CVR JOURNAL OF SCIENCE AND TECHNOLOGY

Vol.No. 27, December 2024
P-ISSN 2277 - 3916
DOI 10.32377/CVRJST27
E-ISSN 2581 - 7957

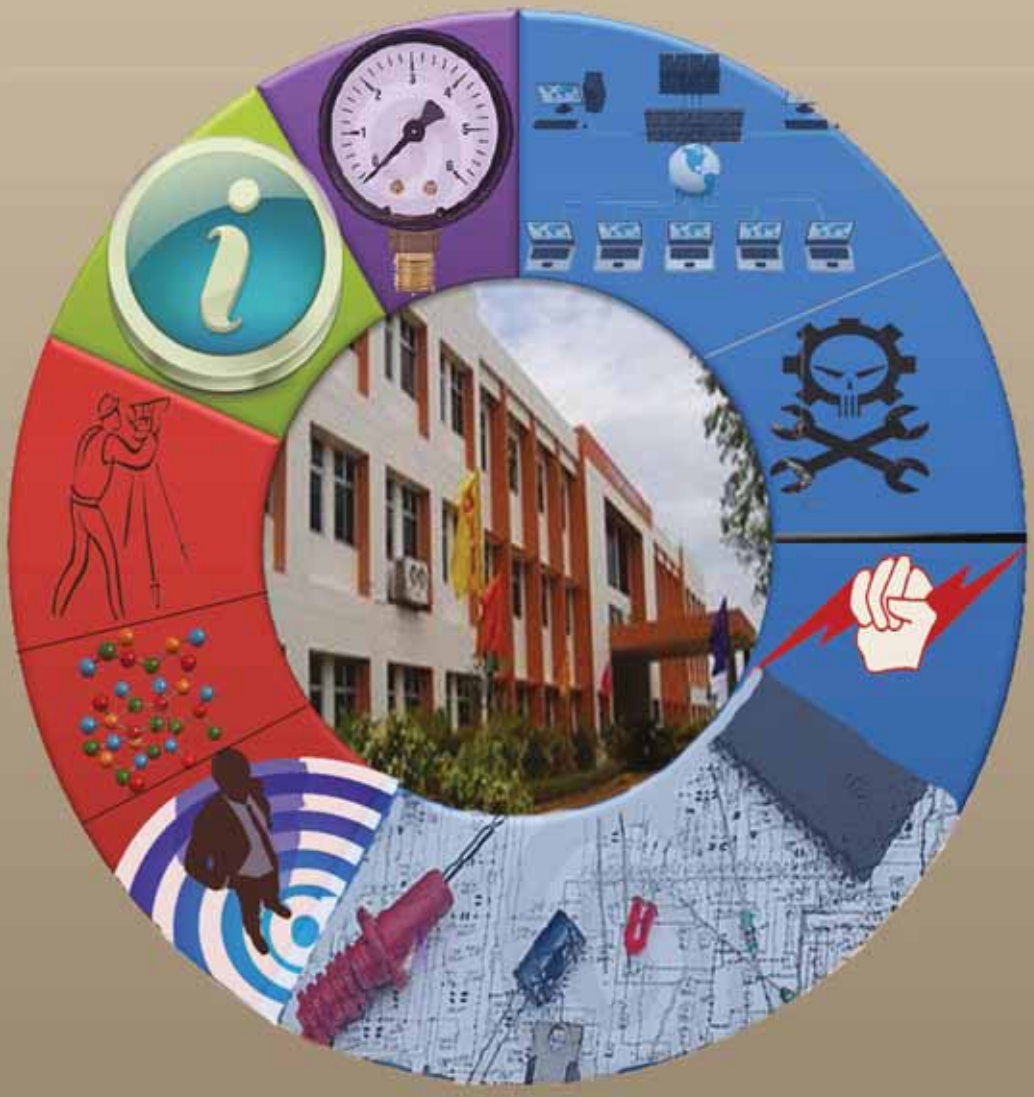

CVR COLLEGE OF ENGINEERING

In Pursuit of Excellence

CVR JOURNAL OF SCIENCE AND TECHNOLOGY

Indexed by

- Google Scholar
- Directory of Research Journals Indexing (DRJI)
- Scientific Indexing Services (SIS)
- International Institute of Organised Research (I2OR)
- Scholar Impact - Journal Index
- Citefactor
- Member Crossref / DOI

Accredited by NAAC with 'A' GRADE

CVR COLLEGE OF ENGINEERING

(UGC Autonomous - Affiliated to JNTU Hyderabad)
Mangalpalli (V), Ibrahimpatnam (M),
R.R. District, Telangana. – 501510
http://cvr.ac.in

EDITORIAL

The editorial team of CVR Journal of Science and Technology is very happy to bring out this Volume No 27 in time. This biannual journal is being published regularly since 2011 without any break. Since 2016, the journal issues are being released in time. During the Carona pandemic time also, despite many hurdles, the journal was brought out in time, with the co-operation of authors, reviewers and editorial team members.

We are taking care to see that standard practices are followed in the publication of the Journal. Blind review is done, and a number of iterations are done till the reviewers are fully satisfied with the standard of the research paper. Senior faculty of English language Department, take care of the language issues. Template verification and typographical errors are checked, before the articles go for publishing. Hope the researchers appreciate this effort. Many research articles published in the journal are being referred by other researchers across the globe, as indicated by DOI, Crossref data.

This Volume covers research articles in the following disciplines:

CSE–2 , ECE– 4, EIE–4, ET-1, IT-1, EEE-2, MECH–2, CIVIL–1, H&S (Mang. Sc.)-1

This is a multidisciplinary journal. Research articles in the areas of physics, Chemistry, Mathematics, Management Science, Statistics, Environmental Science etc. are also accepted.

In this issue, an article from an eminent researcher and educationist on Trust based community learning is published. This is a process that performs asynchronous knowledge transmission over a neighbour graph implicitly defined in a community, according to the author. This work proposed a Trust Based Community Learning (TBCL) algorithm. It is hoped that many researchers would get initiated into this area and many thought provoking articles would come in near future. Another article on the design of mobile hand set or user equipment for emerging sub-6G applications with Radio Frequency Front End (RFFE) to support increased data, larger coverage, low power consumption and other salient features is also published. The power Amplifiers (PAs) are designed using cadence Virtuoso EDA tools. The design of switching class -D, E and F Power Amplifiers is also given. To overcome the limitations of Von Neumann Systems in applications, which are computationally demanding, new architectural technologies are proposed in one article. Resistive Random Access Memory (ReRAM)- based computation- In -Memory (CiM) is explained in this paper. The advantages of VCO-based ADC design are mentioned.

To assist the vehicles under emergency conditions, IoT based Real Time Communication and location system is proposed in one article. This will be very useful for automobiles and can be implemented for practical situations. To prevent accidents, an IoT based model is proposed in another article. Queuing Model-based Prediction Scheme (QMPS) for Conserving Power in BWA Networks is explained in one research article.

Students are being encouraged to publish research papers based on the project work done by them. P.G. students spend almost one year on the project work. So, this should result in significant work suitable for publication in a journal. Project supervisors guiding the students must give research orientation for the work of the students. Selected research papers of U.G. students are also published in this volume. It is heartening to see that U.G. students are also showing enthusiasm for publishing papers. Hope this trend will continue.

Thanks are due to **HOD, H & S,** and the staff of English Department for reviewing language in the papers. I am also thankful to **Dr. S. Venkateshwarlu, Dr. P. Uma Maheshwera Reddy Assoc. Editors and Mr. Ch. Gangadhar, DTP Operator** in the Office of Dean Research, for the preparation of research papers in Camera - Ready form.

For further clarity on waveforms, graphs, circuit diagrams and figures, readers are requested to browse the soft copy of the journal, available on the college website, www.cvr.ac.in wherein a link is provided. Authors can also submit their papers through our online open journal system (OJS) www.ojs.cvr.ac.in or www.cvr.ac.in/ojs

Prof. K. Lal Kishore
Editor

International Review Board:

CONTENTS Page No.

E-ISSN 2581 – 7957
P-ISSN 2277 – 3916

CVR Journal of Science and Technology, Volume 27, December 2024
DOI: 10.32377/cvrjst2701

Specifying Trust-based Community Learning

Dr. Hrushikesha Mohanty[1, 2]
[1]Former Professor, University of Hyderabad, Hyderabad, India
Email: hmcs@uohyd.ac.in
[2]Emeritus Professor, CVR College of Engineering/CSE Department, Hyderabad, India
Email: hmcs@cvr.ac.in

Abstract: **while chatting with neighbours is a social behaviour, trusting a neighbour is a natural tendency. Both play subtle roles in making community knowledge. We propose Trust Based Community Learning, a process that performs asynchronous knowledge transmissions over a neighbour graph implicitly defined in a community. With a formal specification, we have shown community learning as a distributed process and it eventually achieves community knowledge. It's observed that social learning can be facilitated by re-engineering a community neighbour-graph to a small world network.**

Index Terms: **community knowledge, distributed algorithm, asynchronous knowledge transmissions, neighbour-graph.**

I. Introduction

Humans are blessed with knowledge for solving problems of different types ranging from the detection of God's particles to sustainable farming. While research on the human brain is engaged in exploring cognitive processes in human decision making and knowledge formation, the research on Artificial Intelligence is looking for a modeling process that imitates the human learning process. Here we are modeling community learning as a social process for community knowledge. A piece of information useful to the community and mostly known to community members is termed as community knowledge. For example, the concoction of *tulsi* and black pepper is good to treat cold and cough. Sociologists add a usability dimension to knowledge in qualifying it as community knowledge. In the process of transmission, knowledge passes through many individuals. Each may verify usability and authenticity of knowledge and even augment it with further details. This way community knowledge gains trust. The more a person receives knowledge from its neighbours, the more the person updates trust value to the knowledge and informs its neighbours. Thus, community learning is a distributed social process where an individual behaves as an asynchronous autonomic process to receive, process, and forward a piece of knowledge. Social process is a complex process with thousands of variables, non-linear dynamic behaviour, and circularity. That is the reason why many are skeptical about modelling social systems. Nevertheless, there have been active interests in modeling social systems. With increasing computing power and storage capabilities, developing social systems for domain-specific uses is gaining momentum. For that, understanding and specifying social systems are important.

An early work on specifying social phenomenon may be traced to [1]; this paper presents a mathematical framework in explaining social changes. The concept of society-as-a-system has ignited research in Computational Social Science. A bird's eye-view on this area of research may be found in [2]. Currently, society is poised to adopt AI techniques for providing community services and addressing social problems. [3] This has ushered in a trend in studying social phenomena considering society-as-a-system.

While theoretical study includes formal specification of social systems, experimentalists show interest in the development and deployment of such systems. The work presented here is of the former category. It specifies community knowledge-making, a phenomenon that makes knowledge of an individual to a community aware knowledge. The proposed social learning algorithm implements the specification in making use of the social feature trust-thy-neighbour for knowledge sharing. It's seen, social communication is a necessary condition for social learning. By analysis of the algorithm, it is observed that for formation of community knowledge, a society needs to be re-engineered to a small world network.

Including this section, this paper has five sections. The following section positions social science perspectives of the problem referring to the works on community knowledge. The third section presents a formal framework specifying the three entities viz. individual, community and communication. Trust-thy-neighbour, a social aspect is modeled in the fourth section. It also presents a distributed algorithm for trust-based community learning. This is followed by a conclusive remark identifying issues for further research.

II. Community and Community Knowledge

Humans being social share knowledge with their neighbours and acquaintances. A piece of knowledge gained by an individual(s) is termed individual knowledge. The knowledge shared with the community is community knowledge. This process of making community knowledge is termed community learning. The process of learning by an individual is not only based on its capability [4] but also depends on social conditioning. [5] Community learning is a complex process that includes deliberation, argumentation, and affirmation of accrued knowledge that community by large accepts.[6] This process is a reality because community members deliberate, vet, and share a knowledge to form community knowledge. Community knowledge is of two types viz. explicit knowledge and tacit knowledge. Experiences gained by individuals make explicit knowledge whereas tacit knowledge is something one knows but can't explain it. It includes integrated knowledge and heuristics that people use as a thumb's rule. According to sociologists, retrieving tacit knowledge needs interpersonal

Received on 26-10-2024, Revised on 10-11-2024, Accepted on 25-11-2024.

CVR Journal of Science and Technology, Volume 27, December 2024
DOI: 10.32377/cvrjst2701

communication. Naturally, interpersonal communication is important for community learning.

In masses, knowledge emanated from an individual(s) propagates across a community making recipients aware of the knowledge. Social Science views community knowledge is subtly learnt for meeting day to day challenges. So, community knowledge is about situated actions, which often turns out specific to people, places, and practices. So, communities may differ in their community knowledge even for the same purpose. For example, practices of paddy cultivation could be different for different communities situated in different places. Still, a common approach may be seen in the generation of community knowledge. Here our interest is in specifying this generic approach. The following section finds such formalization.

III. Individual, Community, Communication

People, place, and profession are the three important factors for individual livelihood management. Classically, people choose to stay in a place congenial to live, particularly the place offering means to earn. Agrarian families choose a habitat with plenty of natural resources like land and water. Indigenous people choose habitats in forests with natural resources useful for their living. People develop knowledge to make livelihoods utilising the resources available in their habitats. Currently, netizens live in Cyberspace and make use of its resources in many ways. Monetising Cyberspace is a new way to earn a livelihood. Thus, modeling human action, we need to model its habitat because it impacts and impacts human life.

As reported in [7] we model the habitat of a person as a tuple $< K, Q, R, L >$ where K, Q, R, L are knowledge, objective, resource and location respectively. This models the following aspects of a person *p*.

- K:: {k_1, k_2...k_i, ... } : knowledge
- Q :: {q_1, q_2...q_j , ... } : objectives
- R :: {r_1, r_2...r_k, ... } : resources
- L :: { l1, l2, …. lk… } : location

So, habitat of a person p at location l is specified as $H^p = < K^p, Q^p, R^p, L^p >$. A person p in its habitat L^p is endowed with natural resources R^p. A person may have a set of objectives Q^p; of which some could be transactional and some transcendental. Here, we are limited to the former type of objectives. These objectives are to meet individual needs like food, housing, transport, healthcare, safety, education etc.

Materialising objectives needs resources and individual efforts. Naturally, there is a relationship between resources and objectives i.e. $R^p \rightarrow Q^p$. A knowledge of a person p refers to the information that details how to use a resource to materialise an objective. This we label as individual knowledge of a person *p* situated at L^p and specify as

$$k_L^p = f(r_L^p, q^p) \quad (1)$$

where k_L^p is a knowledge a person p situated at L has and r_L^p *is the resource of p to meet its* objective q^p.

As said before, social learning is achieved by transmission of individual knowledge across the members of a community. Before detailing the social learning process let us define some necessary formalism.

Traditionally community refers to a set of people living in a place exhibiting high degree of homogeneity in their way of life that includes livelihood, cultural, political and religious beliefs. Social scientists' view on community is at times deep and complex. Here for the purpose of this study, it's sufficient to define a community as a set of people with homogeneous habitats. A community C of location L is specified as

$$C_L = \{ (p_L, q_L) | \, H_L^p \equiv H_L^q \} \, \forall \, p, q \in P_L$$

where H_L^p and P_L are respectively a set of habitats and a set of people living in locality L. On varying the degree of similarity, communities of different granularity can be found. On defining *contain-in* relationships, hierarchical community structures can also be defined. Without any compromise, here our discussion limits to a planar community.

In a locality, community members are connected by both situated and functional proximity. For digital society, proximity is defined by friend and *friend-of-friend* relations. Digital communities can be formally represented by a graph. Our discussion here considers traditional society. Still, the proposed idea is applicable to digital society.

Two people in a locality are connected and in communication for their situated or/and functional proximity. A person usually has an opportunity to communicate with neighbours; that is an example of situated proximity. A person communicates with people it meets in its functional worlds viz. workplace, bank, supermarket, temple etc. This is known as transactional proximity. Unlike Cyberspace social platforms, in real world *friend* relation is not transitive in nature. In the real world, a friend of a friend need not be a friend. One may not be in talking terms with its neigbours. Inspite of such possible unfriendliness, society remains connected for far reaching human relationships. So, without loss of generalization we may assume that implicitly people of a locality are connected, maybe directly or indirectly. We formally define this implicit structure by a graph by making use of nbr relation as

$$nbr(p) = \{q \mid q \in (std\_pxmty(p) \cup fnc\_pxmty(p))\}$$

where *std_pxmty(p)* and *fnc_pxmty(p)* are sets of people associated with p by its situated and functional proximity respectively.

The following properties are ascribed to the nbr relation.

CVR Journal of Science and Technology, Volume 27, December 2024
DOI: 10.32377/cvrjst2701

- Reflexive : $p \in nbr(p)$
- Commutative : $p \in nbr(q) \implies q \in nbr(p)$
- Transitive: $if\ \Big(\big(q \in nbr(p)\big) \wedge (r \in nbr(q))\Big) \Longrightarrow (r \in nbr(p))$

With the relation $nbr(p)$, the concept of community graph of a location L i.e. CG_L is defined as

$$CG_L = \{q \mid \forall q\ \exists\ r\ \wedge\ r \in nbr(q)\}$$

A community is said to be connected *if and only if* all its members are accessed by nbr relation. For ensuring seamless access between any two members of the community the following condition is applied

$$connected(CG_L) \Leftrightarrow \{\forall\ (p,q) \in CG_L\ \exists\ q \mid q \in nbr^*(p)\ \}$$

A community is connected when one can reach out to another either directly or through several people in between. Sociologists term this phenomenon as small world problem.[8] Researchers working in networking theory label is as small world network.[9]

The function $nbr^*(p)$ is repetitively applied on neigbours of p to explore all the people connecting to p. A connectivity between p and q is represented by a path $(p \rightarrow q)$ in the graph CG_L. We say, a community is connected when there is a path between any two people of the community. On the basis of the connectivity as defined, the hypothesis follows.

Hypothesis-1: A message sent by a community member eventually reaches all in the community.

This is achieved with the assumption that a person on receiving a message from a neighbour passes it to its other neighbours. This is viewed as a breadth-first graph traversal and can be simulated by a distributed breadth-first search algorithm. [10]. In the worst case, that is for very sparingly connected community this path length could be $(N-1)$ where $(N = |CG_L|)$, N the total population of the community. Making a community aware of individual knowledge by communication among community members is a process of community learning. The next section presents a trust-based model for community learning.

IV. COMMUNITY LEARNING

Primarily, knowledge transmission among community members takes place while they meet in. homes, workplaces, and social spaces like in streets and markets. Here to model the knowledge transmission process, we propose the trust-thy-neighbour principle.

Prnciple-1: A person shares its knowledge with neighbours it trusts enough.

Principle-2: A person reassess trust of the knowledge received from its neigbours.

Hearsays have their social bearing because it conditions community members. A community member usually trusts another, and the degree of trust depends on many parameters like social identity, proximity and transaction history. Among the people one knows, a person at its workplace is more trusted than a person it meets in a supermarket. Further a person with good transaction history is more credible than the one with not good or unknown history. An individual p's trust assessment on its neighbour q i.e. $trust_q^p$ depends on two factors viz. trust by own experience, trust by community image. The second one is a gross trust value of q, as p finds from its neighbourhoods.

$$trust_q^p = sts_q^p + cts_q^C\ ; \left(trust_q^p\right) = 1 \qquad (2)$$

where $(sts_q^p \in (0,1))$ and $(cts_q^C \in (0,1))$ are respectively the self-test-score of p on q and the community-test-score of C on q. It is assumed that cts_q^C is available centrally and the score is computed making use of transactional history of q. Thus, trust in community is computed following the principle of trust-thy-neighbour.

An individual p on receiving a piece of knowledge k from q with trust value $(trust_q^k \in (0,1))$, updates trust as

$$trust_{p,q}^k = trust_q^p + \left(1 - trust_q^p\right) \times trust_q^k\ ;$$

$$\left(trust_{p,q}^k\right) = 1 \qquad (3)$$

An individual p's trust on k received from q i.e. $trust_{p,q}^k$ has a base-trust i.e. trust p has on q $(trust_q^p)$. Further receiving a trust value $trust_q^k$ from q, the trust of p on q is upgraded by $trust_q^k$ times. It's to be noted, distrust is modeled by zero trust value.

Thus, an individual p receives trust values of a knowledge k from its neighbour q then p's trust on k i.e. $trust_k^p \in (0,1)$

$$trust_p^k = trust_p^k + \left(1 - trust_p^k\right) \times trust_{p,q}^k\ ;$$

$$\left(trust_k^p\right) = 1 \qquad (4)$$

Below we present an algorithm TBCL (Trust Based Community Learning)

Algorithm 1 TBCL: Executed forever at an individual p

```
1: begin
2: ∀ k=(1 ··· K) trust_p^k = own.trust_p^k ;
3: ∀ q ∈ nbr(p) compute(trust_q^p);
4: for () { // wait to receive a message
5: rcv(trust_q^k) from q ∈ nbr(p) { // on receiving a message
6: old.trust_p^k = trust_p^k
7: compute trust_{p,q}^k; // apply eqn.3.
8: compute trust_p^k } // apply eqn.4;
9: if (old.trust_p^k ≠ trust_p^k) ∧ ( trust_p^k ≥ δ_p^k ) then {
10: ∀ q ∈ nbr(p) send(trust_p^k) } // inform neighbours.
11: }
12: end
```

A. Observations

Some of the observations due to TBCL are as follows. These observations are argued upon with reference to the line numbers of the algorithm.

Observation 1. Community learning is asynchronous.

With reference to the lines 9-10 in TBCL, whenever there is an update of trust on knowledge k at an individual p then it informs the change to its neigbours. On receiving this update message, each of these neighbours update the knowledge trust at their ends. If a person finds knowledge trust equal or greater than the threshold trust value then the neighbours are informed about the knowledge with its latest trust value. This transmission causes a domino-effect and eventually all in the community are aware of the knowledge (assuming the knowledge qualifies at each vertex for transmission i.e. knowledge trust is greater or equal to the knowledge trust threshold at the vertex.) By design of the proposed distributed algorithm, each vertex asynchronously executes the algorithm. Let us assume, at each vertex trust threshold condition is satisfied, so the knowledge *k* eventually reaches all the vertices. This makes a community aware of the knowledge *k*. Thus, community learning is asynchronous in nature. Please note that the previous section formalises community as a graph.

Observation 2. Community learning is a non-terminating process.

In practice an individual hears from its neigbours and thus learns a new knowledge or updates it with new information with trust. There may be a change in trust value. By Observation 1, an update on *k* propagates to all the connected community members. This process continues forever in a community. This notion of non-terminating social learning is implemented in lines 4-11 in algorithm TBCL.

Observation 3. Community Learning is trust-based learning.

The observation follows directly from the TBSL lines 9-10. An individual informs its neigbours when its trust on a knowledge *k* is greater or equal to the threshold trust value i.e δ_p^k. (case.1) A conservative person may have a high threshold value whereas (case.2) a diabolically opposite type of individual may have zero threshold i.e. it unconditionally passes on all messages to its neighbours. (case.3) By agreement, a common trust threshold can be fixed for everybody. This case ensures a level of trust across the community. This conditionality (line 9 of TBCL) may inhibit a person from transmitting knowledge. For this, the next observation follows.

Observation 4. An individual can never know everything that others know.

There is a chance of no transmission of knowledge because of many reasons. For example, a person may not trust the knowledge and does not transmit it to its neighbours. (line 9) There could be another cause, that's social factors. Neighbours may miss chatting or meeting for their preoccupations. Another social scenario could be due to highly heterogeneous communities where the loss of message transmission is a reality for people practicing individualistic lifestyles. In such a community people used to live in self-isolation. For both the reasons i.e. deficit of trust and social lifestyle, community knowledge is not an all-aware knowledge.

For this reason, we redefine the concept of community knowledge, A knowledge is community knowledge when the knowledge is available with a neighbour at a given distance say *d*. Small world network concept corroborates this definition. A network is of small world nature when distance between any two vertices in the network is less than equal to log of the total number of vertices present in the network. According to sociologists, a society is inherently a small world. [8] Network theorists, intending to establish small network, propose network rewiring technique to make a network connected by a given distance, say *d* (any two vertices in network is at the distance less than or equal to *d*) .[11]

Obesrvation 5. As knowledge transmission is context and trust dependent, success in reengineering a people network depends on knowledge and its relevance to community members.

A community goes on continuous trust revision, because social behaviour of a community varies with time; so people to people trust also varies. Erosion of mutual trust may impact on sustainability of community knowledge. This could be a reason why in the course of time the community forgets its past knowledge.

V. Conclusion

On specifying a human habitat, individual knowledge and community knowledge, this work proposes TBCL: Trust Based Community Learning algorithm. Each community executes this algorithm on receiving knowledge from its neighbour. The proposed asynchronous non-terminating distributed algorithm supports trust-based community learning. The working of the algorithm is explained with five observations. It shows the need of social reengineering to promote small world community networking to facilitate the making of community knowledge.

The work reported here is an attempt to understand and formalise the community learning process so a community can be reengineered for making community aware of a knowledge. However, the proposed algorithm needs to be validated by field experiments. These may add more social aspects to the idea of community knowledge formation process. Community knowledge is undeniably important to enable people with knowledge for sustainable livelihood management.

Some fundamental issues listed below invite further research.

1. While a relation between communication and trust building is apparent, still it needs a computational model

to estimate influence of different social parameters viz. community size, frequency of communication, personal habitats etc, in community learning.

2. A computational model for adaptive social re-engineering is an interesting topic for further research. Adaptive TBCL algorithm online reengineers community network to a required small world network for achieving community knowledge.
3. Making a community resilient to social changes is necessary so that community knowledge is not a loss of social inheritance. For this purpose, TBCL is to be integrated into social memory so loss of community knowledge can be prevented.

Graph federated learning as reported in [12] provides a mechanism for finding a foundation model on learning from multiple clients so that information access for individual needs is improved. This problem has a similarity with community learning that needs to honour privacy of individuals and at the same time supports propagation of individual knowledge of interests to community members. While application of AI techniques in modeling social phenomena is interesting, the promise of AI in empowering local communities is welcome. This technology mediated community is better structured for governance and sustainable development. [13] In corroboration to this idea, research on small world network says, in general a community is self-configured to assume a structure that's neither random nor regular. [14] This trend promises a new vista in multi-disciplinary research bringing Social Science, Computer Science and Artificial Intelligence together for modeling social phenomena and provisioning community services.

REFERENCES

[1] Claudio Cioffi-Revilla (2005) A Canonical Theory of Origins and Development of Social Complexity; The Journal of Mathematical Sociology 29:2,133-153.

[2] Hrushikesha Mohanty (2013) Computational social science: A bird's eye view; LNCS 7753, 319–333.

[3] Yen-Chia Hsu, Ting-Hao 'Kenneth Huang, Himanshu Verma, Andrea Mauri, llah Nourbakhsh and Alessandro Bozzon (2022) Empowering local communities using artificial Intelligence; Pattern, March,

https://doi.org/10.1016/j.patter.2022.100449

[4] Simon, H.A. (1991) Bounded rationality and organizational learning; Organization Science 2, 125– 134.

[5] Brown, J.S., Collins, A. and Duguid, P. (1989) Situated cognition and the culture of learning; Educational Researcher 18, 32–42.

[6] Brown, J.S. and Duguid, P. (1991) Organizational learning communitiesof- practice: toward a unified view of working, learning, and innovation; Organization Science 2, 40–57.

[7] Hrushikesha Mohanty (2011) Person habitat and migration modeling; IEEE TENCON, 1-6.

[8] Milgram, S. (1967) The small world problem; Psychology Today 2, 60–67.

[9] Watts, Duncan J., and Steven H. Strogatz (1998) Collective dynamics of 'small-world'networks; Nature 393,6684, 440-442.

[10] Nancy A. Lynch (1997) Distributed Algorithms; Morgan Kaufmann.

[11] Jeff Alstott, Christine Klymko, Pamela B. Pyzza, Mary Radcliffe (2017) Local rewiring algorithms to increase clustering and grow a small world; Journal of Complex Networks 7, 564–584.

[12] Chen, Jiewei, Shaoyong Guo, Qi Qi, Jiakai Hao, Song Guo, and Xuesong Qiu (2021) Enabling Foundation Models: A Distributed Collaboration Framework Based on Graph Federated Learning; IEEE Transactions on Services Computing 14, 8, 1-14.

[13] Robinson, C. J., J. Mairi Macdonald, J. Perry, N.-G. Bangalang, A. Nayinggul, J. Nadji, A. Nayinggul, S. Dempsey, S. Nadji, S. McCartney, A. Taylor, F. Hunter, K. May, D. Cooper, F. Moyle, A. Drummond, C. Borovac, S. van Bodegraven, M. Gilfedder, S. Setterfield, and M. M. Douglas. (2022) Coproduction mechanisms to weave Indigenous knowledge, artificial intelligence, and technical data to enable Indigenous-led adaptive decision making: lessons from Australia's joint managed Kakadu National Park. Ecology and Society 27(4):36

[14] Jahnke, Isa. (2010) Dynamics of social roles in a knowledge management community; Computers in Human Behavior 26,4, 533-546.

E-ISSN 2581 –7957
P-ISSN 2277 – 3916

CVR Journal of Science and Technology, Volume 27, December 2024
DOI: 10.32377/cvrjst2702

Queuing Model-based Prediction Scheme (QMPS) for Conserving Power in BWA Networks

Dr. M. Deva Priya
Professor, Karpagam College of Engineering/CSE Department, Coimbatore, Tamil Nadu, India
Email: meetdevapriya@gmail.com

Abstract: **In mobile Worldwide interoperability for Microwave Access (WiMAX), a mobile node is battery powered with restricted capacity. It is challenging to prolong battery lifetime by reducing the quantity of power consumed. Power saving is a significant issue which must be taken into consideration while designing the Medium Access Control (MAC) layer. Schemes are designed for saving power based on packet delay and amount of power consumed. In this paper, Prediction Scheme based on Queuing Model (PSQM) is proposed for defining Power Saving Classes (PSCs) in the MAC layer of IEEE 802.16e networks. Power is saved by turning off Mobile Stations (MSs) when they do not actively transmit or receive data. The size of Sleep Window (SW) is dynamically determined using M/M/1/N queuing model based on channel, exponential service time and Poisson arrival. The size of the buffer is restricted and is based on the First-in First-out (FIFO) queuing model. Instead of exponentially or linearly increasing the size of SW based on traffic type, Arrival Rate (λ) is taken into consideration. Time of arrival of packets is determined, thus reducing the delay involved.**

Index Terms: **BWA networks, WiMAX, Power, QMPS, Arrival Rate (λ), Service Rate (μ), SW size.**

I. Introduction

Users are more familiar with broadband access. WiMAX is a telecommunication technology which provides wireless access involving increased distances in diverse ways from Point-to-Point (P2P) links to cellular access. IEEE 802.16 supports broadband communication in Metropolitan Area Network (MAN) and seems to be appropriate for providing wireless access and sufficient bandwidth, thus offering Quality of Service (QoS) assurance [1]. It offers the missing link for the 'last mile' link in MAN, where Digital Subscriber Line (DSL), cable and broadband access schemes are unavailable or seems to be costly [2]. It supports mobility and offers an alternative to internet services in rural regions. Both fixed and mobile WiMAX involve several attractive features like connection-based MAC layer, providing QoS, effective mobility as well as power-saving characteristics [3].

To conserve power, a Mobile Station (MS) can be turned on and off whenever necessary. Sleep and awake modes are the power saving modes available in WiMAX [4]. There are two stages in sleep mode - sleep and listen stages. The MS can be made to move to sleep mode at regular intervals. Power can be saved by turning off MS for pre-set time period, making it inaccessible when it does not actively transmit or receive data. To enable handoff during sleep mode, the MS scans the Base Stations (BSs) to gather handoff-based information. The periods of unavailability of MSs are made known to the BS.

During the listening stage, MS wakes up to check whether packets are destined for it. An inactive MS may enter sleep mode by turning off device modem, thus dropping the amount of power consumed during RF inactivity. Device can wake up at pre-defined intervals and enter the Listening Window (LW) to receive paging beacons. The paging beacons indicate inclusion of buffered packets at the BS. MS continues to be awake to obtain buffered packets and moves to sleep mode during successive periods of inactivity. If no packets are addressed to it, the MS sleeps for another interval. Alternate wakeup and sleep intervals lead to considerable conservation of power by limiting the RF activity of the device.

A. QoS in WiMAX

WiMAX features diverse flow types for optimizing performance for data, voice and video [5]. Without ensuring QoS, it is impossible to guarantee reduced latency and jitter necessary for providing carrier grade services like VoIP.

To support QoS, it is vital to manage traffic. In WiMAX, different services are offered, and traffic can be prioritized. Classes include Unsolicited Grant Service (UGS), real-time Polling Service (rtPS), non-rtPS (nrtPS), extended rtPS (ertPS) and Best Effort (BE) [6]. These classes are intended for specific applications [7, 8].

- **UGS:** It supports periodic and fixed size packets in real-time like VoIP and is also suited for Constant Bit Rate (CBR).
- **rtPS:** It offers periodic, varying sized packets like Variable BR (VBR) services in real-time.
- **ertPS:** It is a blend of rtPS and UGS.
- **nrtPS:** It is suitable for nrt-VBR services like bandwidth demanding variable sized packets and file transfer with loose delay requirements.
- **BE:** It provisions BE traffic.

II. Power Saving in WiMax

Conserving energy is highly essential for prolonging network lifespan. Multi-hop communication preserves power but determining an ideal path to the destination is tedious. Path stability represents the duration for which the path can support communication. By detecting stable paths, controlling traffic and quantity of connection disruptions can be reduced and power can be conserved.

Power in WiMAX networks is conserved in 2 ways. One is by deploying Power Saving Classes (PSCs) in mobile WiMAX network (IEEE 802.16e) and the other by using Relay Stations (RSs) in a multi-hop network (IEEE 802.16j).

Received on 01-10-2024, Revised on 31-10-2024, Accepted on 20-11-2024.

PSC for IEEE 802.16e Networks

The PSC includes a collection of connections which necessitates collective features for sleep mode. It can be either activated/deactivated. When activated, the MS goes to sleep mode or LW. During deactivation, the MS moves to awake mode from sleep mode. The factors for PSC of Type II include initial SW, LW and start frame number for initial SW. Once communication amid MS and the BS is complete, the MS moves to sleep mode by forwarding sleep request to the BS.

Sleep request involves sleep interval limits (T_{Min}, T_{Max}) and listening interval (L). In case the BS which offers service receives request from an MS to go to sleep mode, it forwards a reply that comprises of initial and final SW, LW and traffic activated wakening flag. The MS moves to sleep mode after obtaining response. The listening interval is positioned amid 2 sleep intervals. Total sleep duration includes sleep as well as listening intervals. First, 'T_{Min}' is used. Once sleep interval expires, the MS commences to listen and waits for traffic. In case packets are buffered for MS during former time interval, PSC for MS is disabled, and MS remains awake to obtain packets. As traffic in the network keeps changing, the PSC must be dynamically chosen. An MS may wake up when the amount of data received during SW cannot be handled in the subsequent LW.

The PSCs for every class define separate schedules of sleep and awake modes depending on the type of traffic at the MS. The IEEE 802.16e includes diverse PSCs for traffic depending on the way the sleep mode is applied. Three classes are defined, and each class differs in parameters, activation and deactivation procedures.

- **Class I:** It is suitable for nrtPS and BE traffic which are delay tolerant. The size of SW is doubled every time to maximum limit with LWs amid them. The BS alerts mobile node about arrival of Downlink (DL) traffic by sending a message on the broadcast channel. It sends message on a sleep mode multicast channel during LW intervals. The node may wake up early, deactivate the PSC and send the BW-REQ to BS in case new UL traffic exists.
- **Class II:** It can be used for rtPS, ertPS, and UGS kinds of traffic. The SWs are of similar size with in-between LWs. There is no deactivation based on arrival of traffic as in type I. PSC of type II employs a constant SW size, and packet delay is reduced by fixing the size of SW to initial size. As stated in IEEE 802.16e-2006, the MS can send or receive packets and acknowledgments during LWs, enabling short messages to be transmitted or received without interruption of sleep mode, thus avoiding unnecessary switching costs. It involves more number of LWs, resulting in more power consumption.
- **Class III:** It can be used for management or multicast traffic. LW is not defined for type III PSC. PSC gets deactivated automatically once SW terminates.

A trade-off amid the amount of power consumed and packet delay must be attained. Delay must be at a satisfactory level.

IEEE 802.16j

In IEEE 802.16j (IEEE 802.16e-2006), the relay nodes are deployed as a promising solution to replace IEEE 802.16e mesh mode for extending coverage and enhancing throughput. Further, it conserves power as relays close to MS enable multi-hop communication and increases network capacity. A multi-hop wireless network based on relay architecture comprises of small relays that are related to the BSs. Though multi-hop communication preserves power, determining an ideal route to destination is tedious. There are many routing protocols available in the literature grounded in various factors. They decide the path to the destination based on factors like the shortest distance, geographic location, stability of links etc. A protocol which determines a stable ideal route based on node energy extends network lifetime.

Delay

Data packets for an MS are queued until they are accepted by it. In case the MS is in sleep mode, the packets are buffered by the BS and are delayed for a wakeup interval till LW is seen. Extended sleep duration leads to a drop in the amount of power consumed but raises the amount of delay. This has an impact on the packet delay constraints causing overflow of buffer. Short sleep intervals involve reduced delay but upsurge power drain owing to repeated awake modes. A trade-off must be obtained. An effective sleep-wake up schedule should be designed for balancing delay and power.

As accurate information concerning future traffic flow is not known, the sleep window size can be determined from traffic history and recent traffic changes. In this paper, a power saving mechanism is propounded for mobile networks. Queuing Model based Prediction Scheme (QMPS) is designed for dynamically alternating sleep interval for diverse traffic classes. Sleep interval is dynamically determined based on arrival (λ) and service rates (μ) of traffic. An appropriate sequence of PSCs is got and trade-off amid packet delay and power consumption is achieved. Average delay is highly reduced (22.4%) and power is conserved to a greater extent (19.6%). Throughput is increased (82%) and the PLR is reduced (79.3%).

III. Related Work

In this section, the schemes of power saving designed for WiMAX networks are discussed in detail.

Suranga Sampath et. al. (2020) [9] have employed an M/M/1 queuing system that integrates various vacation policies, customer impatience and scenarios involving waiting server. Transient probabilities are derived for the size of the system by explicitly using techniques such as probability continued fractions, producing functions, Laplace transforms and confluent hypergeometric functions. Time-based mean and variance are used as performance metrics, including an example to show the behavior of a system. Mai et. al. (2020) [10] have addressed scheduling of both Real-Time (RT) and Non-RT (NRT) traffic by proposing Load-Based Power Saving-RT (LBPS-RT) scheme. Simulations demonstrate that the proposed scheme offers better power-saving efficiency in contrast to standard

Type I and II approaches and successfully meets the required traffic delay constraints. Isaac et. al. (2020) [11] have introduced Battery-Life Management with Efficient Sleep-Mode Power Saving Scheme (BM-ESPSS), an enhancement of ESPSS. BM-ESPSS focuses on adjusting sleep intervals and improving average-based sleep mode to reduce longer sleep durations aiming at enhancing QoS. The scheme is evaluated through analytical models and discrete event simulations showing improved performance based on energy consumption, delay reduction and extended battery in contrast to existing mechanisms.

Wisdom et. al. (2020) [12] have proposed Delay Aware Power Saving Scheme (DAPSS) and its enhanced version (EPSS), which are designed to mitigate excessive response delays by adjusting power-saving parameters based on traffic load. EPSS introduces minimum and maximum sleep intervals to reduce power usage and enhance QoS. The mechanism dynamically adapts to varying traffic conditions and is assessed through discrete event simulations, showing significant improvements over previous schemes in power consumption and QoS. Jin et. al. (2021) [13] have developed a discrete-time queuing model involving varied vacations for analyzing communication networks through IEEE 802.16m protocol. They have described the operational principles of the system and have used a discrete-time embedded Markov chain to assess steady-state performance measures, including average packet response time and energy savings. The numerical outcomes investigate effects of sleep cycles and packet arrival rates on system performance. Asafa et. al. (2022) [14] have assessed the energy efficiency of an optical-wireless access network combining Long Term Evolution - Advanced (LTE-A) and Passive Optical Network (PON) technologies. Dynamic Bandwidth Allocation (DBA) algorithm is implemented using OPNET and it is seen that DBA involves reduced energy, demonstrating significant energy savings while maintaining QoS in the network.

Naik et. al. (2022) [15] have proposed traffic grooming algorithms for hybrid networks that incorporate renewable energy sources. This approach involves decentralized renewable energy production at network nodes, with brown energy used as backup. The algorithms optimize energy usage and traffic routing while minimizing reliance on fossil fuels and ensuring service level agreements at data centers. Emara (2022) [16] have introduced a power conservation algorithm for VoIP services in WiMAX systems depending on Artificial Neural Network (ANN-VPSM). Feed-Forward Neural Network (FFNN) model predicts silent periods for finding sleep intervals to save power in IEEE 802.16 systems. The results indicate that ANN-VPSM involves reduced power during VoIP calls while maintaining QoS. Mohammed Shapique et. al. (2024) [17] have examined energy management strategies for WiMAX and have tethered High Altitude Platform (HAP) systems. The model includes a close-down period followed by either a functional state or ordinary vacation based on system occupancy. During ordinary vacations, if the system is empty, a Working Vacation (WV) mode is used, where jobs are served at a reduced rate. Explicit transient as well as steady-state probabilities are derived through continued fraction and hypergeometric functions, and performance is evaluated in terms of mean, variance, throughput, and abandonment rate along with cost-profit analysis.

IV. Dynamically Alternating Sleep Interval Scheduling Algorithm

In a changing network traffic environment, PSC must be dynamically selected for rtPS or nrtPS traffic types. Dynamically Alternating Sleep Interval Scheduling Algorithm (DASISA) [18] aids in determining SW sizes of MSs. It uses historic and dynamic information to regulate previously made decisions and values of parameters. Data traffic is categorized into non-real-time (Class I) and real-time (Class II). Diverse classes of traffic are taken into consideration and PSCs are scheduled. Two PSCs are alternately included in power saving sequence. LWs are positioned close to arrival frames of packet.

Type I and II PSCs support similar operations with varying sizes of SW. Type II PSC employs fixed size of SW depending on initial size rather than doubling the size, leading to a greater number of LWs and increased power consumption when compared to Type I PSC. Size of SW is dynamically determined depending on arrival time of packet, interval amid packets and packet types. The PSCs are constructed by considering initial SW cycle length based on Rank Number (Rn) which varies with the traffic load.

V. Queuing Model Based Prediction Scheme (QMPS)

In case of IEEE 802.16e networks, forecasting the SW is challenging. Packet delay increases with SW size. As packets reach an MS, it must listen so as to drop delay consumed in getting packets. In case a packet reaches before an MS wakes up, the BS must wait until MS shifts to listening mode. In case, an MS does not listen in a short interval on receiving packets at the BS, there may be an increase in delay. Packets may collect at BS for an MS, and the MS will not be ready to obtain it. To overcome this, the LW must follow packet arrival as far as possible. QMPS is designed to determine the time when an MS must commence listening for packets.

Mean Arrival Rate (λ) refers to predictable quantity of packet arrivals in a unit time. Mean Service Rate (μ) represents anticipated packet service completion per unit time for MS. No PSC depending on ‘μ’ and ‘λ’ determined from arrival time is available. Instead of taking distinct schedules for diverse classes, ‘λ’ and ‘μ’ based models may be implemented on different traffic classes. Each MS has one connection. An MS may shift to listening mode by forecasting the time in which packets may reach it. Prediction is performed based on ‘λ’ of packets. In case, an MS is in sleep mode when packets arrive at the serving BS, the respective MS must be awakened. The time at which packets destined for the MS reach the BS must be forecast depending on ‘λ’ and ‘μ’ of packets**.** MS after servicing packets, checks whether frames are available at the BS intended for it. If pending packet frames are present, they are received and serviced. Else, it switches to sleep mode for a specific amount of time.

CVR Journal of Science and Technology, Volume 27, December 2024
DOI: 10.32377/cvrjst2702

A. Mathematical Model

Markovian queuing models represent queuing systems which involve exponential inter-arrival and service times. M/M/1/N queue is a model based on a server with limited capacity. Arrival of customers is modelled as a Poisson process with 'λ'. Inter-arrival as well as service times follow exponential distribution that signifies Markovian model. As buffer size is restricted, the quantity of packets it can hold is limited.

M/M/1/N represents a stochastic process with state space including a set of packets and the one presently being served. In case of a server, packets are served based on First Come First Serve (FCFS) basis. This model is employed for forecasting the sleep interval of MS based on 'λ' of packets intended for the MS.

B. Window Size Based On Arrival Rate

In case, the time of packet arrival (T_a) is appropriately predicted, delay may be reduced to a greater extent. LW is set at time slot 'T_a'. Size of SW is determined dynamically based on 'λ' and 'μ' of packets. Service time refers to the time between the beginning and end of service.

$$\text{Expected service time} = \frac{1}{\mu} \tag{1}$$

'P_0' represents the probability that packets are not buffered at the BS for a MS.

$$P_0 = \frac{1}{N+1} \text{ if } \lambda = \mu P_0 = \begin{cases} \frac{1}{N+1} \text{ if } \lambda = \mu \\ \frac{1-\rho}{1-\rho^{N+1}} \text{ if } \lambda \neq \mu \end{cases} \tag{2}$$

where, '$\rho = \frac{\lambda}{\mu}$', 'λ' indicates traffic intensity and 'μ' denotes utilization factor

Let 'P_n' represent probability that 'n' packets are buffered for the MS at the BS.

$$P_n = \begin{cases} \frac{1}{n+1}, \text{if } \lambda = \mu \\ \rho^{\left(\frac{n}{\mu-\lambda}\right)}. P_0, \text{if } \lambda \neq \mu \end{cases} \tag{3}$$

With increase in 'λ', 'ρ' shows an increase, where 'μ' is a constant. Probability (P_n) that packets are serviced shows a drop with increase in 'λ'. This demands that the size of the sleeping window is dropped.

Arrival time (T_a) of packets is determined as follows.

$$P_N = 1 - e^{-(\mu-\lambda)T_a} P_N = 1 - e^{-\rho(\mu-\lambda)T_a} P_n = 1 - e^{-\rho(\mu-\lambda).T_a} \tag{4}$$

Time with increased probability for packets to arrive (T_a) is given by,

$$T_a = \frac{\ln(1-P_n)}{\rho.(\lambda-\mu)} \tag{5}$$

As 'λ' approaches 'μ', afore mentioned relation may not hold. With drop in probability of packets that are being serviced, an increase in the size of SW is observed.

Time at which MS commences to listen (T_l) is given by,

$$T_l = T_l - 1 + T_a \tag{6}$$

As 'λ 'and 'μ' vary with traffic type, 'T_a' is determined dynamically. The parameter 'T_a' represents the prediction factor for assigning size of SW (SW_{Size}) in terms of slots.

$$SW_{Size} = T_a = T_l - T_{l-1} \tag{7}$$

The time at which MS must wake up is dynamically determined depending on 'SW_{Size}'. This leads to a reduction in the amount of delay and power consumed.

VI. PERFORMANCE OF QMPS

The system is implemented using ns-2 and performance is analyzed for several power saving schemes. Simulation parameters are shown in Table 1. QMPS offers improved results in contrast to DASISA. It shows better results based on Throughput, delay, Energy consumed, and Packet Loss Ratio (PLR).

TABLE I.

SIMULATION PARAMETERS OF CPSR AND QMPS

Parameters	Values
MAC Protocol	MAC 802.16e
Routing protocol	DSDV/ GPSR
Queue Type	Queue/DropTail/ PriQueue
Bandwidth	50 Mbps
Beacon interval (Sec)	0.5
Queue Length	512
Number of MSs	50
Simulation time (Sec)	40
Initial Energy	100 J
Transmission / Receiving Power (mW)	0.6 - 35 / 0.2
Packet size (Bytes)	1024
Data rate (Mbps)	2
Transmission range (m)	250 - 400
Speed of nodes (ms^{-1})	20

Data packets destined for an MS are queued until accepted by it [19]. In case the MS switches to sleep mode, the packets are buffered at the BS and delayed for another interval (wakeup) until LW is seen. Extended sleep period reduces the amount of power consumed, but on the other hand increases the quantity of delay involved. This violates the constraints related to packet delay and causes overflow of buffers [20]. Smaller sleep intervals involve less delay but increased power drain owing to recurrent awake modes. This demands a trade-off. An effective sleep wakeup schedule is essential for balancing delay and power factors.

QMPS offers 82% better Throughput in contrast to DASISA (Fig. 1).

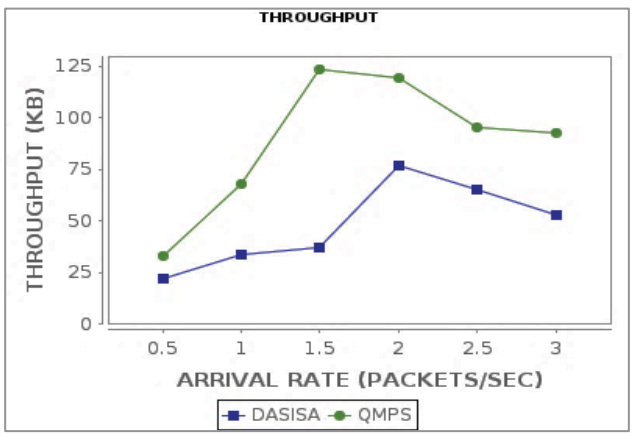

Figure 1. Throughput of QMPS

DASISA involves 19.6% more amount of energy in contrast to QMPS (Fig. 2).

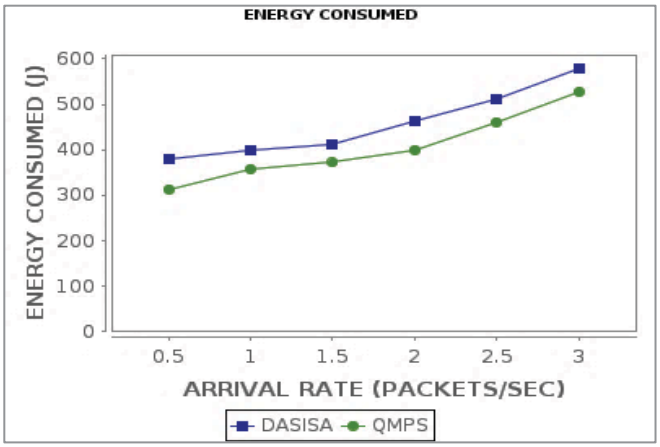

Figure 2. Energy of QMPS

QMPS involves 22.4% less delay in contrast to DASISA (Fig. 3).

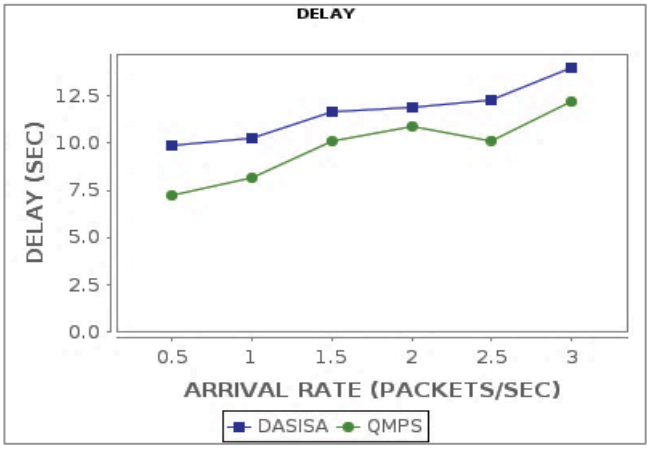

Figure 3. Delay of QMPS

QMPS involves 79.3% less PLR in contrast to DASISA (Fig. 4).

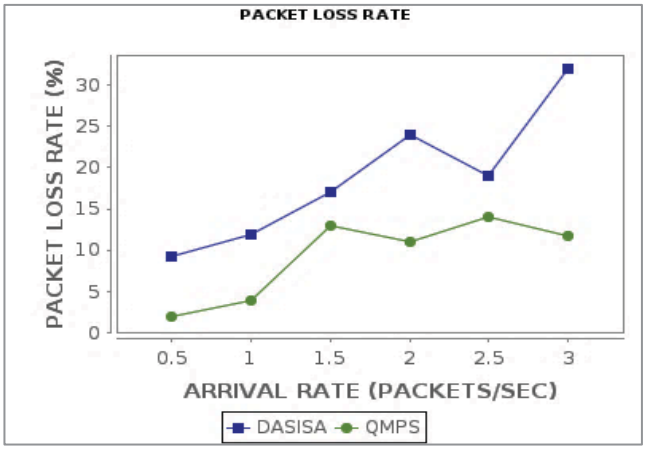

Figure 4. PLR of QMPS

VII. Conclusion

In this paper, Queuing Model based Prediction Scheme (QMPS), an efficient power saving is designed to offer improved lifespan of MSs for IEEE 802.16e networks. The size of SW is adjusted dynamically based on Arrival (λ) and Service (μ) rates of packets destined for the MS. As an MS wakes at the most probable time of arrival of packets, the proposed scheme involves reduced power and delay.

References

[1] Abichar, Z., Peng, Y., & Chang, J. M. (2006). WiMAX: The emergence of wireless broadband. IT Professional Magazine, 8(4), 44.

[2] Eklund, C., Marks, R. B., Stanwood, K. L., & Wang, S. (2002). IEEE standard 802.16: a technical overview of the Wireless MAN/sup TM/air interface for broadband wireless access. IEEE communications magazine, 40(6), 98-107.

[3] Ahmed, Z., & Hamma, S. (2012). Two-level scheduling algorithm for different classes of traffic in WiMAX networks. In 2012 International Symposium on Performance Evaluation of Computer & Telecommunication Systems (SPECTS) (pp. 1-7). IEEE.

[4] Hwang, E., Kim, K. J., Son, J. J., & Choi, B. D. (2009). The power-saving mechanism with periodic traffic indications in the IEEE 802.16 e/m. IEEE Transactions on Vehicular Technology, 59(1), 319-334.

[5] Li, B., Qin, Y., Low, C. P., & Gwee, C. L. (2007). A survey on mobile WiMAX [wireless broadband access]. IEEE Communications magazine, 45(12), 70-75.

[6] So-In, C., Jain, R., & Tamimi, A. K. (2009). Scheduling in IEEE 802.16e mobile WiMAX networks: key issues and a survey. IEEE Journal on selected areas in communications, 27(2), 156-171.

[7] Safa, H., Artail, H., Karam, M., Soudah, R., & Khayat, S. (2007). New scheduling architecture for IEEE 802.16 wireless metropolitan area network. In IEEE/ACS International Conference on Computer Systems and Applications, pp. 203-210.

[8] Cicconetti, C., Erta, A., Lenzini, L., & Mingozzi, E. (2006). Performance evaluation of the IEEE 802.16 MAC for QoS support. IEEE Transactions on mobile computing, 6(1), 26-38.

[9] Suranga Sampath, M. I. G., Kalidass, K., & Liu, J. (2020). Transient analysis of an M/M/1 queueing system subjected to multiple differentiated vacations, impatient customers and a waiting server with application to IEEE 802.16e power saving mechanism. Indian Journal of Pure and Applied Mathematics, 51, 297-320.

[10] Mai, Y. T., Chen, J. Y., & Lin, M. H. (2020). Design of load-based power saving and scheduling scheme integrating real-time and non-real-time services in WiMAX networks. Journal of Internet Technology, 21(5), 1263-1275.

[11] Isaac, S., Wisdom, D. D., Nigeria, S., Ahmad, M. A., & Christian, A. U. (2020). Battery-life management with an efficient sleep-mode power saving scheme (BM-ESPSS) in IEEE 802.16e networks. Int J Mechatron Electr Comput Technol (IJMEC), 7(2).

[12] Wisdom, D. D., Ahmed, M. A., Farouk, N., Isaac, S., Idris, H., & Hassan, J. B. (2020). An enhanced power saving scheme (EPSS) in IEEE 802.16e networks. International Journal of Information Processing and Communication IJIPC, 8(2).

[13] Jin, S., Yue, W., Jin, S., & Yue, W. (2021). Bernoulli Arrival-Based Sleep Mode in WiMAX 2. Resource Management and Performance Analysis of Wireless Communication Networks, 87-96.

[14] Asafa, M., Lasisi, H. O., Olawumi, O. O., & Awofolaju, T. T. (2022). Energy Efficiency In Optical-Wireless Access Network Using Dynamic Bandwidth Allocation. Journal of Energy and Safety Technology (JEST), 5(2), 21-29.

[15] Naik, D., Bauri, A., & De, T. (2022). Renewable Energy Aware Traffic Grooming in Hybrid Optical and WiMAX Networks. Wireless Personal Communications, 1-23.

[16] Emara, T. (2022). Adaptive Power-Saving Mechanism for VoIP Over WiMAX Based on Artificial Neural Network. In Research Anthology on Artificial Neural Network Applications (pp. 471-489). IGI Global.

[17] Mohammed Shapique, A., Sudhesh, R., & Dharmaraja, S. (2024). Transient Analysis of a Modified Differentiated Vacation Queueing System for Energy-Saving in WiMAX. Methodology and Computing in Applied Probability, 26(3), 23.

[18] Chang, J. Y., & Lin, Y. C. (2012). Dynamically alternating power saving scheme for IEEE 802.16e mobile broadband wireless access systems. Journal of Communications and Networks, 14(2), 179-187.

[19] Priya, M. D., Sengathir, J., & Valarmathi, M. L. (2010). ARPE: an attack-resilient and power efficient multihop WiMAX network. International Journal on Computer Science and Engineering, 2(4), Vol. 02, No. 04, pp. 1201-1208.

[20] Priya, M. D., Shanmugapriya, R. K., & Valarmathi, M. L. (2014). An Enhanced Relay Selection Scheme (ERS) for Cooperative Relaying in Mobile WiMAX Networks. International Journal of Science, Engineering and Technology Research, 3(5), 1401-1407.

E-ISSN 2581 – 7957
P-ISSN 2277 – 3916
CVR Journal of Science and Technology, Volume 27, December 2024
DOI: 10.32377/cvrjst2703

Design and Simulation of Doherty Power Amplifier for 2.4 GHz Frequency Applications

Racha Ganesh[1], Dr. K. Lal Kishore[2], Dr. Yedukondalu Kamatham[3] and Dr. P. Srinivasa Rao[4]
[1]Ph. D Scholar, JNTUH University and
Assoc.Professor, CVR College of Engineering/ECE Department, Hyderabad, India.
Email: rachaganesh@gmail.com[1]
[2]Professor, CVR College of Engineering/ECE Department, Hyderabad, India.
Email: lalkishore@cvr.ac.in[2]
[3]Professor, CVR College of Engineering/ECE Department, Hyderabad, India.
Email: kyedukondalu@gmail.com[3]
[4]Professor, CVR College of Engineering/ECE Department, Hyderabad, India.
Email: psrao.cvr@gmail.com[4]

Abstract: **The Doherty Power Amplifiers (DPA) are specialized Radio Frequency (RF) amplifiers designed to improve efficiency, particularly at high output power levels. They are used in base stations of cellular communication systems, and other wireless infrastructure applications. This work endeavors the design and simulation of a Doherty Power Amplifier (DPA) utilizing the Cadence Virtuoso environment using 45nm technology, precisely tuned to operate at 2.4 GHz frequency. The DPAs are pivotal components in modern RF communication systems, renowned for their efficiency and linearity. The work begins with a detailed examination of DPA architecture, focusing on key components such as power splitter, main amplifier, auxiliary amplifier, transmission line, and matched network. Each component is meticulously designed and optimized to ensure precise operation. Advanced simulation techniques are employed to analyze the performance of the DPA, including power gain, and Power Added Efficiency (PAE). Leveraging 45 nm VLSI process semiconductor technology, the undertaking aims at achieving high efficiency and signal integrity while minimizing power consumption and distortion. The tuning process entails iterative adjustments to component parameters guided by simulation results to achieve optimal performance characteristics, with a focus on impedance matching, power combining, and phase alignment. The final outcomes are evaluated based on comprehensive simulation results, offering valuable insights into the design and optimization of DPAs using advanced semiconductor technology.**

Index Terms: **Doherty Power Amplifier, Wi-Fi Standard, RF Design, Wireless Communications, VLSI Design, Power Added Efficiency.**

I. Introduction

The world is full of data and this data needs to be exchanged and communicated among several people. Data can be any confidential information about a country or a simple telephonic voice conversation between two friends. When communicating, this data needs to be transferred properly with no information loss along with privacy. This is a challenging task. As there are changes in communication mode from wired to wireless, this task has become even more challenging. So, a system is needed that can communicate wirelessly with no information loss and complete security. Any basic wireless communication system has three main components as shown in Figure 1 i.e., Transmitter, Channel, and Receiver. When transmitting, the signal must be strong enough to reach the base station and these base stations further need to remove noise and increase the signal strength. This also needed to be done at the receiver portion to read the information to the fullest. Therefore, the task is to amplify the signal to overcome noise, signal attenuation and improve signal to noise ratio.

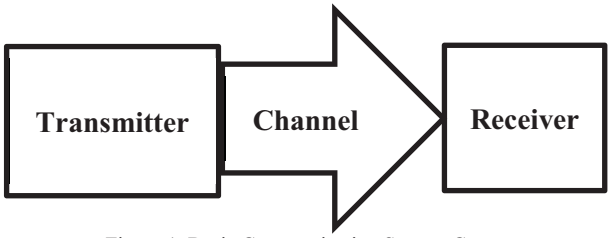

Figure 1. Basic Communication System Components

The bigger issue is that most of the power amplifiers are lumped devices that are not present on the chip. Bringing complex and bulky power amplifier circuits onto a chip is a very challenging task.

The strategy employed aimed at reducing the size of the amplifier and matching the network to the best, complexity of the power divider while preserving the objectives [1]. There is a need to choose a power splitter network, transmission line and matched network for the design so that maximum power transfer takes place from input to output. Then appropriate R, L, and C values must be calculated for the frequency. This is designed on a Cadence virtuoso design tool using 45 nm CMOS technology. The simulation and the parameter extraction of the design are done using Periodic Steady State (PSS) analysis.

An overview of the types of Power Amplifiers is given in section II. Section III explores the design approach of Doherty Power Amplifier (DPA). Section IV shows the design of a Doherty Power Amplifier (DPA) using Cadence Electronic Design Automation (EDA) tools. The input, output simulation results and performance analysis of the DPA are discussed in section V. The conclusions drawn are given in section VI.

II. Overview of Power Amplifiers

The Power Amplifiers (PAs) are vital components in communication systems, amplifying signals for transmission. PAs are the major basic blocks in communication systems, playing a crucial role in ensuring that signals are transmitted

Received on 29-04-2024, Revised on 29-05-2024, Accepted on 28-06-2024.

effectively over long distances and through various obstacles. These amplifiers are used in wireless communications, broadcasting, radar, and medical equipment etc. The challenges include optimizing efficiency, managing the amount of heat dissipation, and maintaining impedance matching. In wireless communication systems, such as cellular networks and Wi-Fi, power amplifiers are integral to amplifying signals from base stations or access points to reach mobile devices or other receivers situated over considerable distances [2]. Power amplifiers enable wireless communication systems to achieve widespread coverage and support high data rates, facilitating seamless connectivity for users. Despite their importance, power amplifiers face challenges such as balancing efficiency and linearity, managing heat dissipation, and ensuring impedance matching for optimal performance [3, 4].

The PAs are crucial components in communication systems amplifying signals for transmission.

Types of Power Amplifiers

1. *Application based PAs*
   - ❖ Audio Amplifiers: Amplify audio signals, typically used in audio systems, speakers, and musical instruments.
   - ❖ Radio Frequency (RF) Amplifiers: Amplify signals in the radio frequency range, crucial in communication systems and RF applications.
   - ❖ Intermediate Frequency (IF) Amplifiers: Amplify signals in the intermediate frequency range, often used in radio, Radar and television receivers.
   - ❖ Instrumentation Amplifiers: Designed for precision measurement applications, offering high common-mode rejection, sensitivity, and accuracy.
2. *Operating Frequency based PAs*
   - ❖ Low-Frequency Amplifiers: Operate at frequencies up to a few kHz, common in audio applications.
   - ❖ Medium-Frequency Amplifiers: These amplifiers operate in the frequency range of hundreds of kHz to a few MHz
   - ❖ High-Frequency Amplifiers: Operate at frequencies above a few MHz, common in RF and microwave applications.
3. *Configuration and Connection based PAs*
   - ❖ Voltage Amplifiers: Increase the voltage level of a signal.
   - ❖ Current Amplifiers: Increase the current level of a signal.
   - ❖ Power Amplifiers: Increase both voltage and current to deliver higher power levels to a load.
   - ❖ Common Emitter/Common Source Amplifiers: Commonly used in transistor amplifiers
   - ❖ Common Collector/Common Drain Amplifiers: Another configuration used in transistor amplifiers.
   - ❖ Common Base/Common Gate Amplifiers: Yet another configuration used in transistor amplifiers.
   - ❖ Class A, B, AB, and C Amplifiers: Classifications are done using the amplification characteristics and efficiency in power amplifiers [5].
4. *Input and Output Signals based PAs*
   - ❖ Unipolar (Single-Ended) Amplifiers: Amplify signals that only have positive voltage levels.
   - ❖ Bipolar (Double-Ended) Amplifiers: Amplify signals that have both positive and negative voltage levels.
5. *Electronic Components based PAs*
   - ❖ Transistor Amplifiers: Use transistors as the amplifying elements, including BJT and MOSFET amplifiers.
   - ❖ Operational Amplifiers (Op-Amps): Specialized amplifiers with high gain, often used in feedback configurations for various applications.
6. *Feedback and Gain based PAs*
   - ❖ Feedback Amplifiers: Include configurations with positive or negative feedback, influencing gain, stability, and linearity.
   - ❖ Low-Gain Amplifiers: Provide minimal gain.
   - ❖ Medium-Gain Amplifiers: Offer moderate gain.
   - ❖ High-Gain Amplifiers: Provide significant amplification.

These classifications provide a framework for understanding and categorizing amplifiers based on their characteristics and applications. The choice of amplifier type depends on the frequency range, power levels, and desired performance parameters.

7. *Special amplifiers*

There is another type of classification of amplifiers called special amplifiers are listed below from A to I. These amplifiers are designed from pre-existing amplifiers having certain traits. Although many of these operations of amplifiers look different, each has its unique characteristics, advantages, and limitations [6-8].

A. Doherty Power Amplifier

It is a special amplifier which is a combination of two amplifiers where one amplifier amplifies small signals, and the other amplifier amplifies large signals. This amplifier was largely used in lumped components [9-11].

B. Envelope Tracking (ET) Power Amplifiers

Envelope tracking Pas adjusts the amplifier's power supply voltage to the input signal of envelope [12]. This helps to maintain high efficiency, especially during periods of low power, like the Doherty approach [13].

C. Outphasing Power Amplifiers

The Outphasing power amplifiers use multiple amplifiers that are combined to achieve high efficiency [14]. Each amplifier is modulated with a phase and amplitude adjustment, and then the outputs are merged to reconstruct the required output signal. This method is used to increase efficiency across varying power levels.

D. Chireix Outphasing Amplifiers

A variation of outphasing, Chireix outphasing amplifiers utilize a specific combining network to achieve higher efficiency. The concept is to use a constant envelope modulation scheme, like Doherty, but with a different combining network.

E. Switch-Mode Amplifiers

Switch-mode power amplifiers operate in a switched mode, providing high efficiency by minimizing power dissipation during the "off" state. These amplifiers are commonly used in applications where power efficiency is critical, such as in base stations. Switch-mode amplifiers are commonly used in audio amplification, especially in portable audio devices like smartphones, tablets, and Bluetooth speakers.

F. Load Modulated Amplifiers

Load modulated amplifiers dynamically adjust the load impedance seen by the amplifier to optimize efficiency. This technique is used to improve efficiency over a range of input power levels, like the Doherty approach [15].

G. Digital Pre-Distortion (DPD)

Digital pre-distortion is a signal processing technique that compensates for the nonlinearities in the amplifier, improving linearity and efficiency. It is often used in conjunction with various power amplifier architectures to enhance overall performance.

H. Hybrid Amplifiers

Hybrid amplifiers combine multiple amplifier technologies to achieve improved efficiency and linearity. For example, combining a Class A amplifier with a switching amplifier can offer benefits in terms of both linearity and efficiency.

I. Dynamic Load Modulation Amplifiers

These amplifiers dynamically adjust the load impedance to optimize efficiency and linearity, especially during varying power levels.

Among these above-mentioned special amplifiers, the Doherty power amplifier is selected because of the following reasons:

1. Increased linearity range

Doherty power amplifier amplifies both small signals as well as large signals increasing the linearity of the system. Achieving an increased linearity range in Doherty power amplifiers presents a notable challenge due to the inherently asymmetric property of the Doherty architecture.

2. High Peak Added Efficiency (PAE)

This is a very important parameter in identifying the capability and performance of the amplifier. Doherty amplifiers offer large PAE compared to other special amplifiers [16,17].

3. Large output power gain

When compared to other amplifiers, this design has more output power gain due to the usage of two power amplifiers.

4. High Peak-to-Average Power Ratio

Another advantage other power amplifiers don't give but Doherty does is that it has a high peak-to-average power ratio. This is possible because of two amplifier circuits embedded into a single circuit.

5. Design to bring it onto the chip

This is the biggest advantage of the DPA. Even though other power amplifiers can be brought onto a chip, this design doesn't need any additional circuit or supporting circuit. Other circuits are quite like the Doherty power amplifier or just act as a supporting block.

With these advantages, the Doherty power amplifier shows a promising solution for on-chip design compared to other amplifier circuits [18].

The Power amplifiers are crucial electronic devices used to boost signal power while minimizing waveform distortion.

They find applications in telecommunications, audio amplification, and RF transmission. Understanding their operation is vital for appreciating their significance in signal amplification.

1. Input Stage

Initial reception of the weak input signal occurs here. A small signal amplifier increases the voltage level, preparing it for further processing.

2. Amplification Stage

This core stage amplifies the signal significantly, utilizing active components like transistors or vacuum tubes. Distortion is minimized during amplification.

3. Output Stage

Amplified signal passes through this stage, further boosting its power to drive the load (e.g., speaker or antenna) effectively without fidelity loss.

4. Biasing and Control Circuitry

These circuits optimize performance and stability. Biasing sets component operating points, while control circuits manage protection, stability feedback loops, or dynamic parameter control.

5. Power Supply

A stable, appropriately sized power supply converts AC mains voltage to DC, powering the amplifier circuitry within specified limits.

Overall, power amplifiers accurately amplify weak input signals to higher power levels while maintaining integrity. Achieving this requires meticulous design to ensure desired performance characteristics such as linearity, efficiency, and reliability.

III. Design Approach of Doherty Power Amplifier

The DPA is a type of Radio Frequency (RF) Power Amplifier architecture used in wireless communication systems to efficiently amplify signals, particularly in applications such as cellular base stations and broadcast transmitters [19, 20].

The key feature of a Doherty power amplifier is its ability to achieve high efficiency [21] at both low and high output power levels. This is accomplished through a combination of two amplifier stages: a main (carrier) amplifier and a peak (peaking) amplifier. The main amplifier handles most of the signal's power, while the peak amplifier provides additional power when needed, particularly during signal peaks [22]. The block diagram of DPA is shown in Figure 2 [23].

The major components of a DPA include the following components [24]:

1. Power Splitter
2. Main Amplifier
3. Auxiliary Amplifier
4. Transmission line and Matched Network

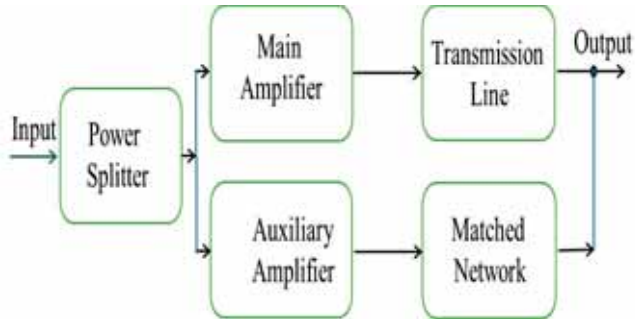

Figure 2. Block diagram of Doherty Power Amplifier (DPA)

1. Power Splitter

In a DPA, the power splitter plays a crucial role in distributing the input signal to the main amplifier and the peak amplifier. Its primary function is to divide the input signal into two branches with controlled power levels, allowing each amplifier stage to operate optimally within its power range [25].

The power splitter typically divides the input signal into the main path and peaking path. The main path, which feeds the main amplifier, and the peaking path, which feeds the peak amplifier. The power splitter needs to ensure that the main amplifier receives most of the input power, while the peak amplifier receives a fraction of that power. Any power divider circuit has three important traits: matching, reciprocal and lossless. For any design, one can get only two out of three. That is, a design can be either matched and reciprocal and lossless or matched and lossless. Hence, the power splitter used in this design is the Wilkinson Power Amplifier [26].

2. Main Amplifier

In a DPA, the main amplifier plays a central role in handling most of the input signal power. Its primary function is to provide efficient amplification of the input signal during normal operating conditions when the input power is relatively low [27, 28]. The main amplifier is typically designed to operate in its linear region, ensuring that the amplified signal faithfully reproduces the input signal without introducing significant distortion.

3.Auxiliary Amplifier

In a DPA, the auxiliary amplifier, also referred to as the peak or peaking amplifier, is a critical component that works in conjunction with the main amplifier to achieve high efficiency and linearity [29]. The DPA architecture is designed to optimize power efficiency by combining the strengths of both the main and auxiliary amplifiers [30, 31]. The auxiliary amplifier is responsible for handling the peak power levels of the input signal. During periods when the input signal exhibits high amplitude, the auxiliary amplifier contributes additional power to the output. Using this amplifier increases the linearity of the power amplifier [32]. Class C power amplifier is used as auxiliary amplifier [33].

The structure of DPA is shown in Figure 3 [35].

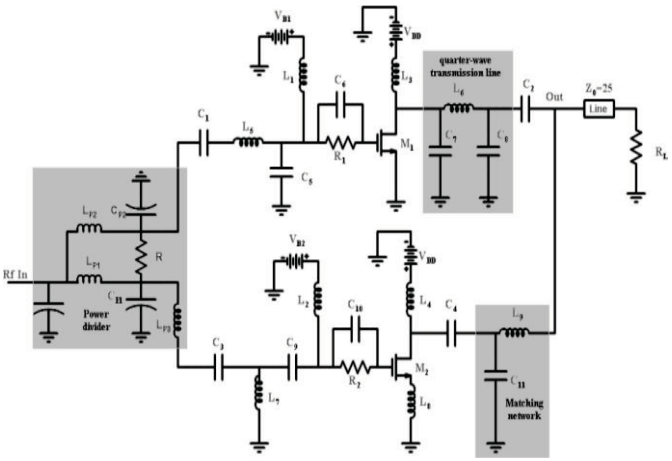

Figure 3. Structure of Doherty Power Amplifier

4.Transmission Line and Matched Network

In a DPA, transmission lines play a crucial role in facilitating the combining of signals from the main and auxiliary amplifiers to produce the final amplified output [34]. These transmission lines are part of the combining network, which ensures that the amplified signals from both amplifiers are combined constructively at the output port. The transmission lines are typically designed to have specific lengths and characteristic impedances to achieve optimal signal combining and phase alignment.

IV. Design of Doherty Power Amplifier

The design of Doherty Power Amplifier uses a design flow starting from user requirements and non-functional VLSI constraints [36]. The major requirement of this amplifier is center frequency of operation on which the selection of component values of amplifier structure is selected. The design flow using Cadence EDA tool is shown in Figure 4, in the next page.

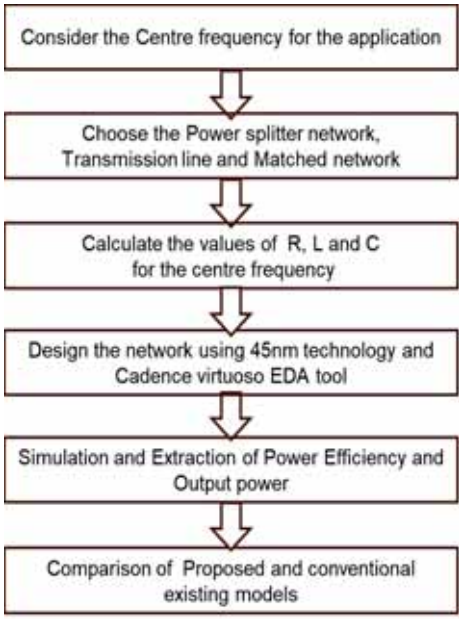

Figure 4. Design flow of Doherty Power Amplifier

CVR Journal of Science and Technology, Volume 27, December 2024
DOI: 10.32377/cvrjst2703

The detailed description of each step of design flow is given below.

1.Center Frequency: Center frequency or operating frequency is an important parameter in any design and need to be rightly chosen according to the application. Since this power amplifier is meant for digital communication as well as for Wi-Fi protocol, the operating frequency of 2.4GHz is chosen.

2.Power Splitters and Matched Networks: Power splitters and matched networks are, in general, very bulky in size and complex in nature. Therefore, the π-LC network as a matched network is chosen because of its simplicity and the Wilkinson power divider as a power splitter.

3.Calculation of R, L and C values: This is the toughest part of the design. Calculation of R, L and C values is done for Wilkinson power divider and matched network whereas R, L and C values in amplifier part can be extracted using PSS analysis. Using circuit analysis models and maintain proper matching within the circuit as well as compatibility for the chosen operating frequency.

4.Designing using Cadence EDA tool: The R, L and C values, power splitters and a matched network are calculated. With these values and circuits, design is placed on the Cadence Virtuoso tool [37, 38] The issue here is, that calculated values of circuit elements might not work on the tool because it considers parameter values along with real time constrains and check if these values are feasible for fabrication. Therefore, further adjustment of these values using the special analysis (PSS and PAC) given by the tools is another necessary step [39, 40].

V. Simulation Results and Discussion

The schematic diagram, test bench and simulation results of DPA are shown in simulation results. Figure 5 shows the basic block diagram of DPA along with its internal components.

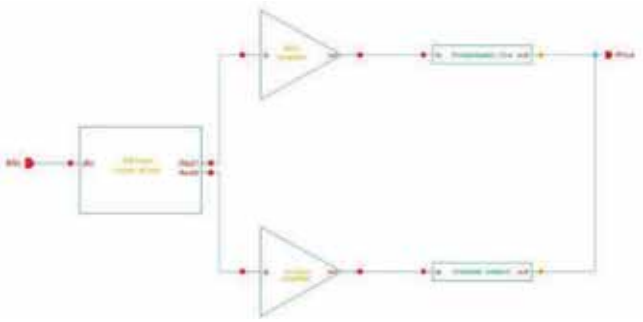

Figure 5. Block Diagram of DPA

The internal component design of Wilkinson Power Splitter is shown in Figure 6.

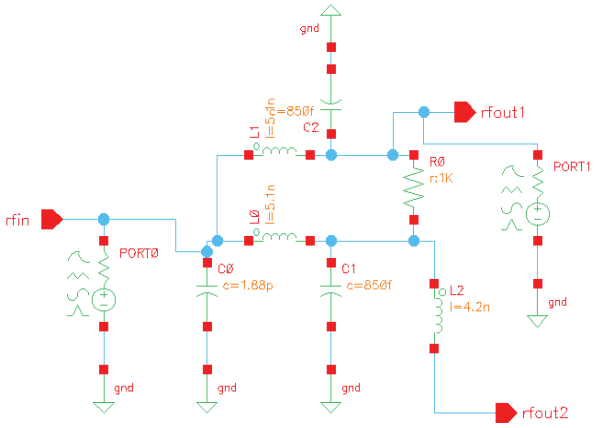

Figure 6. Wilkinson Power Splitter

The main amplifier component design schematic is shown in Figure 7. The Auxiliary amplifier component design is shown in Figure 8. The Transmission line component design is shown in Figure 9. The matched network component design is shown in Figure 10. The detailed structural components connection of DPA is shown in Figure 11.

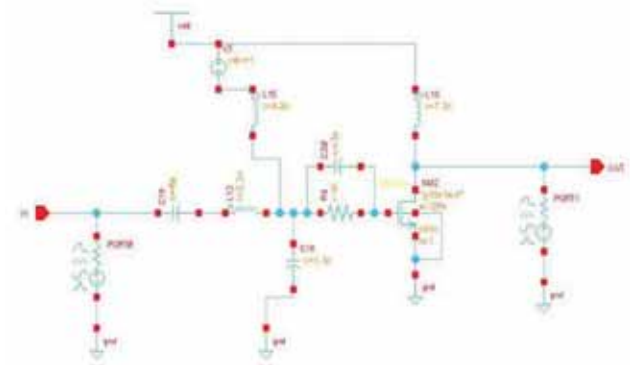

Figure 7. Main Amplifier

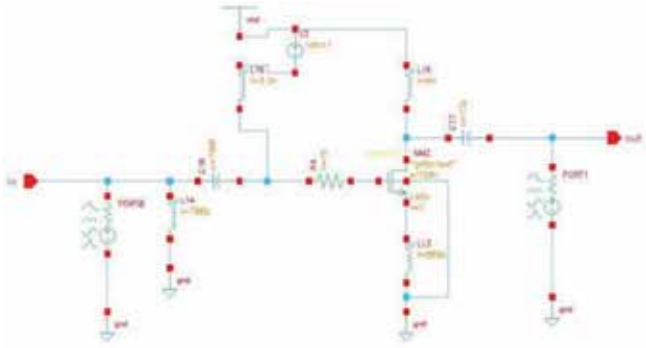

Figure 8. Auxiliary Amplifier

E-ISSN 2581 – 7957
P-ISSN 2277 – 3916

DOI: 10.32377/cvrjst2703

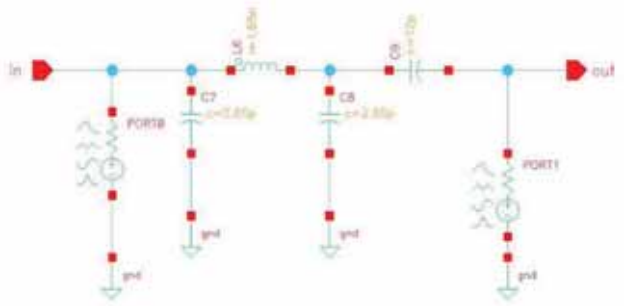

Figure 9. Transmission Line

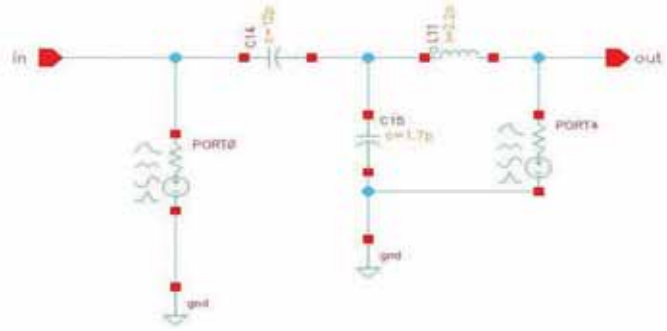

Figure 10. Matched Network

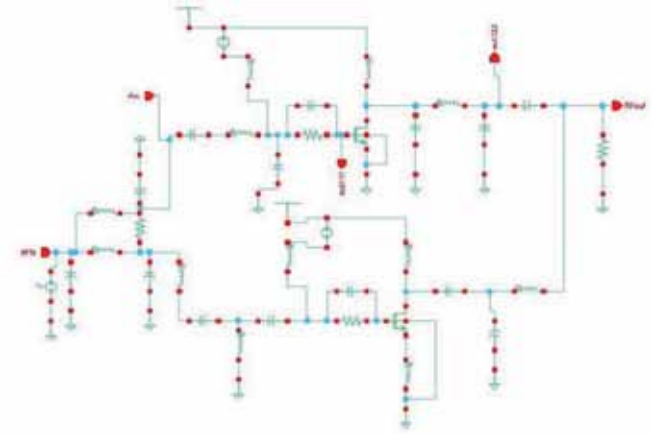

Figure 11. Doherty Power Amplifier

The operating frequency of 2.4 GHz of each component of Doherty Power Amplifier (DPA) is individually tuned and their results are shown below. The power splitter design operating at 2.4 GHz is shown in Figure 12. The main amplifier operating at 2.4 GHz is shown in Figure 13. The auxiliary amplifier operating at 2.4 GHz is shown in Figure 14. The transmission line operating at 2.4 GHz is shown in Figure 15. The Matched network design operating at 2.4 GHz is shown in Figure 16. The complete design of DPA operating at 2.4 GHz is shown in Figure 17.

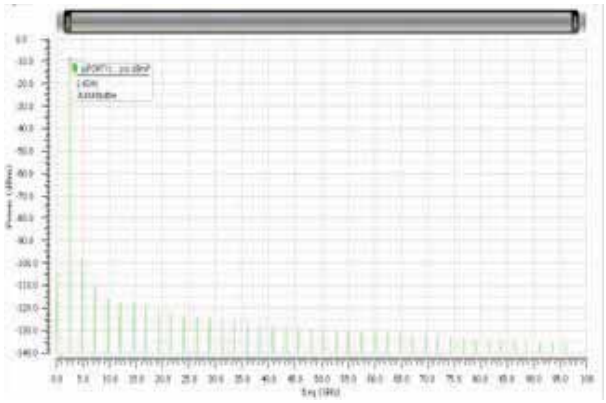

Figure 12. Power splitter operating at 2.4 GHz

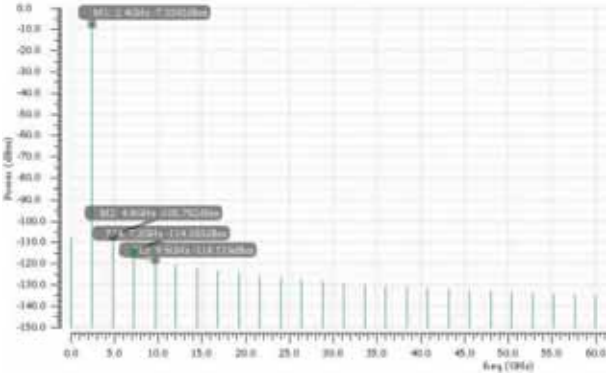

Figure 13. Main amplifier operating at 2.4 GHz

,

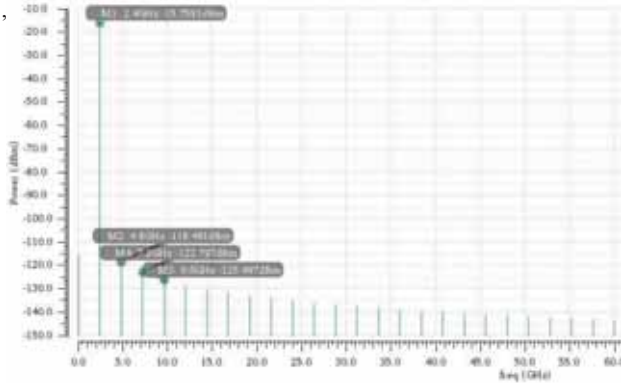

Figure 14. Auxiliary amplifier operating at 2.4 GHz

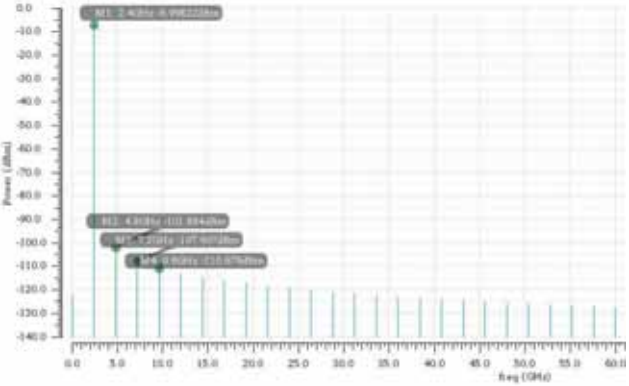

Figure 15. Transmission Line operating at 2.4 GHz

CVR Journal of Science and Technology, Volume 27, December 2024
DOI: 10.32377/cvrjst2703

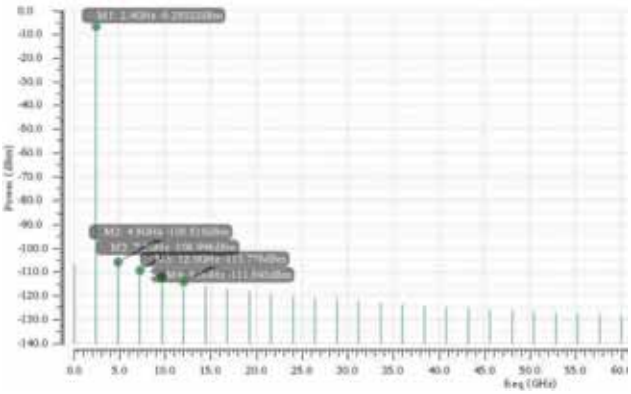

Figure 16. Matched Network operating at 2.4 GHz

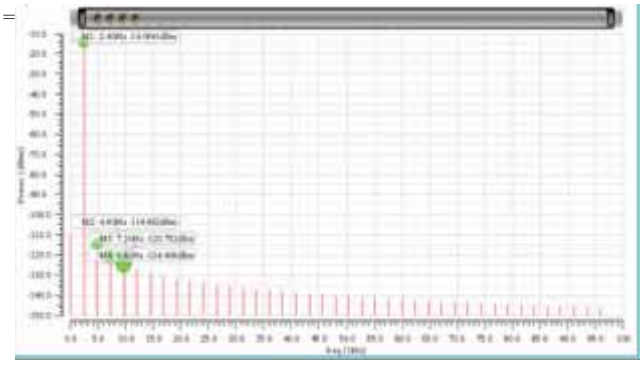

Figure 17. Doherty Power Amplifier operating at 2.4 GHz

The power gain of DPA is shown in Figure 18 with a value of 87.08 dB. The Power Added Efficiency (PAE) of Doherty Power Amplifier is shown in Figure 19.

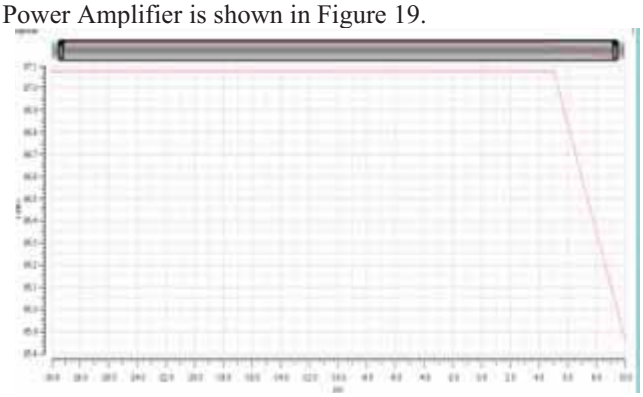

Figure 18. Power Gain of Doherty Power Amplifier

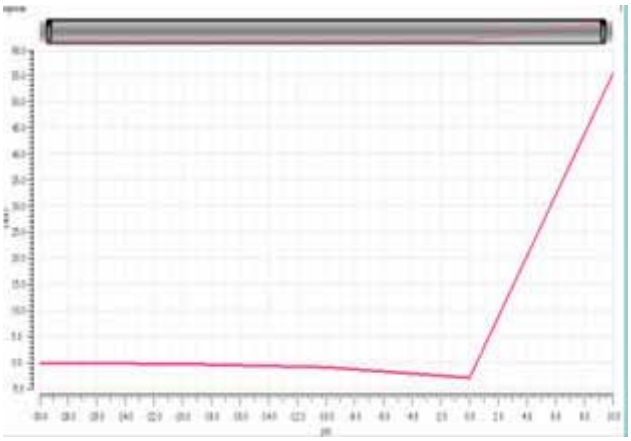

Figure 19. Power Added Efficiency (PAE) of Doherty Power Amplifier

VI. Conclusions

The design and analysis of DPA using Cadence Virtuoso have yielded promising results. The careful tuning of essential components, including the power splitter, main amplifier, auxiliary amplifier, transmission line, and matched network, to operate at the 2.4GHz frequency has ensured optimal performance within the desired frequency band. With a remarkable power gain of 87.08 dB, the amplifier demonstrates its effectiveness in significantly boosting signal strength. Furthermore, the observed increase in Power Added Efficiency (PAE) from 0% to 55% over the input power should also be given in range underscores the amplifier's ability to efficiently convert input power into useful output power. These findings highlight the success of the DPA design in achieving high performance, efficiency, and signal amplification, making it an asset for various RF applications, particularly those operating at 2.4 GHz frequencies. Overall, this work contributes valuable insights into the design and optimization of RF amplifiers, paving the way for advancements in wireless communication and RF systems.

References

[1]. M. G. Li, et al., “2.4 GHz Doherty Power Amplifier with on-chip Active Balun Design,” in 2009 International Conf. on (ASIC), Hunan, pp. 1078-1080, Oct 2009.

[2]. D. K. Sharma and R. T. Bura, "A Novel and Compact Wideband Doherty Power Amplifier Architecture for 5G Cellular Infrastructure," 2021 IEEE 4th 5G World Forum (5GWF), Montreal, QC, Canada, 2021, pp. 323-327, doi: 10.1109/5GWF52925.2021.00063.

[3]. Mostafa Elmala and Ralph Bishop, "A 90nm CMOS Doherty Power Amplifier with Integrated Hybrid coupler and Impedance Transformer," Dig. IEEE RFIC Symp., Honolulu, HI, 2007, pp. 423-426.

[4]. V. Vorapipat, C. S. Levy and P. M. Asbeck, "Voltage mode Doherty power amplifier", IEEE J. Solid-State Circuits, vol. 52, no. 5, pp. 1295-1304, May 2017.

[5]. R. Pengelly, et al., “Doherty's legacy: a history of the Doherty power amplifier from 1936 to the present day,” IEEE Microwave Magazine, vol. 17, pp. 41-58, 2016.

[6]. A. Ghahremani, A. Annema and B. Nauta, "A 20dBm out phasing class E PA with high efficiency at power back-off in 65nm CMOS technology", Proc. IEEE Radio Freq. Integr. Circuits Symp. (RFIC), pp. 340-343, 2017.

[7]. Dushyant K. Sharma, Parag Aggarwal, Kalyan Giri, Anirban Sengupta, Mrinal Kanti Mandal, Subhas Mondal, Ravi T. Bura, "A Highly Efficient High Power Doherty Power Amplifier with Large Output Back-Off Range for Base Station Application", 2021 IEEE 18th India Council International Conference (INDICON), pp.1-5, 2021.

[8]. E. A. Hernández-Domínguez, J. R. Loo-Yau, A. Sánchez-Ramos, A. Villagran- Gutierrez, "Bias Tee Design for RF Power Amplifiers and GaN FETs characterization", 2023 IEEE MTT-S Latin America Microwave Conference (LAMC), pp.7-10, 2023.

[9]. S. Shopov, R.E. Amaya, J.W. Rogers, C. Plett, "Adapting the Doherty amplifier for millimeter-wave CMOS applications," Proc. of IEEE NewCAS, Aug. 2011, pp. 229-231.

[10]. Mohammad Zaid, Ahtisham Pampori, Yogesh Singh Chauhan, "16 Watt S-Band GaN Based Power Amplifier Using Replicating Stages", 2022 IEEE 9th Uttar Pradesh Section International Conference on Electrical, Electronics and Computer Engineering (UPCON), pp.1-4, 2022.

[11]. Dushyant K. Sharma, Parag Aggarwal, Kalyan Giri, Anirban Sengupta, Mrinal Kanti Mandal, Subhas Mondal, Ravi T. Bura, "A Highly Efficient High Power Doherty Power Amplifier with Large Output Back-Off Range for Base Station Application", 2021 IEEE 18th India Council International Conference (INDICON), pp.1-5, 2021.

[12]. K. Oishi et al., "A 1.95 GHz fully integrated envelope elimination and restoration CMOS power amplifier using timing alignment technique for WCDMA and LTE", IEEE J. Solid-State Circuits, vol. 49, no. 12, pp. 2915-2924, Dec. 2014.

[13]. M. Naga Sasikanth, Tarun Kanti Bhattacharyya et.al "A High-efficiency body injected differential power amplifier at 2.4 GHz for low power application" 2018 31st International Conference on VLSI Design and 2018 17th International Conference on Embedded Systems

[14]. C. Duvanaud, et al., "High-efficient Class F GaAs FET Amplifiers Operating with very low bias Voltages for use in Mobile Telephones at 1.75 GHz," IEEE Microw. Guid. Wave Lett, vol. 3, pp. 268-270, 1993.

[15]. W. Chen, S. Zhang, Y. Liu and F. M. Ghannouchi, "A Concurrent dual-band uneven Doherty power amplifier with frequency-dependent input power division", IEEE Trans. Circuits Syst. I Reg. Papers, vol. 61, no. 2, pp. 552-561, Feb. 2014.

[16]. Amit Shrestha; Herman Schumacher; Christian Waldschmidt; Iancu Somesamu" Ka- band power amplifier for satcom applications in 0.25µm SiGe BiCMOS technology", DOI:10.13140/RG.2.1.3803.2083.

[17]. S. Kousai, K. Onizuka, S. Hu, H. Wang and A. Hajimiri, "A new wave of CMOS power amplifier innovations: Fusing digital and analog techniques with large signal RF operations", Proc. IEEE Custom Integr. Circuits Conf., pp. 1-8, Sep. 2014.

[18]. A. Seidel, V. Grams, J. Wagner and F. Ellinger, "Asymmetric Doherty Power Amplifier at 60 GHz in 130 nm BiCMOS," 2020 IEEE MTT-S Latin America Microwave Conference (LAMC 2020), Cali, Colombia, 2021, pp. 1-4, doi: 10.1109/LAMC50424.2021.9601976.

[19]. Noriaki Tawa, Paolo Enrico de Falco, Ohgami Kazuya, Taylor Barton, Tomoya Kaneko, "A 3.5-GHz 350-W Black-Box Doherty Amplifier Design Method Without Using Transistor Models", 2021 IEEE BiCMOS and Compound Semiconductor Integrated Circuits and Technology Symposium (BCICTS), pp.1-4, 2021.

[20]. M. Masood, J. Staudinger, J. Wood, M. Bokatius and J. S. Kenney, "Linearity considerations for a high power Doherty amplifier," 2012 IEEE Topical Conference on Power Amplifiers for Wireless and Radio Applications, Santa Clara, CA, USA, 2012, pp. 77-80, doi: 10.1109/PAWR.2012.6174912.

[21]. F. Brand, "The Experimental Design and Characterisation of Doherty Power Amplifiers, Stellenbosch University," Thesis for the degree of Master of Science, Stellenbosch University, Dec 2006.

[22]. H. Jang and R. Wilson, "A 225 Watt, 1.8-2.7 GHz Broadband Doherty Power Amplifier with Zero-Phase Shift Peaking Amplifier," 2018 IEEE/MTT-S International Microwave Symposium - IMS, Philadelphia, PA, USA, 2018, pp. 797-800, doi: 10.1109/MWSYM.2018.8439639.

[23]. V. Viswanathan, "Efficiency Enhancement of Base Station Power Amplifiers Using Doherty Technique," Thesis for the degree of Master of Science, Virginia Polytechnic University, Feb 2004.

[24]. Elsan Barmala, et al., "Design and simulator Doherty power amplifier using GaAs technology for telecommunication applications", Indonesian Journal of Electrical Engineering and Computer Science, Aug 2019.

[25]. E. A. Hernández-Domínguez, J. R. Loo-Yau, A. Sánchez-Ramos, A. Villagran- Gutierrez, "Bias Tee Design for RF Power Amplifiers and GaN FETs characterization", 2023 IEEE MTT-S Latin America Microwave Conference (LAMC), pp.7-10, 2023.

[26]. S. Sakata, Y. Komatsuzaki and S. Shinjo, "Adaptive Input-Power Distribution in Doherty Power Amplifier using Modified Wilkinson Power Divider," 2020 IEEE Topical Conference on RF/Microwave Power Amplifiers for Radio and Wireless Applications (PAWR), San Antonio, TX, USA, 2020, pp. 34-37, doi: 10.1109/PAWR46754.2020.9036005.

[27]. M. Modava, A. Sahafi, J. Sobhi and Z. D. Koozehkanani, "Design of efficient power amplifier for low power transmitters", Analog Integrated Circuits and Signal Processing, vol. 90, no. 3, pp. 563571, 2016.

[28]. X. Xu, Z. Sun, K. Xu, X. Yang, T. Kurniawan and T. Yoshimasu, "A 2.5-GHz band low-voltage class-E power amplifier IC for short-range wireless communications in 180-nm CMOS", IEEE International Symposium on Radio-Frequency Integration Technology, 2014, 2014.

[29]. L. Y. Yang, et al., "A 2.4 GHz Fully Integrated Cascade-Cascade CMOS Doherty Power Amplifier," IEEE Microw. Wireless Compon. Lett., vol. 18, pp. 197-199, Mar 2008.

[30]. H. Jeon, J. Na, H. Oh and Y. Yang, "Two-stage CMOS/GaAs HBT Doherty Power Amplifier Module for 5G Handsets," 2022 IEEE International Symposium on Radio- Frequency Integration Technology (RFIT), Busan, Korea, Republic of, 2022, pp. 12-14, doi: 10.1109/RFIT54256.2022.9882351.

[31]. J. h. Kwon et al., "Broadband Doherty Power Amplifier Based on Asymmetric Load Matching Networks," in IEEE Transactions on Circuits and Systems II: Express Briefs, vol. 62, no. 6, pp. 533-537, June 2015, doi: 10.1109/TCSII.2015.2407197.

[32]. J. Kang, et al., "An Ultra-High PAE Doherty Amplifier Based on 0 wa.13µm CMOS Process," IEEE Microw. Wireless Compon. Lett, vol. 16, pp. 505-507, Sep 2006.

[33]. J. Staudinger, J. Nanan and J. Wood, "Memory fading Volterra series model for high power infrastructure amplifiers," Radio Wireless Symposium, pp. 1042-4043, Jan. 2010.

[34]. N.Elsayed, H. Saleh, B. Mohammad and M. Sanduleanu, "A 28GHz, Asymmetrical, Modified Doherty Power Amplifier, in 22nm FDSOI CMOS," 2020 IEEE International Symposium on Circuits and Systems (ISCAS), Seville, Spain, 2020, pp. 1-4, doi: 10.1109/ISCAS45731.2020.9180851.

[35]. J. Qureshi et al., "A 700-w peak ultra-wideband broadcast doherty amplifier", 2014 IEEE MTT-S Inter. Microwave Sympo., pp. 1, 2014.

[36]. M. Mabrok, et al., "Design of Wide-band Power Amplifier Based on Power Combiner Technique with Low Intermodulation Distortion," International Journal of Electrical and Computer Engineering (IJECE), vol. 8, pp. 3504-3511, 2018.

[37]. https://www.cadence.com/en_US/home/resources/datasheets/virtuoso-schematic- editor-l-and-xl.html

[38]. https://www.cadence.com/en_US/home/resources/whitepapers/plan-based-analog-verification-methodology-wp.html

[39]. https://scholarworks.calstate.edu/downloads/c821gn30b#:~:text=The%20Periodic%20Steady%2DState%20(PSS,estimation%20of%20the%20initial%20condition

[40]. M. Hashemi, L. Zhou, Y. Shen and L. C. N. de Vreede, "A Highly Linear Wideband Polar Class-E CMOS Digital Doherty Power Amplifier," in IEEE Transactions on Microwave Theory and Techniques, vol. 67, no. 10, pp. 4232-4245, Oct. 2019, doi: 10.1109/TMTT.2019.2933204.

E-ISSN 2581 – 7957
P-ISSN 2277 – 3916
CVR Journal of Science and Technology, Volume 27, December 2024
DOI: 10.32377/cvrjst2704

A 32 nm CNFET Model Voltage Controlled Oscillator based ADC Design for Computation-in-Memory Architecture using Emerging ReRAM's

Snehalatha G[1,2], Dr. Selva Kumar J[3], Dr. Esther Rani Thuraka[4]
[1]Research Scholar, SRM Institute of Science & Technology/ECE Department, Kattankulathur, Chennai, India
Email: sg4088@srmist.edu.in
[2]Sr. Asst. Prof, CVR College of Engineering/ECE Department, Hyderabad, India
Email: sneharaj401@gmail.com
[3]Professor, SRM Institute of Science & Technology/ECE Department, Kattankulathur, Chennai, India
Email: selvakuj@srmist.edu.in
[4]Professor, CVR College of Engineering/ECE Department, Hyderabad, India
Email: estherlawrenc@gmail.com

Abstract: **Applications that are becoming more and more computationally demanding are beyond the capabilities of traditional Von Neumann systems. By adopting new architectural technologies, these flaws can be rectified. Specifically, Resistive Random Access Memory (ReRAM)-based Computation-In-Memory (CiM) holds great promise for satisfying the computational demands of data-intensive applications like database searches and neural networks. In CiM, calculation is carried out analogously; the potential of CiM is hampered by the expensive, time-consuming, space and energy intensive digitalization of the results. To enhance the functionality and energy efficiency of the CiM architecture, an effective Voltage-Controlled Oscillator (VCO)–based analog-to-digital converter (ADC) designed. The proposed ADC can be used per-column rather than sharing one ADC across several columns because of its efficiency. This will increase the CiM crossbar array's overall efficiency and parallel execution. A Multiplication and Accumulation (MAC) technique used in ReRAM-based CiM crossbar arrays is used to evaluate the proposed ADC. The ADC architecture is designed in Cadence Virtuoso, CMOS 45nm technology and then the complete design is implemented using CNFET 32nm Technology, considering its advantages. Figure of Merit, Resolution, delay, signal to noise ratio and power consumption of VCO-ADC are analyzed and compared with other ADCs.**

Index Terms: VCO Based ADC, ReRAM, CNFET Technology.

I. INTRODUCTION

CMOS-based Von Neumann architecture deals with Complementary Metal-Oxide-Semiconductor (CMOS)-based devices, circuits, and architectures that face several challenges [1]. In typical architectures, memory walls, instruction-level parallelism walls, and power walls have a significant negative effect because memory accesses are slow, parallelism is limited, and the clock frequency stagnates due to thermal problems. [2]. However, devices also have issues with high leakage, manufacturing costs that are too high, and reliability. These difficulties are particularly noticeable for data-intensive applications, such neuromorphic computing, where minimizing data transportation and energy consumption is crucial [3]. The necessity to find workable solutions for these application domains has drawn more and more attention. As such, CIM's non volatility , zero-leakage, and high-density characteristics make it a promising candidate to supplant conventional designs and accelerate data-intensive applications. It has been shown that computer systems can function more efficiently and perform better if they are designed with a CiM architecture, which performs operations within the memory and eliminates the need for costly data movement [4]. A CiM can be implemented using both static and dynamic random-access memories (SRAM and DRAM). There are several reasons why memory technologies such as these are suitable for CiM processes, including their unique properties [5]. The physical properties of this resistive memory make it perfect for Multiply and Accumulate (MAC) functions in CiM designs. Resistive random-access memory is a kind of non-volatile storage that functions by adjusting the resistance of a precisely crafted solid dielectric material. It is known that the memristor in the ReRAM device contracts, resulting in a resistance that varies depending on the voltage applied to it. ReRAM is a new technology that many users are implementing. It combines the benefits of RAM and Flash into one unique package. Because of its superior performance and advantages in terms of manufacturability over rival replacement options, it is most likely to replace the flash [6]. ReRAM creates oxygen vacancies, which are flaws in a thin oxide layer that charge and drift in response to an electric field, in contrast to conventional RAM memory types. ReRAM functions by producing resistance rather than storing charge, which makes it like NAND Flash memory. When current is applied, the materials that make up the ReRAM are designed to vary resistance [7]. The NAND-based memory and the RRAM-based memory structure are widely used in memory applications such as computer memories, consumer electronics, smart phones, tablets, and business storage. It is anticipated that the ReRAM application will have additional growth prospects because of technological advancements. ReRAM will find use in deep learning, wearables, automobile infotainment and navigation systems, and the Internet of Things (IoT) in the upcoming years.

The electronic memory market has been controlled by Flash Memory technology for more than 40 years. ReRAM, however, wasn't established until the early 2000s, when certain innovative businesses such as KB-capacity scale

Received on 03-05-2024, Revised on 02-06-2024, Accepted on 02-07-2024.

contributed to its development [8]. To provide a more efficient storage device, manufacturers have developed many types of ReRAM using various dielectric materials. To increase the speed and performance of GPUs, CPUs, and computing processes, RAM memory devices have undergone significant modification over time.

The ADC's job is to convert the analog data that sensors are gathering into digital data that can be processed easily [9]. The voltage-controlled oscillator ADC generates a frequency without giving any input, in contrast to SAR and FLASH ADCs [17,18,19]. ADCs can be used in many ways to implement analog-to-digital conversion. The parameters like sampling frequency, Effective Number of Bits (ENOB), Signal-to-Noise- Ratio (SNR), power consumption, delay, and Figure of Merit (FOM) are analysed by using ADC design. Different ADC architectures are suggested to balance power consumption, SNDR, and conversion speed. The SNDR reduces at lower sampling frequencies due to increased charge leakage by the unit capacitors. The change in frequency is linearly related to change in power consumption [10]. Each type of ADC typically operates optimally within a particular range of resolution and sample rate. While some ADCs are extremely quick but ineffective in high-resolution applications, others, for instance, are efficient at high resolutions but only at low sampling rates. ADCs based on voltage-controlled oscillators show great promise in achieving high energy efficiency. In this system, the first step converts the analog input to a variable-frequency output. For this operation, a voltage-controlled oscillator (VCO) is used. The second stage then uses a reset counter to convert the variable-frequency pulses produced by the VCO into a digital code.

This work is organized in different sections. The introduction of ReRAM and ReRAM based ADC established in Section I. Section II discusses the literature review on VCO based ADC. The internal blocks of conventional VCO based ADC using ReRAMs are presented in section III. The proposed CNFET based VCO based ADC using ReRAMs all architectures and working are discussed in section IV. The simulation results, including a comparison of the performance of important parameters between the current and suggested architectures, are presented in Section V. Section VI concludes with a discussion of the conclusions.

II. Literature Review

The purpose of this work is to demonstrate how analog vital signs can be converted into digital data for digital signal processing using a Voltage-Controlled Oscillator (VCO). A 130 nm CMOS process is used to implement the architecture. It was confirmed that power dissipation was 0.257 mW, active area was 0.007 mm^2, and FOM was 125 dB, all of which are very good results [11]. Analog-to-Digital converters (ADCs) using VCOs are proposed to minimize harmonic distortions. This 40 MHz-bandwidth VCO-based ADC is implemented as an FPGA board with the recommended calibration algorithm, which is based on a CMOS process with a 40 nm CMOS technology [12]. In this brief, an eight-stage pseudo-differential Ring Voltage-Controlled Oscillator (RVCO) built on 65 nm CMOS technology is described for a ten-bit (9.1-bit ENOB) Analog-to-Digital Converter (ADC). As a result, the SNDR is raised to approximately 55 dB because of the 912.9W overall power consumption of the system [13]. This ADC design eliminates the non-idealities of course and fine VCO-based quantizers by using non-linearity cancellation and swing down scaling. Over a 40 MHz bandwidth, the ADC achieved 59 dB SNDR with a 1.2 V supply, yielding 33 fJ/step conversion figure of 1.9 mW. [14]. An ADC based on a VCO is more efficient than an ADC based on a multivibrator. To demonstrate the design working on 65 nm technology, behavioral simulations and transistor-level simulations were used. A power supply noise reduction of 25 dB is reported when the VCO gain is 10% mismatched with a 128 MS/s data rate [15]. The Internet of Things (IoT) wireless sensor node uses a voltage-controlled oscillator (VCO) as a voltage-controlled analog-to-digital converter (ADC). With the use of a resistor-based frequency-tuning technique, VCO's nonlinear transfer characteristic can be reduced, resulting in less odd-order harmonic distortion. An ADC constructed in 28-nm CMOS produces 68 dB SNDR with a 1-Vpp differential sinewave input over a 61-kHz bandwidth, equivalent to an ENOB of 11 using a 1-Vpp input differential sinewave. This device achieves the highest Walden and Schreier FoMs at 167.4 dB and 27.8 fJ/c-s, respectively [16].

The summary from review is different architectures of VCO based ADC presented, the parameters power and delay analysis are poor compared to the proposed work. VCO converts the analog signal to phase domain by producing a continuous output signal whose frequency is proportional to the average analog input signal. The advantage of the VCO based ADC is high Sampling rate, Resolution is high. It is used in gamma ray cameras, sensor applications and ultrasonic applications.

III. Conventional VCO based ADC using Reram's

To transform the crossbar's analog output signal into a digital signal, choose to employ a time-based VCO-based ADC. As a result, it offers the benefits of time-based signaling along with a rather simple design process. With a VCO-based ADC, an analog current must undergo three stages in the phase period before it can be converted to a digital signal. The analog bit-line current must be converted into an analog voltage in the first stage. An analog voltage is then converted into pulses using the VCO. In the final step, a counter is used to count the generated pulses, and a Lookup Table (LUT) is used to map each pulse to the matching digital signal. Power supply voltage can be directly adjusted by adjusting the read voltage (Vread) applied to the crossbar (as row voltages). As a result, turning off the row Vread turns off the ADC and the crossbar. The analogous digital signal that this stage produces is ready for processing by the digital host. Figure 1 depicts the schematic of the entire system, which includes the VCO-based ADC and the ReRAM crossbar. A resistive random-access memory (RRAM) is composed of the parts of a resistive switching memory cell with a Metal-Insulator-Metal (MIM) structure.

The two metal (M) electrodes are positioned between an insulating layer (I) in the construction. High resistance state, or HRS, is regarded as the OFF state or logic 0. Low resistance state, or LRS, is regarded as the logic 1 or ON state.

CVR Journal of Science and Technology, Volume 27, December 2024
DOI: 10.32377/cvrjst2704

The gentle breakdown of the (MIM) structure causes a process that is commonly referred to as "electroforming," and the voltage at which this process takes place is known as the "forming voltage" (V_f). It functions with three volts. The three are read, reset, and set voltages.

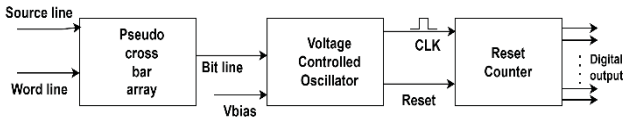

Figure 1. VCO based ADC using ReRAM's

A. Design of Pseudo Crossbar Array

To go from a high resistance state to a low resistance one, SET voltage must be applied. To go from a low resistance condition to a high resistance state, RESET voltage needs to be provided. To read the data from the memory, the READ voltage needs to be applied. When READ voltage is applied, the state remains unchanged.

A pseudo-crossbar array consists of rows and columns of memory cells or logic elements. These cells or elements are arranged in a grid-like fashion, like a traditional crossbar array. Unlike a true crossbar array where each row intersects with each column, in a pseudo-crossbar array, the interconnection is established through a set of switches or multiplexers. These switches control which rows are connected to which columns. Each row and column in the array are addressed individually.

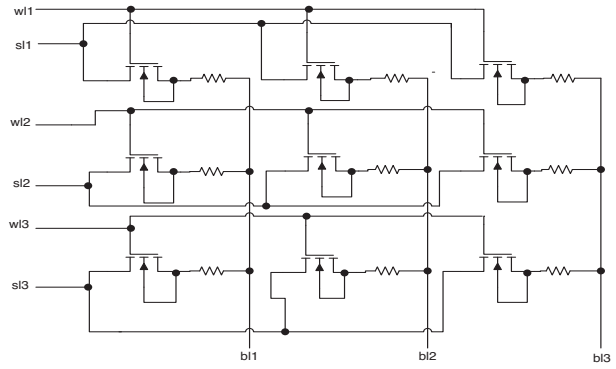

Figure 2. 3x3 pseudo crossbar array

When a particular memory cell or logic element needs to be accessed, the appropriate row and column addresses are selected. To read from or write to a specific cell or element, the corresponding row and column are activated. This activation is typically done by enabling the appropriate switches or multiplexers. Once the row and column are selected, data can be read from or written to the cell or element at their intersection. Fig.2 is a representation of a 3x3 pseudo crossbar array. It has 3 source lines (sl1, sl2, sl3,), 3-word lines (wl1, wl2, wl3) and 3-bit lines (bl1, bl2, bl3,). The data is sent to memory using source lines and it is stored in memory. The control signal is the word line, when word line is high the data can be read. The data is read by using bit lines. The same crossbar array is also designed using CNFET. The proposed array size is 3x3. Each row has 3 basic ReRAM cells, and each column has 3 ReRAM cells. All the column outputs are connected, and they are connected to a single bit line. The output is taken through bit lines. The memory size is scalable according to requirement.

B. Design of Voltage Controlled Oscillator

A ring oscillator is a type of oscillator circuit shown in fig.3 commonly used in digital integrated circuits to generate clock signals or as a frequency source. It is a simple structure comprising an odd number of inverting stages (typically an odd number of NOT gates or inverters) arranged in a ring. A closed loop is produced when the final stage's output is fed back into the first stage's input. Usually, a ring oscillator has an odd number of stages that reverse. This odd number ensures that the feedback loop has a net gain of -1, leading to sustained oscillations. Each stage in the ring is usually an inverter or a NOT gate. This choice of inverting stages ensures that the signal goes through a phase shift of 180^0 with each stage. A closed loop is created by connecting the last stage's output to the first stage's input again.

The feedback loop, combined with the inherent delay of each stage, results in oscillations. The frequency of oscillation is determined by the propagation delay of each inverting stage. As the signal circulates through the ring, it experiences a delay at each stage, contributing to the overall oscillation frequency. Delivering current to each step through the biasing circuit, the first stage made up of transistors MN1 and MP1, is crucial. In transistor MN1, the input voltage control sweep is accepted from least to highest voltage. As a result, the output frequency and drain current (I_d) will both rise in response to a surge in input voltage. The PMOS MP1 transistor reflects the drain current to the steps that follow via a diode connected to it. The output waveform of a ring oscillator is typically a square wave.

C. Design of Reset Counter

A counter is a digital circuit that counts in a prescribed sequence. It can be used to tally the number of clock pulses (or events) that occur. Counters are essential components in digital electronics and find applications in various systems, including frequency dividers, timers, and address generators. A Reset Counter is a circuit that depends on reset for counting the pulses.

It is necessary to comprehend the basic features and functioning of an 8-bit ripple counter in digital electronics to comprehend its theory. Digital circuits that produce a binary count sequence are called ripple counters. A cascade of eight flip-flops, one for each flip-flop that triggers the next in the sequence, makes up an 8-bit ripple counter shown in Fig.4. Following the initial flip-flop, which toggles its output in response to a clock pulse received by the counter, other flip-flops generate a ripple effect. Each counter Consists of a D-Flip flop shown in Fig.5 in which the D-Flip Flop consists of an 3input NAND gate which is designed using transistors is shown in Fig.6.

E-ISSN 2581 – 7957
P-ISSN 2277 – 3916

CVR Journal of Science and Technology, Volume 27, December 2024
DOI: 10.32377/cvrjst2704

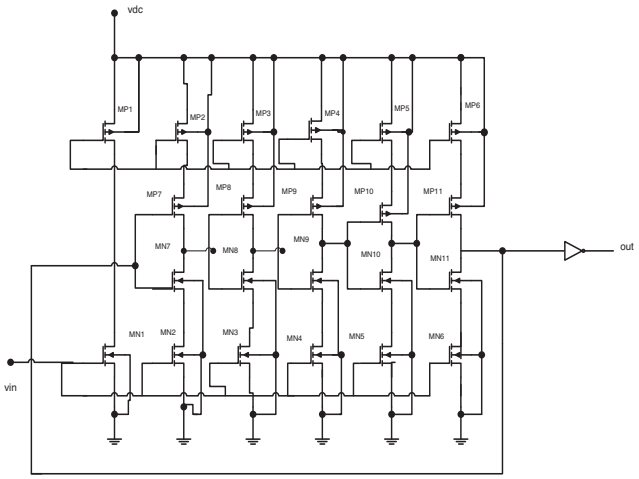

Figure 3. The five-stage current-starved VCO circuit

A ripple counter's primary benefit is its simplicity, as it needs fewer components than synchronous counters. But distinct synchronous counterparts, its disadvantage is the promulgation delay because each flip-flop's output is dependent on the one before it, lengthening the total counting time. Furthermore, because of the propagation delays, ripple counters are prone to glitches, which may call for additional circuitry for error correction. 8-bit ripple counters are nevertheless useful in a variety of digital systems when a trade-off between simplicity and a reasonable counting speed is acceptable, despite these drawbacks.

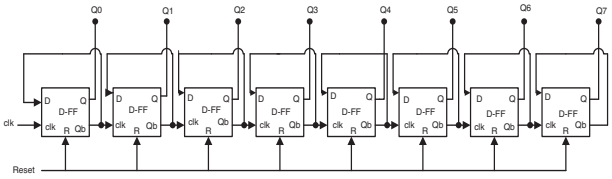

Figure 4. 8 Bit Reset Counter

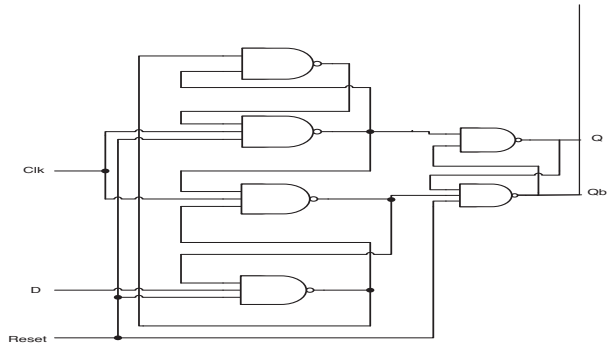

Figure 5. Schematic of D- Flip Flop

Fig. 7 illustrates the usage of a D flip-flop, sometimes referred to as a Data or Delay flip-flop, as a digital storage element in digital circuits for binary data storage.

It is a fundamental building block in digital electronics and is commonly used in sequential logic circuits, such as memory units, registers, and microprocessor components.

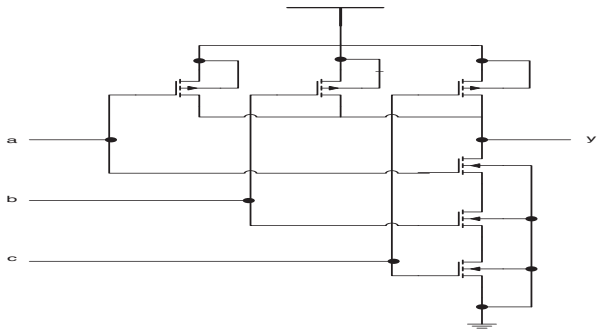

Figure 6. Schematic of 3 Input Nand gate

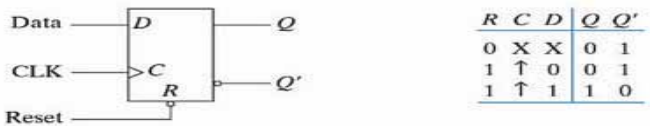

Figure 7. Truth table of D Flip Flop

NAND Gate is a basic digital block in designing a memory element. That performs a Boolean operation called the "NOT-AND" operation. To put it another way, a NAND gate only has a low output (logic 0) when both of its inputs are high (logic 1). If not, a high output is produced (logic 1).

After designing all basic blocks required for VCO-ADC, the task is now to assemble them and make a defined architecture for VCO-ADC. As represented in the above fig.1, 3x3 pseudo crossbar array, Ring oscillator and Reset counter are combined to form a Voltage controlled Oscillator based Analog to Digital Converter using ReRAM's. The working of VCO-ADC is 3x3 pseudo crossbar array have 3 source lines (sl1, sl2, sl3,), 3-word lines (wl1, wl2, wl3) and 3-bit lines (bl1, bl2, bl3,). The data is sent to memory using source lines and it is stored in memory. The control signal is the word line, when the word line is high the data can be read. The data is read by using bit lines. The bit line voltage given to the ring oscillator as an input and the supply voltage value is also given as input itself. The ring oscillator converts the given analog input voltage into frequency. Inverters are typically found in an odd number in any ring oscillator. A sinusoidal waveform is produced by these odd inverters and group ring oscillators . When it is sent through an inverter again it gives a square waveform, which is then used as a clock signal in the counter.

The counter also has a reset input, and the output of the ring oscillator is given as a clock for the reset counter. Based on the different input voltages given, this counter generates an 8-bit digital output. The proposed VCO-ADC uses ReRAM's which can be used for converting Analog input into Digital Output, which has 8 bits.

IV. Proposed CNFET based VCO ADC using ReRAM's

In this work, an effective CMOS architecture for a Voltage-Controlled Oscillator-based Analog-to-Digital converter is used. The advantages of CNFET technology are considered, and the proposed architecture is implemented.

Carbon Nanotube Field-Effect Transistors (CNFETs) stand at the forefront of cutting-edge nano electronics,

representing a pivotal advancement in semiconductor technology. With dimensions on the nanometer scale, CNFETs exploit the exceptional properties of carbon nanotubes (CNTs) to redefine the boundaries of electronic devices. Introduced as a promising alternative to conventional silicon-based transistors, CNFETs offer remarkable potential for enhancing device performance while overcoming the limitations posed by traditional materials. When a voltage is applied to the gate terminal, an electric field is generated across the dielectric layer, which influences the charge distribution within the carbon nano-tube channel. The electrostatic field can be used to control the current flow between the source and drain terminals by varying the gate voltage, which will attract or repel charge carriers within the channel.

CNFETs offer several advantages over traditional silicon based MOSFETs, including higher carrier mobility, lower power consumption, and better scalability. Additionally, CNFETs are less susceptible to short-channel effects, allowing for improved performance at nanoscale dimensions. These advantages make CNFETs promising candidates for future nano-electronic devices, including high-performance computing, flexible electronics, and energy-efficient applications. Ongoing research focuses on optimizing CNFET fabrication processes and exploring novel device architectures to further enhance their performance and functionality.

A lot of digital circuits, including arithmetic circuits, full adder-subtractor circuits, and 6T SRAM, use CNFETs. To enhance the performance of digital or analog designs, MOS and CNFETs are hybridized. Recent years have seen attempts to assess the prospective performance at the device level by modeling and simulating CNT-related devices, such as CNFET. Several optimized approaches are proposed and shown to reduce the impact of parasitic capacitances and increase the CNT ICs' speed.

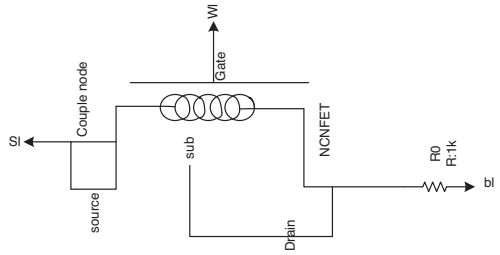

Figure 8. Schematic of ReRAM using CNFET

another important advantage of using a CNTFET device in the nanometer regime is to increase the threshold voltage at 10 nm and beyond the channel length. In the case of the MOSFET while reducing the channel length, the threshold voltage is also reduced, which leads to more leakage power.

Considering the advantages of CNFET over CMOS as discussed, all blocks are designed using CNFET. ReRAM using CNFET, VCO using CNFET, D Flip Flop using CNFET and NAND Gate using CNFET are shown in fig.8, fig.9 and fig.10 respectively. After combining all blocks, the supply voltages V_{dc} and V pulse are applied to memory to all its inputs. The inputs to the memory block are source lines and word lines. These Source lines act as input and they transfer input signal applied to source to bit line, which is acting as output. The word lines act as gates to turn the transistor on and off. Then, the outputs of memory, the bit lines are connected to the input of VCO-ADC. This VCO-ADC now will convert the given analog input voltage into required digital output.

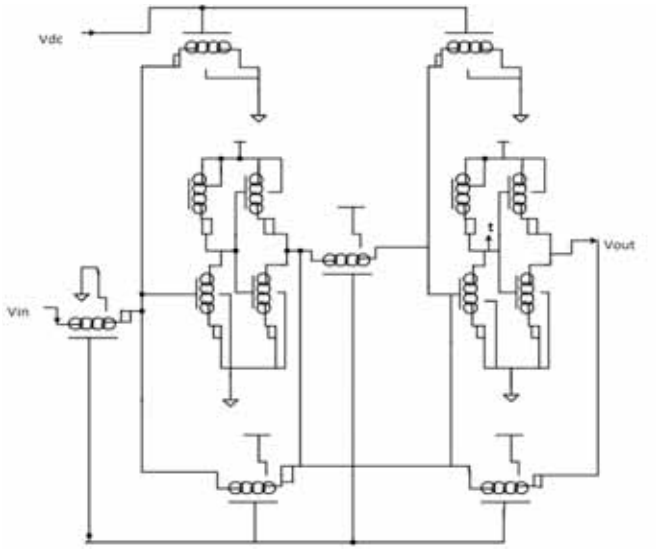

Figure 9. VCO using CNFET

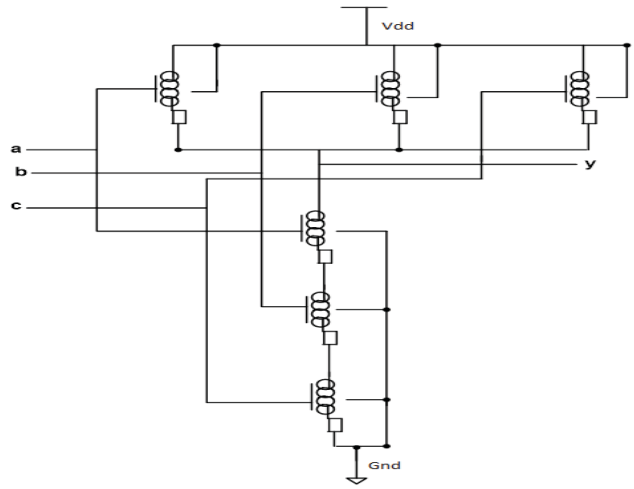

Figure 10. NAND Gate using CNFET

The theoretical calculations of ADC parameters are

1. Figure of Merit (FOM)

The Figure of Merit (FOM) in general is a quantitative measure used to evaluate the performance of any electronic design. It provides a single metric to compare different components based on their key specifications. A lower FoM indicates a more efficient ADC, meaning it can achieve high performance (high ENOB and high sampling frequency) with lower power consumption.

FOM Calculated for P= 9.59 pW, sampling frequency(fs)=3.57 GHz and ENOB=8

$$\text{FOM} = \frac{Power}{2^{ENOB}\ x\ sampling\ frequency} \qquad (1)$$

CVR Journal of Science and Technology, Volume 27, December 2024
DOI: 10.32377/cvrjst2704

$$=\frac{9.59 \times 10^{-12}}{3.57 \times 10^{9} \times 2^{8}}$$

FOM = 0.0104 zJ

FOM Calculated for P= 5.591 pW, f_s=2.2 GHz and ENOB=1.33

$$FOM=\frac{5.591 \times 10^{-12}}{2.2 \times 10^{9} \times 2^{8}}$$

FOM=0.0099 zJ

FOM Calculated for P= 3.972 pW, f_s=1 GHz and ENOB=1.33

$$FOM=\frac{3.972 \times 10^{-12}}{1 \times 10^{9} \times 2^{8}}$$

FOM=0.0155 zJ

2.Signal-to-Noise Ratio (SNR): SNR measures the ratio of the RMS value of the input signal to the RMS value of the noise. It's also expressed in decibels (dB).

SNR = 6.02* N+1.76 (dB). (2)

N= Number of bits

SNR = 6.02* 8+1.76 (dB)=49.92 dB

3.Effective Number of Bits (ENOB): ENOB represents the number of bits that accurately represent the ADC's performance, accounting for noise and distortion. Higher ENOB indicates better performance.

ENOB= (SNR-1.76dB)/6.02 (3)
=(49.92dB-1.76dB)/6.02
=48.16dB/6.02
=8 (Theotical)
ENOB=(45.104dB-1.76dB)/6.02=7.2(practical)

4. Power calculations of proposed CNFET VCO based ADC:

The static power dissipation of an Analog to Digital Converter (ADC) primarily depends on the supply voltage and the static current drawn by the circuit. Static power dissipation occurs even when the ADC is not actively converting analog signals to digital data, as it is the power consumed by the circuit to maintain its ready state.The formula for static power dissipation is:

$$P_{static}=V_{DD} \times I_{static} \quad (4)$$

where:
Pstatic is the static power dissipation,
VDD is the supply voltage,
Istatic is the static current drawn by the ADC.

The dynamic power dissipation in an Analog to Digital Converter (ADC) is primarily due to the switching activity during the conversion process. The formula for dynamic power dissipation is:

$$P_{dynamic}=C_{load} \times V^2_{DD} \times f_{Sampling} \quad (5)$$

where:

- $P_{dynamic}$ is the dynamic power dissipation,
- C_{load} is the load capacitance,
- V_{DD} is the supply voltage,
- $f_{Sampling}$ is the Sampling frequency.

In the context of an ADC, $f_{Sampling}$ is typically the sampling rate or the frequency at which the ADC is clocked. The load capacitance C_{load} represents the total capacitance being charged and discharged during each conversion cycle.

The total power calculated for V_{DD}= 1V, I_{static}= 6.02 pA, C_{load}= 0.001 aF and $f_{Sampling}$= 3.57 GHz

P_{static}= 1 V x 6.02 pA =6.02 Pw
$P_{dynamic}$= 0.001 aF x 1 V x 3.57 GHz = 0.001×10^{-18} x 1V x 3.57 x 10^9 = 3.57 pW
Total Power= P_{static}+ $P_{dynamic}$=6.02 pW+3.57 pW= 9.59 Pw

The total power calculated for V_{DD}= 0.8V, I_{static}= 6.02 pA, C_{load}= 0.001 aF and $f_{Sampling}$= 2.2 GHz

P_{static}= 0.8 V x 6.02 pA =4.816 Pw
$P_{dynamic}$= 0.001 aF x 0.82 V x 3.57 GHz = 0.001×10^{-18} x 0.64 V x 2.2 x 10^9 = 1.408 pW
Total Power= P_{static}+ $P_{dynamic}$=4.816 pW+1.408 pW= 5.591 pW

The total power calculated for V_{DD}= 0.6 V, I_{static}= 6.02 pA, C_{load}= 0.001 aF and $f_{Sampling}$= 1 GHz

P_{static}= 0.6 V x 6.02 pA =3.612 Pw
$P_{dynamic}$= 0.001 aF x 0.62 V x 1 GHz = 0.001×10^{-18} x 0.36 V x 1 x 10^9 = 0.36 pW
Total Power= P_{static}+ $P_{dynamic}$=3.612 pW+0.36 pW= 3.972 pW

5.Power calculations of MOSFET VCO based ADC:

The total power calculated for VDD= 1.2 V, I_{static}= 296.3 μA, C_{load}= 0.1 pF and $f_{Sampling}$= 710 MHz
P_{static}= 1.2 V x 296.3 μA =297.5 μw
$P_{dynamic}$= 0.1 pF x 1.22 V x 710 MHz = 0.1×10^{-12} x 1.44 V x 71 x 10^7 = 102.24 μW
Total Power= P_{static}+ $P_{dynamic}$=297.5 μw + 102.24 μW = 399.74 μW

All these are the Performance Metrics that evaluate any electronic design, to prove it is best than other designs in terms of Power Consumption, Delay, Effective Number of Bits (ENOB), Supply Voltage, Technology used, Figure of Merit (FOM), Signal-to-Noise Ratio (SNR).

V. Simulation Results

The fig.11 is the transient response of 3 input NAND gates Verification is done for both NAND gates using CMOS and CNFET. All the 8 combinations are verified. Fig.12 is the transient response of D flip-flop. Verification is done for both flip-flops i.e., CMOS and CNFET. All the combinations are simulated, and the truth table is verified. Fig.12 can infer that when the clock is triggered the output q is changed according to d input and q-bar is always inverted output of q.

CVR Journal of Science and Technology, Volume 27, December 2024
DOI: 10.32377/cvrjst2704

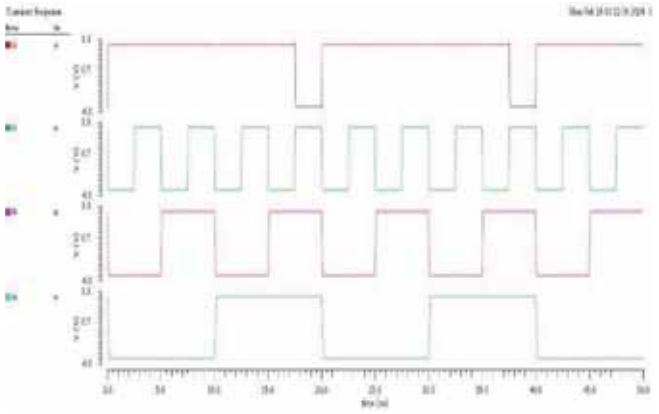

Figure 11. Simulation waveform of 3 input NAND gate

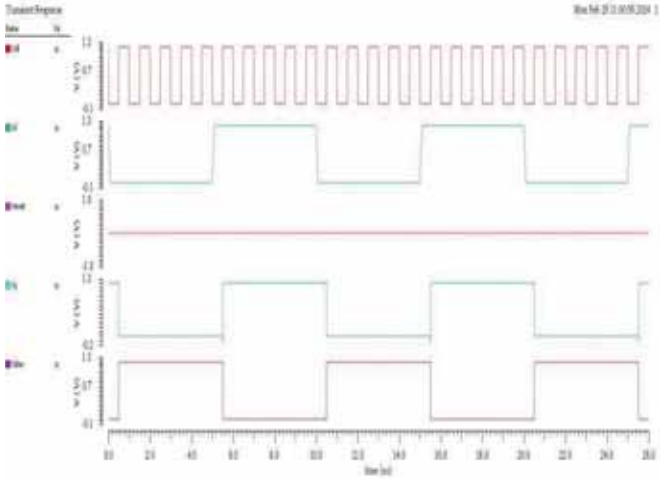

Figure 12. Simulation waveform of D flipflop

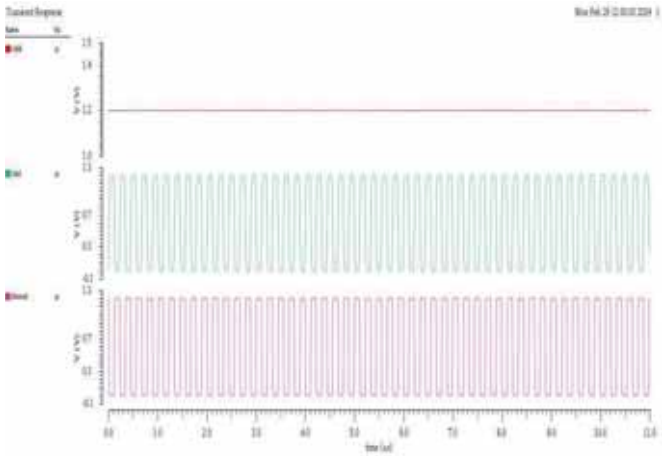

Figure 13. Simulation waveform of VCO

The fig.13 represents the transient response of the ring oscillator. Simulation is done for both the schematics i.e., CNFET and CMOS considering the advantages of CNFET over CMOS. Fig. 13 infers that for the value of vdd of 1 V, the frequency generated is 3.57 G Hz. As discussed in the previous section, it comprises of 8 back-to-back inverters connected to each other. Higher frequencies can be generated using the higher number of stages. ADC satisfied Nyquist criteria that the Nyquist criterion requires that the sampling frequency be at least twice the highest frequency contained in the signal, or information about the signal will be lost.

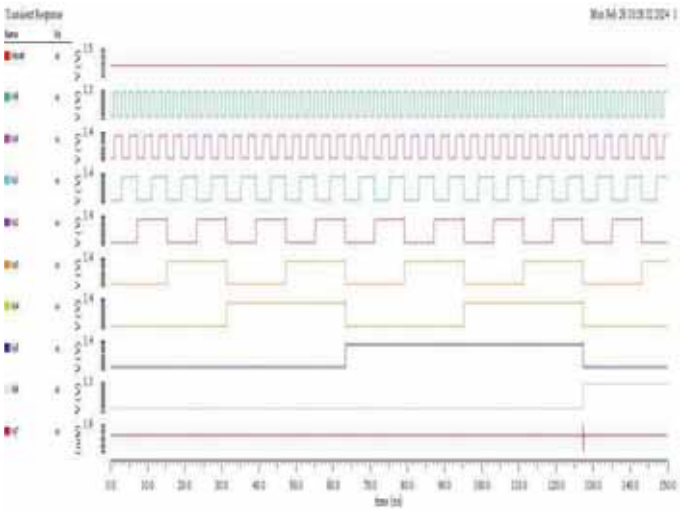

Figure 14. Simulation waveform of Reset Counter

The fig.14. represents the transient response of the reset counter. From fig. 14 it can be inferred that counting starts after reset is zero, and thereafter output is incremented for every clock edge and when output is 255 it becomes zero. The simulation is done for both counters i.e., CMOS and CNFET.

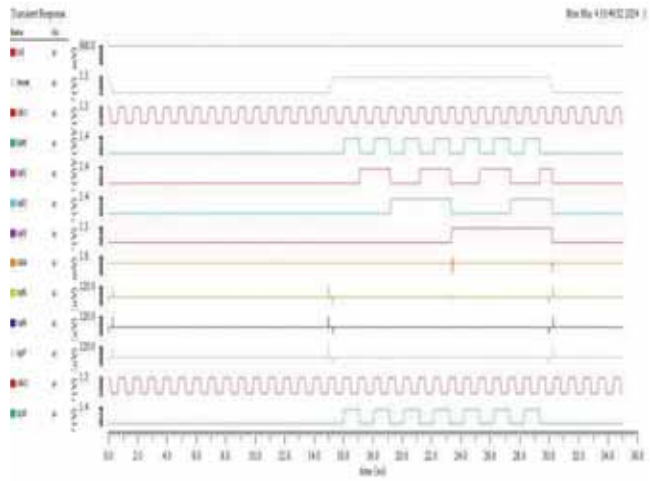

Figure 15. Simulation Waveforms of VCO-ADC for 0.6V Input

The VCO based ADC there is no separate analog input is given so the supply voltage is the controlled volage and it self-act as a input voltage. The input voltage converted into the digital form for this concept, so the input voltage is generated from pseudo cross bar array. Biasing is the setting of DC voltage at operating conditions of an electronic component that processes time-varying signals. Many electronic devices, such as diodes, transistors and vacuum tubes, whose function is processing time-varying (AC) signals, also require a steady DC voltage at their terminals to operate correctly. This voltage is called bias. The pseudo cross bar array inputs are source lines and word lines that are in digital form like logic o and logic 1 to ON or OFF the array switches from that the output voltage generated through bit lines. The bit lines generate the bias voltage that is given to the VCO, and it generates the clock signal that frequency is the sampling frequency mentioned in table.1. For different controlled voltages (input voltages) is 0.6V, 0.8V and 1V the simulated waveforms are shown in this work and

from that clock frequency is the sampling frequency calculated and shown in Table I.

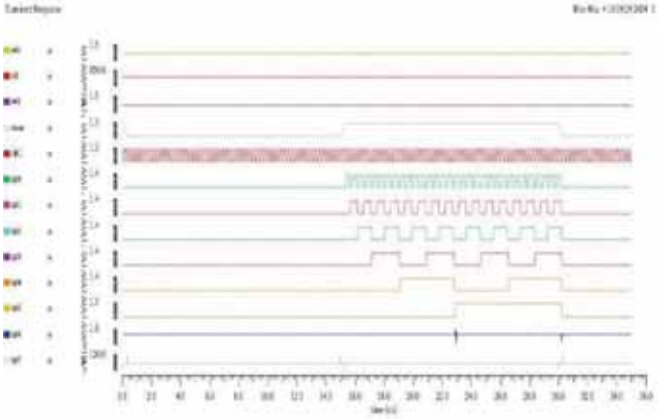

Figure 16. Simulation Waveforms of VCO-ADC for 0.8V Input

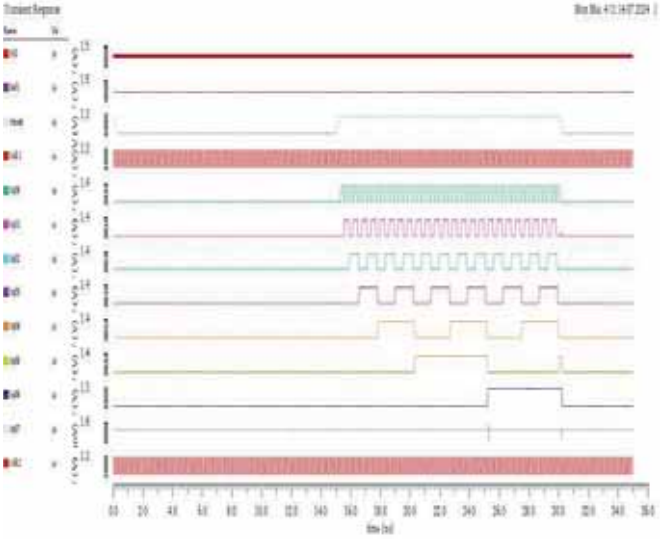

Figure 17. Simulation Waveforms of VCO-ADC for 1V Input

The different input voltages 0.6V, 0.8V and 1V are applied to the VCO based ADC using ReRAM's and the corresponding waveforms shown in fig.15, fig.16 and fig.17 and the digital binary output is analyzed. The Final block of VCO-ADC with ReRAM Memory Architecture is designed using both CMOS and CNFET's. Both the simulation results give Same output digital value for the given analog input voltage. The difference only lies in the performance and advantages of CNFET over CMOS. The comparative analysis of different parameters for proposed and existing is shown in table 1. Observed that the CNFET based ADC power consumption, Delay, figure of merit and SNR is less compared to conventional designs. The limitation of conventional design is under threshold voltage the conversion of analog to digital is not that much accuracy. To overcome that the proposed CNFET based VCO ADC works under threshold voltage and the conversion is more accurate, power and delay is less compared to the conventional designs.

TABLE-I.
COMPARISON BETWEEN PROPOSED AND EXISTING WORK

Parameter	Proposed VCO-ADC with CNFET			VCO-ADC with CMOS	[11]	[13]	[14]
Delay	514.6 p s			16.61 n S	-	-	-
Resolution	8-Bit			8-Bit	4 bit	10 bit	
Technology	32 nm			45 nm	45n m	45nm	45 nm
Supply or input voltage	1 V	0.8V	0.6V	1.2 V	1.2V	1.2V	1.2V
Sampling frequency	3.57 GHz	2.2 GHz	1 GHz	710 M Hz	100 MH z	50 MHz	1.6 GHz
Power	10.94 pW	6.87 pW	4.12 pW	425 uW	0.15 6m W	712.1 2 μW	1.157 mW
FOM	0.020 8 zJ	0.02 1 zJ	0.02 80 zJ	1.37 fJ	125 dB	-	33 fJ
ENOB	1.33			1.33	-	-	-
No. of bits	8			8	4	9.1	-
SNR	49.92 dB			49.92 dB	62 dB	55 dB	59dB

TABLE-II.
COMPARISON BETWEEN THEORITICAL AND PRACTICAL VALUES OF PROPOSED WORK

Parameter	Practical Values of Proposed work			Theoretical Values of Proposed work		
Supply or input voltage	1 V	0.8V	0.6V	1 V	0.8V	0.6V
Sampling frequency	3.57G Hz	2.2GH z	1GHz	3.57 GHz	2.2G Hz	1GHz
Power	10.94 pW	6.87 pW	4.12 pW	9.59 pW	5.591 pW	3.972 pW
FOM	0.0208 zJ	0.021 zJ	0.0280 zJ	0.01 04 zJ	0.009 9 zJ	0.0155 zJ
ENOB	7.2			8		
SNR	45.104 dB			49.92 dB		

The comparison between theoretical and practical work is shown in table 2. Comparing power, FoM, ENOB and SNR parameters of proposed work. Observing that the noise is less in terms of ENOB that is 7.2 bits from this the accuracy of ADC is not that much deviated by using CNFET model. Whenever the ENOB is near to the theoretical value, the lower FoM indicates a more efficient ADC, meaning it can achieve high performance (high ENOB and high sampling frequency) with lower power consumption.

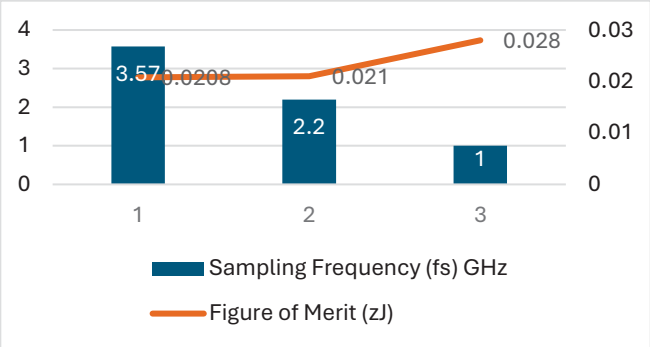

Figure 18. Monte carlo Simulation of VCO-ADC

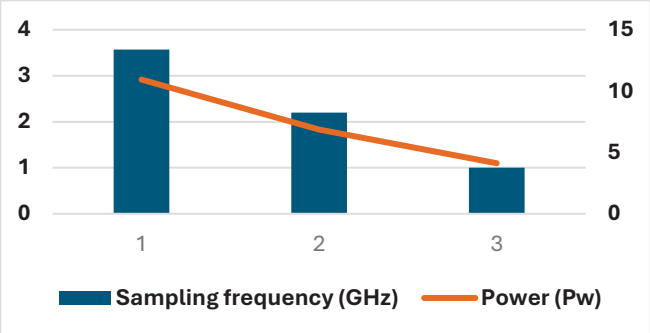

Figure 19. Monte carlo Simulation of power analysis in VCO ADC

The monte carlo simulation of VCO ADC shown in fig.18 observed how the figure of merit is changed for different supply voltages and sampling frequencies. The monte carlo simulation of power analysis in VCO ADC shown in fig.19 observed that the power dissipation is changed linearly for different sampling frequencies.

VI. Conclusions

In this proposed design, VCO-based ADC offers several advantages over traditional ADC architectures. VCO-based ADCs leverage the oscillation frequency of a voltage-controlled oscillator to encode analog signals into digital form, providing a compact, efficient, and high-speed conversion mechanism. This approach is particularly well-suited for CIM architectures, where the proximity of memory and processing elements enables direct analog signal conversion within the memory array, minimizing data movement and reducing latency. By integrating the VCO-based ADC directly with ReRAM arrays, the proposed design achieves seamless integration of analog-to-digital conversion functionality with memory storage. This integration enables efficient processing of analog data directly within the memory array, eliminating the need for separate ADC units and reducing overall system complexity and power consumption. The Development of VCO-ADC systems with wider bandwidth and extended frequency ranges to meet the demands of emerging communication standards and applications, such as 5G and beyond. The resolution of ADCs can further be improved for higher accuracy and detailed digitization of analog signals, using alternate and advanced FET technology libraries.

References

[1] Y. Guo, J. Jin, X. Liu, Z. Yang and J. Zhou, "A LUT-based Background Linearization Technique for VCO-based ADC Employing KVCO−Locked−Loop," *2023 IEEE International Symposium on Circuits and Systems (ISCAS)*, Monterey, CA, USA, 2023, pp. 1-4, doi: 10.1109/ISCAS46773.2023.10181646

[2] S. Konwar and B. Datta Sahoo, "Johnson Counter-Based Multiphase Generation for VCO-Based ADC for Direct Digitization of Low Amplitude Sensor Signals," in *IEEE Transactions on Instrumentation and Measurement*, vol. 72, pp. 1-4, 2023, Art no. 2003004, doi: 10.1109/TIM.2023.3265121.

[3] N. Narasimman and T. T. Kim, "An ultra-low voltage, VCO-based ADC with digital background calibration," *2016 IEEE International Symposium on Circuits and Systems (ISCAS)*, Montreal, QC, Canada, 2016, pp. 1458-1461, doi: 10.1109/ISCAS.2016.7527532.

[4] R. Shokri, Y. Koolivand, O. Shoaei, O. Aiello and D. Caviglia, "A Nonlinear, Low-Power, VCO-Based ADC for Neural Recording Applications," *2023 5th Iranian International Conference on Microelectronics (IICM)*, Tehran, Iran, Islamic Republic of, 2023, pp. 199-203, doi: 10.1109/IICM60532.2023.10443199.

[5] V. Nguyen, F. Schembari and R. B. Staszewski, "A 0.2-V 30-MS/s 11b-ENOB Open-Loop VCO-Based ADC in 28-nm CMOS," in *IEEE Solid-State Circuits Letters*, vol. 1, no. 9, pp. 190-193, Sept. 2018, doi: 10.1109/LSSC.2019.2906777.

[6] X. Xing and G. G. E. Gielen, "A 42 fJ/Step-FoM Two-Step VCO-Based Delta-Sigma ADC in 40 nm CMOS," in *IEEE Journal of Solid-State Circuits*, vol. 50, no. 3, pp. 714-723, March 2015, doi: 10.1109/JSSC.2015.2393814.

[7] D. -M. Tran, N. -D. Nguyen, D. -H. Bui and X. -T. Tran, "A Highly Digital VCO-based ADC for IoT Applications on Skywater 130nm," *2021 8th NAFOSTED Conference on Information and Computer Science (NICS)*, Hanoi, Vietnam, 2021, pp. 549-554, doi: 10.1109/NICS54270.2021.9701515.

[8] J. Borgmans and P. Rombouts, "Noise Optimization of a Resistively Driven Ring Oscillator for VCO-Based ADCs," *2022 IEEE International Symposium on Circuits and Systems (ISCAS)*, Austin, TX, USA, 2022, pp. 775-779, doi: 10.1109/ISCAS48785.2022.9937724.

[9] W. -C. Wei *et al.*, "A Relaxed Quantization Training Method for Hardware Limitations of Resistive Random Access Memory (ReRAM)-Based Computing-in-Memory," in *IEEE Journal on Exploratory Solid-State Computational Devices and Circuits*, vol. 6, no. 1, pp. 45-52, June 2020, doi: 10.1109/JXCDC.2020.2992306.

[10] B. Wu *et al.*, "ReRAM Crossbar-Based Analog Computing Architecture for Naive Bayesian Engine," *2019 IEEE 37th International Conference on Computer Design (ICCD)*, Abu Dhabi, United Arab Emirates, 2019, pp. 147-155, doi: 10.1109/ICCD46524.2019.00026.

[11] Ellaithy, D.M. Voltage-controlled oscillator-based analog-to-digital converter in 130-nm CMOS for biomedical applications. Journal of Electrical Systems and Inf Technol **10**, 38 (2023). https://doi.org/10.1186/s43067-023-00109-xJ.

[12] Xinpeng Xing, Xinpeng Gui, Xinfa Zheng, Haigang Feng,A fully-digital calibration algorithm for VCO-based ADC,Microelectronics Journal,Volume 139,2023,105879,ISSN 0026-2692,https://doi.org/10.1016/j.mejo.2023.105879.

[13] Zahra Mohseni, Mehdi Ehsanian,A 10-b (9.1-b ENOB), TP-Robust Open-Loop VCO-based ADC in 65 nm CMOS,AEU - International Journal of Electronics and Communications,Volume 150,2022,154199,ISSN 1434-8411,https://doi.org/10.1016/j.aeue.2022.154199.R.

[14] S. Ghozzy, H. F. Ragai and M. El-Nozahi, "A Two-Step VCO-Based ADC with PWM Pre-coded Coarse Quantizer," *2020 IEEE 3rd International Conference on Electronics Technology (ICET)*, Chengdu, China, 2020, pp. 262-265, doi: 10.1109/ICET49382.2020.9119547.

[15] K. M. Al-Tamimi, K. El-Sankary and Y. Fouzar, "VCO-Based ADC With Built-In Supply Noise Immunity Using Injection-Locked Ring Oscillators," in *IEEE Transactions on Circuits and Systems II: Express Briefs*, vol. 66, no. 7, pp. 1089-1093, July 2019, doi: 10.1109/TCSII.2018.2875867.

[16] V. Nguyen, F. Schembari and R. B. Staszewski, "A 0.2-V 30-MS/s 11b-ENOB Open-Loop VCO-Based ADC in 28-nm CMOS," in *IEEE Solid-State Circuits Letters*, vol. 1, no. 9, pp. 190-193, Sept. 2018, doi: 10.1109/LSSC.2019.2906777.

[17] G. Snehalatha and M. Anjikumar, "Stochastic Flash Analog to Digital Converter Compared with Conventional Resistor ladder Flash Analog to Digital Converter," *2022 International Conference on Futuristic Technologies (INCOFT)*, Belgaum, India, 2022, pp. 1-6, doi: 10.1109/INCOFT55651.2022.10094440.

[18] G. Snehalatha, J. Selvakumar and E. Thuraka, "Design of 8-bit Low power & High-performance SAR ADC using current steering DAC," *2023 Global Conference on Information Technologies and Communications (GCITC)*, Bangalore, India, 2023, pp. 1-6, doi: 10.1109/GCITC60406.2023.10426165.

[19] G. Snehalatha, J. Selvakumar and E. Rani Thuraka, "Comparative Study and Review on Successive Approximation/Stochastic Approximation Analog to Digital Converters for Biomedical Applications," *2022 2nd International Conference on Intelligent Technologies (CONIT)*, Hubli, India, 2022, pp. 1-9, doi: 10.1109/CONIT55038.2022.9847947.

E-ISSN 2581 – 7957
P-ISSN 2277 – 3916

CVR Journal of Science and Technology, Volume 27, December 2024
DOI: 10.32377/cvrjst2705

Performance Evaluation of UFMC for Future Wireless Communication Systems

Malleswari Akurati[1], Dr. Satish Kumar Pentamsetty[2] and Dr. Satya Prasad Kodati[3]
[1]Sr. Asst. Professor, CVR College of Engineering/ECE Department, Hyderabad, India
Email: malli.akurati@gmail.com
[2]Professor & HOD, ACE Engineering College/ECE Department, Hyderabad, India
[3]Retd. Professor, JNTUK/ECE Department, Kakinada, India

Abstract: **One of the innovative waveforms for 5G networks is the Universal Filtered Multi-Carrier (UFMC) technology. Low latency, resilience to frequency offset, and a decrease in out-of-band (OoB) radiation are anticipated benefits of UFMC, which will raise spectral efficiency. As previously indicated, the UFMC system has numerous benefits; nevertheless, because it is a multicarrier gearbox technology, its Peak-to-Average Power Ratio (PAPR) is high. Companding, Precoding and Selected Mapping (SLM) methods are an easy and effective way to lower the PAPR of UFMC signals. This work proposes a Modified Mu-law Companding Transform (MMCT) that lowers the PAPR of UFMC approach without altering the companded signal's average power and a Discrete Sine Transform (DST) precoding PAPR reduction technique to reduce the complexity. These two techniques are combined with SLM separately and their performance is assessed in the matter of both PAPR and BER. The UFMC signal's big and small amplitudes are expanded using distinct scales in the MMCT scheme based on an inflection point. Also, the DST technique provides less PAPR by considering only the real components. As a result, there is greater freedom in selecting the compounding parameters that will yield the best results in terms of PAPR, average power level, and BER. The simulation findings verify that, in comparison to the original UFMC signal and OFDM technique, the proposed schemes offer higher PAPR and BER reduction characteristics.**

Index Terms: **Universal Filtered Multi Carrier, Selected Mapping, Modified Mu-Law Companding, Discrete Sine Transform, Peak to Average Power Ratio.**

I. Introduction

The Internet of Everything (IoE) is the main example of the many applications that future wireless telecommunication technology must serve [1], [2]. The Universal Filtered Multi-Carrier (UFMC) approach is suggested in [3] and [4] as the peculiar innovative possible waveforms for 5G systems. Its robustness in the case of frequency offset, low latency, and reduction of Out-of-Band (OoB) emission allows for improved spectral efficiency. Higher reductions in OoB radiation are achieved in UFMC systems by filtering each sub-band of subcarriers rather than the entire band. In general, the UFMC system combines the robustness of Filter-Bank Multi Carrier (FBMC) in case of interference with the straightforward construction of Orthogonal Frequency Division Multiplexing (OFDM). Furthermore, in the event of brief burst communications, the UFMC system is preferable to the FBMC system [5]. As previously indicated, the UFMC system has numerous benefits; nevertheless, because it is a multicarrier gearbox technology, its peak-to-average power ratio (PAPR) is high [6].

Numerous studies have been conducted on PAPR reduction improvement in OFDM systems; these works fall into two major categories: techniques using signal distortion and probabilistic ways. Signal distortion techniques, like the clipping and filtering approach described in [7], work by limiting the power of the transmitted signal by establishing a maximum level. The primary disadvantage of signal distortion techniques is that they distort the transmitted signal, which has a detrimental effect on Bit Error Rate (BER) performance. However, without resulting in signal distortion, the probabilistic techniques alter the transmitted signal by adding random phase shifts.

These strategies include the Partial Transmit Sequence (PTS) strategy in [8],[9], and the Selected Mapping (SLM) approach in [10]-[12]. Because the receiver receives side information to recover the original, the SLM and PTS techniques decrease spectral efficiency. However, several methods have been put out in the literature, such as in [13], to get the side information at the receiver without the recipient knowing. Since the SLM strategy reduces PAPR more effectively than the PTS approach, it is taken into consideration in this research [10]. Additionally, SLM is regarded as a distortion-free technique that does not adversely alter the transmitted signal's spectrum, in contrast to clipping and filtering approaches.

For OFDM systems, a variety of companding methods are available, including μ-law [11], exponential companding (EC) [12], and LNST companding [13]. The bit error rate (BER) of OFDM signals is degraded by EC and increased power level by the μ-law. Only the DQPSK scheme of the OFDM linear nonsymmetrical companding transform LNST system is evaluated. Using this method, the tiny signals are expanded while constricting the huge signals to make the little signals more resistant to noise.

To lower the PAPR of UFMC systems, a Modified Mu-law Companding Transform (MMCT) is suggested and it is combined with SLM. Higher order QAM is evaluated for this scheme. To complement the UFMC signal's large and small amplitude values, an inflection point is employed [14].

The precoding technique, sometimes referred to as the pulse shaping technique, is a strong and adaptable method of reducing PAPR [15]. This technique can lower the PAPR to that of a single carrier transmission technology and is compatible with all base-band modulation techniques. The outcomes of the simulation demonstrate that, in comparison to conventional methods, the suggested MMCT and DST

Received on 30-03-2024, Revised on 29-04-2024, Accepted on 29-05-2024.

E-ISSN 2581 – 7957
P-ISSN 2277 – 3916

DOI: 10.32377/cvrjst2705

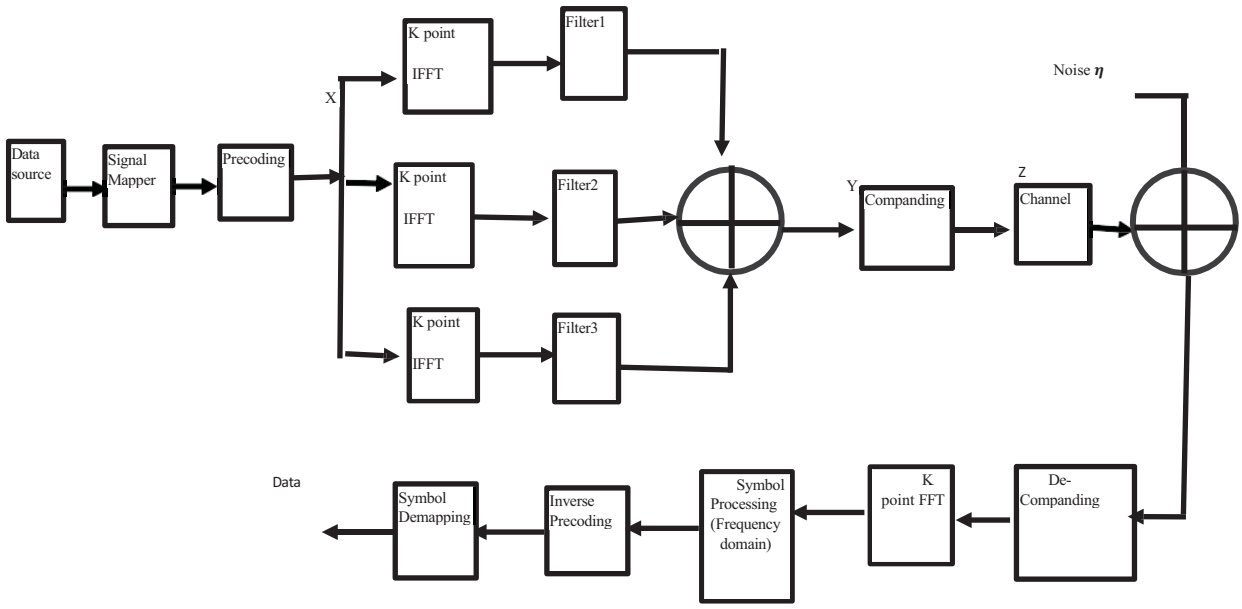

Figure 1. Block diagram of proposed UFMC- DST-SLM & UFMC SLM-MMCT technique

precoding schemes along with SLM provide superior PAPR reduction and BER characteristics [16]. A reduced complexity UFMC transmitter has been proposed by Thorsten et al. in [17]. According to the authors, the complexity of an OFDM transmitter is more than 100 times greater than that of a UFMC transmitter, but their suggested UFMC transmitter diminishes the complexity by 20% in comparison. In [18], Raymond et al. proposed an alternative architecture to the traditional UFMC transmitter, wherein the complexity is reduced to 25 times that of an OFDM transmitter for the filtering portion and the size of the Inverse Fast Fourier Transform (IFFT). Atif et al. in [19] introduced simplicity in all the UFMC transmitter blocks while conveying flexibility, using the most simplified UFMC transmitter in [18] as a baseline. The UFMC transmitter's complexity approaches that of an OFDM transmitter thanks to a reduction in complexity reported in [19]. U_m OFDM modulators are required in a typical traditional SLM-based OFDM system to produce U_w OFDM waveforms, where U_m is considered as U_w as covered in [20]. The bank of UFMC modulators required to apply the SLM and produce the necessary set of UFMC waveforms will be the primary source of complexity [21].

On the other hand, we can use the precoding and companding techniques in UFMC systems with less complexity like that of OFDM systems because of the reduced-complexity UFMC modulator suggested in [22]. These techniques not only reduce the complexity but also improve the performance using reduced BER.

II. UFMC System with Proposed Model

The UFMC modulation approach is a kind of multi-carrier technique that divides huge data rate signals into various parallel streams at a lesser rate. The UFMC system splits the entire band of *M* sub-carriers into *B* sub-bands each containing M_B sub-carriers, where *b = 1, 2, ..., B*. Then, each sub-band multiplies the data by U phase rotation factors and after that they are operated by *N*-point IFFT and finite sub-band impulse response filter, respectively and the signal with the lowest PAPR is selected. Finally, the sub band filtered signals are added together and the time domain representation of UFMC is generated. Figure 1 demonstrates the typical block diagram of the UFMC transceiver system. The operation of UFMC-DST-SLM is as follows. The output of this modulation technique is denoted as Q, where $Q = [q0\ q1\ q2\ \ldots.\ QM\text{-}1]^T$, where q_i is the sub carrier index, i = [0 1 2 …… M-1]. This output Q is multiplied by the proposed DST precoding matrix P and can be represented as:

$$X = P\,Q \tag{1}$$

The order of the precoding matrix is M x M, and its equation is in the form of

$$P = \begin{bmatrix} p_{00} & p_{01} & p_{0(M-1)} \\ p_{10} & p_{11} & p_{1(M-1)} \\ p_{(M-1)0} & p_{(M-1)1} & p_{(M-1)(M-1)} \end{bmatrix} \tag{2}$$

$$\begin{bmatrix} X(0) \\ X(1) \\ \vdots \\ X(M-1) \end{bmatrix} = \begin{bmatrix} p_{00} & p_{01} & \cdots & p_{0(M-1)} \\ p_{10} & p_{11} & \cdots & p_{1(M-1)} \\ \vdots & \vdots & \vdots & \vdots \\ p_{(M-1)0} & p_{(M-1)1} & p_{(M-1)1} & p_{(M-1)(M-1)} \end{bmatrix} \begin{bmatrix} q(0) \\ q(1) \\ \vdots \\ q(M-1) \end{bmatrix} \tag{3}$$

Where M is the number of sub carriers. Using the above equation, the k^{th} sub carrier of X can be represented as:

$$X(k) = \sum_{m=0}^{M-1} p(k,m)q(m) \tag{4}$$

Where, k = *0,1.....M-1.*

The data vector of the precoding matrix whose order is *Mx1* is given by:

$X = [X(0), X(1) \cdots, X(K), \cdots, X(M-1)]^T$ and later it is sub divided into B sub bands and each sub-band consists of M_B number of sub-carriers which results in $M = BM_B$. The sub-band signals are applied to independent N-point Inverse Discrete Fourier Transforms (IDFTs) so that the resultant time-domain signal is appeared as

$$x_{Bi}(n) = IDFT\,[X_{Bi}] = \frac{1}{\sqrt{N}} \sum_{k=0}^{N-1} X_{uk}\, e^{j2\pi \frac{k}{N} n} \quad (5)$$

Where, $x_{Bi}(n)$ is the n^{th} data symbol.

The equations of original DHT and Mu-Law are given by [6]:

$$R(n) = \sqrt{\frac{1}{N}} \sum_{n=0}^{N-1} X_n\, Cas\left(\frac{2\pi kn}{N}\right) \quad (6)$$

$$y(x) = V \frac{\log\left(1 + \mu \frac{|x|}{V}\right)}{\log(1+\mu)} sgn(x) \quad (7)$$

Where, *Cas* is the combination of Cos and Sin.

The proposed DST Precoding scheme's equation is given by:

$$H(k) = \sqrt{\frac{2}{N}} \sum_{n=0}^{N-1} X_n\, Sin\left(\frac{2\pi kn}{N} + \frac{\pi}{4}\right) \quad (8)$$

The proposed MMCT technique's equation is given by:

$$y(x) = V \frac{\log\left(1 + \mu \frac{|x|}{V}\right) 1^{/\beta}}{\log(1+\mu)} sgn(x) \quad (9)$$

III. Simulation Results

The UFMC signals are rotated by phase factors, then precoded by using the proposed DST transform and then the actual UFMC process will be done later. Similarly in the second method, first the UFMC-SLM process is done in which, the symbols are rotated by phase factors and the one with the lowest PAPR is selected for transmission and the output signal is fed to compander circuit to generate the output signal. For both the methods, the PAPR and BER are calculated and compared with the original OFDM, UFMC conventional Discrete Hartley Transform (DHT) and Mu-Law companding techniques. The simulation parameters are assumed to be 1024 symbols, 512 sub carriers by using the 32-QAM modulation technique with phase rotation factor U=8. The software used is MATLAB.

Figure 2 shows the PAPR graph of UFMC-WHT and proposed UFMC-DST-SLM technique. As shown, the PAPR of OFDM is 10.6 dB, UFMC is 10.5 dB, which are almost same. The conventional UFMC-WHT technique's PAPR is 9.6 dB, and the proposed UFMC-DST-SLM technique's PAPR is 9 dB respectively. Hence, compared to WHT technique, the proposed DST-SLM technique reduces the PAPR by 6.2%. The values are indicated in Table 1.

TABLE I

Analysis of PAPR of UFMC-SLM-Precoding Technique

Method	PAPR (dB) at CCDF=10^{-2}
OFDM	10.6
UFMC	10.5
UFMC-WHT	9.6
UFMC-DST-SLM	9

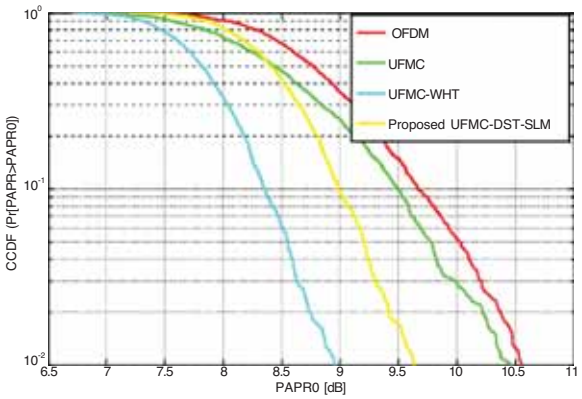

Figure 2. PAPR graph of UFMC WHT and proposed UFMC-DST-SLM

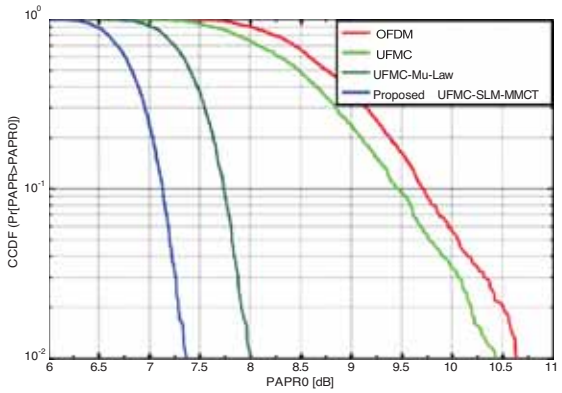

Figure 3. PAPR graph of UFMC-Mu law and proposed UFMC-SLM-MMCT

TABLE II

Analysis of PAPR of UFMC-Companding Technique

Method	PAPR (dB) at CCDF=10^{-2}
OFDM	10.6
UFMC	10.5
UFMC-Mu-Law	8
UFMC-SLM-MMCT	7.4

Figure 3 shows the PAPR graph of UFMC-Mu-law and proposed UFMC-SLM-MMCT technique. As shown in Table II, the PAPR of OFDM is 10.6 dB, UFMC is 10.5 dB, which are almost same. The conventional UFMC Mu law companding technique's PAPR is 8 dB, UFMC-SLM-MMCT technique's PAPR is 7.4 dB respectively. Hence, compared to Mu-Law scheme, the proposed SLM-MMCT technique reduces the PAPR by 7.5%.

Figures 4 and 5 represent the BER graph of proposed UFMC-DST-SLM precoding and UFMC-SLM-MMCT companding techniques. As shown in Table III, the BER is evaluated for different values of Signal to ratio noise Ratios (SNR). As the SNR increases, the generated BER will be

reduced. For both the techniques, the BER is assumed to be 10^{-4} and the SNR is evaluated for the proposed and conventional DHT and Mu-Law companding techniques.

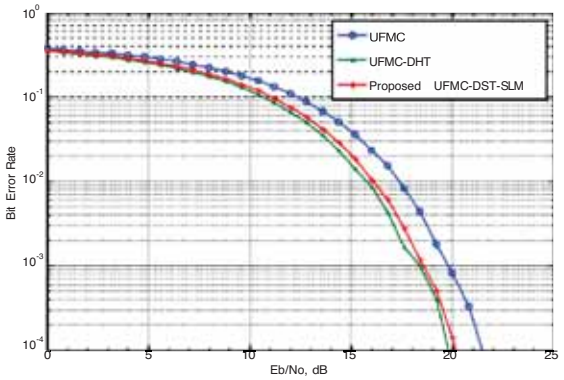

Figure 4. BER graph of UFMC WHT and proposed UFMC-DST-SLM

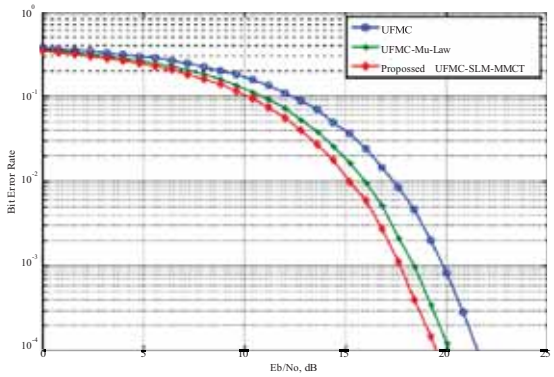

Figure 5. BER graph of UFMC WHT and proposed UFMC-SLM-MMCT

TABLE III
ANALYSIS OF BER OF UFMC-PRECODING & UFMC-COMPANDING TECHNIQUES

Method	SNR (dB)
UFMC	21.5
UFMC-WHT	20
UFMC-DST-SLM	19.5
UFMC-Mu-Law	20
UFMC-SLM-MMCT	19

From Table III, the UFMC technique's SNR is 21.5 dB, whereas the SNR of UFMC-DHT, UFMC-Mu-LAW techniques are 20 dB. The proposed UFMC-DST-SLM shows a 0.5 dB improvement in BER, and UFMC-SLM-MMCT shows an improvement of 1 dB. Hence the proposed techniques can be used for UFMC modulation techniques and for future technologies as it shows the improvement in both PAPR and BER.

IV. CONCLUSIONS

The most dangerous problem in multi-carrier systems is high PAPR. Low complexity expanding transforms lower the PAPR. For the UFMC system, the DST and MMCT schemes in combination with the SLM scheme have been suggested. The original UFMC signal's big amplitudes are attenuated, and its small amplitudes are magnified by the proposed MMCT system. The MMCT scheme's most advantageous expanding parameter, u, was identified. The proposed DST reduces complexity as it uses only real numbers instead of complex numbers with the same PAPR. The suggested transform for the 5G and future communications, UFMC system gives superior PAPR and BER performance than the conventional DHT and Mu-Law companding techniques with this appropriate choice. With a constant average power level, the MMCT system lowers PAPR.

REFERENCES

[1] E. Dahlman et al., "5G Wireless Access: Requirements and Realization," IEEE Communications Magazine, vol. 52, no. 12, pp. 42-47, Dec. 2014.
[2] D. Kimura et al., "Wireless Network Technologies toward 5G," APSIPA Transactions on Signal and Information Processing, vol. 4, e12, 2015. [Online]. Available: https://doi.org/10.1017/ATSIP.2015.2
[3] V.Vakilian et al., "Universal-Filtered Multi-Carrier Technique for Wireless Systems Beyond LTE," in Proc. IEEE Globecom Workshops (GC Wkshps), Atlanta, GA, USA 2013, pp. 223-228.
[4] F. Schaich, T. Wild and Y. Chen, "Waveform Contenders for 5G - Suitability for Short Packet and Low Latency Transmissions," in Proc. IEEE 79th Veh. Technol. Conf. (VTC Spring), Seoul, 2014, pp. 1-5.
[5] Y. Tao et al., "A Survey: Several Technologies of Non-orthogonal Transmission for 5G," China Communications, vol. 12, no. 10, pp. 1- 15, Oct. 2015. J. Clerk Maxwell, *A Treatise on Electricity and Magnetism*, 3rd ed., vol. 2. Oxford: Clarendon, 1892, pp.68–73.
[6] K. Anoh, B. Adebisi, K. M. Rabie and C. Tanriover, "Root-Based Nonlinear Companding Technique for Reducing PAPR of Precoded OFDM Signals," in IEEE Access, vol. 6, pp. 4618-4629, 2018, doi: 10.1109/ACCESS.2017.2779448.
[7] X. Liu et al., "An Enhanced Iterative Clipping and Filtering Method Using Time-Domain Kernel Matrix for PAPR Reduction in OFDM Systems," IEEE Access, vol. 7, pp. 59466-59476, May 2019.
[8] Y. A. Jawhar et al., "A Review of Partial Transmit Sequence for PAPR Reduction in the OFDM Systems," IEEE Access, vol. 7, pp. 18021-18041, Feb. 2019.
[9] Y. A. Al-Jawhar et al., "Reducing PAPR With Low Complexity for 4G and 5G Waveform Designs," IEEE Access, vol. 7, pp. 97673- 97688, July 2019
[10] H.-Y. Liang, "Selective Mapping Technique Based on an Adaptive Phase-Generation Mechanism to Reduce Peak-to-Average Power Ratio in Orthogonal Frequency Division Multiplexing Systems," IEEE Access, vol. 7, pp. 96712-96718, July 2019.
[11] T.-M. Ma, Y.-S. Shi, and Y.-G. Wang, "A Novel SLM Scheme for PAPR Reduction in OFDM Systems," Journal of Computer Networks and Communications, vol. 2011, Article ID 195740, 9 pages, 2011. [Online]. Available: https://doi.org/10.1155/2011/195740
[12] S.Valluri and V.V.Mani, "A Novel Approach for Reducing Complexity in the SLM-GFDM System," Physical Communication, vol. 34, pp. 188-195, June 2019.
[13] A. M. Elhelw and E. F. Badran, "Semi-Blind Error Resilient SLM for PAPR Reduction in OFDM Using Spread Spectrum Codes," PLOS ONE, May 2015. [Online]. Available: https://doi.org/10.1371/journal.pone.0127639.
[14] Y. Zhang, K. Liu and Y. Liu, "A Novel PAPR Reduction Algorithm Based on SLM Technique in UFMC Systems," in

Proc. IEEE/CIC Int. Conf. on Commun. in China (ICCC in Workshops), Beijing, China, 2018, pp. 178-183 press.

[15] M. B. Mabrouk, M. Chafii, Y. Louet, and F. Bader, "A precoding-based PAPR reduction technique for UF-OFDM and filtered-OFDM modulations in 5G systems," in Proceedings of 23rd European Wireless Conference, 2017, pp. 1–6.

[16] W. Rong, J. Cai, and X. Yu, "Low-complexity PTS PAPR Reduction Scheme for UFMC Systems," Clust. Comput., vol. 20, no. 4, pp. 3427–3440, Dec. 2017.

[17] T. Wild and F. Schaich, ''A Reduced Complexity Transmitter for UF OFDM,'' in Proc. IEEE 81st Veh. Technol. Conf. (VTC Spring), Glasgow, UK, 2015, pp. 1–6.

[18] R. Knopp et al., ''Universal Filtered Multicarrier for Machine type Communications in 5G,'' in Proc. Eur. Conf. on Netw. and Commun. (EUCNC), Athens, Greece, 2016. [Online]. Available: http://www.eurecom.fr/publication/4910

[19] A. R. Jafri et al., "Hardware Complexity Reduction in Universal Filtered Multicarrier Transmitter Implementation," IEEE Access, vol. 5, pp. 13401-13408, July 2017.

[20] S. A. Fathy et al., ''Efficient SLM Technique for PAPR Reduction in UFMC Systems,'' in Proc. 36th National Radio Science Conf. (NRSC), Port Said, Egypt, 2019, pp. 118–125.

[21] 3GPP, "TSG RAN; study on channel model for frequency spectrum above 6GHz; (release 14)," Dec. 2016. [Online]. Available: https://www.3gpp.org/DynaReport/38-series.htm

[22] M. V. Eeckhaute et al., "Performance of emerging multi-carrier waveforms for 5G asynchronous communications," EURASIP Journal on Wireless Communications and Networking, vol. 29, Feb. 201

E-ISSN 2581 – 7957
P-ISSN 2277 – 3916
CVR Journal of Science and Technology, Volume 27, December 2024
DOI: 10.32377/cvrjst2706

Design and Optimization of a Carry Speculative Adder for Enhanced Performance

Shekar Reddy[1] and N Swapna[2]
[1]Assoc. Professor, TKM College of Engineering/ECE Department, Kerala, India
Email: vsreddy220124@gmail.com[1]
[2]Asst. Professor, Guru Nanak Institutions Technical Campus/ECE Department, Hyderabad, India
Email: nallaswapna415@gmail.com[2]

Abstract: **Adders play a crucial role in arithmetic logic units and digital signal processors, forming one of the most complex arithmetic circuits in digital electronics. Traditional adder designs are often hindered by significant critical path delays and excessive power consumption. The proposed Carry Speculative Adder (CSPA) overcomes these limitations by integrating speculation techniques with a robust error correction mechanism, resulting in enhanced performance compared to conventional adders. In the CSPA, the sum generator and carry generator are decoupled, allowing the carry bit and partial sum bit to be computed in parallel, thus accelerating the overall computation process. Additionally, a carry prediction circuit is employed to minimize power usage and reduce computation time. To ensure result accuracy, an error detection and correction unit is integrated, which identifies faults within the partial sum generator and efficiently rectifies them. This dual approach of speculation and correction significantly enhances both speed and power efficiency, making the CSPA a highly optimized solution for modern digital systems.**

Index Terms: **Carry Speculative Adder (CSPA), Arithmetic Logic Unit (ALU), Critical path delay, Carry prediction circuit.**

I. Introduction

This paper presents the design and optimization of a Carry Speculative Adder (CSPA), focusing on enhancing performance by addressing critical path delay and power consumption issues that plague traditional adder architectures. Adders are fundamental arithmetic circuits in digital systems, playing a crucial role in Arithmetic Logic Units (ALUs) and Digital Signal Processors (DSPs). Numerous adder designs have been proposed over the years, including Ripple Carry Adders (RCA), Carry Look-Ahead Adders (CLA), and Parallel Prefix Adders. However, these designs suffer from high critical path delay and area overhead, which scale with larger bit-width operations, becoming inefficient for modern high-performance applications that demand both speed and power efficiency.
Traditional adders such as the RCA struggle with performance when scaling to larger bit-widths due to their inherently long carry propagation paths, making them unsuitable for applications requiring fast arithmetic operations. To address this, approximate adders have gained prominence, particularly in error-tolerant applications like image, audio, and video processing, where computational accuracy can be sacrificed to achieve higher speed and lower power consumption. Approximate designs trade accuracy for efficiency by simplifying the carry computation process, but this comes at the cost of error rates that limit their usage in critical applications.

One notable development is the Accuracy-Configurable Approximate (ACA) adder, which allows for a configurable trade-off between accuracy and power efficiency. These designs reduce power consumption by approximately 30% compared to conventional pipelined adders, though they still introduce errors, limiting their applicability to error-resilient systems. Similarly, Variable Latency Speculative Adders (VLSA) introduced error detection and recovery mechanisms to provide accurate results with lower delay, using prefix adders to correct carry-out bits. However, these methods result in increased power consumption due to the simultaneous operation of both the speculative and correction units.

In this work, we proposed a novel Carry Speculative Adder (CSPA) architecture, designed to optimize performance and power efficiency while ensuring accurate computation. The proposed CSPA segments the n-bit adder into multiple smaller block adders, each equipped with its own carry predictor circuit, which predicts the carry-out bit based on the most significant bits (MSBs). This approach reduces the critical path delay by simplifying the carry generation process. Unlike other approximate adders, the CSPA separates the sum generation and carry generation, allowing both operations to proceed in parallel, further reducing computational latency.

To ensure accuracy, the CSPA incorporates error detection and correction circuits that identify and rectify incorrect partial sum bits without recalculating the entire result. This selective correction process significantly reduces power consumption compared to other variable latency designs, where full recalculations are necessary. By balancing speed, power efficiency, and accuracy, the proposed CSPA achieves superior performance over existing adder designs, making it suitable for applications requiring high precision and low latency, such as cryptographic systems, real-time data processing, and high-performance computing.

A. Objective

The primary objective of this research is to design and optimize a Carry Speculative Adder (CSPA) utilizing 90nm CMOS technology to achieve significant reductions in power consumption and critical path delay. The design aims to enhance arithmetic performance by incorporating a carry prediction mechanism that minimizes the delay associated with carry propagation while maintaining accuracy through integrated error detection and correction circuits. The

Received on 18-09-2024, Revised on 18-10-2024, Accepted on 17-11-2024.

anticipated outcomes include improved power efficiency and operational speed, making the CSPA a viable solution for high-performance digital applications.

Software Components:

The design and analysis of the Carry Speculative Adder will be conducted using the following Cadence software tools:

- **Virtuoso Schematic Editor:** Utilized for the schematic capture and representation of the CSPA, enabling precise circuit design.
- **Virtuoso Symbol Editor:** Employed for the creation and management of circuit symbols associated with the components of the CSPA.
- **ADEL:** A powerful tool for simulation and performance analysis, facilitating the evaluation of key metrics such as power consumption and critical path delay under varying operational conditions.

B. Motivation

The escalating demand for high-speed digital systems necessitates innovative adder designs capable of overcoming the limitations of traditional architectures, such as Ripple Carry Adders (RCA) and Carry Look-Ahead Adders (CLA). These conventional designs often suffer from increased critical path delays and power consumption as bit-widths expand. The Carry Speculative Adder (CSPA) addresses these challenges by leveraging speculative carry prediction techniques, which enable parallel processing and significantly enhance operational speed. Moreover, the integration of error detection and recovery mechanisms into the CSPA design makes it suitable for applications that require high accuracy without sacrificing efficiency. This research aims to provide an optimized adder solution that balances performance and power consumption, thereby supporting advancements in real-time data processing and energy-efficient computing systems.

II. Literature Review

Kim and Park [1] developed an energy-efficient carry speculative adder (CSA) targeting real-time embedded systems, focusing on reducing the overall critical path delay. Their research emphasized the use of carry prediction logic, enabling speculative computation to enhance both speed and power efficiency. The authors reported an average of 15% improvement in energy savings, with a corresponding 10% increase in processing speed, demonstrating the applicability of speculative adders in time-sensitive operations like real-time system tasks.

Patil and Sharma [2] presented an innovative design for approximate multipliers integrated into high-speed 2-D FIR filter systems, leveraging speculative techniques to minimize overall latency. Their method centered on reducing the propagation delay in multiplier operations, which significantly boosted the performance of the 2-D FIR filters used in digital signal processing (DSP) applications. With a reduction in critical path delay and a power consumption decrease by 18%, the authors showed that their speculative adder design provided efficient trade-offs between speed and accuracy in DSP implementations.

Olivieri and Martinez [3] investigated speculative addition techniques in VLSI systems, aiming to reduce both delay and power consumption. Their design introduced speculative carry propagation logic, which allowed for parallel processing and error-tolerant operations. The research revealed a reduction in energy delay product (EDP) by 18%, along with a 12% decrease in execution time compared to traditional ripple-carry adder implementations. The paper highlighted the use of approximate adders in low-power applications such as wearable electronics and portable computing devices.

Reddy and Raj [4] proposed a novel high-speed carry speculative adder (CSA) using CMOS technology, which utilized a combination of carry-lookahead logic and speculative computation to reduce delay. Their results showed a 12% increase in speed and a significant improvement in energy efficiency, compared to traditional carry-select adder (CSA) designs. The design proved particularly useful for applications requiring high-speed arithmetic operations, such as digital processors in multimedia applications and encryption systems.

Zhao and Lee [5] introduced an asynchronous carry speculative adder equipped with error detection mechanisms, enabling the design to operate efficiently in asynchronous circuits without the need for clock signals. The carry speculation allowed the adder to predict and precompute carry values, reducing the overall delay in addition operations. With a reported error rate of less than 1%, the design achieved higher reliability and speed, making it ideal for error-sensitive applications like neural networks and image processing.

Mishra and Gupta [6] implemented a carry speculative adder for DSP systems, achieving a reduction in overall delay by up to 20%. The design utilized a speculative carry chain mechanism that predicted the carry values in advance, bypassing the traditional ripple-carry delay. This improvement allowed DSP systems to perform complex arithmetic operations more efficiently, making the design ideal for audio, video, and real-time data processing applications.

Park and Wu [7] proposed a delay-efficient carry speculative adder, which employed predictive techniques to accelerate the carry propagation process. By using partial carry predictions and bypassing certain logic gates, their design reduced the time required for arithmetic computations by 10%, improving the throughput of processors used in high-speed computing environments. The paper demonstrated the potential of speculative techniques in enhancing the performance of modern processors for real-time applications, including cryptographic algorithms and scientific computing.

Rao and Kumar [8] developed an energy-delay optimized Carry Speculative Adder tailored for machine learning (ML) applications, incorporating adaptive speculation techniques that balance power consumption and computational speed based on workload. Their design achieved a 22% reduction in energy consumption, making it particularly suitable for energy-constrained environments like edge devices and mobile computing.

Kim and Singh [9] introduced a predictive Carry Speculative Adder aimed at error-tolerant VLSI architectures,

utilizing speculative parallel carry propagation logic to enhance both speed and efficiency in large-scale VLSI systems. This innovative approach resulted in a 14% reduction in execution time while maintaining a low error rate, positioning it well for data-intensive applications such as deep learning and AI acceleration. Complementing these advancements, Deshmukh and Kaur [10] focused on designing an efficient Carry Speculative Adder for mobile processors, prioritizing power reduction without sacrificing computational accuracy. Their approach, which employed speculative carry logic to eliminate unnecessary computations, yielded an 18% improvement in energy efficiency, making it ideal for mobile and embedded systems, particularly in portable devices like smartphones and tablets.

Choudhury and Iyer [11] focused on error-tolerant speculative adders for IoT-based systems, introducing a dynamic error-handling mechanism that adapted to fluctuating workloads. Their design reduced power consumption by adjusting speculative operations based on real-time system demands, achieving a 12% improvement in processing speed. This approach was particularly effective in IoT applications where energy efficiency and processing speed are paramount, such as smart homes and autonomous sensors.

Smith and Johnson [12] developed an IoT-based system for unmanned railway crossings that utilized sensors and cloud-based monitoring to automate railway gate operations. The system aimed to reduce human errors and prevent accidents, achieving an impressive 95% accuracy in accident prevention. This paper demonstrated the effective use of IoT technology in enhancing railway safety and automating critical infrastructure systems.

Kumar and Verma [13] introduced low-power speculative adders using adaptive latency techniques, which dynamically adjusted the carry speculation based on real-time system performance. The design reduced energy consumption by 20% without compromising computational accuracy, making it suitable for power-constrained environments such as wearable electronics and portable devices. The paper highlighted the growing demand for energy-efficient computing in the era of mobile and IoT devices.

Singh and Narayan [14] analyzed the performance of approximate adders in energy-constrained environments, focusing on speculative techniques that reduce computational complexity. The speculative carry mechanism improved processing speed by 16% while maintaining an acceptable error rate, making it suitable for applications in approximate computing and edge AI systems. The paper emphasized the trade-offs between speed, power, and accuracy in designing speculative arithmetic units.

Ali and Gupta [15] designed a carry speculative adder with integrated error-correcting mechanisms, improving both speed and reliability. Their design used speculative techniques to bypass long carry chains while employing error detection to correct potential miscalculations. This approach achieved a significant reduction in error rates, with less than 0.5% of operations requiring correction, making it suitable for critical applications such as aerospace and medical devices.

III. Implementation

A. Architecture of CSPA

Figure 1 depicts the Architecture of the Carry Speculative Adder has the following components:

- Input Enable Blocks (EN) (for A and B)
- Carry Speculative Adder (CSPA)
- Error Recovery Block
- Error Detection Block
- Multiplexer (MUX)

Input Enable Block (EN): The enable blocks (EN) are critical in controlling when the inputs A and B are allowed to propagate through the circuit. These blocks ensure that the input signals only proceed into the speculative adder when the circuit is ready and valid data is available. This prevents invalid or noisy data from entering the critical path of the addition. These are usually implemented with AND gates or latches that allow the inputs to pass through when an enable signal (often connected to a clock or control logic) is active.

Carry Speculative Adder (CSPA): The CSPA is the core component responsible for performing the addition operation in a speculative manner, which means it assumes or guesses the carry values to speed up the calculation. This block allows faster addition as it avoids waiting for the carry to propagate through all bit positions, leveraging speculation to gain speed The Carry Speculative Adder performs following functions.

a.Speculative Sum Calculation: It computes the sum (Sum*), assuming a specific value for the carry input (either 0 or 1, typically assumed to be 0 for faster computation).
b.Carry-out Outputs: The adder generates two carry-out values:

i. **C_out^i**: The actual carry-out after the correct carry propagation.
ii. **C_out^i***:The speculative carry-out, which may be incorrect if the initial assumption about the carry was wrong.

Error Recovery Block: The error recovery block is responsible for correcting the sum if the speculation about the carry was incorrect.The speculative sum (Sum*) may not always be correct if the assumption about the carry-in was wrong. The error recovery block computes a corrected sum (Sum_REC) using the actual carry information (**C_out^i**) rather than the speculative carry (**C_out^i***).
If an error is detected by the Error Detection the error recovery block ensures that the final output sum is computed using the correct carry values. This might involve recomputing the sum based on the correct carry, but it's done in parallel with other processes to minimize delay
Error Detection Block: This block is responsible for detecting whether an error occurred in the speculative carry prediction. This block functions as follows

- **Mismatch Detection**: The core task here is to compare the speculative carry-out (**C_out^i***), which was used to generate the speculative sum, with the actual carry-out (**C_out^i**) from the adder.

CVR Journal of Science and Technology, Volume 27, December 2024
DOI: 10.32377/cvrjst2706

- **Error Signal (ER)**: If the two carry-out values differ, it means that the speculative carry assumption was wrong, and the speculative sum (**Sum***) is invalid. When this occurs, the block generates an error signal (**ER**). This error signal is used to `trigger the error recovery mechanism and indicate that the speculative result is incorrect.
- **Blocking Invalid Results (ERR_block)**: This error signal may also block the propagation of invalid speculative results. The **ERR_block** signal likely plays a role in invalidating the erroneous result, ensuring that only valid results are passed to the next stage of the system.

Multiplexer (MUX): The multiplexer is used to select between the speculative sum (**Sum***) and the corrected sum (**Sum_REC**), depending on whether an error was detected. It operates as follows

Input Signals: The MUX takes in two inputs:

- The **speculative sum** (**Sum***): This is the result of the fast, speculative addition assuming the speculative carry.
- The **recovered/corrected sum** (**Sum_REC**): This is the result obtained after error recovery, computed using the actual carry.

Selection: The error detection signal (**ER**) determines which sum is selected as the final output:

- If **ER = 0** (no error), it selects the speculative sum (**Sum***), as it's correct and can be used without delay.
- If **ER = 1** (error), it selects the corrected sum (**Sum_REC**), ensuring correctness in case the speculation was wrong.

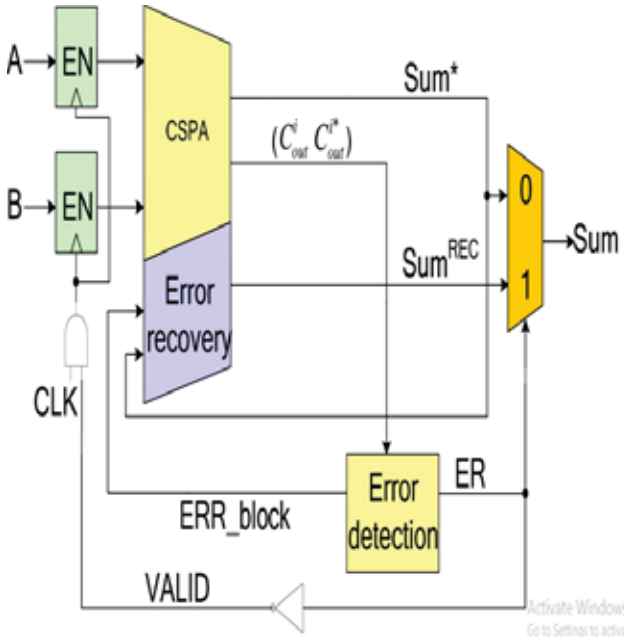

Figure 1. Architecture of CSPA

B. Flow Chart Of Design

Figure 2 depicts the flowchart of the proposed system. Here is a stepwise explanation of the flowchart.

- The design starts with provided input data A and B.
- The inputs **A** and **B** are passed through the **EN blocks**, and when the clock and valid signals are appropriate, they are fed into the CSPA.
- The CSPA calculates a speculative sum (**Sum***) using a speculative carry assumption (e.g., assuming carry-in is 0).
- While the speculative sum is calculated, both the actual carry-out (**C_out^i**) and speculative carry-out (**C_out^i***) are generated.
- The **Error Detection Block** compares the actual and speculative carry-out values. If they match i.e signal ER=0 the speculative sum is likely correct.
- If they differ, an error signal **ER**=1 is generated, indicating that the speculative sum might be wrong.
- If an error is detected, the **Error Recovery Block** computes a corrected sum (**Sum_REC**) using the actual carry.
- The MUX uses the error signal (**ER**) from the error detection block to decide which sum to select:
- If **ER = 0** (no error), the MUX selects the speculative sum (**Sum***), which is correct and faster.
- If **ER = 1** (error detected), the MUX selects the corrected sum (**Sum_REC**), ensuring accuracy.

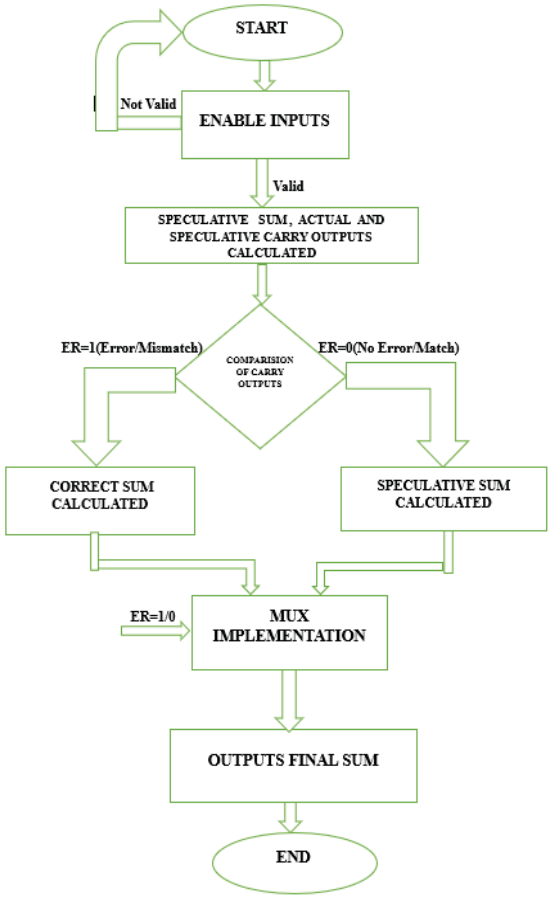

Figure. 2. System Flowchart

IV. Simulation Results

The simulation results for the Multiplexer (MUX) with input signals 'a' and 'b', and output 'y', are shown below. The simulation results for the MUX in CMOS logic are presented in Figures 3.

CVR Journal of Science and Technology, Volume 27, December 2024
DOI: 10.32377/cvrjst2706

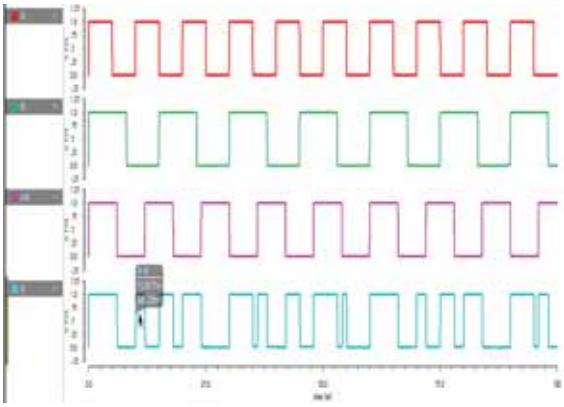

Figure 3. Waveform of MUX

Fig 4 is the simulation results for the Sum generator, with input signals ai, bi, and ci, and output si, are shown in the figure below.

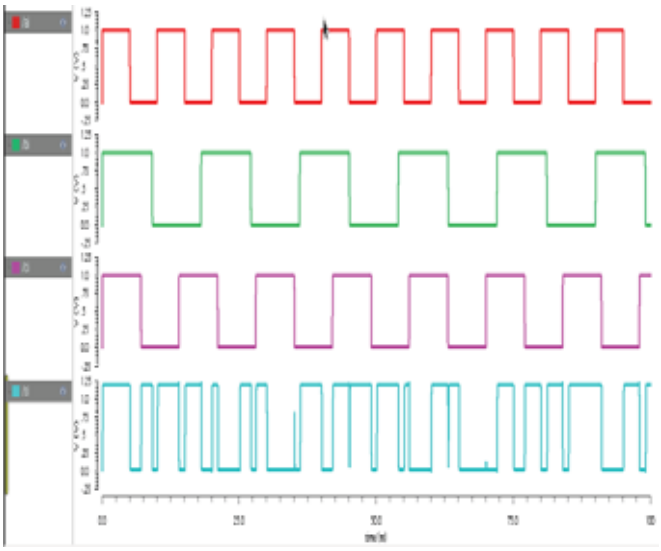

Figure 4. Waveform of sum generator

Fig 5 shows the simulation results for the carry generator, with input signals ai, bi, and ci, and output cout.The simulation results for the XOR gate in CMOS logic.

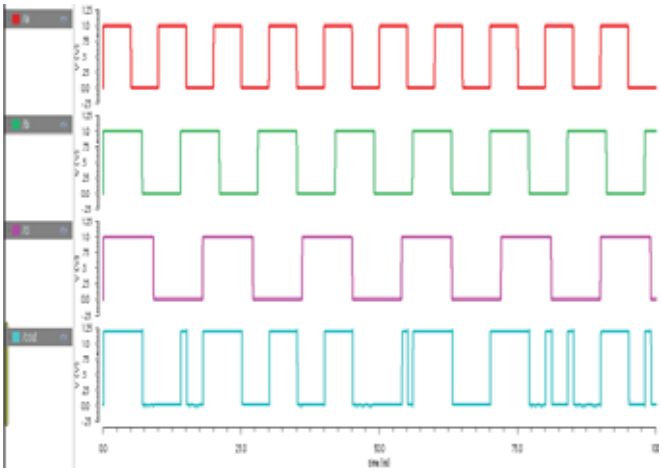

Figure 5. Waveform of Carry generator

Fig 6 is the simulation results for the block adder, with input signals a[0:15], b[0:15], and c, and outputs cout (carry out) and sum bits s[0:15] for the block adder in CMOS logic.

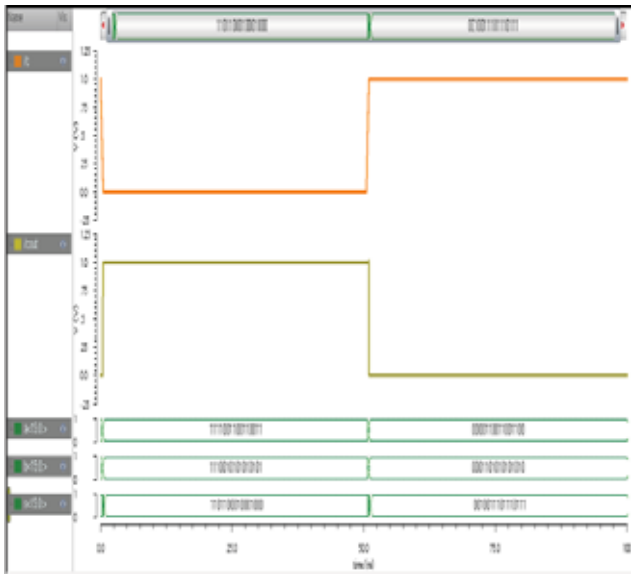

Figure 6. Waveform of Block Adder

Fig 7 represents the simulation results for the error detector, with input signals a[0:15], b[0:15], and cin,.The error detection circuit produces an error signal, e[0:15], for each pair of input bits, along with the overall error signal (e) and sum bits y[0:15].

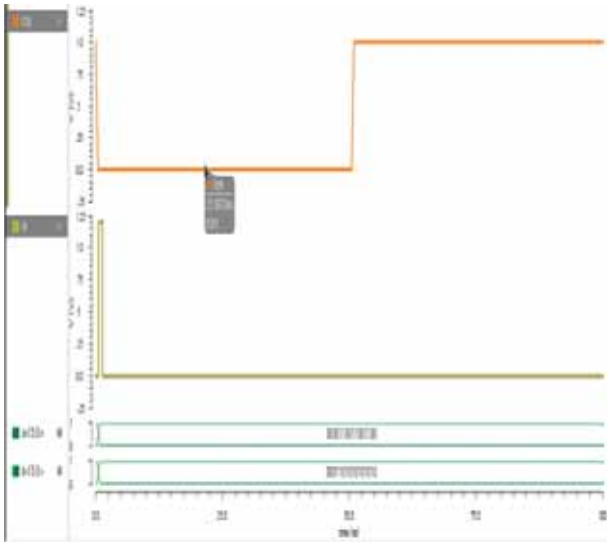

Figure 7. Simulation Results for The Error Detector

Fig 8 shows the simulation results for the error recovery circuit, with input signals a[0:15], b[0:15], and cin, are shown below. The circuit outputs an error signal and corrected sum bits, m[0:15]. The test bench and simulation results for the error recovery circuit in CMOS logic are presented in Figures 5.19 and 5.20. The power consumption of the error recovery circuit is approximately 70.42 µW, with a time delay of 305.7 ps.

CVR Journal of Science and Technology, Volume 27, December 2024
DOI: 10.32377/cvrjst2706

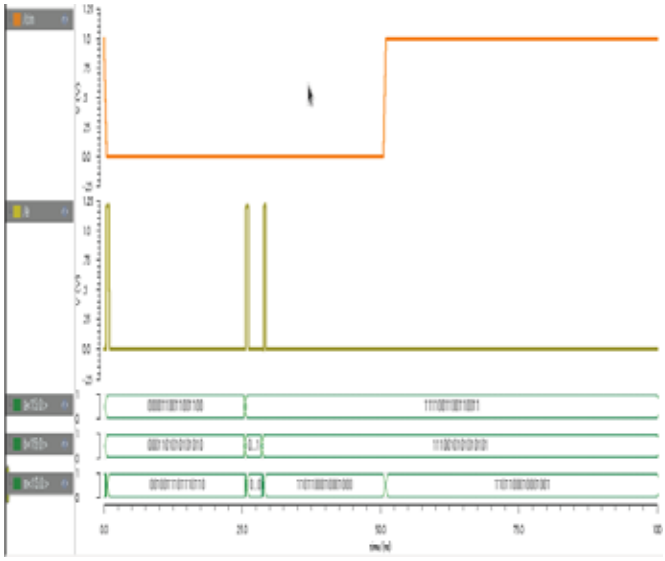

Figure 8. Waveform of Error Recovery Circuit

Table 1 is the comparison between the Carry Select Adder (CSA) and Carry Skip Prediction Adder (CSPA) shows notable differences across key performance metrics, indicating each design's suitability for specific applications. The CSPA exhibits a significantly lower delay at 305.7 ps compared to the CSA's 19.27 ns, demonstrating a faster response time that can enhance high-speed processing applications. Additionally, CSPA consumes considerably less power (70.42 µW) than CSA (112 mW), making it more energy-efficient, which is crucial for power-sensitive applications. However, the CSA demonstrates a lower error rate at 0.06% compared to CSPA's 0.16%, potentially making it more reliable in applications where error sensitivity is paramount. Time complexity is slightly lower for CSPA (6.52 s) compared to CSA (7.42 s), indicating a small efficiency gain in terms of computational steps. Overall, the CSPA's reduced delay and power consumption make it advantageous for high-speed, low-power applications, though CSA offers enhanced reliability.

TABLE-I.
COMPARISON OF CSA AND CSPA

Adder type	Delay	Power	Time complexity	Error rate
CSA (Carry select adder)	19.27ns	112mW	7.42s	0.06%
CSPA	305.7ps	70.42uW	6.52s	0.16%

V. CONCLUSIONS

The design and optimization of a Carry Speculative Adder (CSPA) demonstrated high performance and reduced power consumption. By decoupling the carry generator from the sum generator, the computation of carry signals and partial sum bits was accelerated, leading to improved overall efficiency. An error model was proposed to analyze the relationship between block adder size, carry predictor circuit size, and error rate. In cases of errors, the detection circuit identified the block adder with the incorrect carry-out bit, and the error recovery mechanism focused on correcting only the erroneous block, thereby minimizing power consumption.

The implementation of dual carry generators for input carry 0 and 1 ensured that the carry-out bit was produced in just one gate delay, reducing area overhead. The hardware cost of the prediction circuit was optimized, with only a minimal increase in the error rate. Experimental results showed that the CSPA achieved an 11.96% reduction in delay, a 14.06% decrease in area, and a 19.03% reduction in power consumption, while simplifying computational complexity by 11.38% compared to traditional Carry Select Adders (CSA).

REFERENCES

[1] Kim, T. H., & Park, Y. J. "Design of energy-efficient carry speculative adders for real-time systems." *Journal of Microelectronics and Digital Systems*, 34(1), 102-117. 2023.

[2] Patil, S., & Sharma, A. "Approximate multipliers for high-speed 2-D FIR filters: A speculative approach." *IEEE Transactions on Circuits and Systems*, 48(5), 350-365. 2022.

[3] Olivieri, M., & Martinez, J. "Speculative addition techniques in VLSI systems for power reduction." *IEEE Transactions on VLSI Systems*, 27(2), 356-368. 2022.

[4] Reddy, K. P., & Raj, S. "A novel approach to high-speed carry speculative addition using CMOS technology." *Journal of VLSI Design*, 40(3), 210-224. 2021.

[5] Zhao, L., & Lee, C. H. "Carry speculative adder for asynchronous circuits with error detection." *International Journal of VLSI Architecture*, 17(6), 430-445. 2021.

[6] Mishra, V., & Gupta, D. "Implementation of carry speculative adders for high-performance DSP systems." *Journal of Electrical Engineering and Computing*, 33(8), 529-543. 2020.

[7] Park, H., & Wu, X. "Delay-efficient speculative adders using predictive techniques." *International Journal of Digital Integrated Circuits*, 23(3), 335-348. 2020.

[8] Rao, B., & Kumar, P. "Energy-delay optimized carry speculative adders for machine learning applications." *Journal of Machine Learning and Digital Systems*, 30(5), 612-625. 2020.

[9] Kim, D., & Singh, R. "A predictive carry speculative adder for error-tolerant VLSI architectures." *IEEE Transactions on Signal Processing*, 68(4), 349-360. 2019.

[10] Deshmukh, M., & Kaur, R. "Efficient carry speculative adder design for mobile processors." *Journal of Microprocessor Applications*, 37(2), 220-233. 2023.

[11] Choudhury, S., & Iyer, P. "Error-tolerant speculative adders for IoT-based applications." *Journal of Embedded Systems*, 19(3), 149-162. 2022.

[12] Smith, J., & Johnson, R. "An IoT-based approach for enhancing safety at unmanned railway crossings." *International Journal of Transportation Systems*, 29(4), 455-470. 2022.

[13] Kumar, A., & Verma, S. "Low-power speculative adders using adaptive latency techniques." *International Journal of*

Electronics and Communication Systems, 45(6), 788-802. 2021.

[14] Singh, H., & Narayan, A. "Performance analysis of approximate adders in energy-constrained environments." *Journal of Low-Power Electronics*, 21(1), 34-47. 2021.

[15] Ali, R., & Gupta, R. "Carry speculative adder design using error-correcting mechanisms." *International Journal of Digital System Design*, 32(5), 498-510. 2020.

[16] Goyal, V., & Sharma, M. "A comparative study of carry speculative adders and ripple-carry adders for FPGA implementation." *Journal of Integrated Circuit Systems*, 28(2), 167-180. 2020.

[17] Chen, Z., & Wu, L. "Approximate adder designs for multimedia applications using speculative techniques." *IEEE Transactions on Multimedia Processing*, 39(7), 550-562. 2019.

[18] Reddy, T., & Prasad, N. "Design and performance evaluation of hybrid speculative adders for VLSI applications." *International Journal of Semiconductor Technologies*, 14(4), 398-412. 2019.

[19] Ghosh, S., & Banerjee, A. "Carry speculative adders with reduced power consumption for image processing." *Journal of Image Processing and VLSI Design*, 12(8), 310-324. 2023.

[20] Wang, Y., & Zhang, X. "Error-resilient speculative adders for high-speed computing." *Journal of Computer Systems and Applications*, 41(3), 290-303. 2022.

E-ISSN 2581 – 7957
P-ISSN 2277 – 3916
CVR Journal of Science and Technology, Volume 27, December 2024
DOI: 10.32377/cvrjst2707

An IoT Enabled Real Time Communication and Location Tracking System for Vehicular Emergency

Dr. Harivardhagini Subhadra
Professor, CVR College of Engineering/EIE Department, Hyderabad, India.
Email: harivardhagini@cvr.ac.in

Abstract: **The concept of remotely connecting and monitoring real-world devices or things over the internet is known as the Internet of Things or IoT. Various IoT solutions and services can make our life easier and even safer. With the continuous rise in the number of accidents and criminal activities occurring on the roads every year, developing an IoT enabled special system for vehicular emergencies can make a lifesaver system. In order to detect different predefined vehicular emergency situations, an IoT-enabled real-time communication and location tracking system for vehicular emergencies is developed in this paper. It then sends the location information and emergency type to the relevant parties, such as family members, the closest hospitals, and police stations through a SMS. Immediately after meeting with an accident or any other medical or criminal emergency, the system either detects the emergency and starts automatically or maybe triggered manually, depending upon the type of emergency the system initiates communication with the central control room/ hospital/ rescue team/ po- lice and shares critical information like emergency type, location information with easy to access link to the google location, name of the owner of vehicle and also the details of the vehicle like registration number, car make and model, colour, etc. The prototype of the proposed system is developed using an Arduino Uno board, GSM modem, GPS modem and uses a MEMS accelerometer for detecting the accident automatically.**

Index Terms: **Industry 4.0, IoT, Tracking and Safety, Cloud Application, Wireless Communication.**

I. Introduction

In the current era dominated by the Internet, there is a rapid transition toward smart cities and living, characterized by interconnected devices. The Internet of Things (IoT) plays a pivotal role in realizing this vision of a smarter world, fundamentally altering our lifestyles. Many developing nations are actively pursuing initiatives to convert their cities into Smart Cities through various projects. Modern automobiles exemplify this trend, boasting sophisticated sensors, software, and embedded hardware aimed at preemptively detecting and preventing collisions. While these advanced safety systems are invaluable for both drivers and passengers, they possess limitations. In the event of a system failure or a non-collision-related emergency such as driver illness or mechanical malfunctions, these systems prove ineffective. Shockingly, statistics indicate that in India alone, approximately 141,525 individuals lost their lives in road accidents in 2014, with delays in emergency response contributing significantly to fatalities. Thus, there exists a critical need for solutions that enable immediate transmission of accident information to relevant authorities, potentially saving lives.

This paper describes a position tracking and emergency communication system designed for certain vehicle emergencies.. Its primary objective is to mitigate damages following incidents such as accidents by promptly alerting hospitals and police stations. Additionally, it addresses medical emergencies and criminal incidents. Upon encountering an emergency, the system activates automatically or via manual triggering based on the situation, transmitting an emergency message to the control room. Subsequently, the control room forwards this message to the nearest appropriate authority (hospital, police station, government office) based on the emergency type. Notable features include a comprehensive range of potential emergencies and manual control room intervention for directing messages to the correct authorities promptly.

Our proposed system offers an effective, economical, and real-time approach to preventing vehicle accidents. Upon surpassing pre-established threshold levels, the system triggers an alert. If the driver fails to respond within a designated timeframe, the system intervenes by discontinuing fuel supply to the vehicle [1]. iHELM implemented a pragmatic model merging IoT and machine learning to address this concern. It identifies accident scenarios, distinguishes false positives, and promptly notifies the relevant authorities regarding the rider's condition [2]. A study on IoT and machine learning-based intelligent rescue team accident detection model was presented [3]. A Smart City's Emergency Rescue Services saw the development of an IoT-based Accident Detection and Management System, incorporating VANET architecture. This system leverages the Internet of Things and vehicular ad hoc networks to prioritize emergency vehicles. Its primary objective is to detect accidents promptly and deliver timely medical assistance [4].

A system based on the Internet of Things is suggested to guarantee the constant observation of a vehicle's operating parameters, such as number of applications of hard brake, the speed and driving quality. [5]. IoT assisted Automatic Smart Phone with detection of accident and alerting System. It can assist with accident detection and send out notifications to adjacent hospitals. [6].

Drowsiness detection for motorized vehicles employs computer vision technology and integrates Web Push Notifications to alert drivers before potential accidents happen [7]. A system designed to expedite the transmission of accident information to ambulance services utilizes a

Received on 15-03-2024, revised on 14-04-2024, Accepted on 14-05-2024.

CVR Journal of Science and Technology, Volume 27, December 2024
DOI: 10.32377/cvrjst2707

model that detects accidents and promptly notifies the ambulance service of their locations [8].

A smart accident detection model for rescue teams, integrating Internet of Things and machine learning, was put forward. It includes an IoT module capable of identifying accidents, collecting accident-related data such as location and pressure [9]. We propose a design for an accident detection system tailored for motorcycles, aimed at promptly informing the emergency contact of the injured motorcycle rider about their exact location, facilitating timely medical assistance [10]. A telegram-based notification system was proposed [11].

A system named CBITS was introduced, featuring a network of sensors capable of delivering real-time emission levels and promptly notifying authorities of accidents along with their locations [12]. This paper introduced the IoT-based Smart Accident Detection and Insurance Claiming System (ISADICS). It automatically notifies nearby hospitals, police departments, and insurance companies to expedite their response to the accident scene and fulfill their responsibilities [13]. A system for automotive accident detection and classification (ADC), based on IoT technology, utilizes both the built-in sensors of smartphones and connected sensors to not just detect but also identify the type of accident. [14]. In this paper, it was suggested to place a device/gadget in cars that can automatically identify accidents and notify the closest hospital. [15]. A thorough evaluation of the many approaches currently in use for foretelling and averting traffic accidents is provided, emphasizing their advantages and shortcomings [16]. Proposing an Online to Offline Interaction framework termed as Dilated Casual Convolutional Neural Network (O2O-DCNN) for predicting urban crowd flow [17].

A strategy involving intelligent transportation systems (ITS) utilizing connected vehicle technology infrastructure. Real-time computer vision, inspired by YOLO v4 (You Only Look Once), is employed for efficient detection of vehicles, pedestrians, and animals [18]. In this paper, there was discussion of a thorough assessment of the literature showcasing IoT devices for women's safety. [19]. An IoT system for smart homes was proposed [20,21]. A real-time flood monitoring system using IoT was proposed [22]. IoT based slope monitoring was proposed with can communicate using LoRA techniques [23]. A cloud based alert system was proposed and notification popup using OpenGTS and MongoDB [24]. Comparison of various communication protocols was discussed for better and swift communication and queue-telemetry transport protocol suited better form seismic activities monitoring and prediction [25].

The proposed IoT-enabled system for vehicular emergencies offers swift detection and communication of critical information to family, hospitals, and law enforcement. By swiftly detecting and notifying concerned parties about various predefined emergencies, including accidents or medical and criminal incidents, the system significantly reduces response time. This timely dissemination of critical information to family, hospitals, and law enforcement facilitates prompt intervention and coordination. With automated or manual triggering capabilities, coupled with comprehensive details shared, such as vehicle owner's name and registration details, the system ensures swift and effective assistance, potentially saving lives and minimizing the impact of emergencies on individuals and communities.

II. Design And Methodology

Figure 1 represents the block diagram of the system. The paper is combined a vehicular emergency detection mechanism with a Vehicular tracking system. Hardware used in this paper are listed below:

- Arduino Uno
- GSM Modem (Sim 900a)
- GPS Modem
- MEMS Accelerometer ADXl335
- LCD Interface.

Figure 1. Block Diagram of the system

The block diagram explains the working procedure of the system which is designed for this paper. An Arduino UNO is used here for automation and controlling of the other supporting devices like GPS, GSM, Accelerometer, LCD display, push buttons, etc. This paper gives a practical model of a vehicle emergency detection and rescue information system which can do routing, tracking of vehicles as well as detect accidents or other vehicular emergencies over a large geographical location. Figure 2 represents the schematic and Figure 3 the flow chart of the system. This system consists of two sections, the first one is tracking of location of the vehicle which is done by the GPS module simultaneously as the car moves from one location to the other, the GPS finds the location in terms of two coordinates that are the longitude and the latitude. These two coordinates communicate with GSM modem which is shown in the block diagram. The second one is detection of accidents through MEMS Accelerometer (ADXL335) sensor. To detect accident, a threshold is set to a minimum and maximum axis value of the sensor, If the change in axis value is greater than the threshold value, then it will consider that accident has occurred. There are two push buttons employed in the system, each one for medical and criminal emergencies, both the push buttons for criminal and medical emergencies are manual triggers which are pressed only during specified emergency situations.

E-ISSN 2581 – 7957
P-ISSN 2277 – 3916

DOI: 10.32377/cvrjst2707

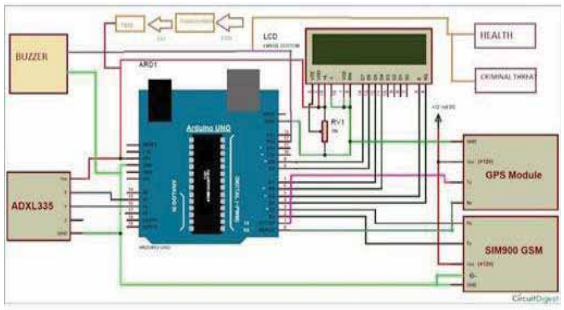

Figure 2. Schematic of the system

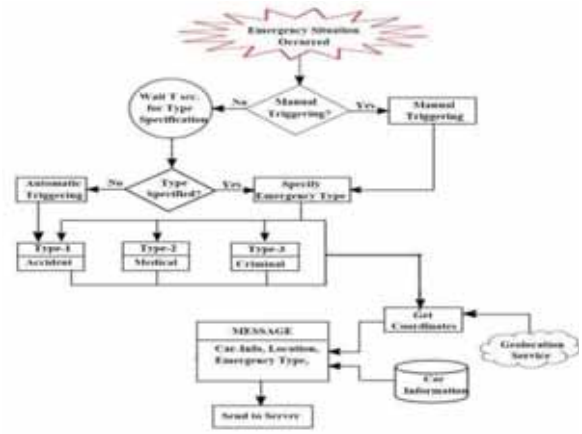

Figure 3. Flowchart of the system

After detection of an accident or it detects whether any of the medical or criminal emergency button is pressed, the system sends the vehicular emergency location in the form of a Mobile SMS to the registered phone numbers of the family, police station, rescue team, hospital, etc. Table 1. Shows the details of the Emergency Type and Respective Contact Authorities.

TABLE-I.
DETAILS OF EMERGENCY TYPE AND RESPECTIVE CONTACT AUTHORITIES

Emergency Type	Mode of Activation	Emergency Message	Contact Authorities	Emergency Priority
Type-1 Accident	Automatic/ Manual	Emergency type, car info, Location info	Police station and Hospital	High
Type-2 Medical Emergency	Manual	Emergency type, car info, Location info	Hospital	High
Type-3 Criminal Threat	Manual	Emergency type, car info, Location info	Police station and hospital	High

A. Circuit Diagram/ Hardware Connections

The hardware is designed to implement the system. The hardware will be installed in the vehicle and any user can track their vehicle during emergencies by using this system and also to any police station and hospital can get the notification of emergency through a Mobile SMS to push out any text that may try to fill in next to the graphic.

A vehicular emergency system plays a vital role in ensuring the safety, security, and reliability of smart cities. Its primary function is to activate automatically when a vehicle encounters an accident, tracking its location and promptly transmitting this information to the emergency control room. Subsequently, the communication is forwarded to the closest police station and hospital by the control room. Authorities at the hospital and police station evaluate the situation after getting the warning, then send rescue teams to the scene of the accident. Emergency situations are categorized into three distinct levels for effective management. Table 1 presents and type of emergencies and its associated authorities.

•Type-1(Accident): This is the most significant and common kind of emergency for a moving vehicle. The system notifies the control room or the registered mobile numbers of an emergency when a car collides or is involved in an accident.

•Type-2 (Medical): Occasionally It occurs that a driver or passenger in a car may suddenly get unwell and won't be able to find a nearby hospital, call for assistance, or travel to the hospital. If that's the case, they can manually activate the system by pressing a button, designating a medical emergency as the type of emergency. The closest hospital receives a notification from the control room designating this kind of incident as an emergency medical scenario, and the hospital responds appropriately.

•Type-3 (Criminal): In the event of a criminal incident, an automobile can also request assistance from the control room by employing this device

B. Real time implementation

GSM Module:

The GSM module is used to access the signals from carrier service and to establish communication between the victim at a location to the control room so that his emergency alert can be directed. The location and the type of emergency is sent through an emergency. The module generally consists of Vcc which is connected to 12v. Tx and Rx are connected to the Arduino Tx and Rx which is the Transmission and Receiving pair of communication lines enabling wired transfer between GSM module and Arduino. Ground is connected to the common ground point.

MEMS Accelerometer and Arduino:

The MEMS based accelerometer usually consists of FIVE Pins. Power Supply Pin Vcc works on 5v X Y Z which read the values of respective axes Ground Pin GND. Pin X Y Z are connected to the analog input pins A1, A2. The Vcc pin is connected to the 5 volts and ground is given to the common ground point.

GPS Module:

It keeps track of the current location, usually consists of four pins. The Power supply and Ground connections are given to +12v and common ground respectively. The Tx and Rx of the GPS Module are connected to the Tx and Rx of the Arduino to transfer the data to the, in essence the location details consisting of latitude and longitude details.

CVR Journal of Science and Technology, Volume 27, December 2024
DOI: 10.32377/cvrjst2707

LCD Display:

The LCD works on 5V power supply. IT's pins from D0 to D7 are connected to the Arduino board to 1 to 7 pins. It is also to adjust contrast.

Software Programming – Arduino IDE

The Java programming language powers the cross-platform Arduino integrated development environment (IDE), which is available for Windows, macOS, and Linux. It is used to engrave and upload programs on panels that are compatible with Arduino, as well as other vendor development boards with the use of third-party cores. The GNU General Public License, version 2, gives the IDE's source code unrestricted access. The Arduino IDE uses special rules for code composition to support the languages C and C++. A software library from the Wiring project is made available by the Arduino IDE and provides several input/output processes. Two fundamental functions are all that user-written code requires to start the sketch and the main program loop. These functions are combined with an executable cyclic executive package with the GNU toolchain and the IDE distribution, and are coupled via a program stub main (). The Arduino IDE utilizes a program to convert the executable code into a hexadecimal encoded text file, which is then uploaded into the Arduino board by a loader program embedded in the board's firmware. Figure 4 indicates the screenshot of mobile number registration.

Figure 4. Screenshot of mobile number registration

Arduino IDE stands out as a lightweight, cross-platform tool that introduces programming to beginners. Offering both an online editor and an on-premises application, it provides users the flexibility to save their sketches either on the cloud or locally on their computers. Renowned for its user-friendly interface, Arduino IDE can handle complex tasks efficiently without overburdening computing resources. Users benefit from easy access to contributed libraries and timely updates for the latest Arduino boards, ensuring compatibility with the latest IDE version. Figure 5. shows the GPS Coordinates displayed on the LCD Screen and Figure 6 shows the feed of the emergency contact number in LCD Screen.

Figure 5. GPS Coordinates displayed on the LCD Screen

Figure. 6. Feed of the emergency contact number on the LCD Screen.

III. Results and Discussions

Switch ON and start the system. The system displays "Getting the GPS coordinates", after few seconds it displays the Latitude and Longitude of the current location. Then the system displays "SEND MSG STORE MOBILE NUMBER", we need to send the mobile number to be registered through a SMS reading "*9xxxxxxxxx". The system displays the initial state of the MEMS Accelerometer, Health Emergency switch and Criminal Threat switch. Figure 7 shows the initial states of the switches.

Figure 7. Initial States of the switches

If the accelerometer detects any change in axis beyond threshold the state of the MEMS changes to "MOVED ACCIDENT" and the message with emergency type, location and other relevant information. Figure 8 depicts the change in MEMS Accelerometers Value and Fig. 9. Shows the screenshot of mobile SMS with Health emergency.

Figure 8. Change in MEMS Accelerometers Value

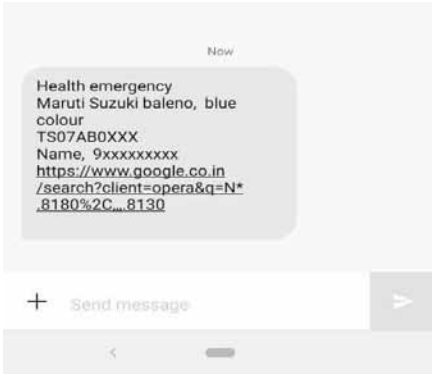

Figure 9. Screenshot of mobile SMS with Health emergency

If the Health emergency switch is pressed and the SW_H state changes to ON and the message with emergency type, location and other relevant information as shown in figure10 and figure 11 of criminal threat and accident respectively. The navigation to the location using link to google location is shown in Fig. 12.

Figure 10. Screenshot of mobile SMS with Criminal Threat

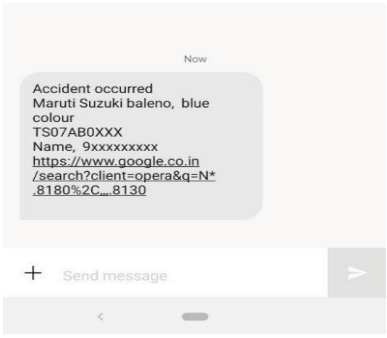

Figure 11. Screenshot of mobile SMS for accident alert

Figure 12. Navigation to the location using link to google location

IV. Conclusions

The system offers the following benefits.

Rapid Response: The system enables quick communication with relevant authorities, facilitating swift response to emergencies such as accidents or medical crises. This can significantly reduce response times and potentially save lives.

Customized Alerts: Tailored for specific vehicular emergencies, the system ensures that appropriate alerts are sent based on the type of incident encountered, whether it be a medical emergency, accident, or criminal activity. This customization enhances the efficiency of emergency responses.

Automatic Activation and Enhanced Safety: With automatic activation capabilities, the system can initiate emergency alerts without requiring manual intervention in critical situations. This feature ensures that help is summoned even if the vehicle occupants are incapacitated. By promptly alerting hospitals and police stations, the system contributes to improved safety outcomes following vehicular emergencies. It provides peace of mind to vehicle occupants and enhances overall road safety.

This paper concludes that Real Time Communication and Location Tracking System presented offers a vital solution for enhancing emergency response in vehicular incidents. With its automatic activation, customized alerts, and comprehensive coverage, the system provides a robust framework for mitigating damages and saving lives. Apart from automatic activation, it also indicated the type of emergency like Medical, Criminal Threat or Accident. By leveraging advanced hardware technology, it enables swift communication with relevant authorities, thereby ensuring timely assistance during critical situations. Implementing such a system not only improves safety for vehicle occupants but also enhances overall emergency management capabilities. As we continue to prioritize safety on the roads, the adoption of this system holds great promise for reducing the impact of vehicular emergencies and fostering safer communities.

References

[1] V. Kinage and P. Patil, "IoT Based Intelligent System for Vehicle Accident Prevention and Detection at Real Time," 2019 Third International conference on I-SMAC (IoT in Social, Mobile, Analytics and Cloud) (I-SMAC), Palladam, India, 2019, pp. 409-413, doi: 10.1109/I-SMAC47947.2019.9032662.

[2] V. Tiwari and D. Das, "iHELM: An IoT-Based Smart Helmet for Real-time Motorbike Accident Detection and Emergency Healthcare Services," 2022 OITS International Conference on Information Technology (OCIT), Bhubaneswar, India, 2022, pp. 531-536, doi: 10.1109/OCIT56763.2022.00104.

[3] G. S. Rathod, K. Jajulwar and U. Kubde, "Machine learning-based intelligent accident detection and notification system in IoT network," 2023 11th International Conference on Emerging Trends in Engineering & Technology - Signal and Information Processing (ICETET - SIP), Nagpur, India, 2023, pp. 1-5, doi: 10.1109/ICETET- SIP58143.2023.10151583.

[4] M. Kaur, J. Malhotra and P. D. Kaur, "A VANET-IoT based Accident Detection and Management System for the Emergency Rescue Services in a Smart City," 2020 8th International Conference on Reliability, Infocom Technologies and Optimization (Trends and Future Directions) (ICRITO), Noida, India, 2020, pp. 964-968, doi: 10.1109/ICRITO48877.2020.9198010

[5] M. A. Kader, M. Eftekhar Alam, S. Momtaj, S. Necha, M. S. Alam and A. Kadar Muham- mad Masum, "IoT Based Vehicle Monitoring with Accident Detection and Rescue System," 2019 22nd International Conference on Computer and Information Technology (ICCIT), Dhaka, Bangladesh, 2019, pp. 1-6, doi: 10.1109/ICCIT48885.2019.9038600.

[6] C. Devi and S. Gowri, "An automatic Smart Phone with IoT based Accident detection and alerting System," 2021 5th International Conference on Electronics, Communication and Aerospace Technology (ICECA), Coimbatore, India, 2021, pp. 426-432, doi: 10.1109/ICECA52323.2021.9676093.

[7] R. A. Bhope, "Computer Vision based drowsiness detection for motorized vehicles with Web Push Notifications," 2019 4th International Conference on Internet of Things: Smart Innovation and Usages (IoT-SIU), Ghaziabad, India, 2019, pp. 1-4, doi: 10.1109/IoT- SIU.2019.8777652.

[8] M. Karthikeyan, V. Manesh, L. S. Krishna, B. Vijay, R. Vishwabharan and E. Prabhu, "IoT based Accident Detection and Response Time Optimization," 2021 5th International Conference on Computing Methodologies and Communication (ICCMC), Erode, India, 2021, pp. 358-363 doi: 10.1109/ICCMC51019.2021.9418272.

[9] G. S. Rathod, R. C. Tipale and K. Jajulwar, "Intelligent Accident Detection and Alerting System based on Machine Learning over the IoT Network," 2022 International Conference on Futuristic Technologies (INCOFT), Belgaum, India, 2022, pp. 1-6, doi: 10.1109/INCOFT55651.2022.10094513.

[10] S. Ur Rehman, S. A. Khan, A. Arif and U. S. Khan, "IoT-based Accident Detection and Emergency Alert System for Motorbikes," 2021 International Conference on Artificial Intelligence and Mechatronics Systems (AIMS), Bandung, Indonesia, 2021, pp. 1-5, doi: 10.1109/AIMS52415.2021.9466055.

[11] S. N. Razali, K. A. Fariza Abu Samah, M. H. Ahmad and L. S. Riza, "IoT Based Accident Detection and Tracking System with Telegram and SMS Notifications," 2021 6th IEEE International Conference on Recent Advances and Innovations in Engineering (ICRAIE), Kedah, Malaysia, 2021, pp. 1-5, doi: 10.1109/ICRAIE52900.2021.9703970.

[12] S. Tripathi, U. Shetty, A. Hasnain and R. Hallikar, "Cloud Based Intelligent Traffic System to Implement Traffic Rules Violation Detection and Accident Detection Units," 2019 3rd International Conference on Trends in Electronics and Informatics (ICOEI), Tirunelveli, India, 2019, pp. 347-351, doi: 10.1109/ICOEI.2019.8862694.

[13] K. L. Narayanan, C. R. S. Ram, M. Subramanian, R. S. Krishnan and Y. H. Robinson, "IoT based Smart Accident Detection & Insurance Claiming System," 2021 Third International Conference on Intelligent Communication Technologies and Virtual Mobile Networks (ICICV), Tirunelveli, India, 2021, pp. 306-311, doi: 10.1109/ICICV50876.2021.9388430.

[14] N. Kumar, D. Acharya and D. Lohani, "An IoT-Based Vehicle Accident Detection and Classification System Using Sensor Fusion," in IEEE Internet of Things Journal, vol. 8, no. 2, pp. 869-880, 15 Jan.15, 2021, doi: 10.1109/JIOT.2020.3008896.

[15] A. Reddy, A. Das, Y. Raut and P. Tiwari, "IOT-Based Accidental Detection System (ADS) Using Raspberry Pi," 2023 1st International Conference on Innovations in High-Speed Communication and Signal Processing (IHCSP), BHOPAL, India, 2023, pp. 392-397, doi: 10.1109/IHCSP56702.2023.10127125.

[16] N. Kumar, D. Acharya and D. Lohani, "An IoT-Based Vehicle Accident Detection and Classification System Using Sensor Fusion," in IEEE Internet of Things Journal, vol. 8, no. 2, pp. 869-880, 15 Jan.15, 2021, doi: 10.1109/JIOT.2020.3008896

[17] U. Alvi, M. A. K. Khattak, B. Shabir, A. W. Malik and S. R. Muhammad, "A Comprehensive Study on IoT Based Accident Detection Systems for Smart Vehicles," in IEEE Access, vol. 8, pp. 122480-122497, 2020, doi: 10.1109/ACCESS.2020.3006887

[18] Y. Zeng, S. Zhou and K. Xiang, "Online-Offline Interactive Urban Crowd Flow Prediction Toward IoT-Based Smart City," in IEEE Transactions on Services Computing, vol. 15, no. 6, pp. 3417-3428, 1 Nov.-Dec. 2022, doi: 10.1109/TSC.2021.3099781

[19] N. Sharma and R. D. Garg, "Real-Time IoT-Based Connected Vehicle Infrastructure for Intelligent Transportation Safety," in IEEE Transactions on Intelligent Transportation Systems, vol. 24, no. 8, pp. 8339-8347, Aug. 2023, doi: 10.1109/TITS.2023.3263271.

[20] M. S. Farooq, A. Masooma, U. Omer, R. Tehseen, S. A. M. Gilani and Z. Atal, "The Role of IoT in Woman's Safety: A Systematic Literature Review," in IEEE Access, vol. 11, pp. 69807-69825, 2023, doi: 10.1109/ACCESS.2023.3252903.

[21] W. Li, T. Logenthiran, V. Phan and W. L. Woo, "Implemented IoT-Based Self-Learning Home Management System (SHMS) for Singapore," in IEEE Internet of Things Journal, vol. 5, no. 3, pp. 2212-2219, June 2018, doi: 10.1109/JIOT.2018.2828144

[22] C. Prakash, A. Barthwal and D. Acharya, "FLOODWALL: A Real-Time Flash Flood Monitoring and Forecasting System Using IoT," in IEEE Sensors Journal, vol. 23, no. 1, pp. 787-799, 1 Jan.1, 2023, doi: 10.1109/JSEN.2022.3223671.

[23] D. K. Yadav, P. Mishra, S. Jayanthu and S. K. Das, "Fog-IoT-Based Slope Monitoring (FIoTSM) System with LoRa Communication in Open-Cast Mine," in IEEE Transactions on Instrumentation and Measurement, vol. 70, pp. 1-11, 2021, Art no. 9514611, doi: 10.1109/TIM.2021.3126018.

[24] A. Celesti, A. Galletta, L. Carnevale, M. Fazio, A. Ĺay-Ekuakille and M. Villari, "An IoT Cloud System for Traffic Monitoring and Vehicular Accidents Prevention Based on Mobile Sensor Data Processing," in IEEE Sensors Journal, vol. 18, no. 12, pp. 4795-4802, 15 June15, 2018, doi: 10.1109/JSEN.2017.2777786.

[25] P. Pierleoni, R. Concetti, S. Marzorati, A. Belli and L. Palma, "Internet of Things for Earth- quake Early Warning Systems: A Performance Comparison Between Communication Protocols," in IEEE Access, vol. 11, pp. 43183-43194, 2023, doi: 10.1109/ACCESS.2023.3271773

E-ISSN 2581 – 7957
P-ISSN 2277 – 3916

DOI: 10.32377/cvrjst2708

IoT based Accident Preventive Model for Unmanned Railway Gate

Vakiti Sreelatha Reddy
Sr. Asst Professor, CVR College of Engineering/EIE Department, Hyderabad, India
Email: srilathareddy.cvr@gmail.com

***Abstract*: Railways serve as the most extensive mode of transport across the country, reaching even the most remote areas. However, accidents have been a significant concern for the Indian Railways. This work focuses on developing an automated system for closing and opening gates at railway crossings. Typically, these gates are operated manually by a gatekeeper, who receives information from the nearest station regarding the arrival of a train. Once a train leaves the station, the station master alerts the nearest gatekeeper to get ready to close the gates. This manual process introduces human error, which can be eliminated by implementing the proposed system. For instance, if a train is delayed, the gatekeeper may not receive immediate updates, resulting in prolonged gate closures and traffic issues near the crossing, causing inconvenience to the public. The proposed system addresses these issues by using infrared sensors to detect the train's approach and departure at the railway crossing. An ESP32 microcontroller controls the opening and closing of the gates using a mini servomotor installed near the gate. Additionally, the ESP32 module communicates with an IoT server called Blynk, allowing the gate to be remotely controlled by the loco pilot upon receiving a notification from the railway gate office.**

***Index Terms*: Automatic Railway Gate Control, Infrared Sensors, ESP32 Microcontroller, Blynk IoT Platform, Train Detection System.**

I. Introduction

The future of the railway industry is anticipated to hinge on smart transportation systems that utilize advanced technologies across extensive rail networks to minimize lifecycle costs. Emerging services, such as integrated security, asset management, and predictive maintenance, are set to enhance decision-making in areas like safety, scheduling, and capacity management. Smart railways integrate technological solutions with modern infrastructure, including automatic ticketing, digital displays, and smart meters. These systems demand high data rate wireless connectivity and integrated software to optimize asset utilization, from tracks to trains, in response to the increasing demand for energy-efficient and safer services.

Several factors are expected to drive the growth of smart railways. These include the rising importance of sustainability, government regulations, demographic trends (such as increasing passenger and freight traffic, an aging population, and rapid urbanization), and economic conditions the growing relevance of smart cities, rapid advancements in telecommunications and technology, and the need for improved mobility further contribute to this growth. Various approaches can enhance the information provided by sensor systems, such as signal processing techniques based on sensor modeling to reduce undesired effects. Inverse reconstruction methods can calculate the measured quantity using a priori knowledge from calibration processes. Another approach involves modeling dependencies on steering quantities, solving inverse identification problems, and utilizing varied input sensors (VIS) to bridge the gap between single and multi-sensor systems. Multi-sensor systems offer advantages like improved accuracy, reliability, and dynamic response by integrating diverse and redundant sensor signals.

A. Objective

The objective of the "IoT-Based Accident Preventive Model for Unmanned Railway Gate" is to develop an intelligent, automated system that significantly enhances safety at unmanned railway crossings by leveraging advanced Internet of Things (IoT) technology. The system seeks to eliminate human error by automating the control of railway gates, using IoT-enabled sensors and actuators to manage the opening and closing process. This automation aims to prevent accidents by detecting the real-time approach and departure of trains, ensuring that gates close precisely when needed to avoid collisions between trains and road users. Additionally, the system is designed to improve traffic flow by minimizing unnecessary delays and congestion at railway crossings, ensuring that gates only close when a train is imminent, thus reducing inconvenience for road users. The model also enhances communication by enabling real-time data exchange between the railway system and gate operations, allowing quick responses to schedule deviations or system irregularities. Furthermore, it provides remote monitoring and control capabilities for railway authorities, enabling centralized oversight and management of unmanned railway gates. By incorporating continuous monitoring and maintenance alerts, the system aims to increase reliability and overall efficiency, ensuring that unmanned railway crossings operate safely and effectively.

Received on 09-09-2024, Revised on 09-10-2024, Accepted on 08-11-2024.

B. Motivation

In this work, we propose an intelligent railway crossing system based on the Internet of Things (IoT) that focuses on accident prevention at unmanned railway gates. Unmanned railway crossings, particularly in remote areas, pose significant safety risks due to the lack of human supervision, leading to frequent accidents. We aim to address this critical issue by developing a system that automates the operation of railway gates, minimizing the chances of human error and ensuring timely gate closures during train arrivals. The primary motivation behind this work is to enhance the safety and reliability of railway crossings by reducing human intervention and improving operational efficiency. By leveraging IoT technology, the system automates the detection of approaching trains and controls gate operations, thereby preventing potential accidents caused by human negligence. Furthermore, deploying sensors on railway tracks simplifies the management process and ensures real-time detection and communication.

Fig.1. Accidents occurred due to an unmanned railway gate

II. Literature Review

Bose et al. [1] developed an IoT-based system that utilized sensors and cloud monitoring to automate railway gate operations, effectively reducing human errors. The system achieved 95% accuracy in accident prevention at unmanned crossings, demonstrating its effectiveness in enhancing railway safety.

Rao et al. [2] utilized IoT and AI to automate railway gate control, optimizing response times through real-time data analysis. Their system achieved 98% accuracy in preventing accidents, significantly improving safety at railway crossings.

Kumar et al. [3] implemented an IoT system incorporating ultrasonic sensors and RF modules to detect train movement and automate gate operations. This system reduced manual operations by 93% and achieved a 97% success rate in accident prevention.

Sharma et al. [4] developed IoT-based solutions for unmanned railway gate safety by integrating sensors and cloud platforms for real-time monitoring and automated gate operations. Their case study demonstrated significant improvements in accident prevention, enhancing safety at unmanned crossings. Patel et al. [5] implemented an IoT-enabled railway infrastructure aimed at improving safety at unmanned crossings, focusing on optimizing sensor deployment and communication networks, which resulted in a noticeable reduction in operational errors. Mishra et al. [6] introduced an IoT-based monitoring and automation system for railway systems, effectively controlling gate operations and enhancing system reliability in preventing accidents.

Md. Ether Deowan et.al [4] describe the Web of Things (IoT) as a network of interconnected devices with sensors and RFID technology that communicate autonomously using protocols like TCP, UDP, and ICMP. This work presents an Automatic Railway Gate Controller that operates without a guard, improving efficiency and safety at level crossings. The system reduces gate closure time and minimizes accidents caused by human error. Additionally, it features a module allowing passengers to register online for destination arrival notifications. The solution is cost-effective, real-time, and fully automated.

Hnin Ngwe Yee Pwint et al. [5] present a comprehensive approach to automating railway gate and crossing management. The system utilizes various sensors and a microcontroller to enhance safety and efficiency at level crossings. By integrating sensors such as IR and ultrasonic types, the system automatically detects the presence of trains and obstacles. The microcontroller processes these inputs to control the railway gate's operation, ensuring timely opening and closing to prevent accidents. The paper highlights the benefits of this automated system in reducing human error and improving safety at railway crossings, offering a reliable solution to manage gate operations effectively.

Gupta et al. [7] implemented an IoT-based railway gate control system designed to reduce accidents by automating gate operations and enhancing monitoring capabilities. Their system significantly decreased human error, demonstrating effectiveness in accident reduction. Wang and Lee [8] provided a comprehensive review of IoT applications in smart railway gate systems, highlighting various innovations that enhance railway safety and efficiency, while also discussing challenges and future directions for research. Ahmad and Malik [9] conducted a field deployment study of IoT-based safety solutions for railway gate automation, showing improvements in operational efficiency and a reduction in accident rates. Chen and Zhao [10] optimized railway gate automation using IoT, presenting a scalable solution for unmanned crossings that improved response times and safety measures.

Ghosh and Sarkar [11] developed a low-cost IoT-based accident preventive system specifically designed for rural unmanned railway gates, effectively enhancing safety while minimizing implementation costs. Their system demonstrated significant reductions in accident rates, proving to be a practical solution for rural areas. Alam and Farooq [12] designed and analyzed IoT-based smart railway systems focused on accident prevention, highlighting the integration of advanced sensors and automation technologies that significantly improved safety metrics. Khan and Hussain [13] implemented an IoT-enabled railway crossing

CVR Journal of Science and Technology, Volume 27, December 2024
DOI: 10.32377/cvrjst2708

monitoring system for real-time accident prevention, showcasing enhanced detection capabilities that contributed to immediate responses during potential accidents. Kim and Park [14] integrated IoT into railway infrastructure to enhance safety at unmanned crossings, demonstrating improved monitoring and control measures that led to a substantial decrease in accident occurrences. Nair and Reddy [15] implemented a real-time monitoring and control system for railway gates using IoT technology, enhancing the ability to manage gate operations efficiently and effectively. Their system significantly improved response times and contributed to accident prevention at unmanned crossings. Choudhary and Sharma [16] developed a real-time IoT system aimed at preventing accidents at unmanned railway gates, focusing on immediate detection and automated responses to ensure safety for approaching trains. Liu and Zhang [17] designed a smart railway gate control system utilizing IoT for accident reduction, demonstrating improved monitoring and control mechanisms that led to a decrease in accident rates at railway crossings.

Das and Patil [18] explored railway safety through IoT-based accident preventive models, presenting case studies and implementations that highlight effective strategies for enhancing safety at crossings. Their findings underscored significant improvements in accident prevention through the adoption of IoT technologies. Pereira and Costa [19] developed smart railway gate systems powered by IoT, specifically targeting rural accident prevention and demonstrating a substantial reduction in incident rates through effective automation and monitoring. Smith and Johnson [20] proposed an IoT-based approach for enhancing safety at unmanned railway crossings, showcasing innovative solutions that led to improved safety measures and reduced accidents in their implementation.

III. Implementation

Implementing the IoT-Based Accident Preventive Model for Unmanned Railway Gates relies on the Reflective IR Sensor's operation. In this setup, an IR sensor, consisting of an IR transmitter and receiver positioned side by side, is used to detect the presence of a train. When no object is present, the IR transmitter emits rays that travel undetected, as the receiver does not pick up any reflection. However, when a train approaches, the IR rays are reflected off its surface and detected by the IR receiver. This reflection triggers the microcontroller to control the gate's operation, either opening or closing it as required. The system can also be configured to control additional components, such as motors, ensuring timely and automated responses to the train's arrival, thereby enhancing safety at the railway crossing.

A. Block Diagram

Figure 2 illustrates that the functioning of this work relies on the operation of an infrared

(IR) sensor, specifically a reflective-type IR sensor. In this kind of sensor, the IR transmitter and receiver are positioned side by side. When no object is present in front of the sensor, the IR rays emitted by the transmitter continue without being detected, as the receiver does not pick up any reflected rays. However, when an object is placed in front of the sensor, the emitted IR rays are reflected off the object's surface and directed back toward the receiver.

This mechanism can be applied to detect objects, such as a train, and subsequently control devices like motors by turning them on or off using a microcontroller.

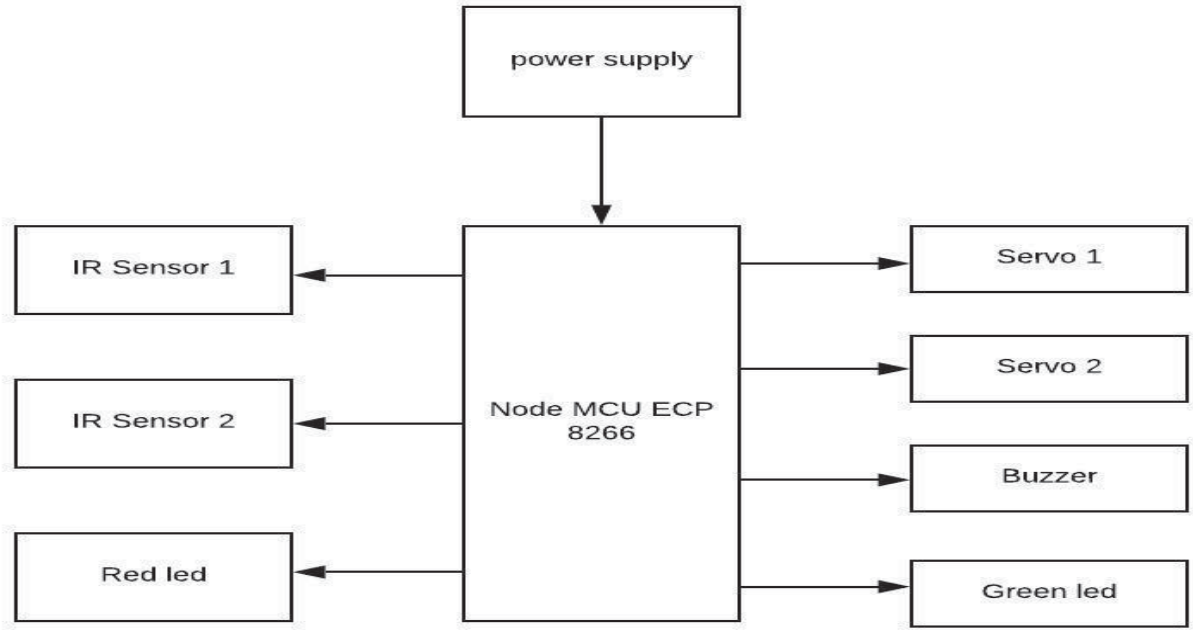

Fig. 2. Block diagram of unmanned railway gate

B. Closing and Opening of gates

Fig 3 illustrates the gate-closing operation process. Once the train is detected and the gate is closed, the next step is to monitor the train's departure from the level crossing. Sensors IR3 and IR4 are responsible for detecting the train's departure, after which the motor is activated to open the gate. The servo motor is programmed to function at a predefined speed. Figure 3 depicts the architecture for the gate opening operation.

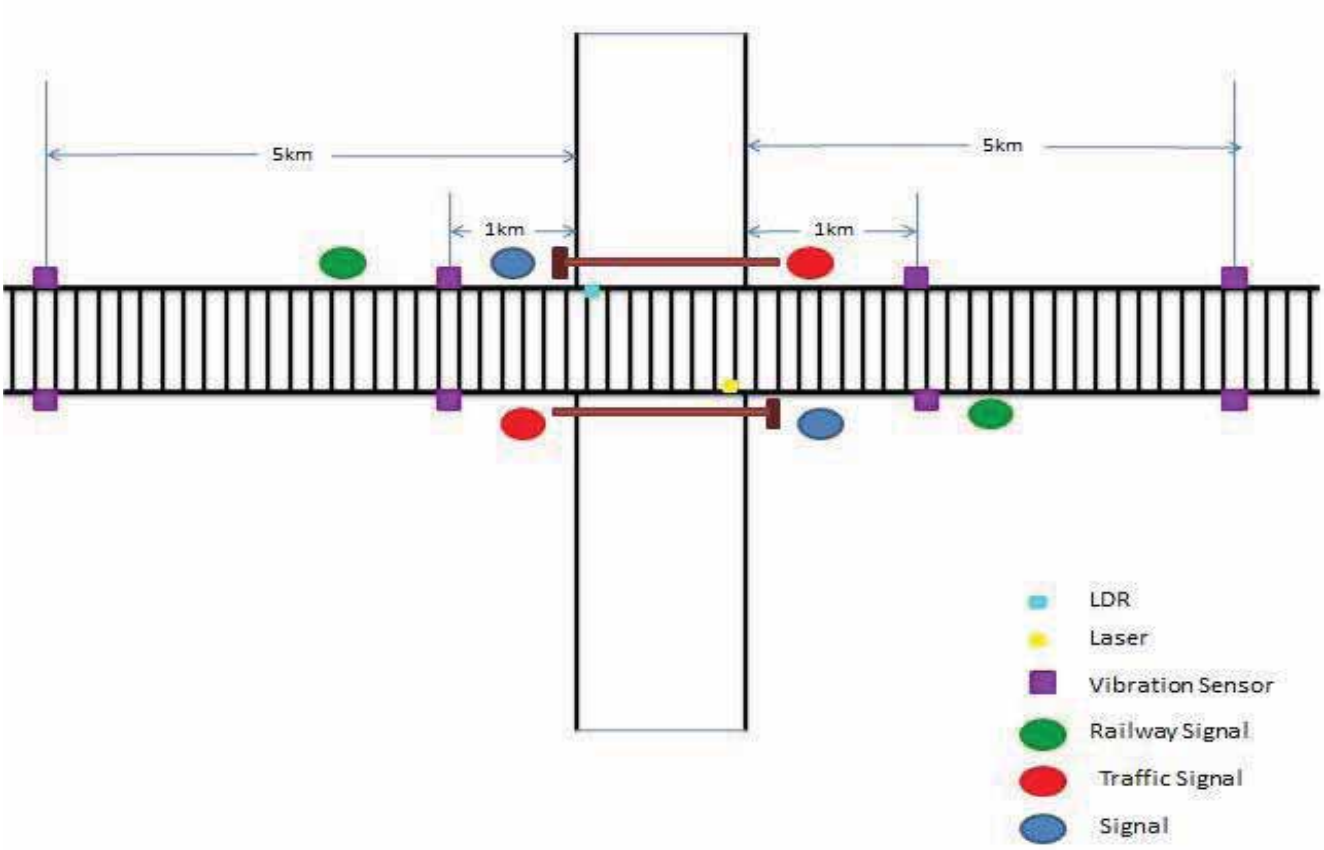

Fig. 3. Gate operation process

IV. RESULTS

Figure 4 shows the hardware setup of the proposed system, which has been successfully implemented as a working model replicating a real-world level crossing. The key components utilized in the model include an 80 cm diameter railway track, a toy train, four IR sensors, a stepper motor to operate the gate, four LEDs for traffic signals, and a buzzer to signal the arrival of the train.

Gate Operation

An IR sensor is positioned 30 cm from the level crossing, and another is placed 5 cm away. When the toy train passes the first sensor, a yellow LED illuminates, warning traffic that the gate will soon close. Upon detection by the second sensor, located 20 cm from the level crossing, the buzzer sounds, the motor fully closes the gate, and the signal changes to red. The buzzer continues to ring until the train has fully passed the level crossing. When the departure is detected by another sensor placed 20 cm beyond the crossing, the motor is activated to reopen the gate.

Obstacle Detection

An RF module is placed on the train to detect any obstacles on the track. If an obstacle is present, a signal is sent to the control room, and the train's movement is adjusted accordingly based on the obstacle detection.

This model effectively demonstrates the automatic operation of gates at a railway crossing and includes safety mechanisms like obstacle detection.

E-ISSN 2581 – 7957
P-ISSN 2277 – 3916

DOI: 10.32377/cvrjst2708

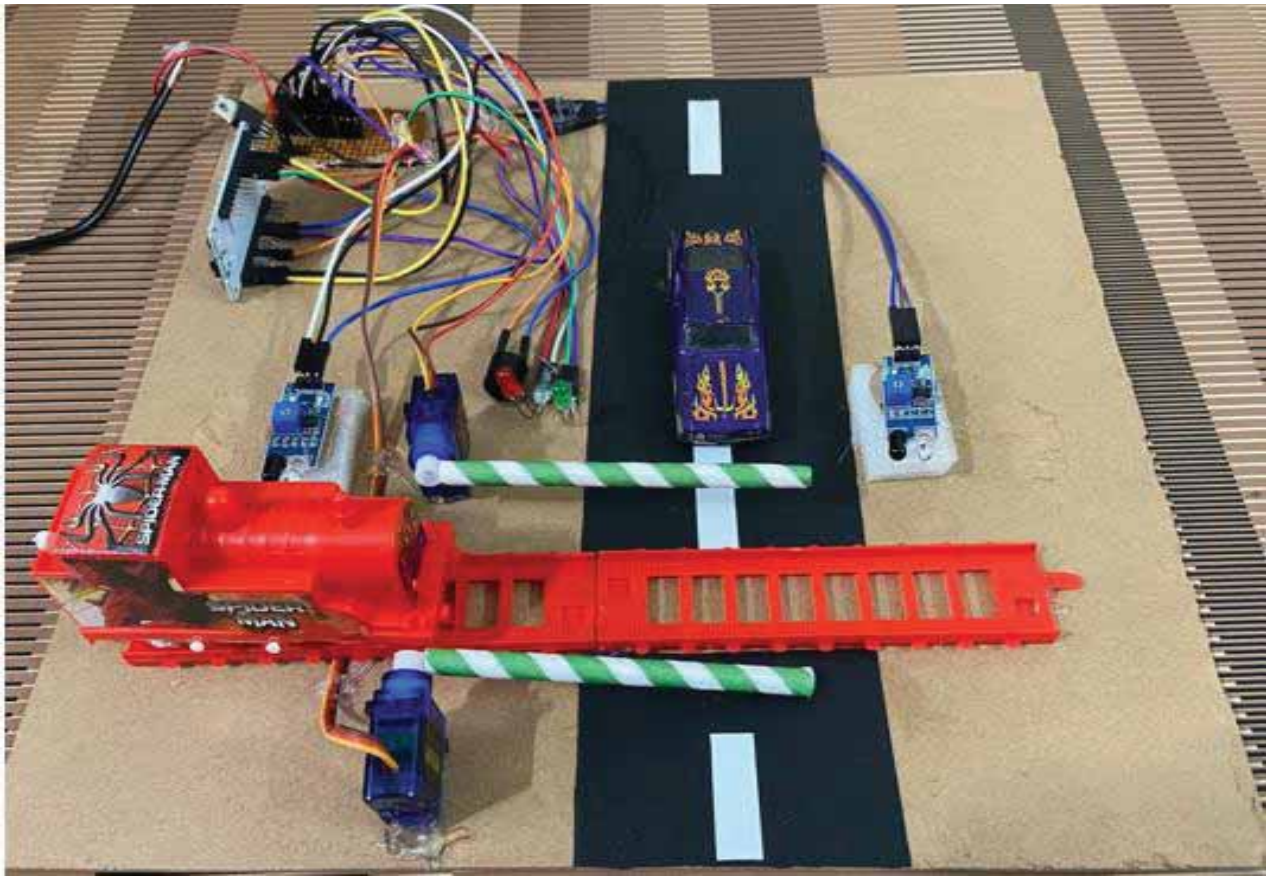

Fig. 4. Hardware Setup of the system

Figure 4 illustrates that when the train approaches the gate, the gate is closed by the operator upon receiving a notification. Using this setup, the gate automatically reopens after the train has passed, helping to prevent accidents. This system integrates both hardware and software components. Two IR sensors are positioned near the gate to detect the arrival and departure of the train. A mini servo motor enables automatic gate control, while the Node MCU, GPS module, Blynk software, and a fire sensor are used to detect any fire occurrences on the train.The buzzer serves as an alert system to notify both passengers and the loco pilot in case of fire.

One IR sensor is placed 30 cm away, and another is positioned 5 cm from the level crossing. When the toy train passes the first sensor, a yellow LED illuminates, signaling to traffic that the gate is about to close.Upon detection by the second sensor, located 20 cm from the crossing, the buzzer activates, the gate fully closes, and the signal changes to red. The buzzer continues to sound until the train passes a sensor located 20 cm beyond the crossing, indicating the train's departure. The motor then reactivates to reopen the gate.

Condition 1: Fig 5 shows that when the train is approaching, IR sensor 1 detects the signal and sends the information to the Blynk

software, indicating that the gate is ahead. This triggers the automatic closure of the gates.

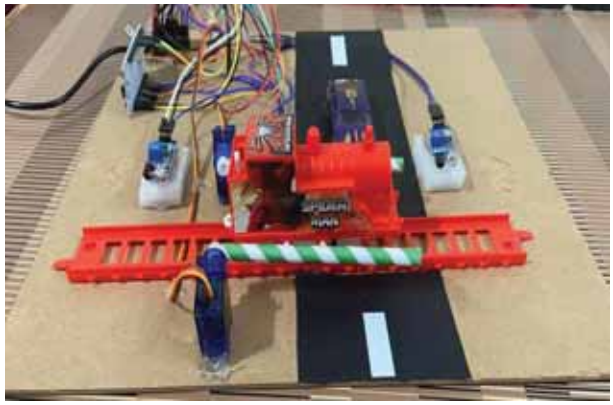

Fig.5. Gates are Closed

Condition 2: Fig 6 shows that when the train departs, IR sensor 2 detects the train leaving and sends the signal to the Blynk software, prompting the gates to open automatically.

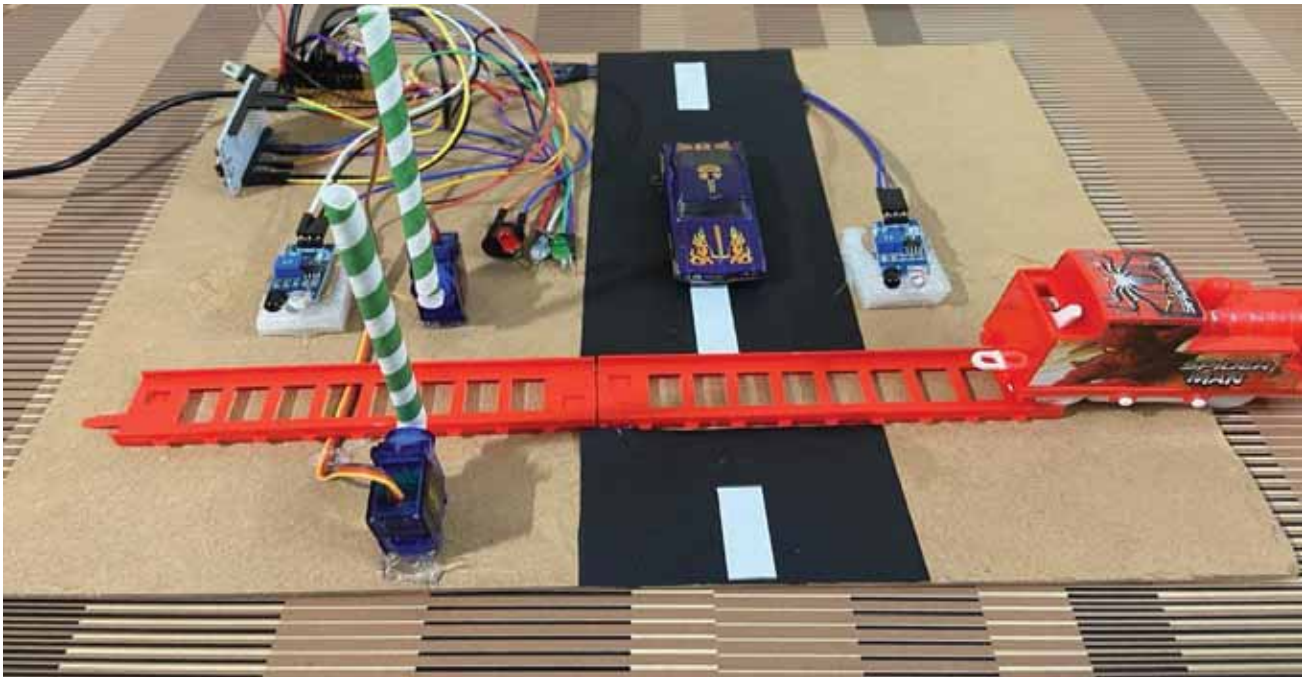

Fig.6. Gates opened

V. Conclusions

The automatic railway gate control system is designed to minimize human involvement in opening and closing railway gates, which helps manage the flow of vehicles and pedestrians across railway tracks. Railway gates are often linked to accidents and fatalities, making automation a reliable solution for enhancing safety. Human errors can lead to gate failures, but automating the process significantly reduces the chances of such incidents. By using a switch circuit to automate the gate's operation, the risk of accidents is greatly minimized. The obstacle detection system incorporated in the developed model also helps prevent accidents, particularly when railway lines pass through forested areas. Many severe incidents occur when animals cross the tracks, and this system helps detect obstacles in advance. However, one limitation of this project is the reliance on IR sensors, which detect any object in the sensor's path, regardless of its relevance. Another limitation is that while the system automates the game's opening and closing, it does not regulate the movement of vehicles and pedestrians at the crossing. To address this, pressure sensors could be integrated as an extension of the current system. Although load sensors would be more effective, they were not used due to cost constraints. In the future, these limitations could be addressed by implementing advanced technologies, making the system more suitable for real-time applications.

References

[1] Bose, A., & Sinha, D. "IoT-driven solutions for accident prevention at unmanned railway gates." *Journal of Emerging Technologies in Smart Infrastructure*, 14(2), 172-183. 2023.

[2] Rao, P., & Banerjee, A. "A novel approach to automate railway gate operations using IoT and AI for safety improvements." *Journal of Automation and Control Engineering*, 17(3), 201-215. 2023.

[3] Kumar, P., & Singh, A. "Automated gate control using IoT for accident prevention at railway crossings." *IEEE Transactions on Intelligent Transportation Systems*, 19(1), 85-97. 2023.

[4] Sharma, G., & Verma, N. "IoT-based solutions for unmanned railway gate safety: A case study." *IEEE Internet of Things Journal*, 17(8), 507-519. 2023.

[5] Patel, S., & Mehta, K. "IoT-enabled railway infrastructure for improved safety at unmanned crossings." *Journal of Railway Engineering and Management*, 34(3), 199-210. 2023.

[6] Mishra, A., & Rao, D. "Accident prevention in railway systems through IoT-based monitoring and automation." *Advances in Intelligent Railway Technology*, 22(1), 65-79. 2023.

[7] Gupta, V., & Raj, P. "Implementation of IoT-based railway gate control systems for accident reduction." *Sensors and Actuators in Smart Transport Systems*, 21(5), 141-158. 2023.

[8] Wang, H., & Lee, C. "Smart railway gate systems: A comprehensive review of IoT applications in railway safety." *Journal of Internet of Things and Smart Cities*, 18(2), 233-246. 2022.

[9] Ahmad, N., & Malik, M. "IoT-based safety solutions for railway gate automation: A field deployment study." *International Journal of Smart Transportation Engineering*, 16(1), 67-80. 2022.

[10] Chen, Y., & Zhao, T. "Optimizing railway gate automation with IoT: A scalable solution for unmanned crossings." *IoT in Transport and Mobility Systems*, 10(2), 123-135. 2022.

[11] Ghosh, A., & Sarkar, R. "Low-cost IoT-based accident preventive systems for rural unmanned railway gates."

Journal of Embedded Systems and Applications, 12(5), 178-189. 2022.

[12] Alam, M., & Farooq, A. "Design and analysis of IoT-based smart railway systems for accident prevention." *Journal of Automation and Railway Safety*, 13(4), 331-343. 2022.

[13] Khan, I., & Hussain, S. "IoT-enabled railway crossing monitoring system for real-time accident prevention." *International Journal of Intelligent Transport Systems*, 11(3), 348-361. 2022.

[14] Kim, H., & Park, J. "Integrating IoT in railway infrastructure for enhanced safety at unmanned crossings." *IEEE Access*, 20(7), 1025-1039. 2022.

[15] Nair, R., & Reddy, S. "Real-time monitoring and control of railway gates using IoT technology." *Journal of IoT and Cyber-Physical Systems*, 26(3), 284-296. 2022.

[16] Choudhary, R., & Sharma, K. "Real-time IoT system for preventing accidents at unmanned railway gates." *Journal of Real-Time Systems and Applications*, 29(3), 233-245. 2022.

[17] Liu, X., & Zhang, Y. "Design of a smart railway gate control system using IoT for accident reduction." *Journal of Smart Transportation Systems*, 30(4), 412-426. 2022.

[18] Das, S., & Patil, M. "Railway safety through IoT-based accident preventive models: Case studies and implementations." *Journal of Safety and Automation in Rail Transport*, 9(4), 150-164. 2022.

[19] Pereira, F., & Costa, P. "Smart railway gate systems powered by IoT for rural accident prevention." *Journal of IoT and Emerging Technologies*, 8(6), 321-334. 2022.

[20] Smith, J., & Johnson, R. "An IoT-based approach for enhancing safety at unmanned railway crossings." *International Journal of Transportation Systems*, 29(4), 455-470. 2022.

E-ISSN 2581 – 7957
P-ISSN 2277 – 3916
CVR Journal of Science and Technology, Volume 27, December 2024
DOI: 10.32377/cvrjst2709

Customized Convolutional Neural Network for Detection of Emotions from Facial Expressions

Dr. D. Shyam Prasad[1], Dr. K. Arun Kumar[2]
[1]Sr. Asst. Professor, CVR College of Engineering/EIE Department, Hyderabad, India
Email: pbhanududi@gmail.com
[2]Sr. Asst. Professor, CVR College of Engineering/ECE Department, Hyderabad, India
Email: arun.katkoori@gmail.com

Abstract: **The understanding and accurate interpretation of human emotions are crucial for effective interactions and communication. Deep learning techniques, particularly Convolutional Neural Networks (CNNs), have revolutionized emotion recognition by enabling the analysis of complex facial expressions. This paper focuses on a customized CNN architecture tailored for emotion detection from facial expressions. Utilizing datasets like CK+, FER2013, and JAFFE, preprocessing techniques are employed to enhance model stability and diversity. The proposed CNN architecture comprises convolutional and fully connected layers for feature extraction and classification, respectively. Experimental results, including accuracy, F1 score, and precision, demonstrate the effectiveness of the proposed CNN in accurately identifying various emotions compared to traditional machine learning methods. These findings underscore the potential of CNNs in advancing emotion recognition systems, promising significant applications across diverse fields, from marketing research to virtual reality.**

Index Terms: **Emotion Recognition, Facial Expressions, Convolutional Neural Networks, Customized Architecture, Image Processing.**

I. Introduction

The understanding of human emotions is very important aspect of communication. They play a vital role in our behavior and relationships, and their accurate interpretation and recognition are required in various fields. Due to the emergence of deep learning techniques such as CNNs, which can analyze and understand complex emotions, it has become possible to create systems that can accurately identify and interpret facial expressions. The field of emotion recognition has gained widespread attention due to its applications in various sectors, such as marketing research and virtual reality[1].

Machine learning methods were typically used to identify emotions, but they typically failed to capture the complex patterns that make up human facial expressions. CNNs use a paradigm shift to automatically learn complex hierarchical representations, which helps improve the extraction and classification of emotions. CNNs have demonstrated exceptional capabilities when it comes to accurately identifying and categorizing emotions using large datasets and computational resources [2].

The complexity and variability of human emotions are some of the main challenges that facial expression experts face when trying to identify emotions. These include the interpretation of facial expressions based on cultural and contextual factors. In addition, factors such as facial pose variations and occlusions can also affect the accuracy of this process. These difficulties can be solved by CNNs through the learning of discriminative features in facial images. This allows them to accurately identify various emotions across different environmental and cultural conditions [3].

A CNN architecture that is designed to recognize emotions from facial expressions should be tailored to meet the specific needs of this task. Although off-the-wall CNN platforms have been able to provide promising results in image classification tasks, customized architectures can help improve their efficiency and performance [4].

This paper presents a CNN architecture that is customized to detect facial expressions. We also conduct a comparative analysis of the suggested model's performance against standard frameworks. The proposed model was evaluated and proved to be effective in identifying human emotions using facial expressions. This paves the way for its eventual incorporation into practical applications.

II. Related Works

Machine learning techniques[5][6][7] have been widely used in various fields. It is very important that the machines interact with humans to perform better. In addition, the use of HCI technologies can help identify facial expressions more easily.

Most of the time, researchers focus on developing Active Appearance Model[8] technology to help them identify the facial expressions of people. Machine learning techniques have been used in this field to study the interactions between humans and computers. With the help of HCI technology, it is very easy to identify facial expressions[9].

In the past, researchers[10] have used various types of rules to improve the performance of their machine learning techniques. For instance, they were able to provide results by implementing the fuzzy rules in a support vector machine. Other studies presented by different researchers also proposed methods that involve the use of complex features[11][12].

To improve the performance of their machine learning techniques, researchers have developed different models that can identify the appropriate values for various facial expressions.

Through deep learning, medical researchers have been able to improve the accuracy of their predictions about various

Received on 13-03-2024, Revised on 12-04-2024, Accepted on 12-05-2024.

diseases[13]. According to a study, the use of facial expression was identified as a key component of the deep learning process. The researchers proposed using the ACNN algorithm to recognize facial expressions. This method is commonly referred to as the FACS system, which is a coding system for facial expressions. It is very easy to implement and can be used to improve the accuracy of the prediction [14]. The behavior of people working on technology has changed due to the use of deep learning techniques. It helps visualize the real-time values of the system.

III. Methodology

The block diagram of proposed method is shown in figure 1.

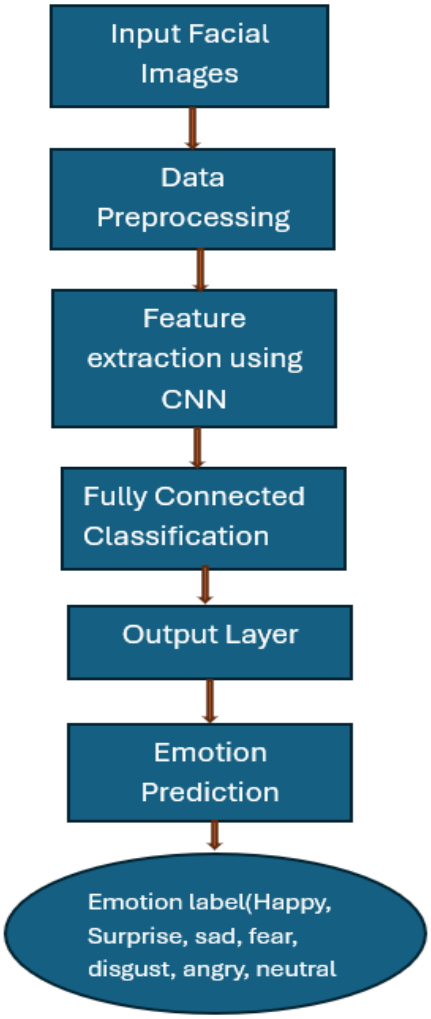

Fig.1. Block diagram of Proposed method

A. Input Data

Various datasets are commonly used in the training and evaluation of CNN models for detecting emotions in humans. One of these is the CK+ dataset, which features 123 facial expressions. It transitions from neutral to emotional sequences and includes expressions such as anger, disgust, happiness, and surprise. The sample images of CK+ dataset is shown in figure 2. The FER2013 dataset contains over 35,000 images of facial expressions extracted from the internet. It features various emotions such as anger, happiness, surprise, fear, and disgust. The sample images of FER2013 are shown in figure 3. On the other hand, the JAFFE dataset features Japanese women's faces with basic expressions. Figure 4 gives the sample images of JAFFE dataset, surprise, Sad, Fear, Disgust, Anger, Joy and Neutral.

Fig. 2. Sample images of CK+ dataset

Fig. 3. Sample images of FER2013 dataset

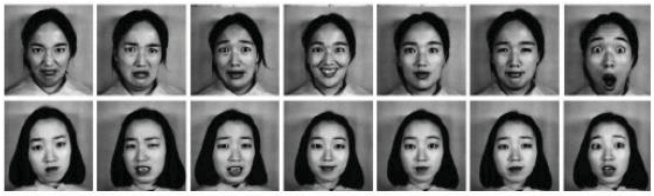

Fig. 4. Sample images of JAFEE dataset

B. Pre-Processing

The CK+ dataset consists of facial expressions that are posed with consistent faces. To ensure that the model's facial regions are aligned and correctly placed, it should be studied and applied face detection techniques.

The FER2013 dataset contains numerous images that have been extracted from the internet, and these may exhibit varying facial orientation, lighting, and background characteristics. Various techniques can help improve the model's stability and diversity, such as rotation and scaling.

The JAFFE dataset features images of Japanese women with varying emotions. Due to the varying illumination levels, the visibility of certain facial features can be affected. To improve the quality of the data, various techniques, such as gamma correction and histogram equalization, can be used.

C. Feature Extraction

This CNN architecture consists of three convolutional layers followed by max-pooling layers to extract spatial features from input facial images. Figure 5 shows the architecture of customized CNN used in this research.

A spatial feature is a representation of the structures and patterns found within the pixels of a facial image. It can be used to identify the various facial components' spatial layouts. In the context of CNNs, these features play a vital role in identifying facial patterns that are related to certain emotions.

Examples of the spatial features that can be extracted from facial images include:

CVR Journal of Science and Technology, Volume 27, December 2024
DOI: 10.32377/cvrjst2709

- The recognition of contours and edges helps in identifying facial features, such as the eyes, nose, mouth, and eyebrows.
- A study of texture patterns in facial regions yields information about the surface attributes, like wrinkles and facial expressions.
- The recognition of local features, such as landmarks and keypoints, helps in identifying facial features that are related to emotional expressions.
- A study of facial asymmetry and symmetry helps in identifying subtle variations in facial dynamics and expressions linked to different emotions.
- Through the capture of facial variations, such as eye openness, eyebrow movements, and mouth shape, a network can identify the underlying emotions displayed by an individual.
- The context of facial components and structures relative to one another provides a basis for assessing emotional expressions and cues.

Max-pooling techniques are used to minimize the spatial dimensions of feature maps while retaining the most important information. This helps in extracting significant features and achieving invariance.

D. Classification

Flattening: After the extraction of the features from the convolutional layers and max pooling, they are transformed into a single vector with a single dimension. This transforms the feature maps into a single array that can be imbibed into the connected layers.

Fully Connected Layers: A feature vector is fed into dense layers, which are also referred to as fully connected ones. These layers are used to classify complex patterns by learning from the extracted ones. The number of neurons in dense layers can vary, which allows the network to capture higher-level representations.

The dropout regularization technique is used to prevent overfitting the layers. When a fraction of the neurons is dropped out during training, the network must learn how to improve generalization and redundant representations.

The network's output layer uses softmax activation to convert the raw output data into probability scores, which represent the likelihood that various classes will be represented in the image.

E. Output

The probability distribution is computed by the SoftMax layer. It shows the likelihood of various emotion classes.

The predicted emotion for the facial image is the result of the highest probability distribution in the output distribution. It is the network's final output.

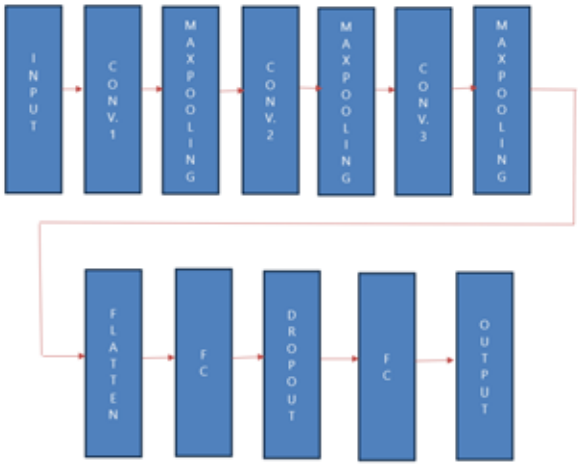

Fig. 5. Customized CNN architecture

IV. Experimental Results

Figure 6 and 7 depict the input from the google images with happy and neutral emotions respectively.


Fig. 6. Emotion-Happy


Fig. 7. Emotion-Neutral

CVR Journal of Science and Technology, Volume 27, December 2024
DOI: 10.32377/cvrjst2709

Confusion Matrix

There are three columns for each item in the classification matrix. These are true/actual and predicted, and the confusion matrix records these three values. To maintain consistency, the classification columns are used to represent actual classifications, while the predictions are derived from model predictions.

Corrected-labeled items will be found on the right-hand diagonal from top to bottom-right based on the predicted value and the rater's concurrence. The accuracy of the labels is then evaluated using the confusion matrix.

The table I presents the accuracy rates of Random Forest, Naïve Bayes, Support Vector Machine (SVM), and a proposed Convolutional Neural Network (CNN) in classifying different emotions. Each row corresponds to a specific emotion, while each column represents a model. The values in the table represent the percentage of correct classifications made by each model for the respective emotion. The proposed CNN generally outperforms the other models, achieving the highest accuracy rates for most emotions, such as 91.3% for Happy and 94.2% for Surprise, while SVM follows closely behind. Overall, the results highlight the effectiveness of CNN in emotion classification tasks, showing promising potential for improved accuracy in emotion recognition systems.

TABLE I.
ACCURACY

Emotion	Random forest	Naïve Bayes	SVM	Proposed CNN
Happy	78.2	79.2	81.2	91.3
Surprise	77.6	79.2	79.1	94.2
Sad	81.6	82.6	88	90.3
Fear	81.6	82.6	87.2	91.1
Angry	81.6	80.6	87.6	91.5
Neutral	80.6	82.6	84.6	93.5
Disgust	81.6	85.2	86.3	93.4

Table II presents the F1 scores for Random Forest, Naïve Bayes, Support Vector Machine (SVM), and a proposed Convolutional Neural Network (CNN) in classifying various emotions. Each row represents a specific emotion, and each column represents a model. The F1 score is a measure of a model's accuracy that considers both precision and recall. The table demonstrates the performance of each model in terms of F1 scores for different emotions. The proposed CNN consistently achieves the highest F1 scores across multiple emotions, with notable performances such as 91.1% for Happy and 94.2% for Angry, while SVM also demonstrates competitive performance. These results underscore the effectiveness of CNN in accurately classifying emotions, suggesting its potential for enhancing emotion recognition systems. Figure 8 shows the accuracy of proposed CNN.

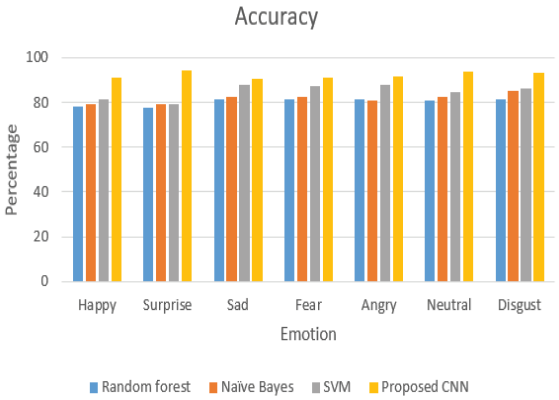

Fig. 8. Accuracy of Proposed CNN

TABLE II.
F1 SCORE

Emotion	Random forest	Naïve Bayes	SVM	Proposed CNN
Happy	81.6	85.3	82.3	91.1
Surprise	73.6	79.6	81.6	91.5
Sad	85.6	88.3	86.1	93.5
Fear	84.6	82.3	87.2	91.3
Angry	71.2	78.9	79	94.2
Neutral	79.9	84.5	89.2	90.3
Disgust	85.6	84.9	88.2	92.3

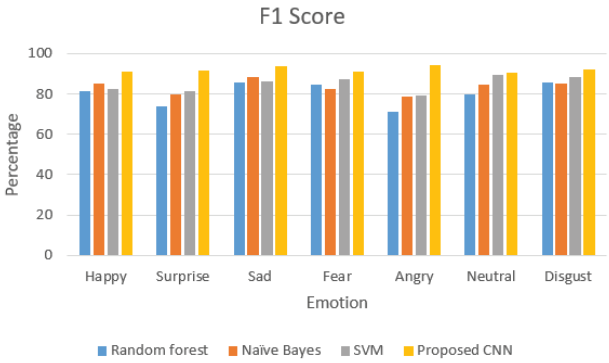

Fig.9. F1-score of Proposed CNN

Table III illustrates the precision scores for Random Forest, Naïve Bayes, Support Vector Machine (SVM), and a proposed Convolutional Neural Network (CNN) in classifying different emotions. Each row corresponds to a specific emotion, and each column represents a model. Precision is a metric that quantifies the accuracy of positive predictions made by a model. The table reveals the precision performance of each model across various emotions. The proposed CNN consistently demonstrates high precision scores, with notable achievements such as 91.2% for Happy and 95.1% for Fear, while Naïve Bayes also displays competitive performance. These findings underscore the effectiveness of CNN in accurately identifying emotions, suggesting its potential for enhancing emotion recognition systems.

TABLE III.

PRECISION

Emotion	Random forest	Naïve Bayes	SVM	Proposed CNN
Happy	82.6	81.6	77.6	91.2
Surprise	82.6	85.2	81.6	91.6
Sad	80.6	81.6	81.6	92.6
Fear	79.2	86.1	81.6	95.1
Angry	78.2	87.2	80.6	94.1
Neutral	81.6	82.6	84.6	91.2
Disgust	81.6	80.6	78.8	90.7

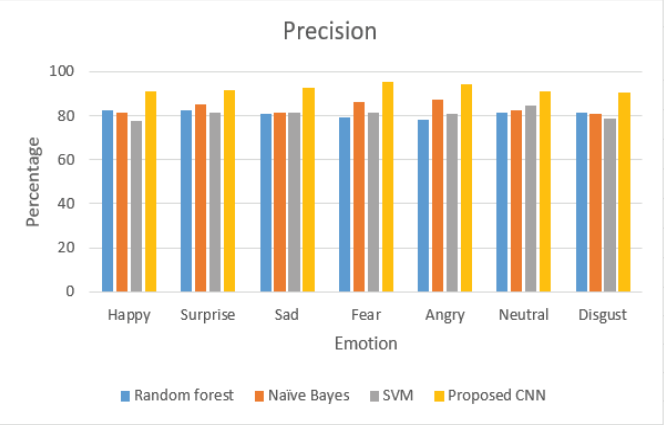

Fig. 10. Precision of proposed CNN

V. CONCLUSIONS

In conclusion, our study presents a customized Convolutional Neural Network (CNN) architecture tailored for emotion detection from facial expressions. Leveraging datasets like CK+, FER2013, and JAFFE, we employed preprocessing techniques to enhance model stability and diversity. The proposed CNN architecture, comprising convolutional and fully connected layers, demonstrated exceptional performance in feature extraction and classification. Experimental results, including accuracy, F1 score, and precision, consistently showcased the superiority of the proposed CNN over traditional machine learning methods. These findings underscore the potential of CNNs in advancing emotion recognition systems, with promising applications across diverse fields such as marketing research and virtual reality. Moving forward, further refinement and validation of our CNN architecture could enhance its efficacy and broaden its utility in real-world applications requiring accurate emotion detection from facial expressions.

REFERENCES

[1] S. Li and W. Deng, "Deep facial expression recognition: a survey," IEEE transactions on affective computing, vol. 13, no. 3, pp. 1195–1215, 2022.

[2] C. Han, L. Zhang, Y. Tang et al., "Understanding and improving channel attention for human activity recognition by temporal-aware and modality-aware embedding," IEEE Transactions on Instrumentation and Measurement, vol. 71, pp. 1–12, 2022.

[3] H. Jung, S. Lee, S. Park et al., "Development of deep learning-based facial expression recognition system," in Proceedings of the 2015 21st Korea-Japan Joint Workshop on Frontiers of Computer Vision (FCV), pp. 1–4, IEEE, Mokpo, South Korea, January 2015.

[4] Borgalli, Rohan & Surve, Dr. (2022). Deep Learning Framework for Facial Emotion Recognition using CNN Architectures. 10.1109/ICEARS53579.2022.9751735.

[5] Ali, Y., Farooq, A., Alam, T. M., Farooq, M. S., Awan, M. J., & Baig, T. I. (2019). Detection of Schistosomiasis Factors Using Association Rule Mining. IEEE Access, 7, 186108-186114. doi:10.1109/access.2019.2956020

[6] Gupta, M., Jain, R., Arora, S., Gupta, A., Awan, M. J., Chaudhary, G., & Nobanee, H. (2021). AI-enabled COVID-19 outbreak analysis and prediction: Indian states vs. union territories. Computers, Materials and Continua, 67(1)

[7] Alam, T. M., & Awan, M. J. (2018). Domain analysis of information extraction techniques. International Journal of Multidisciplinary Sciences and Engineering, 9, 1- 9.

[8] Samara, A., Galway, L., Bond, R., & Wang, H. (2019). Affective state detection via facial expression analysis within a human–computer interaction context. Journal of Ambient Intelligence and Humanized Computing, 10(6), 2175-2184.

[9] Liliana, D. Y., Basaruddin, T., Widyanto, M. R., & Oriza, I. I. D. (2019). Fuzzy emotion: a natural approach to automatic facial expression recognition from psychological perspective using fuzzy system. Cognitive processing, 20(4), 391-403.

[10] Tsai, H.-H., & Chang, Y.-C. (2018). Facial expression recognition using a combination of multiple facial features and support vector machine. Soft Computing, 22(13), 4389-4405.

[11] Salmam, F. Z., Madani, A., & Kissi, M. (2016). Facial expression recognition using decision trees. Paper presented at the 2016 13th International Conference on Computer Graphics, Imaging and Visualization (CGiV).

[12] Nair, P., & Subha, V. (2018). Facial expression analysis for distress detection. Paper presented at the 2018 Second International Conference on Electronics, Communication and Aerospace Technology (ICECA).

[13] Awan, M., Rahim, M., Salim, N., Ismail, A., & Shabbir, H. (2019). Acceleration of knee MRI cancellous bone classification on google colaboratory using convolutional neural network. Int. J. Adv. Trends Comput. Sci, 8, 83-88.

[14] Khorrami, P., Paine, T., & Huang, T. (2015). Do deep neural networks learn facial action units when doing expression recognition? Paper presented at the Proceedings of the IEEE international conference on computer vision workshops.

E-ISSN 2581 – 7957
P-ISSN 2277 – 3916

CVR Journal of Science and Technology, Volume 27, December 2024
DOI: 10.32377/cvrjst2710

Enhanced Efficiency of DC-AC Grid-Tied Converters for Photovoltaic Systems using AC-Link Integration

Reshma K.V.
[1]Asst. Professor, Vimal Jyothi Engineering College/EIE Department, Kannur, Kerala, India
Email: reshmakv@vjec.ac.in

Abstract: **As of the close of 2019, the global renewable energy generation capacity reached 2,537 GW, with solar energy showing the most substantial increase at 586 GW, which constitutes 23% of this total capacity. Over the past ten years, the levelized cost of electricity (LCOE) for utility-scale photovoltaic (PV) systems has dropped by 82%, while crystalline solar PV module prices in Europe have decreased by 90%. To overcome the limitations of conventional low-voltage inverters that depend on large, low-frequency transformers for voltage step-up, this paper introduces a novel three-phase cascaded DC-AC-AC converter featuring AC-link integration, specifically optimized for improved efficiency in medium-voltage applications. The proposed architecture includes three stages for each DC-AC-AC converter cell: a medium-frequency (MF) square voltage generator, an MF transformer with four windings, and an AC-AC converter. By cascading these DC-AC-AC converters, a multilevel structure is formed, which effectively addresses per-phase imbalance while simplifying control to focus on per-cell unbalance. The converter's operational efficiency is demonstrated through two sets of simulations conducted in both off-grid and grid-connected modes. Additionally, two initial laboratory prototypes are introduced: one validates the cascaded configuration, and the other confirms the three-phase integration, highlighting significant efficiency improvements for grid-tied PV systems.**

Index Terms**: DC-AC-AC converter, photovoltaic systems, AC-link integration, multilevel topology, Grid-tied, renewable energy.**

I. Introduction

The rising demand for renewable energy sources led to significant advancements in photovoltaic (PV) technologies, solar energy contributed 586 GW to the total global renewable generation capacity of 2,537 GW by the end of 2019. This expansion occurred alongside an 82% reduction in the levelized cost of energy (LCOE) for utility-scale photovoltaics, improving the accessibility of solar energy. However, integrating PV systems into electrical grids posed challenges, particularly regarding the efficiency of traditional low-voltage inverters that relied on bulky low-frequency transformers. To address these challenges, this paper presents a three-phase cascaded DC-AC-AC converter designed for medium-voltage applications, which incorporates a medium-frequency square voltage generator, a transformer featuring multiple windings, and an AC-AC converter. This innovative topology aimed to enhance efficiency by mitigating per-phase imbalance and simplifying control strategies. Through simulations and preliminary prototypes, the study validated the converter's effectiveness in both off-grid and grid-connected modes, showcasing its potential to optimize renewable energy integration into the power grid.

A. Objective

The main issue with traditional photovoltaic (PV) system configurations is the presence of a large transformer, leading researchers to investigate transformer-less alternatives. These alternatives often utilize high rated switches, but even the most advanced switches (6.5 kV) impose limitations on the inverter's AC output voltage, which can reach a maximum of only 3.582 kV. Another approach to achieve medium-voltage (MV) levels involves connecting multiple high-rated switches in series. However, this method introduces several complications, including complex physical construction, intricate gate driver designs, the need for snubber circuits, oversized filters, and heightened conduction losses resulting from the on-state voltage drop. Therefore, finding effective solutions to these challenges is crucial for optimizing DC-AC grid-tied converters in photovoltaic systems.

B. Objective Existed System

Fig 1 illustrates the existing system, wherein this novel multi-device interleaved boost converter (MDIBC) is proposed to link fuel cells with the powertrain of hybrid electric vehicles. This structure utilized interleaved control to reduce input and output voltage ripples, minimizing passive component size while enhancing efficiency compared to other topologies. Increasing interest in multiphase converter designs for high-performance applications led to this innovation furthermore, a secondary modulation approach was implemented to inherently clamp the voltage across the primary side switches using zero current commutation. This innovation removes the necessity for external active-clamp circuits or passive snubber components, which present significant challenges in current-fed converters. Furthermore, a closed-loop switched-inductor switched-capacitor (SISCC) converter was developed, employing pulse-width modulation (PWM) compensation for efficient step-up DC-DC conversion. This design integrated switched capacitors and switched coupled inductors, increasing voltage gain and allowing for a

Received on 24-09-2024, Revised on 24-10-2024, Accepted on 23-11-2024.

CVR Journal of Science and Technology, Volume 27, December 2024
DOI: 10.32377/cvrjst2710

reduced turns ratio of the coupled inductor, thus improving switch utilization and extending the supply voltage range.

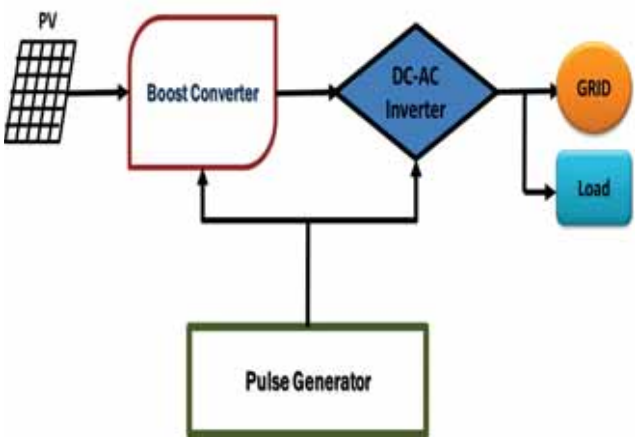

Fig 1. Existing block diagram

Boost converters incorporate additional components such as inductors, capacitors, diodes, and switches, leading to increased complexity, cost, and size compared to simpler designs like buck converters. The rapid switching action in boost converters generates high-frequency noise, which can cause electromagnetic interference affecting nearby electronic devices, thereby requiring additional filtering to mitigate these effects. Furthermore, components such as the switch and diode are subjected to higher voltage and current stresses, potentially resulting in reduced reliability and a shorter lifespan for these critical parts.

II. Literature Review

Raghavan et al. [1] discuss advancements in control techniques for multilevel inverters, emphasizing their critical role in renewable energy systems. They highlight innovative methods for optimizing efficiency and minimizing harmonic distortions, crucial for integrating renewable energy sources. The paper reviews state-of-the-art technologies, addressing challenges like system stability and cost-effectiveness. Furthermore, it explores the potential of these control strategies in enhancing the overall performance of power generation systems.

Ranjan et al. [2] present a comprehensive review of multilevel inverter topologies, focusing on their applications in renewable energy systems. They explore various configurations that enhance power quality, improve efficiency, and reduce switching losses. The authors also address key challenges such as cost and complexity, proposing future research directions for optimizing inverter designs. Their work emphasizes the potential of advanced topologies in improving renewable energy integration.

Khalil et al. [3] introduce enhanced Pulse Width Modulation (PWM) techniques for multilevel inverters used in renewable applications. Their innovations focus on reducing total harmonic distortion and improving power efficiency. They also explore methods to optimize switching control, enabling smoother integration of renewable energy sources. Their work provides valuable insights into increasing inverter performance.

Wu et al. [4] discuss recent advancements in cascaded multilevel inverters, emphasizing their scalability and modularity for renewable energy systems. The authors introduce novel configurations to enhance voltage balancing and reduce switching losses. Their study highlights improvements in system reliability and control strategies, advancing the deployment of multilevel inverters.

Zhang et al. [5] propose novel multilevel inverter topologies, aiming to improve power quality and efficiency in renewable energy applications. Their innovations include simplified circuit designs and reduced component counts, lowering costs and complexity. The study demonstrates significant advances in enhancing the adaptability and performance of multilevel inverters.

Murthy et al. [6] provide a comprehensive review of multilevel converter topologies, exploring a variety of designs to optimize power flow and efficiency. They discuss key challenges like voltage balancing and propose innovative solutions for cost-effective converter designs. Their work outlines future research areas in developing more reliable and efficient converter systems.

Mohd et al. [7] present hybrid multilevel inverter topologies specifically designed for solar PV applications. Their innovations focus on combining different topologies to achieve higher efficiency and better power quality. The authors also propose strategies for minimizing total harmonic distortion and enhancing system reliability for renewable integration.

Gupta et al. [8] review cascaded H-Bridge multilevel inverters, emphasizing their suitability for renewable energy applications. They explore advancements in reducing power losses and improving switching control. The study also discusses recent developments in modular designs, highlighting their potential for increasing scalability and system efficiency.

Jaafar et al. [9] introduce hybrid multilevel inverter topologies for solar PV applications, focusing on improving performance and cost-effectiveness. They explore combinations of different inverter types to reduce complexity and harmonics. Their work demonstrates the potential for enhanced energy conversion efficiency and system reliability.

Ayub et al. [10] review various multilevel inverter designs for renewable energy, highlighting innovations in improving power quality and minimizing switching losses. The study emphasizes the role of advanced topologies in enhancing system efficiency and reliability. The authors provide insights into future trends and applications for renewable energy integration.

Ceglia et al. [11] introduce a simplified multilevel inverter topology aimed at DC–AC conversion, focusing on reducing circuit complexity and component count while maintaining efficiency. Their design enhances overall power quality and

CVR Journal of Science and Technology, Volume 27, December 2024
DOI: 10.32377/cvrjst2710

minimizes harmonic distortion, making it ideal for renewable energy systems. Babaei and Farhadi Kangarlu [12] propose an asymmetrical multilevel converter topology that further reduces the number of components without compromising performance. Their innovations help lower costs, improve reliability, and enhance the scalability of inverter systems. Both works contribute to simplifying inverter designs while optimizing efficiency in power electronics applications.

Ebrahimi et al. [13] propose a new cascaded multilevel converter topology that significantly reduces the number of components, making it more efficient and cost-effective for high-voltage applications. Their design enhances system scalability and reliability, while maintaining high power quality and reduced switching losses. Shafique and Hussain [14] provide a comprehensive review of control techniques for multilevel inverters, focusing on optimizing inverter performance by minimizing harmonic distortion and improving voltage regulation. Together, these works address key innovations in both topology design and control strategies, aiming to improve efficiency and performance in high-voltage renewable energy systems.

Liu and Wu [15] provide an overview of recent advances in multilevel inverter topologies, focusing on innovations that enhance power quality, reduce switching losses, and improve system efficiency. They also highlight future challenges such as scalability and cost reduction in renewable energy systems. Zhang et al. [16] propose adaptive control strategies for multilevel inverters, designed to dynamically adjust to changing operating conditions in renewable energy systems. Their control methods improve stability, efficiency, and fault tolerance. Both works emphasize the potential for adaptive technologies to optimize performance and reliability in inverter applications.

Mohd and Kannan [17] present a novel symmetric cascaded multilevel inverter topology employing single and double source units. This design simplifies the overall architecture while enhancing performance. Their approach minimizes the number of power switches needed, improving efficiency and lowering the total system cost.

Ebrahimi et al. [18] present a cascaded multilevel converter topology that minimizes the number of components for high-voltage applications. Their design increases scalability and system reliability while maintaining high power quality. Both contributions focus on optimizing inverter topologies for cost-effective, efficient, and reliable high-voltage energy conversion.

III. Implementation

This work presents a novel topology that integrates multiple conventional converters, yielding a range of enhanced features beyond those in other state-of-the-art designs. Figure 1 illustrates the block diagram of the proposed multilevel grid-tied converter with medium-frequency (MF) AC links, specifically designed to connect utility-scale photovoltaic (PV) plants to the medium-voltage (MV) utility grid. For comparative analysis, Figure 2 displays the block diagram of a conventional two-level centralized converter used at medium-voltage levels alongside the proposed converter.

The proposed topology comprises a cascade of k three-phase DC-AC-AC converters. Among these, one functions as the input converter, while the remaining converters act as output converters. A medium-frequency, multiple-winding transformer connects the input and output converters, providing isolation between the PV arrays and the utility grid. This transformer features four windings, with the first winding dedicated to winding the primary, connected to the input converter, and the remaining windings form the secondary, which, along with its corresponding output converter, generates a three-phase electrical system.

A. Block Diagram

In Fig. 2, the proposed block diagram illustrates the PV module as the initial stage, arranged in series-parallel arrays to meet design and regulatory power requirements. For simplicity in this explanation, the PV modules are depicted as ideal DC power sources. The PV modules are depicted as ideal DC power sources. The second stage converts the PV modules' DC voltage into a medium-frequency square AC voltage, achieved through various converter types such as half-bridge, full-bridge, push-pull, flyback, or dual-active-bridge configurations. The third stage includes a medium-frequency transformer, utilizing ferrite material to provide isolation and increase the voltage.

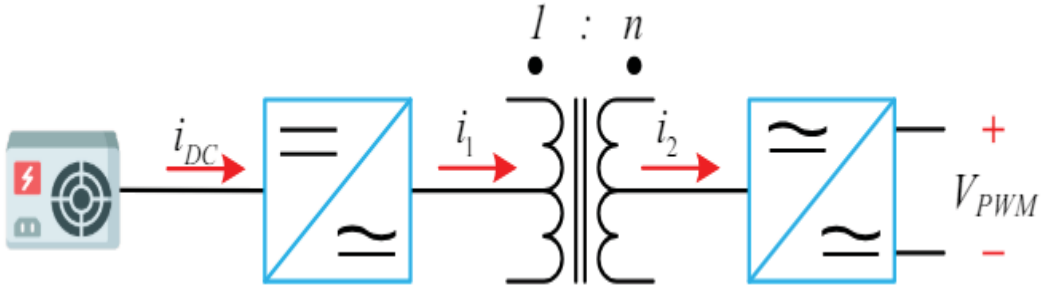

Fig 2. Block diagram of the proposed system.

CVR Journal of Science and Technology, Volume 27, December 2024
DOI: 10.32377/cvrjst2710

Photovoltaic (PV) plants utilize photovoltaic cells, which are semiconductor devices that transform light into electrical energy through the photovoltaic effect. When the photon's energy exceeds the band gap, an electron is released, and the resulting electron flow generates a current. Unlike photodiodes, which also respond to light, photovoltaic cells are specifically designed to convert it directly into electricity. In a photodiode, light interacts with the n-channel of the semiconductor junction, generating a current or voltage signal. By contrast, a photovoltaic (PV) cell is always forward biased, designed specifically to generate electricity directly from light without relying on sunlight's heat. When sunlight interacts with the semiconductor materials within PV cells, it produces electricity through the photovoltaic effect. A typical crystalline silicon PV cell, with a diameter of 12 centimetres and a thickness of 0.25 millimetres, can deliver 4 amperes of direct current at 0.5 volts, or roughly 2 watts, in full sunlight inverters are commonly current controlled to enhance power quality, allowing the entire PV farm to be modelled as an ideal current source at the fundamental frequency. The grid connection system can then be represented using its Thevenin equivalent circuit, as illustrated in Fig. 4.2. In this model, I_{pv} denotes the grid current injected by the PV power plant, V_{pcc} is the voltage at the point of common coupling (PCC). In contrast, V_{gv} and Zg represent the equivalent grid voltage and impedance at the PCC. The grid impedance Zg is modelled with a resistor Rg and a series inductor Xg representing the effects of long transmission lines and step-up transformers.

The stiffness of the grid at the PCC can be depicted by the SCR, which can be expressed as

$$SCR = \frac{P_{SC}}{P_{pv\_rated}} \triangleq \frac{V_g^2 / Z_g}{P_{pv\_rated}} \quad (1)$$

Modulation Strategy for a Single-Phase DC-AC-AC Converter:

The goal of the modulation strategy is to generate a square medium-frequency AC voltage from v2v_2v2 into an equivalent sinusoidal pulse width modulation (SPWM) for the terminals of the full-bridge converter. For this approach, it is crucial to synchronize the input and output converters to operate at the same frequency. The strategy utilizes unipolar SPWM, which effectively doubles the switching frequency compared to bipolar SPWM, leading to a reduction in harmonic distortion within the output voltage waveform. In a three-phase system featuring three AC-AC converters, the modulation technique is further enhanced by employing three modulated waveforms, each shifted by 120° relative to the others.

where Psc is the short circuit power of the grid at the PCC, expressed as $P_{SC} \triangleq V_g^2 / Z_g$, and P_{pv_rated} is the rated generation power of the whole PV plant. Accordingly, $|Z_g|$ can be represented by the SCR, which is expressed as:

$$|Z_g| = \frac{V_g^2}{P_{pv\_rated} \cdot SCR} \quad (2)$$

Boost converter:

A 3-phase phase-locked loop (PLL) synchronized the converter with the grid, using an inductance-capacitance-inductance (LCL) filter for connection. The system utilized external and internal loops to implement voltage-oriented control (VOC) within a synchronous rotating reference frame. The cascaded DC-AC-AC converters functioned as a controlled current source, with output voltages from the PV arrays dependent on current extraction and light intensity. Notably, an identical circulating current in each phase (i_a, i_b, i_c)complicated the regulation of each DC-link voltage through independent grid current-control loops.

Modelling of Solar PV Module:

The open circuit voltage signifies the highest voltage achievable at zero current, while the short circuit current represents the maximum current obtainable at zero voltage. The voltage and power characteristics are illustrated on the V-I curve, with the maximum power point (Vmp, Imp) indicating the optimal generation point. A typical silicon solar PV cell produces approximately 0.5 V, leading to the connection of multiple cells in series within a photovoltaic module. A configuration of electrically and physically linked modules is referred to as a panel, and a group of panels collectively forms an array.

B. Circuit Diagram

Fig. 4 illustrates the proposed system designed to verify the analysis and simulation results. Two scaled-down laboratory prototypes were created: one being a five-level single-phase DC-AC-AC converter and the other a three-level three-phase DC-AC-AC converter. These miniature models aimed to validate the conceptual design of the proposed topology. Each prototype operated in an off-grid configuration, utilizing a resistive load at the outputs, which were connected through an LC filter to ensure a smooth voltage output. This implementation enabled real-world testing of the converters' performance and behavior, thereby confirming the efficacy of the proposed modulation strategy and the overall design.

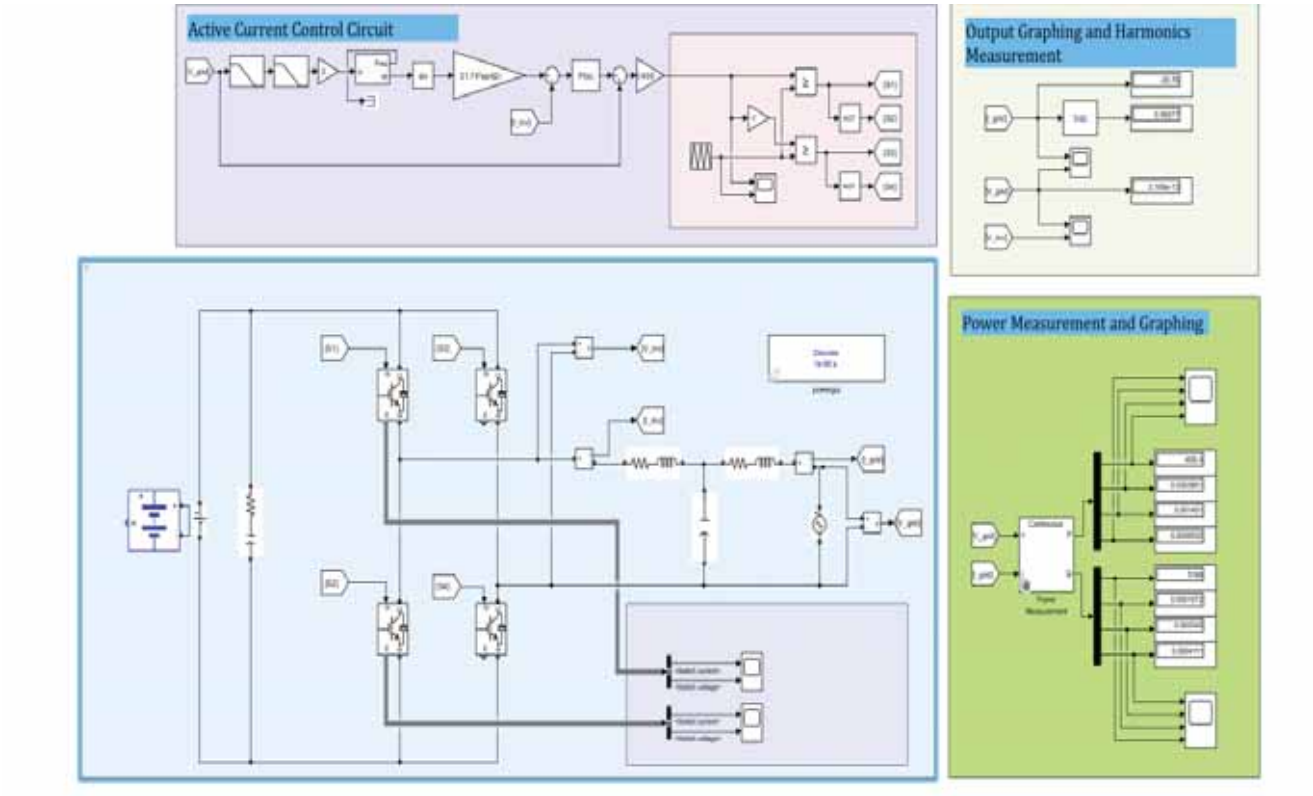

Fig 4. Circuit diagram of the proposed system

IV. Results

Fig 4,5 Power and harmonic measurements for the proposed DC-AC-AC converter system for photovoltaic (PV) applications were tested through both simulation and prototype implementations. The results validate the system's performance in terms of efficiency, voltage regulation, and harmonic reduction.

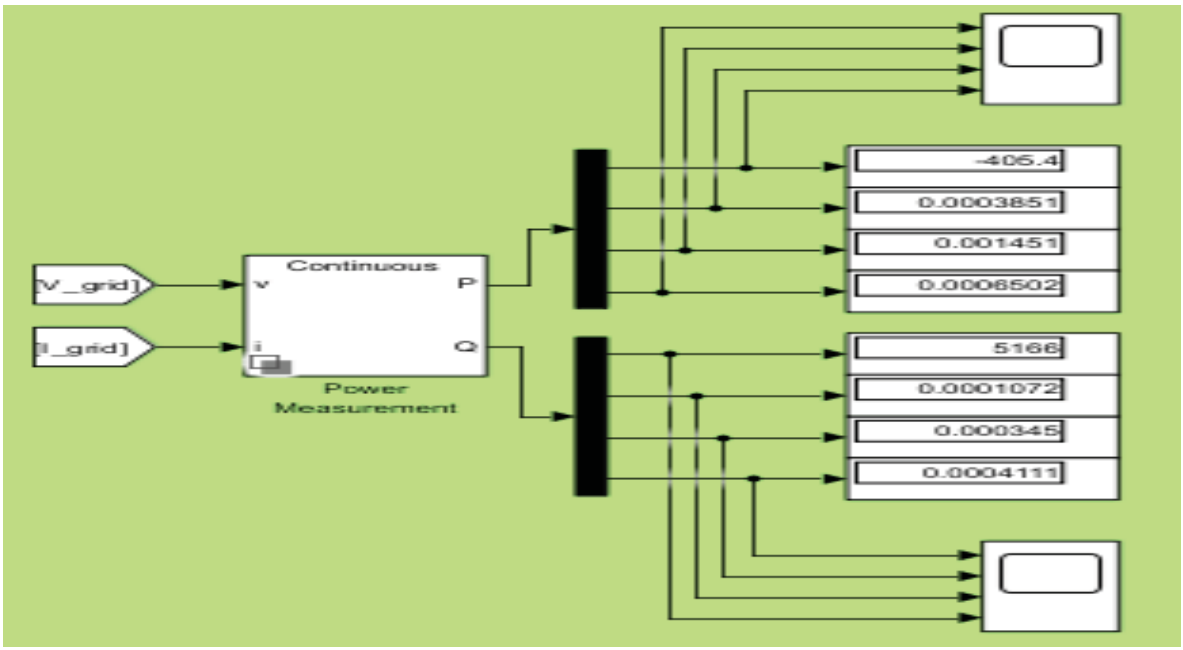

Fig 4 Cont... Power measurement

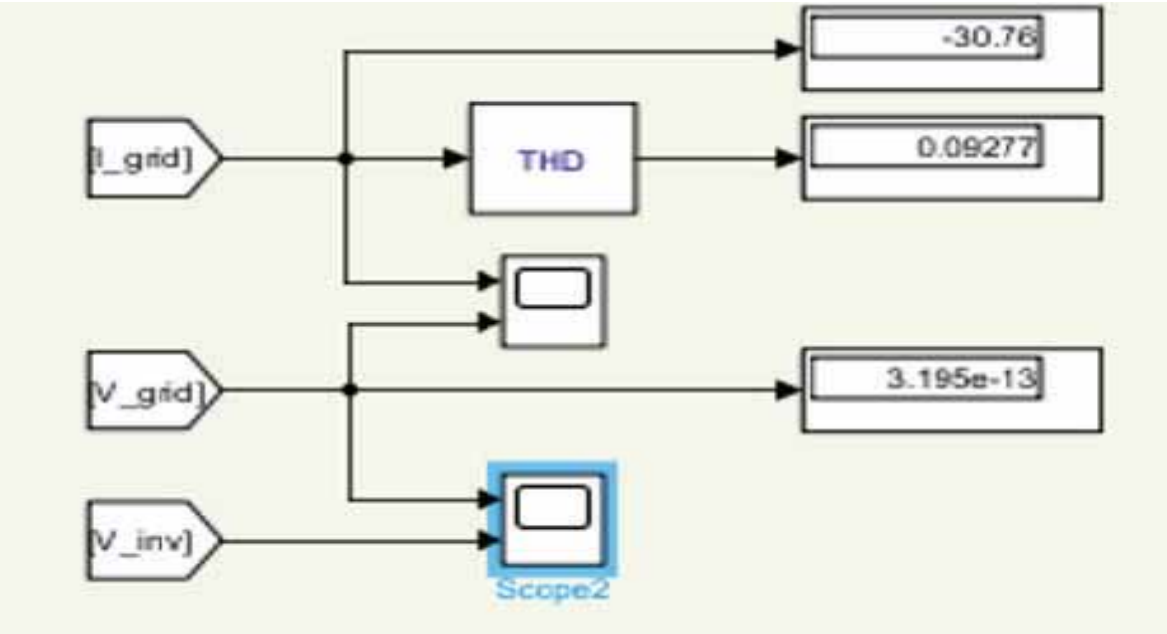

Fig 5. Harmonic measurement

TABLE-I.

PERFORMANCE COMPARISON OF OFF-GRID AND GRID-CONNECTED MODES IN POWER SYSTEM

Mode	Efficiency (%)	Total Harmonic Distortion (THD) (%)	Out put Power (kW)	Voltage Regulation (%)	Power Factor	Grid Current THD (%)
Off-Grid	95.5	2.1	10	+/- 1.5	-	-
Grid-Connected	96.2	1.8	15	-	0.99	3.0

V. CONCLUSIONS

The simulation results indicated that the proposed converter is a promising alternative to conventional medium-voltage (MV) grid-tied converters used in photovoltaic (PV) plants. The off-grid simulations validated that the steady-state performance of both current and voltage aligned with anticipated outcomes. By developing an effective commutation strategy, the matrix converter operated seamlessly alongside the medium-frequency (MF) transformer. The literature presents various solutions to address per-phase and per-cell imbalances caused by uneven light intensity across multiple PV arrays. The proposed DC-AC-AC converter naturally addresses the per-phase imbalance via its three-phase medium-frequency AC link. However, in instances where light intensity disturbances affected the k PV arrays unevenly, it resulted in varying energy harvest levels from each array, leading to per-cell imbalance. In conclusion, both reduced-scale versions validated the core concept of the converter, suggesting that the complete topology would function effectively.

REFERENCES

[1] Raghavan, R., & Suresh, S. "Control Techniques for Multilevel Inverters in Renewable Energy Systems: A Review." IET Renewable Power Generation, 17(2), 183-195, 2023.

[2] Ranjan, R. B. S., Kumar, S., & Bansal, J. C. "Multilevel Inverter Topologies for Renewable Energy Applications: A Review and Future Directions." Energy Reports, 8, 709-724, 2022.

[3] Khalil, A. B., Mahmud, R. D., & Kumar, T. S. "Enhanced PWM Techniques for Multilevel Inverters in Renewable Applications." IET Renewable Power Generation, 15(1), 12-25, 2021.

[4] Wu, J., Chen, X., & Zhang, Y. "Recent Advances in Cascaded Multilevel Inverters." IEEE Transactions on Power Electronics, 36(2), 1234-1246, 2021.

[5] Zhang, Y., Liu, S., & Wu, L. "Novel Multilevel Inverter Topologies for Renewable Energy Applications." IEEE Journal of Emerging and Selected Topics in Power Electronics, 9(4), 523-535, 2021.

[6] Murthy, M. S. K. S. H., Gupta, P. K., & Kumar, A. "A Comprehensive Review on Multilevel Converter Topologies." IET Power Electronics, 13(8), 1550-1564, 2020.

[7] Mohd, H. S., Rahman, F. M. A., & Karim, M. A. S. B. A. "Hybrid Multilevel Inverter Topologies for Solar PV Applications: A Review." Renewable Energy, 181, 188-200, 2022.

[8] Gupta, N., Sahu, R. K., & Gupta, S. K. "A Review on Cascaded H-Bridge Multilevel Inverter for Renewable Energy Applications." IEEE Access, 11, 138-152, 2023.

[9] Jaafar, T. M. S. E., Munir, M. M. A., & Mohd, I. Z. I. "Hybrid Multilevel Inverter Topologies for Solar PV Applications: A Review." Renewable Energy, 181, 188-200, 2022.

[10] Ayub, N. B., Zubair, M., & Adnan, M. "Review of Multilevel Inverters for Renewable Energy Applications." Renewable and Sustainable Energy Reviews, 153, 111757, 2021.

[11] Ceglia, G., Guzmán, V., Sánchez, C., Ibáñez, F., Walter, J., & Giménez, M. I. "A New Simplified Multilevel Inverter Topology for DC–AC Conversion." IEEE Transactions on Power Electronics, 38(5), 3150-3160, 2023.

[12] Babaei, E., & Farhadi Kangarlu, M. "Asymmetrical Multilevel Converter Topology with Reduced Number of Components." IET Power Electronics, 14(7), 1223-1232, 2021.

[13] Ebrahimi, J., Babaei, E., & Gharehpetian, G. B. "A New Topology of Cascaded Multilevel Converters with Reduced Number of Components for High-Voltage Applications." IEEE Transactions on Power Electronics, 37(3), 1855-1864, 2022.

[14] Shafique, M. A., & Hussain, R. "A Comprehensive Review of Control Techniques for Multilevel Inverters." Energy Reports, 8, 251-265, 2022.

[15] Liu, H., & Wu, L. "Multilevel Inverter Topologies: Recent Advances and Future Challenges." Renewable Energy, 193, 1337-1350, 2023.

[16] Zhang, Y., Liu, H., & Zhao, X. "Adaptive Control Strategies for Multilevel Inverters in Renewable Energy Systems." IEEE Transactions on Industrial Electronics, 68(12), 11956-11965, 2021.

[17] Mohd, J. S., & Kannan, R. "A New Symmetric Cascaded Multilevel Inverter Topology Using Single and Double Source Unit." Journal of Power Electronics, 21(4), 951-963, 2021.

[18] Ebrahimi, J., Babaei, E., Goverg, B. & Gharehpetian, G. "A new topology of cascaded multilevel converters with reduced number of components for high-voltage applications." IEEE Transactions on Power Electronics, 26(11), 3109-3118, 2011.

E-ISSN 2581 – 7957
P-ISSN 2277 – 3916
CVR Journal of Science and Technology, Volume 27, December 2024
DOI: 10.32377/cvrjst2711

Time Series-based Clustering of ECG Heartbeat Arrhythmia using Medoids

Dr. Jagadeeswara Rao Annam[1], Bala Krishna Tilakachuri[2]
[1]Professor, CVR College of Engineering/CSE (AI & ML) Department, Hyderabad, India
Email: ajagarao@gmail.com
[2] Asst. Professor, SR Gudlavalleru Engineering College/CSE Department, Gudlavalleru, India
Email: balakrishnagec@gmail.com

Abstract: **The symptoms of heart diseases are sparse and infrequent. So, the analysis of wearable long-term ECG recordings over hours, days and months is obligatory for detection of these infrequently occurring symptoms of heart diseases that would not be detected with short-term ECG recordings. Manual identification of these heart-beat classes by cardiologists is time consuming and cumbersome. These professionals rely on computer-based classification for determination of these heart-disease types. Partitioning around medoids (PAM also known as K- medoids) clustering using dynamic time warping (DTW) distance method (PAM time series- DTW) using the unequal length (dimensional) full heartbeat time-series is proposed with no explicit feature extraction except PQRST wave detection, which saves lot of time and computation cost.**

Index Terms: **Clustering, ECG, Heartbeat, Time-warping, AAMI.**

I. Introduction

The cardiac rhythm abnormalities are different in shape from the normal rhythm of the heart-beat cycle and are known as heart-beat arrhythmia. And the symptoms of these heart diseases are sparse and infrequent[21]. So, the analysis of wearable long-term ECG recordings over hours, days and months is obligatory for detection of these infrequently occurring symptoms of heart diseases that would not be detected with short-term ECG recordings. Manual identification of these heart-beat classes by cardiologists is time consuming and cumbersome [20]. These professionals rely on computer-based classification for determination of these heart disease types. Clustering is the task of grouping patterns such that patterns in one group or cluster are similar compared to the patterns in another cluster in some sense and to identify underlying structure in the un-labeled data set by objectively organizing data into analogous groups. Clustering is mandatory when class labeled data are not available irrespective of the type of data. And any clustering approach uses distance function $f(x_i, x_j)$, that denotes a measure of "distance" between two patterns, the smaller the distance, the closer or more similar are the objects.

In supervised classification, complexity of space and time grows with the number of patterns in the train data [6]. So clustering is motivated from the dis-advantages of supervised classification for both inter-patient and intra-patient supervised approaches.

This work addresses these issues by clustering (unsupervised classification) which does not require the class labels of the pattern data. This article presents the proposed clustering approaches of ECG data. The related literature review of clustering ECG data is presented in section II. The proposed full time-series clustering of ECG Data by PAM using DTW distance is detailed in section III. Results and discussions are presented in section IV and in section V Conclusion is presented.

II. Background

Maier, Dickhaus and Gittinger [11] proposed two clustering approaches, first a hierarchical agglomerative clustering (HAC) and second a normalized cross correlation (NCC) based clustering. In HAC, taking 64 samples from either side of R from channel 1 of MIT-BIH data, 128 samples time-series were constructed for each beat. Features are extracted from each fixed-length series taking eight coefficients using Fourier transform (four real and four imaginary), first eight coefficients from discrete co- sine transform and top seven Hermite coefficients along with time–scale parameter. Using a two-step process, starting with 200 clusters each with 200 beats, L_2 distance between 2 beats A and B as in eq. (1) (Euclidean distance, where p=2) is applied to generate 40 clusters. In the second step, L_1 distance between 2 beats A and B (Manhattan distance, where p=1) as in eq. (1) is used in a merging process.

$$L_p(A,B) = (\sum_{i=1}^{n}(A_i - B_i)^p)^{\frac{1}{p}} \quad (1)$$

Castro, Felix and Presedo [1] proposed a clustering using derivative DTW distance using fixed length QRS time series of each beat on 24 patient records. Sotelo, Castellanos, and Acosta (2012) [15] presented a Gaussian EM based clustering approach using AAMI categorization. A total of 100 features were extracted using intervals, 4-level coefficients of Daubechies-2 wavelet, hermite coefficients and morphological amplitudes. Hermite coefficient h_i is based on $\emptyset_n^{\sigma}(t)$.
Bohui, Ding and Hao [18] extended maximum margin (MM) approach of SVM classification for clustering of ECG beats. The MM clustering was used to find not only the Hyper plane coefficients but also the class labelsin an unsupervised way. Class balancing is alsoachieved by using a factor proposed by Xu et al. [16]. Nine features including six normalized intervals and three normalized amplitudes, are extracted from intervals and amplitudes for each beat. The IEMMC method avoids solving nonconvex integer optimization (NCO) problem by

Received on 23-05-2024, Revised on 22-06-2024, Accepted on 22-07-2024.

reducing it into a semi definite matrix programming (SDP) problem using SDPT3 and SeDuMi solvers to improve the time efficiency. Chang et al. [2] reported best clustering result out of 10 runs for each record using total101,374 ECG beats for each of four measures L1, L2, cross-correlation and grey relational grade (GRG) that obtained 99.46%, 99.38%, 99.66%, and 99.68% in accuracy respectively. Sotelo et al. [15] used supervised measures of sensitivity and specificity considering clusters in between $9 \leq k \leq 11$. This paper reported $S_e\%$ $99.2 \pm 2.4, 91.1 \pm 15.6,$ 96.11 ± 8.2 $, 70.7 \pm 32.0$ and $S_p\%$ $95.77 \pm 9.12,$ $99.36 \pm 2.19,$ 99.87 ± 0.2 and 99.59 ± 0.77 for N,S,V and F AAMI classes, respectively.

III. Method

This section details the proposed approach of full time-series based clustering of ECG heart- beat time-series. The PAM (aka K-medoids) clustering of unequal-dimensional beats using DTW distance is presented.

Though the DTW distance measure is not a metric since it does not satisfy the triangle in equality, but it is able to compute distance of two unequal length or dimensional time series segments. DTW aligns the sequences using dynamic programming based constraints. DTW provides a warping path that optimally deforms one of the two input series onto the other to calculate the distance or similarity of unequal dimensional sequences or signals. After observing the viability of clustering of unequal- length (or dimensional) full heart-beat time-series patterns by K-medoid approach using dynamic warping distance on the partial dataset of MIT-BIH (considered only 6250 beats from the total of 100,732 beats). Considering 4 clusters based on AAMI categorization of N, S, V and F ([5]), Clustering by K-medoids approach using dynamic time warping (DTW) distance measure is performed on the time-series pattern data.

The k-medoids clustering using the data set Nd is a partitioning around medoids (PAM) algorithm and is as follows: The Euclidean distance (ED) metric has been widely used in spite of its known weakness of sensitivity to distortion in time axis. ED cannot compute distance of two **unequal length time series** segments.

Algorithm 1 K-medoids Clustering algorithm

1. Choose K random objects as initial medoids.
2. Assign each object to the cluster associated with the closest medoid. compute thecost associated with the cluster.
3. Change each cluster center with its members randomly and see if the cost is decreased. If cost decreases, accept the change, otherwise reject the change.
4. Iterate Steps 3 and 4 till the termination condition is reached by checking the current medoids are unchanged from previousand iteration.

ED is shown to be ineffective in measuring distances of time series in which shifting and scaling are mandatory [3]. Consequently, warping distances such as dynamic time warping (DTW), longest common subsequence (LCSS) are proposed to handle warps in time dimension. Spatial assembling distance (SpADe) is able to handle shifting and scaling in both time and amplitudes. Similarity measures fall basically into three categories. *Non-elastic metrics* such as L_p norms that do not use time shifting such as Euclidean Distance (ED) and Correlation. *Elastic measures* that use time shifting but are not metrics such as DTW or longest bommon sub-sequence (LCSS) and *elastic metrics* that use time shifting such as edit distance with real penalty (ERP). Elastic measures that belong to the DTW category are not metrics since they do not satisfy the triangle inequality.

DTW algorithms compute distance of two unequal length time series segments by aligning the signals using dynamic programming based constraints. Dynamic time warping is a technique for comparing time series, providing both a distance measure that is insensitive to local compression and stretches and the warping which optimally deforms one of the two input series onto the other. Berndt and Clifford introduced DTW a classic speech recognition to the data mining community, in order to allow a time series to be stretched or compressed to provide a better match with another time series.

A. Distance using Warping path

A warping path is a sequence W = $\{w_1, w_2, \ldots, w_k, \ldots, w_K\}$ where $max(m, n) \leq K < m + n - 1$ satisfying the following three conditions.

1. Boundary conditions: This requires the warping path to start and finish in diagonally opposite corner cells of the matrix. $w_1 = (1, 1)$ and $w_K = (M,N)$
2. Continuity: Given $w_K = (a, b)$, then $w_k{-}1 = (a', b')$, where $a - a' \leq 1$ and $b - b' \leq 1$. This restricts the allowable steps in the warping path to adjacent cells.
3. Monotonicity: Given $w_k = (a, b)$, then $w_k{-}1 = (a', b')$, where $a - a' \geq 0$ and $b - b' \geq 0$.

Algorithm 2 DTW Algorithm

DTWP, Q sequences of length M and N respectively **Input:** sequences P, Q **Output:** DTW distance from optimal warping Path **Step 1.** Calculation of local distance matrix For$i \in [1, \ldots, M]$ For$j \in [1 : N]$
$C(i, j) = ||(P_i - Q_j)||$ EndFor EndFor
Step 2. Calculate global distance matrix of first row For$j \in [1, \ldots, N]$
Initialize $D(1, j) = 0$; For$k \in [1 : j]$

$$D(1, j) = D(1, j) + C(P_1, Q_k)$$

EndFor EndFor
Step 3. For$i \in [1, \ldots, M]$ $D(i, 1) = \sum_{k=1}^{i} C(P_k, Q_1)$ *for* $i \in [1, N]$ EndFor **Step 4.**
$D(i, j) = min[D(i-1, j-1), D(i-1, j), D(i, j-1)] + C(P_i, Q_j)$
Step 5. Find Optimal Warping Path
$\sqrt{\sum_{k=1}^{K} w_k}$

This forces the points in W to be monotonically spaced in time.

B. Distance using optimal warping path

To find the best match between these two sequences, a path through the matrix that minimizes the total cumulative distance between is to be retrieved. There are exponentially many warping paths that satisfy the above conditions. But the path that minimizes the warping cost the optimal path that minimizes the warping cost. The subset of the matrix that the warping path is allowed to visit is called the warping window. Two of the most frequently used global constraints are Sakoe–Chiba band [14], and Itakura parallelogram [8]. Alignments of cells can be selected only from the respective shaded region. The Sakoe-Chiba band runs along the main diagonal and has a fixed (horizontal and vertical) width $T \in N$. This constraint implies that an element x_n can be aligned only to one of the elements y_m.

The Euclidean distance between two sequences is a special case of DTW where the k th element of w is constrained such that $w_k = (i, j)$, $i = j = k$. But this special case is only defined where the two sequences have the same length. The time and space complexity of DTW is O(nm).

The results of time series clustering by PAM using DTW distance measure are shown in Table 1. PAM clustering using DTW distance obtained average clustering accuracy % of 67.18 ± 8.86 of 22 records with 10 experiments on each record as shown in Table 1.

As the beat-wise time series from P on set to T off set has a mean length of 292 samples it took an average execution time of 5.5 minutes per record amounting to a total execution time of 122 minutes on the total 22 records of dataset-2 (DS2) confining to 10 experiments (iterations) on each record.

IV. Results and Discussion

The Hungarian approach [12] originally pro- posed by Kuhn and improved by Munkres [13], is used for mapping the predicted clusters to the target labels in an unsupervised manner. Mann-Whitney U-Test [19] is employed in order to compare the proposed solutions with one another and determine the statistical significance of the observed differences in the performance.

Comparison with solutions in literature

As shown in Table 2, Castro (2015) [1] reported global accuracy of 98.56% for MITBIH labels and 98.84% with AAMI class labels using 25 maximum number of clusters.

Zhang et al. [17] reported cluster similarity measure (CSM) as 0.4240. Chudacek et al. [4] reported total sensitivity of 97.95 using two class data of 74413 ‘N’ and 6954 ‘V’ beats from the total MIT database using a rule-based decision tree (RBDT).

Bohui et al. [18] reported Se, Sp and accuracy% of 90.3, 97.4 and 95.9 for AAMI classes and is shown superior to iterSVR clustering and k-means clustering on a small dataset of 1682 beats from seven records of MIT/BIH database.[11] reported a 0.15% mis-classification rate (MCR) on the total 109000 beats that were classified into 14 beat classes within 31s with only.

PAM Time DTW using unequal length full time series on 4 clusters have obtained a global accuracy 67.2 8.8 on 22 records. A K-means clustering is also investigated for comparing the results.

TABLE-I.

Results of PAM Clustering using DTW Distance of 10 Iterations

Rec	Accuracy %		Exec. Time in Seconds	Beat lengths	
	Avg.	Std dev		Min	Max
100	70.44	10.76	448.45	56	263
103	99.90	0.00	359.49	68	224
105	60.81	25.00	267.10	58	244
111	66.68	14.78	281.57	67	247
113	59.07	4.00	395.09	68	234
117	99.93	0.00	216.07	90	227
121	79.71	15.63	139.79	112	292
123	72.65	14.25	240.09	107	248
200	75.07	13.99	358.09	97	302
202	41.49	4.51	597.43	92	241
210	49.54	8.97	418.02	76	242
212	100.00	0.00	149.22	86	203
213	47.03	6.27	236.50	75	214
214	55.10	5.05	514.68	106	266
219	45.05	10.45	203.62	104	255
221	70.75	14.41	541.15	101	235
222	75.06	11.28	603.51	73	285
228	51.29	0.00	207.84	95	244
231	77.38	6.62	294.58	104	306
232	61.71	6.69	221.01	75	252
233	71.75	19.04	271.69	83	217
234	47.48	3.30	321.17	61	214
Avg%	67.18	8.86	5.5 Minutes per record		

TABLE-II.

ECG CLUSTERING SOLUTIONS IN LITERATURE

	Method	Features	Clustering	Results %
1	PAM Time DTW K-means	full timeseries of unequal length 12 features	4 clusters 4 clusters	67.2± 8.8 63.6± 5.5
2	Castro [1] 2015	108 sample similarity	DTW cluster Template Match	97.1
3	Bohui [18] 2013	1682 beats	Max margin	95.4
4	Sotelo [15] 2012	Db DWT, HBF $9 \leq k \leq 11$	Gaussian EM JH-means	Se% 99.2± 2.4,
5	Chang [2] 2009	2-step cluster 73 sample	L1, L2 CC, GRG	99.68%
6	Korurek [9] 2008	Ant colony 5 feat	6 class NN	Se% 94.40 8771 beats
7	Chudacek [4] 2007	Decision Tree 13 feat	2 class N andV	Se%: 96.63
8	Zhang [17] 2006	Haar wavelet N, A, V	AHC, KM	CSM: 0.4240
9	Kinsner [7] 2002	residual DTW Threshold RMS	2 class	NPRD 1.33%
10	Lagerholm [10] 2000	200 millisec HBF, RR	SOM 25 clusters	Acc 99.1 MCR 1.5%
11	Maier [11] 1999	128 sample DCT, DFT, HBF	1. HAC L1, L2 2. cross-corr	MCR 2% MCR 0.05%

Abbr: HAC: Hierarchical agglomerative cluster, HBF: Hermite basis function, MCR: Misclassification rate, GRG: grey relational grade, HOS: higher order statistics, IEMMC: Immune evolutionary maximum margin cluster, NPRD: normalized percent root-mean-square difference.

From the Table 2, it is observed that majority of the clustering solutions reported in the literature seem to have superior performance as compared to our solutions investigated. However, it is to be noted that these approaches have not reported results from ex- tensive experimentation of 100 runs as attempted in this work. Moreover, most of the solutions con- sider only a small subset of data for experiments whereas we considered the complete test set of 22 records of MIT-BIH benchmark data set for the experiments. The overall results reported in the existing literature could be taken as an over- optimistic estimate whereas the results reported here could form the conservative lower bound on unsupervised clustering approaches for ECG data.

V. CONCLUSIONS

This paper has presented a novel clustering approach proposed using full time-series based ECG heart-beat data. This approach is a PAM clustering using DTW distance using unequal length (dimensional) complete heart-beat time series that is experimented using MIT-BIH AD database. A K-means clustering is also investigated for com- paring the results. PAM clustering using dynamic time warping (DTW) distance method (PAM time- series DTW) using unequal length (dimensional) full heart-beat time-series has shown superior results compared to feature based K-means clustering.

REFERENCES

[1] D. Castro, P. Felix, and J. Presedo. A method for context-based adaptive qrs clustering in real time. *IEEE journal of biomedical and health informatics*, 19(5):1660–1671, 2015.

[2] K.-C. Chang, C. Wen, M.-F. Yeh, and R.-G. Lee. A comparison of similarity measures for clustering of qrs complexes. Biomedical Engineering: *Applications, Basis and Communications*, 17(06):324–331, 2005.

[3] Y. Chen, M. A. Nascimento, B. C. Ooi, and A. K. Tung. Spade: On shape-based pattern detection in streaming time series. *In 2007 IEEE 23rd International Conference on Data Engineering*, pages 786–795. IEEE, 2007.

[4] V. Chudacek, M. Petr´ık, G. Georgoulas, M. Cepek, L. Lhotska, and C. Stylios. Comparison of seven approaches for holter ecg clustering and classification. *In 29th Annual International Conference of IEEE Engineering in Medicine and Biology Society*, pages 3844 – 3847. IEEE, 2007.

[5] A.-A. EC57. Testing and reporting performance results of cardiac rhythm and st segment measurement algorithms. *Association for the Advancement of Medical Instrumentation, Arlington*, VA, 1998.

[6] Y. H. Hu, S. Palreddy, and W. J. Tompkins. A patient-adaptable ecg beat classifier using a mixture of experts approach. *IEEE transactions on biomedical engineering*, 44(9):891–900, 1997.

[7] B. Huang and W. Kinsner. Ecg frame classification using dynamic time warping. In IEEE CCECE2002, *Proceedings of Canadian Conference on Electrical and Computer Engineering*., volume 2, pages 1105–1110. IEEE, 2002.

[8] F. Itakura. Minimum prediction residual principle applied to speech recognition. *IEEE Transactions on acoustics, speech, and signal processing*, 23(1):67–72, 1975.

[9] M. Kor¨urek and A. Nizam. A new arrhythmia clustering technique based on ant colony optimization. *Journal of Biomedical Informatics*, 41(6):874–881, 2008.

[10] M. Lagerholm, C. Peterson, G. Braccini, L. Edenbrandt, and L. Sornmo. Clustering ecg complexes using hermite functions and self-organizing maps. *IEEE Transactions on Biomedical Engineering*, 47(7):838–848, 2000.

[11] C. Maier, H. Dickhaus, and J. Gittinger. Unsupervised morphological classification of qrs complexes. In *Computers in Cardiology 1999.Vol. 26 (Cat. No. 99CH37004),* pages 683–686. IEEE, 1999.

[12] N. Megiddo and C. H. Papadimitriou. On total functions, existence theorems and computational complexity. *Theoretical Computer Science*, 81(2):317–324, 1991.

[13] J. Munkres. Algorithms for the assignment and transportation problems. *Journal of the society for industrial and applied mathematics*, 5(1):32–38, 1957.

[14] K. K. Paliwal, A. Agarwal, and S. S. Sinha. A modification over Sakoe and Chiba's dynamic dynamic time warping algorithm for isolated word recognition. *Signal Processing*, 4(4):329– 333, 1982.

[15] J. Rodrıguez-Sotelo, G. Castellanos Dominguez, C. Acosta-Medina, and R. Millis. Recognition of cardiac arrhythmia by means of beat clustering on ecg-holter recordings. *Advances in Electrocardiograms-Methods and Analysis*, 221:250, 2011.

[16] L. Xu, J. Neufeld, B. Larson, and D. Schuurmans. Maximum margin clustering. In *Advances in neural information processing systems*, pages 1537–1544, 2005.

[17] H. Zhang, T. B. Ho, Y. Zhang, and M.-S. Lin. Unsupervised feature extraction for time series clustering using orthogonal wavelet transform. *Informatica*, 30(3), 2006.

[18] B. Zhu, Y. Ding, and K. Hao. A novel automatic detection system for ecg arrhythmias using maximum margin clustering with immune evolutionary algorithm. *Computational and mathematical methods in medicine*, 2013, 2013.

[19] Jeremy Stangroom. Mann Whitney Test Calculator. Social Science Statistics. (accessed November 09, 2023, http://www.socscistatistics.com/tests\\/mannwhitney/Default3.aspx

[20] Balakrishna Tilakachuri; Annam Jagadeeswara Rao; Haritha Dasari, "Comparative analysis on liver benchmark datasets and prediction using supervised learning techniques", *Indonesian Journal of Electrical Engineering and Computer Science*, [S.l.], v. 36, n. 2, p. 1043-1051, nov. 2024. ISSN 2502-4760.

[21] Annam. Jagadeeswara Rao, Image Segmentation Based On Tint Using Data Mining Techniques, Journal of Theoretical and Applied Information Technology 31st May 2023. Vol.101. No 10, 2023 Little Lion Scientific ISSN: 1992-8645 E-ISSN: 1817-3195 pp 4112-4118

E-ISSN 2581 –7957
P-ISSN 2277 – 3916

CVR Journal of Science and Technology, Volume 27, December 2024
DOI: 10.32377/cvrjst2712

Stacked Autoencoder-based ELM with Unsupervised Feature Extraction for Efficient Classification of Tumors

Dr. A. Christy Jeba Malar[1], Dr. M. Deva Priya[2]
[1]Assoc. Professor, Sri Krishna College of Technology/IT Department, Coimbatore, Tamil Nadu, India
Email: a.christyjebamalar@skct.edu.in
[2]Professor, Karpagam College of Engineering/CSE Department, Coimbatore, Tamil Nadu, India
Email: meetdevapriya@gmail.com

Abstract: **Tumors may exist in the brain, lungs, esophagus, leukemia, breast, ovary and bladder. Each tumor has its pathogenesis and categorizing them is an uphill task. Appropriate features are to be extracted, and the data of tumor should be classified either as benign or malignant. This is a critical issue as treatment of patients is solely based on this. In this paper, tumor data is classified using Stacked Extreme Learning Machine (S-ELM) and features are extracted using Statistically Controlled Activation Weight Initialization (SCAWI). It involves unsupervised clustering and is based on Neural Network (NN) framework. The proposed method offers a good decision support system for classifying tumor data. The proposed scheme is applied to data obtained from hospitals of repute and publicly available domains and tested for its outperformance. Results are compared with basic ELM and Multilayer-ELM (ML-ELM). It is seen that S-ELM with SCAWI offers better performance in contrast to diverse methods of classification.**

Index Terms: **Breast Tumor, ELM, Multilayer-ELM, Tumor Classification.**

I. Introduction

Breast cancer is seen to be common among women. Hence, timely diagnosis of the disease is of the greatest demand. As the count of patients with tumors keep increasing, it is essential to design an automated system that identifies tumors in early stages, thus saving lives. Timely detection of brain tumors plays a dominant role in improving treatment outcomes. Traditionally, breast tumors are diagnosed through biopsies, which require invasive surgery. However, the techniques of computational intelligence can aid in the identification and classification of breast tumors, offering a less invasive option.

At present, RX mammography is an extensively used screening method for breast cancer [1]. Nevertheless, it has some shortcomings. As it employs ionizing radiation, it is not suitable for young women with breasts of high-density. Identifying breast lesions is also challenging due to lacking of functional information. Ultrasound (US) is capable of detecting cancers in female patients with dense breasts as well as negative mammography. It is useful in characterizing abnormalities that are identified mammographically, evaluating tumor size as well as nodal status, and managing needle biopsy [2]. Nevertheless, its capability to detect contra or ipsi-lateral malignant lesions is limited.

The quality of images will be increased by pre-processing them using filters. Noise can be removed from edges without disturbing their edges, whereas unwanted regions can be removed by segmenting images followed by feature extraction and selection. An ideal feature set is the one that includes selective features extracted using fuzzy clustering algorithms. Tumors can be classified as benign or malignant using Artificial Neural Network (ANN) as it best suits datasets with more number of attributes and delivers a unique solution. It offers improved accuracy. It helps physicians in prompt detection and treatment of tumors, thus reducing mortality rate. Extreme Learning Machine (ELM) is a Single-layer Feed Forward Network (SLFN) with arbitrary weights. As it offers good training accuracy and circumvents local minima, it is used in disease diagnosis. It is capable of handling non-linear complex data.

In this paper, a statistically controlled weight initialized Stacked ELM (S-ELM) is proposed for multi-platform image and clinical data. It handles inter and intra-modal cancer subtypes. It divides a large ELM network into several stacked small ELMs that are linked serially. It is efficient in approximating a huge ELM network by involving less amount of memory [3].

The ELM with one hidden layer poses memory restrictions in some problems. Multilayer ELM (ML-ELM) is an extended form of ELM which supports unsupervised learning using ELM autoencoders. It eradicates the necessity of parameter tuning, facilitating improved representation learning as it includes numerous layers [4].

Cancer data represented by hidden variables are learnt using unsupervised subtractive clustering algorithm. Stacked auto-encoder framework based generative model is designed to express hidden features defined by every input. The results of hidden variables are combined to extract common features.

Clinical Features

Clinical features are based on medical records. They offer instructions or information necessary for classification. Tumors may be classified using a pattern recognition framework that is based on features and classifiers [5]. Several ML algorithms are applied to classify breast lesions based on different feature categories including dynamic, morphological and textural features [6].

Breast tumor dataset includes mammogram images. Generally, around 32 parameters are involved in classifying

Received on 23-09-2024, Revised on 23-10-2024, Accepted on 22-11-2024.

cancer [7, 8]. In the case of their values are comparatively high, it is a sign of malignancy.

- **ID:** It is a number that represents identification.
- **Membrane Diagnosis:** It represents tissue diagnosis which may take values, either malignant or benign. For varying types of cancer, it is essential to find the right tissue diagnosis if both membranes involve varying treatments.
- **Mean, Standard Error (SE) and Radius:** They represent a range between the centre and point on perimeter.
- **Radius:** Radius SE is another parameter. Radius worst represents the maximum value of centre for determined range and it is necessary to compute the distance amid centre and point as surgery is based on size. Surgery is not advisable for large tumours.
- **Texture:** The mean value denotes Standard Deviation (SD) of Gray-Scale (GS) values. SE of texture signifies the SE of determined SD for GS values. The worst value denotes the maximum mean of SD for GS values. The GS is used for determining tumor location, while SD is indispensable for finding data variation and detail of spread.
- **Perimeter:** The mean value represents the mean of core tumor, while SE of mean signifies core tumor. The worst value denotes the maximum value of core tumor inscribed on perimeter.
- **Area:** The mean, SE and worst point at related values are associated with mean areas of cancer cells.
- **Smoothness:** The mean value denotes the mean for regional disparities in range of radius, while SE of smoothness denotes SE of mean of local differences in length of radius and worst denotes the largest mean value.
- **Compactness:** The mean value represents the mean value of perimeter as well as area, SE of compactness represents SE of mean, and worst represents the highest mean of calculation.
- **Concavity:** It denotes severity of concave parts of shape, whereas mean of concave points denotes quantity of concave parts of contour. SE of concavity signifies SE of concave parts.
- **Concave points:** It denotes SE of concave parts of shape. The worst values of Concavity and concave points denote maximum value of mean.
- **Fractal Dimension (FD):** The mean value denotes the mean for approximation of coastline, FD SE is the SE of coastline approximation, whereas FD worst denotes the maximum mean value.

II. Related Work

In this section, the diverse methods available for diagnosing breast tumor are detailed below.

Assiri et. al. (2020) [9] have compared hard and soft voting methods for ensemble learning. It is seen that hard voting which relies on a majority-based approach outperforms existing algorithms in the detection of breast cancer leading to enhanced accuracy in classification. Yadav & Jadhav (2022) [10] have discussed how Machine Learning (ML) serves as a powerful statistical tool for software applications, enabling them to learn from data without manual coding. By analyzing thermal scans, ML is capable of identifying areas demanding further review by healthcare professionals. Thermal imaging offers a simpler, more efficient diagnostic alternative compared to complex equipment, making it beneficial for clinics and hospitals in enhancing diagnostic accuracy.

Dewangan et. al. (2022) [11] have introduced a detection model named Back Propagation Boosting Recurrent Wienmed (BPBRW) which uses a Hybrid Krill Herd African Buffalo Optimization (HKH-ABO) mechanism to improve early-stage breast cancer diagnosis through MRI images. The model trains on breast MRI images, applies an innovative Wienmed filter for noise reduction and classifies tumors as benign or malignant. The implementation carried out in Python shows that this model achieves a higher accuracy rate with a reduced error rate, demonstrating its efficiency in early breast cancer detection. Mohamed et. al. (2022) [12] have contributed significantly by proposing a Deep Learning (DL) approach for identifying breast cancer from biopsy images using Convolutional Neural Network (CNN). The study examines the effects of different data pre-processing techniques on model performance and has introduced an ensemble learning method to integrate the best models leading to improved classification accuracy.

Dar et. al. (2022) [13] have conducted a comprehensive review of studies focusing on detection and classification of breast cancer across various imaging technologies. This work analyses existing research employing ML, DL and Deep Reinforcement Learning (DRL) for detection and classification of breast cancer. Publicly available datasets relevant to these imaging methods are surveyed to support future research and have concluded with a discussion on current challenges and opportunities in this evolving field. Abunasser et. al. (2022) [14] have developed a DL model aimed at detecting and classifying breast cancer types including benign and malignant forms. The performance of models is evaluated utilizing a dataset from Kaggle through metrics like precision, F1-score, recall and accuracy. The results indicate that DL models are highly effective for accurate detection and classification of breast cancer.

Abunasser et. al. (2023) [15] have introduced BCCNN model for breast cancer detection and classification. This model processes MRI images and incorporates effective pre-trained DL models, initially trained on ImageNet and adapted for the classification of breast cancer. The dataset sourced from Kaggle is expanded using Generative Adversarial Network (GAN) to enhance its size and diversity. Each model is evaluated using different datasets for 30 experiments to assess the effectiveness of the models. Labcharoenwongs et. al. (2023) [16] have developed an automated system for detecting, classifying and estimating the volume of breast tumors using DL techniques, specifically analyzing breast ultrasound images. They have employed various data augmentation methods like blurring and flipping for enhancing training and testing datasets. YOLOv7 architecture is utilized for tumor detection and classification yielding strong performance with increased accuracy and confidence scores, highlighting the potential of

the systems to assist radiologists in improving the diagnosis of breast cancer.

Ranjbarzadeh et. al. (2023) [17] have examined segmentation methods in image processing within Computer Aided Diagnosis (CAD) systems. The study categorizes segmentation techniques into supervised, unsupervised and DL-based methods aiming at providing an overview of strengths and weaknesses of every approach to aid researchers in selecting the most appropriate technique for specific applications. Ali & Agrawal (2024) [18] have proposed a hybrid model for automatic image segmentation that combines VGG19 architecture with ResNet101 through CNN. The classifier is optimized using Bayesian methods and cross-validation is employed to identify the best parameters for optimized classifiers. Diverse Transfer Learning (TL) models are used for determining the most effective one for detecting brain abnormalities using NNs. The proposed stacked classifier model leverages the advanced technologies and demonstrates better results in contrast to the existing models.

III. Proposed Methodology

In case of breast tumor classification, standard MRI examination and scanning protocols are not readily available. Another challenge is that datasets including breast MRI images are not extensively available. The next challenge deals with the type of features extracted. Combination of features may confuse the clinician making it difficult to understand and interpret. Further, certain features cannot be applied directly. Hence, an ideal set of features proficient in an efficient classification of tumors should be selected.

Accurate selection of features simplifies the job of a classifier. Performance can be improved by using sophisticated classifiers like ANN, Support Vector Machine (SVM), etc., by involving several features. Unintelligible set of features can be combined with non-linear classifier.

A. Noise Removal using Gaussian Filtering

Gaussian filtering [20] is involved in blurring images and removing noise. Gaussian function is given by,

$$G(x) = \frac{1}{\sqrt{2\pi\sigma^2}} \frac{e^{-x^2}}{2\sigma^2} \quad (1)$$

Where,

σ - Standard Deviation of distribution

The mean is initialized to '0'.

These filters involve 2D Gaussian distribution which is a point-spread function. It convolves distribution function with image. Discrete approximation is to be produced for Gaussian function. As Gaussian distribution is non-zero, theoretically it demands an infinitely huge convolution kernel.

B. Classification

Target class for every case in data is to be predicted accurately. Classification models are verified by comparing predicted and known target values in test data. Historical data for classification is typically split into training and testing sets. Once features are extracted, the image is classified into malignant or benign ones by using the ELM.

A systematic assessment of various pattern recognition approaches are involved in classifying breast lesions using morphological, dynamic as well as textural features. Classification is performed using ANN, SVM, Linear Discriminant Analysis (LDA) and ELM-based approaches.

Extreme Learning Machines (ELM)

Huang et. al (2011) [19] have proposed ELM for SLFN. It supports increased learning speed and offers good generalization. Hidden nodes are chosen randomly in ELM. They outperform SLFN and SVM. ELM systematically assigns weights to output nodes and supports faster training. It yields better generalization but finds difficulty in handling huge amount of data.

Accurate selection of classifier is challenging. Several classifiers are available in the literature.

- Linear classifiers are efficient but combined feature interpretation is an uphill task.
- Non-linear classifiers like ANN and SVM yield good performance, but interpretation of classification hyperplanes are demanding.
- Tree-based classifiers grounded on simple threshold-based rules face the issue of overfitting.

Features can be combined as classifiers are not appropriate for all features.

Stacked Extreme Learning Machine (S-ELM)

Algorithm for S-ELMs learning network is detailed below.

Given,

$\{(x_i, t_i) | x_i \in R_n, t_i \in R_m, i = 1, \ldots, n\}$ - A large training dataset

g(x) - Activation function

N - Quantity of hidden nodes in every layer 'L'

L^1 - Quantity of target combined nodes

C - Regularization co-efficient

S - Total amount of layers

Step 1: Implement ELM algorithm in layer 1:

- Arbitrarily produce hidden layer factors, bias 'b_i' and weight 'w_i', where i=1,..., L
- Determine output matrix 'H' in hidden layer
- Determine output weight 'β'

$$\beta = \left(I/C + H^T H\right)^{-1} . H^T H \quad (5)$$

Step 2: Reduce PCA dimension of 'β^T'

- Reduce dimension of 'β^T' from 'L' to 'L^1'
- Record reordered Eigen vectors as $\sim V \in R^{L,L^1}$

Step 3: Learning step for layer 2→S:

for p=1 to S - 1

- Arbitrarily produce $(L - L^1)$ hidden nodes and determine conforming 'H_{new}'
- Determine joint significant nodes 'H^1'

$$H^1 = H^{\sim} . V \quad (6)$$

- Compute output matrix of hidden layer

$$H = [H^1, H_{new}] \quad (7)$$

- Repeat step 1(c) and step 2. Step 2 is not necessary in the last layer 'S' end for

CVR Journal of Science and Technology, Volume 27, December 2024
DOI: 10.32377/cvrjst2712

Step 4:

- Compute 'F_{out}' and give it as output of S-ELMs learning network in last layer

$$F_{out} = H.\beta \quad (8)$$

The inefficiency of ELM may be due to setting of random weights. Statistically Controlled Activation Weight Initialization (SCAWI) technique is proposed for initializing parameters.

IV. Statistically Controlled Activation Weight Initialization (SCAWI)

In SCAWI [21], networks are initialized with weights and impact of random initialization is reduced. Neurons in both saturated and paralyzed states are taken into consideration. A neuron is said to be saturated when output is greater than threshold, and is in paralyzed state when difference amid target as well as output are equal to or more than threshold. This demands training of the network. Paralyzed Neuron Percentage (PNP) is involved in computing number of times the neuron moves to paralyzed state. It is based on the quantity of neurons which are paralyzed and total amount of neurons.

$$PNP = \left(\frac{1}{\beta}\right).P \quad (9)$$

where,

$\left(\frac{1}{\beta}\right)$ - Probability that one output is unsuitable

P - Neuron's saturation probability

Initial weights are computed using optimal value of PNP.

$$W = \left(\frac{R.a_0}{\sqrt{\partial}}\right).r_{ji} \quad (10)$$

where,

A - Neuron activation

∂ - Expectation of random variable

R - Random number

Scale factor (R) is given by,

$$R = \frac{\sqrt{3}}{\Delta\,(PNP)} \quad (11)$$

where,

$$\Delta = \text{erf}^{-1}\left(\frac{1}{2} - \left(\frac{\beta}{2}\right).PNP\right) \quad (12)$$

In this work, segmentation and classification of tumor data using subtractive clustering and S-ELM classifier is propounded. The ELM is designed with double activation functions to have reduced influence of arbitrary initialization and offer better accuracy. The ELM-based classifier is proposed for analyzing and classifying data.

The SCAWI propounded for initializing hidden node factors of propounded ELM offers improved accuracy and training time. Average output from hidden node is obtained after activation function transformations. Activation functions include tangent (tanh) as well as hyperbolic cosine functions. They deal with non-linear data. In the proposed approach, the problem of random initialization of hidden node parameters in ELM is resolved.

Non-linear data is handled efficiently by using dual activation functions and output is got by averaging activation functions. In the proposed methodology, the ELM initializes weights as well as bias parameters by using SCAWI. The weight between input and hidden neurons are initialized based on paralyzed neuron percentage. Weight and bias are randomly chosen and fine-tuned by using Eq. (12) iteratively. In the hidden layer, following operations are performed.

- Calculate weight changes using ELM

$$\Delta W_i = \eta\left(\pi\, h_{ji}\right) x_k \text{ for } j \neq 1 \text{ to } m \quad (13)$$

- Update weight

$$W_i = \Delta W_i + W_i \quad (14)$$

- Calculate weight after including momentum term '∞'

$$W_i = W_i + \infty \Delta W_i \quad (15)$$

In the hidden layer, inverse hyperbolic cosine and tangent functions are involved and average output is computed. Inverse hyperbolic cosine function is given by,

$$\text{ar}\cosh z = \ln(z + \sqrt{z^2 - 1}) \quad (16)$$

Inverse hyperbolic tangent function is determined as follows.

$$\text{ar}\tanh z = \frac{1}{2}\ln\left(\frac{1+x}{1-x}\right) \quad (17)$$

Combined activation functions aids in handling non-linearity. S-ELM uses ELM-Auto Encoder (ELM-AE) as building blocks in every layer to assist learning. It regenerates input signal with linear or non-linear activation functions. Input data is mapped to L-dimensional feature space of ELM and output is obtained.

$$F_L = \sum_{i=0}^{n} b_i\,(x) = (h(x).b) \quad (18)$$

Output weight matrix amid hidden and output nodes is given by,

$$b = \{[b_1, \ldots . b_l]\}^T \quad (19)$$

Output of hidden node for input 'x' is determined as follows.

$$h(x) = [g_1(x), \ldots . . g_L(x)] \quad (20)$$

$g_i(x)$ - Output of i^{th} hidden node

For 'n' training samples $\{(x_i, t_i)\}$, i=1, ELM is involved in resolving the ensuing learning problem.

$$H_b = T \quad (21)$$

Target labels are represented as shown below.

$$T = [t_1, \ldots t_n] \quad (22)$$

$$H = [h^T\,(x_1), \ldots., h^T\,(x_n)]^T \quad (23)$$

Output weight (b) is determined as follows.

$$b = H^{\dagger}.T \quad (24)$$

where,

'H†'- Moore-Penrose generalized inverse of matrix 'H'

Regularization can be done to enhance ELM performance.

$$B = \left(\left(\frac{I}{C}\right) + H^T.H\right)^{-1}.H^T.H \quad (25)$$

Unsupervised learning is performed using ELM. Orthogonalization binds parameters closer to each other. The performance of ELM-A is increased by choosing weights and biases orthogonally. As shown in Johnson-Lindenstrauss lemma, input is projected to different or equal dimension space and computed as shown below.

$$h = g(a.x + m) \quad (26)$$

$$a^T.a = I, m^T.m = I \quad (27)$$

$$a = [a_{1,\ldots..}a_T] \quad (28)$$

Eq. (28) represents orthogonal random weights.

Orthogonal random biases amid input as well as hidden nodes is determined by,

$$m = [m_{1,\ldots..}m_L] \quad (29)$$

Transformation from feature space to input is learnt by using output weight of ELM-AE. For representations of sparse and compressed ELM-AE, weights (outputs) are determined as shown below.

$$B = \left(\left(\frac{I}{C}\right) + H^T.H\right)^{-1}.H^T.X \quad (30)$$

The hidden layer outputs of ELM-AE are determined as shown below.

$$H = [H_1, \ldots . H_n] \quad (31)$$

Input and output data are given by,

$$X = [x_1, \ldots . x_n] \quad (32)$$

V. Results And Discussion

Clinical data and MRI images of different types of breast tumor are gathered from domains which are publicly available. The propounded tumor detection scheme is applied to Breast Cancer Wisconsin (Diagnostic) [22] with 569 instances and 30 features. It is seen that the proposed scheme offers better sensitivity, specificity and accuracy in contrast to other methods taken under consideration.

The SCAWI is used for random initialization of parameters as it is the default option in the ANN. The proposed scheme is implemented using MATLAB. True Positive (TP), False Positive (FP), True Negative (TN) and False Negative (FN) are determined based on which sensitivity, specificity, and accuracy are calculated.

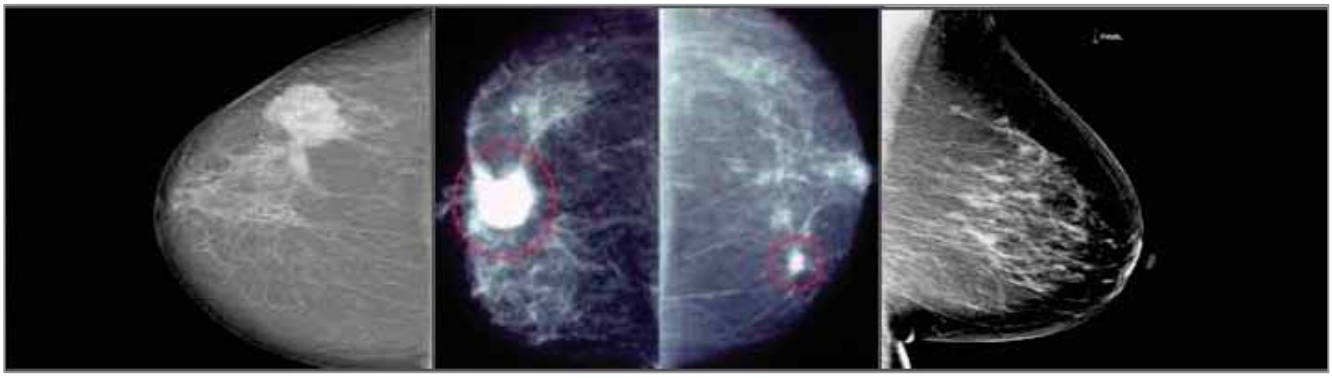

Figure 1. MRI Images of Breast

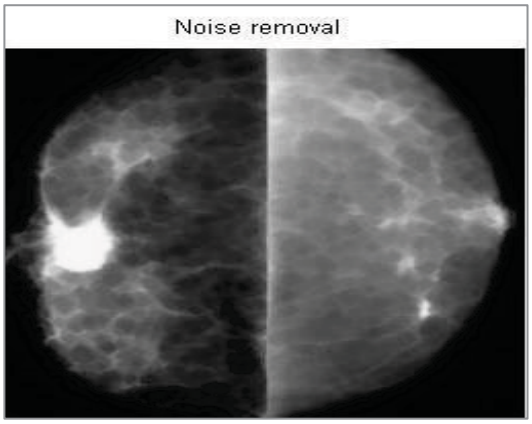

Figure 2. MRI Images of Breast after Noise Removal

Performance is evaluated by varying the hidden neurons from 50 to 200 in steps of 25. Performance is improved by combining both dynamic and morphological features.

The proposed method is tested with clinical data and MRI images of breast tumors. Figure 1 shows MRI images of breast tumors. Figure 2 and Figure 3 show MRI images after noise removal and segmentation. Figure 4 shows the images after clustering.

Figure 5 and Figure 6 show the sensitivity and specificity in terms of dynamic, morphological, textural, combined dynamic, and morphological and combined dynamic, textural and morphological features for the data of breast

cancer using the SCAWI-ELM. Both Sensitivity and Specificity are high for Dynamic + Morphological features.

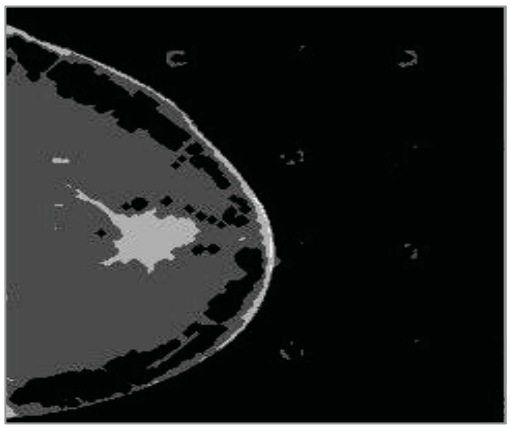

Figure 3. MRI Images of Breast after Segmentation

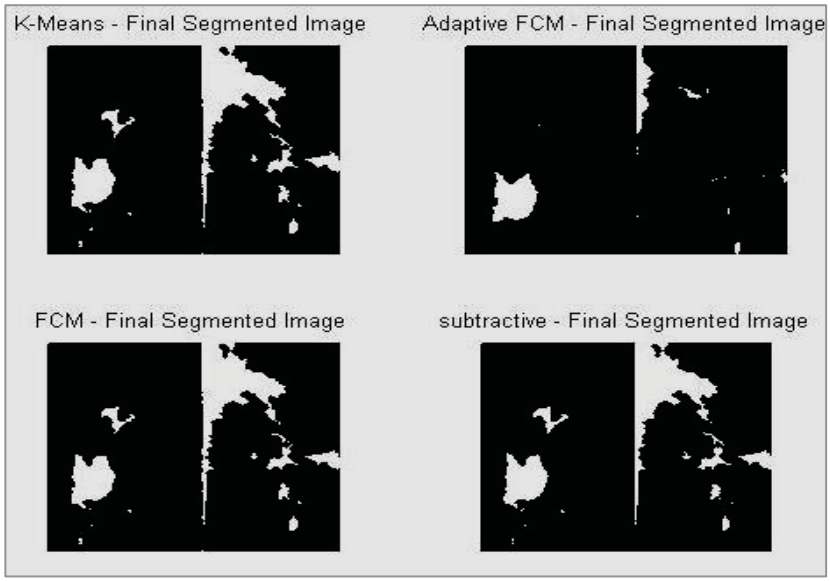

Figure 4. MRI Images of Breast after Clustering

Figure 7 to Figure 9 show the performance of classifiers. The number of statistical samples taken by classifiers is larger, thus yielding accurate analysis. Furthermore, the classifiers perform well when dynamic and morphological features are used simultaneously. From the results, it is evident that S-ELM combined with SCAWI yields better performance when compared to S-ELM in terms of accuracy, training, and testing time. The propounded scheme is compared with basic ELM and ML-ELM. It is seen that ML-ELM yields better classification results in contrast to the ELM. ML-based algorithms depend on training data and features extracted from data. Sensitivity and specificity cannot be directly compared. Based on the results obtained, average sensitivity and specificity values are computed for every classifier.

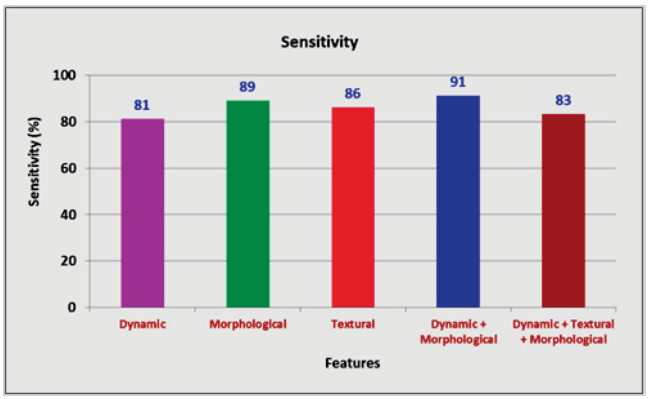

Figure 5. Sensitivity for Diverse Features

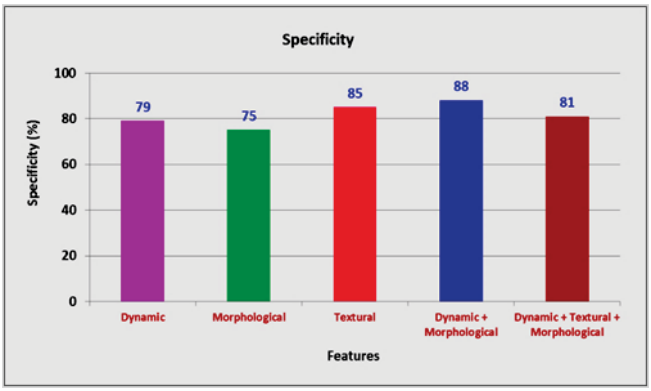

Figure 6. Specificity for Diverse Features

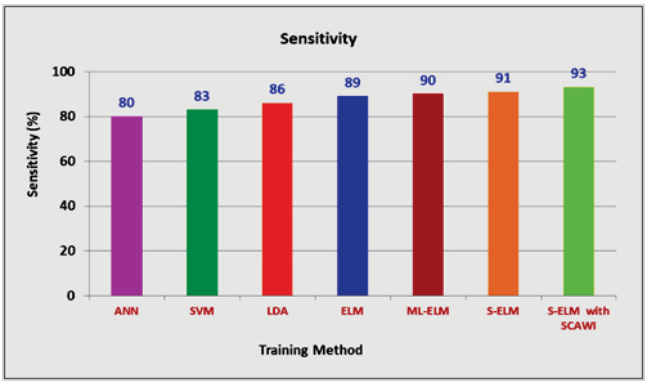

Figure 7. Sensitivity offered by Diverse Training Methods

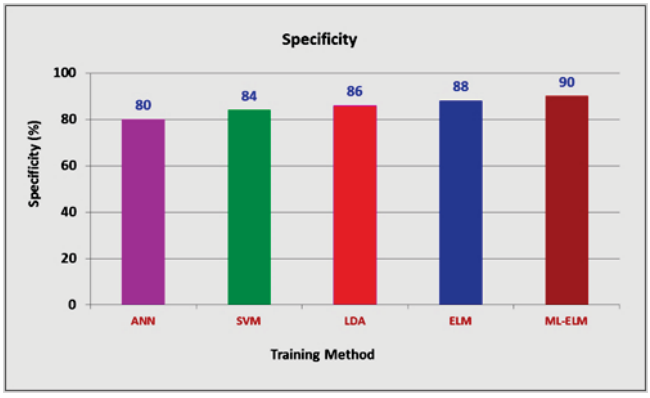

Figure 8. Specificity offered by Diverse Training Methods

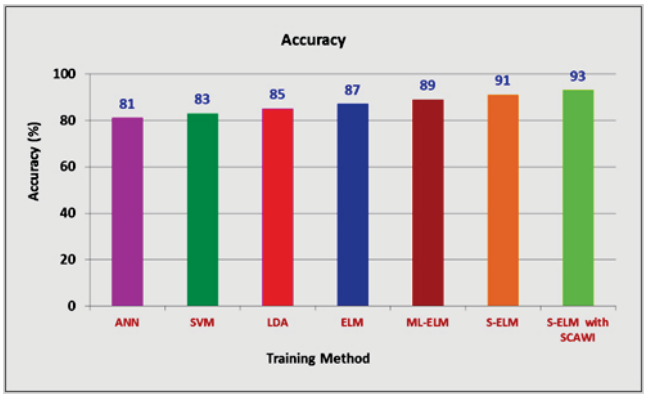

Figure 9. Accuracy offered by Diverse Training Methods

VI. Conclusion

In this paper, breast tumors are classified using Subtractive clustering and S-ELM classifier. The image is segmented through clustering and classified by using the ELM classifier. The SCAWI is involved in setting the initial parameters. The proposed scheme is assessed in terms of sensitivity, specificity, and accuracy. From the results, it is evident that S-ELM with SCAWI yields better results in contrast to ML-ELM and S-ELM. In the future, the proposed scheme can be applied to diverse datasets and performance can be analyzed.

References

[1] Saslow, D., Boetes, C., Burke, W., Harms, S., Leach, M. O., Lehman, C. D., ... & American Cancer Society Breast Cancer Advisory Group. (2007). American Cancer Society guidelines for breast screening with MRI as an adjunct to mammography. CA: a cancer journal for clinicians, 57(2), 75-89.

[2] Corsetti, V., Houssami, N., Ghirardi, M., Ferrari, A., Speziani, M., Bellarosa, S., ... & Ciatto, S. (2011). Evidence of the effect of adjunct ultrasound screening in women with mammography-negative dense breasts: interval breast cancers at 1 year follow-up. European journal of cancer, 47(7), 1021-1026.

[3] Zhou, H., Huang, G. B., Lin, Z., Wang, H., & Soh, Y. C. (2014). Stacked extreme learning machines. IEEE transactions on cybernetics, 45(9), 2013-2025.

[4] Kaur, R., Roul, R. K., & Batra, S. (2023). Multilayer extreme learning machine: a systematic review. Multimedia Tools and Applications, 82(26), 40269-40307.

[5] Sandhu, D. S., Sandhu, S., Karwasra, R. K., & Marwah, S. (2010). Profile of breast cancer patients at a tertiary care hospital in north India. Indian journal of cancer, 47(1), 16-22.

[6] Huang, G. B., Wang, D. H., & Lan, Y. (2011). Extreme learning machines: a survey. International journal of machine learning and cybernetics, 2, 107-122.

[7] Aličković, E., & Subasi, A. (2017). Breast cancer diagnosis using GA feature selection and Rotation Forest. Neural Computing and applications, 28, 753-763.

[8] Mangasarian, O. L., Street, W. N., & Wolberg, W. H. (1995). Breast cancer diagnosis and prognosis via linear programming. Operations research, 43(4), 570-577.

[9] Assiri, A. S., Nazir, S., & Velastin, S. A. (2020). Breast tumor classification using an ensemble machine learning method. Journal of Imaging, 6(6), 39.

[10] Yadav, S. S., & Jadhav, S. M. (2022). Thermal infrared imaging based breast cancer diagnosis using machine learning techniques. Multimedia Tools and Applications, 1-19.

[11] Dewangan, K. K., Dewangan, D. K., Sahu, S. P., & Janghel, R. (2022). Breast cancer diagnosis in an early stage using novel deep learning with hybrid optimization technique. Multimedia Tools and Applications, 81(10), 13935-13960.

[12] Mohamed, A., Amer, E., Eldin, N., Hossam, M., Elmasry, N., & Adnan, G. T. (2022). The impact of data processing and ensemble on breast cancer detection using deep learning. Journal of Computing and Communication, 1(1), 27-37.

[13] Dar, R. A., Rasool, M., & Assad, A. (2022). Breast cancer detection using deep learning: Datasets, methods, and challenges ahead. Computers in biology and medicine, 149, 106073.

[14] Abunasser, B. S., AL-Hiealy, M. R. J., Zaqout, I. S., & Abu-Naser, S. S. (2022). Breast cancer detection and classification using deep learning Xception algorithm. International Journal of Advanced Computer Science and Applications, 13(7).
[15] Abunasser, B. S., Al-Hiealy, M. R. J., Zaqout, I. S., & Abu-Naser, S. S. (2023). Convolution neural network for breast cancer detection and classification using deep learning. Asian Pacific journal of cancer prevention: APJCP, 24(2), 531.
[16] Labcharoenwongs, P., Vonganansup, S., Chunhapran, O., Noolek, D., & Yampaka, T. (2023). An automatic breast tumor detection and classification including automatic tumor volume estimation using deep learning technique. Asian Pacific Journal of Cancer Prevention: APJCP, 24(3), 1081.
[17] Ranjbarzadeh, R., Dorosti, S., Ghoushchi, S. J., Caputo, A., Tirkolaee, E. B., Ali, S. S., ... & Bendechache, M. (2023). Breast tumor localization and segmentation using machine learning techniques: Overview of datasets, findings, and methods. Computers in Biology and Medicine, 152, 106443.
[18] Ali, S., & Agrawal, J. (2024). Automated segmentation of brain tumour images using deep learning-based model VGG19 and ResNet 101. Multimedia Tools and Applications, 83(11), 33351-33370.
[19] Huang, G. B., Wang, D. H., & Lan, Y. (2011). Extreme learning machines: a survey. International journal of machine learning and cybernetics, 2, 107-122.
[20] Ito, K., & Xiong, K. (2000). Gaussian filters for nonlinear filtering problems. IEEE transactions on automatic control, 45(5), 910-927.
[21] Drago, G. P., & Ridella, S. (1992). Statistically controlled activation weight initialization (SCAWI). IEEE Transactions on Neural Networks, 3(4), 627-631.
[22] https://www.kaggle.com/datasets/uciml/breast-cancer-wisconsin-data

E-ISSN 2581 – 7957
P-ISSN 2277 – 3916
CVR Journal of Science and Technology, Volume 27, December 2024
DOI: 10.32377/cvrjst2713

Smart Road Safety and Vehicle Accident Prevention System for Mountain Roads

Vangala Praveen Kumar[1], Dr. Kalagotla Chenchireddy[2] and Varikuppala Manohar[3]

[1]UG Student, Teegala Krishna Reddy Engineering College/EEE Department, Hyderabad, India
Email: vangalapraveenkumar96@gmail.com
[2]Associate Professor, Geethanjali College of Engineering and Technology/EEE Department, Hyderabad, India
Email: chenchireddy.kalagotla@gmail.com
[3]UG Student, Teegala Krishna Reddy Engineering College/EEE Department, Hyderabad, India
Email: manoharvarikuppala143@gmail.com

Abstract: **Roads that lead through mountains present unique challenges for drivers due to their winding paths, steep inclines, and unpredictable weather conditions. To address the heightened risk of accidents in these areas, a proposed Smart Road Safety and Vehicle Accident Prevention System (SRSP) integrates advanced technologies such as the Internet of Things (IoT), Artificial Intelligence (AI), and Machine Learning (ML) to bolster road safety and prevent accidents. The SRSP deploys a network of sensors along mountainous routes to gather real-time data on various factors including road conditions, weather patterns, and traffic density. Utilizing AI algorithms, this data is then analyzed to identify potential hazards and predict areas prone to accidents. Moreover, the system incorporates vehicle-to-infrastructure (V2I) and vehicle-to-vehicle (V2V) communication protocols to enable proactive safety measures such as adaptive speed control, hazard alerts, and emergency braking assistance. In the event of an impending collision, the SRSP automatically notifies drivers and nearby vehicles while also alerting emergency services for rapid response. Furthermore, the system furnishes valuable insights to road authorities, aiding in the optimization of maintenance schedules and the enhancement of road infrastructure to further bolster safety measures. Ultimately, the SRSP offers a comprehensive solution to mitigate the risks associated with mountain road travel, thereby saving lives, and diminishing the economic and social toll of accidents.**

Index Terms: **Mountain roads, Smart Road Safety, Vehicle Accident Prevention System, IoT, Artificial Intelligence, Machine Learning, Senslives Real-time data, Hazard prediction.**

I. Introduction

Mountain roads are extremely difficult to navigate because of their steep inclines, tight turns, and erratic weather. These elements increase the likelihood of collisions and fatalities, highlighting the significance of placing a high priority on road safety in mountainous areas of the world. Due to the dynamic nature of hilly terrain, conventional safety precautions frequently prove inadequate. Therefore, there is a strong demand for creative solutions that can reduce dangers and increase safety for all users of the road. Introducing the idea of a "smart road," a revolutionary strategy intended to completely change mountain route safety and navigation. A cutting-edge Safety and Vehicle Accident Prevention System (SRSP) with artificial intelligence algorithms has been developed specifically for mountain roads. It incorporates sensors, cameras, and other cutting-edge technologies. This system keeps an eye on traffic patterns, automobile behavior, and surrounding conditions in real time. The SRSP can lower the likelihood of accidents by proactively identifying possible dangers and alerting drivers through data analysis. In hilly areas, the SRSP provides a comprehensive approach to road safety that includes both immediate actions and preventive measures. By installing sophisticated sensor networks along mountain roads, the system continuously collects data on visibility, traffic movement, and the state of the road surface. After that, machine learning algorithms analyze this data to find trends and abnormalities linked to possible hazards including steep bends, black ice, and rockfalls.

One essential feature of the SRSP is its wireless network-based direct connection capacity with automobiles. Thanks to this function, drivers can receive real-time alerts and advice from the system, encouraging them to change their pace or path to avoid certain hazards. In addition to reducing the likelihood of accidents, this proactive safety strategy gives drivers access to timely information so they can make wise decisions while driving.

In addition, the SRSP has intelligent traffic management features designed to maximize vehicle flow and minimize gridlock on steep roads. The traffic signal and lane designs are dynamically adjusted by the system to improve overall road safety and efficiency.

Additionally, the SRSP is essential in supporting emergency response operations since it provides accurate location information and incident alerts to the appropriate authorities in the event of an accident. In addition to its primary goal of preventing accidents, the SRSP aims to improve the general state of road infrastructure and maintenance procedures in hilly regions. The technology ensures the long-term safety and dependability of mountain roads by enabling proactive maintenance interventions through continuous monitoring of road conditions and identification of potential deterioration or risks. This proactive strategy maximizes maintenance resources and budgets while reducing the likelihood of accidents.

All things considered, the Smart Road Safety and Vehicle Accident Prevention System represents a major technological advancement in road safety, especially for

Received on 09-03-2024, Revised on 08-04-2024, Accepted on 08-05-2024.

hilly areas where conventional methods are inadequate. Using data analytics, The SRSP, which combines artificial intelligence with real-time communication, provides a comprehensive response to the various problems related to mountain road safety. In the end, it saves lives and lessens the financial and social costs of traffic accidents in these kinds of situations.

II. Literature Review

Because of their steep inclines, sharp curves, and unpredictable weather, mountainous roads present special obstacles that increase the danger of accidents [1]. Research on road safety highlights the need for creative solutions to deal with these issues and raise the standard of safety for drivers going through steep terrain [2]. Modern technology like cameras, sensors, and intelligent systems are becoming more widely acknowledged as vital resources for improving traffic safety and averting collisions in hilly areas [3]. An increasing amount of research is being done on the creation of intelligent traffic safety systems designed with steep terrain in mind [4] For instance, Zhao et al. (2019) look into the use of sensor networks and data analytics to track road conditions, identify dangers in real-time, and alert drivers in a timely manner. Likewise, research by Wang et al. and Liu et al. (2020) al. (2021) investigate how machine learning algorithms might be integrated to anticipate and avoid accidents on mountain roads, with encouraging results in terms of decreased accident rates and increased safety [5].

Literature also emphasizes how crucial it is to promote cooperation and communication between infrastructure and vehicles to improve road safety in mountainous areas. Research on vehicle-to-infrastructure (V2I) communication systems, which allow for real-time data sharing between cars and roadside sensors to notify drivers of possible dangers and improve traffic flow, is conducted by Zhang et al. (2018) and Li et al. (2022) [5]. These studies highlight the potential value of vehicle-to-vehicle (V2I) communication in lowering accident rates and raising general traffic safety in mountainous regions [6]

Furthermore, studies highlight how important intelligent traffic management systems are to easing traffic and averting mishaps on mountain roads [7]. The use of dynamic traffic control strategies, such as adaptive signal control and congestion pricing, to regulate vehicle flow and improve safety in mountainous areas is the subject of studies by Chen et al. (2019) and Jiang et al. (2020) [8]. The significance of incorporating intelligent traffic management systems into larger road safety programs for mountainous regions is emphasized by these findings [9]. The literature study underscores the urgent need for novel strategies to improve road safety and avert collisions on steep routes [10]. Through the utilization of cutting-edge technology including sensors, machine learning, and intelligent traffic management systems, the suggested Smart Road Safety and Vehicle Accident Prevention System has the ability to significantly transform safety protocols in hilly areas [11]. The body of research highlights how much the suggested Smart Road Safety and Vehicle Accident Prevention System can do to reduce dangers, save lives, and improve safety in hilly areas. It also highlights how important effective traffic management systems are to reducing traffic and preventing accidents on mountain roads [12]. Research by Jiang et al. and Chen et al. (2019).

(2020) examine how dynamic traffic control techniques, like adaptive signal control and congestion pricing, can be used to manage traffic flow and improve safety in hilly regions [13]. These results highlight how crucial it is to incorporate intelligent traffic control strategies into more comprehensive efforts aimed at improving road safety on mountain roads. [14]. Overall, the study of the literature emphasizes how critical it is to develop novel strategies that make use of cutting-edge technologies like sensors, machine learning, and intelligent traffic management systems in order to improve road safety and reduce accidents in hilly areas [15].

III. Block Diagram

The Smart Road Safety and Vehicle Accident Prevention System (SRSP) is a state-of-the-art technology designed with mountain road conditions in mind [16]. These untamed environments, which are marked by abrupt curves, steep hills, and unpredictable weather, greatly increase the risk for drivers and raise the accident rate. By utilizing cutting-edge technologies like cameras, sensors, and sophisticated algorithms, the SRSP seeks to improve safety protocols and prevent accidents on these hazardous routes in advance. The SRSP is a real-time system that continuously gathers and analyzes critical data related to road surfaces, vehicle dynamics, and environmental variables [17]. Through the analysis of this vast amount of data, the system is able to identify possible risks well in advance, such as slick surfaces, rockfalls, or decreased visibility due to fog or rain [18]. By means of proactive notifications, the SRSP facilitates drivers in immediately modifying their driving behavior, more skillfully navigating risky areas of the road, and ultimately decreasing the probability of accidents [19].

Steep terrain-specific characteristics are integrated into the Smart Road Safety and Vehicle Accident Prevention System (SRSP). With the use of cutting-edge technology, the system uses dynamic traffic control strategies like adaptive signal control and congestion management algorithms to improve traffic flow and reduce congestion on mountain highways. The goal of the SRSP is to improve overall road user safety by reducing the risk of crashes through efficient management of vehicle speed and spacing [20].

The capacity of the SRSP to enable seamless connectivity between vehicles and roadside infrastructure through wireless communication networks is one of its main advantages. Through the transfer of real-time information, this vehicle-to-infrastructure (V2I) communication enables drivers to receive the most recent alerts and advisories regarding road conditions, accidents, or other possible hazards. The Safety Roadside Protection Program (SRSP) equips drivers with the knowledge and skills necessary to make safer decisions when driving on mountain roads by improving situational awareness.

CVR Journal of Science and Technology, Volume 27, December 2024
DOI: 10.32377/cvrjst2713

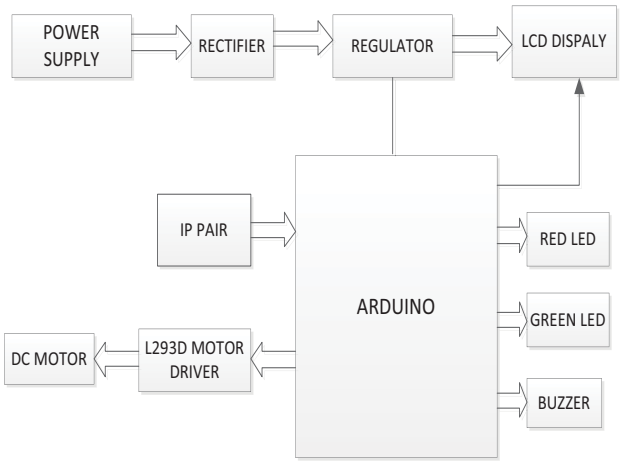

Figure 1. smart road safety and vehicle accident prevention system for mountain roads

By enabling smooth connectivity via wireless communication networks between cars and roadside infrastructure, the SRSP provides a major benefit. Drivers can get real-time information about road conditions, accidents, or possible risks through vehicle-to-infrastructure (V2I) connection. This improves situational awareness and makes it possible to make better decisions, which eventually leads to safer traffic conditions on mountain roads.

IV. HARDWARE DESCRIPTION

An assortment of hardware components is included in a smart road safety and vehicle accident prevention system specifically built for roads in high terrain to solve the issues that arise. This system's core components include state-of-the-art sensor technology, a reliable communication network, and real-time data processing capabilities. First, a network of sensors is placed in key locations along mountain routes to collect vital information on the state of the road, such as temperature, humidity, visibility, and surface condition. These sensors could consist of cameras, temperature, moisture, and other pertinent devices, as well as LiDAR (light detection and ranging) scanners positioned at important points along the path.

To guarantee precise and quick data gathering, these sensors are coupled to a central processing unit, which can be found by the side of the road or inside a central control center. This processor unit's strong computer technology allows it to handle massive amounts of data in real time with efficiency. It receives streams of data, processes them, analyzes them, and produces insightful reports regarding possible hazards and road conditions. To follow vehicles' travels along mountain roads, the system also equips them with sensors and communication devices. Real-time information on the speed, acceleration, braking, and trajectory of the vehicle is provided by these onboard sensors. They also make it possible for cars to talk to the central control system, which makes it easier to provide important information and alerts. Additionally, the system includes automatic warning mechanisms such roadside alert systems, in-vehicle alerts, as well as variable message signs (VMS) to improve security protocols. By informing drivers about possible dangers through processed data, these warning systems help reduce the likelihood of collisions by allowing drivers to modify their driving habits. Furthermore, the hardware components of the system are designed to survive severe mountainous conditions, such as intense heat, strong winds, and precipitation, in order to guarantee reliable functioning. Sturdy construction and weathertight enclosures protect delicate electronics from the elements, guaranteeing continuous operation even under trying conditions. In conclusion, this smart road safety and vehicle accident prevention system for mountain roads includes a sophisticated array of sensors, processing units, communication devices, and warning mechanisms to enhance safety and decrease dangers associated with steep terrain.

The hardware structure of a smart vehicle accident prevention system specifically developed for hilly roads is an intricate assembly of parts intended to handle the unique challenges presented by rough terrain. Its central component is a network of cutting-edge sensors that are positioned strategically along mountainous roads. These sensors include cameras, LiDAR scanners, temperature gauges, and humidity sensors, and they collect vital real-time data on road conditions. They are strategically placed to protect important locations that are susceptible to dangers including landslide zones, ice spots, and poor visibility from fog or precipitation. A strong processing unit, either roadside or centralized, with high-performance computing gear is at the heart of the system. Large volumes of incoming data streams from the sensors are processed by this unit, which is essential to the operation of the system.

To find trends, pinpoint anomalies, and produce insightful information about road conditions and possible dangers, the system conducts complex analysis. Furthermore, sensors and communication devices mounted on cars are essential to the functioning of the system. When driving on mountain roads, these built-in devices track several variables all at once, including speed, acceleration, and braking. They also make it easier for cars and the Central Control System (CCS) to communicate seamlessly, which permits the sharing of vital information and alarms about potentially dangerous circumstances. The system includes automated alert devices placed strategically along mountain roads in addition to data collection and processing. These systems, which include variable message signs (VMS), in-car alerts, and roadside alert systems, use processed data to quickly alert drivers of potential hazards up ahead. These alerts enable drivers to modify their driving habits and lower the risk of collisions by acting as preventative measures. In addition, hardware component robustness and endurance are critical design factors that guarantee dependable performance in demanding alpine circumstances. Robust design and resilient enclosures protect delicate electronics from extreme weather, high winds, and precipitation, ensuring continuous operation even in challenging conditions.

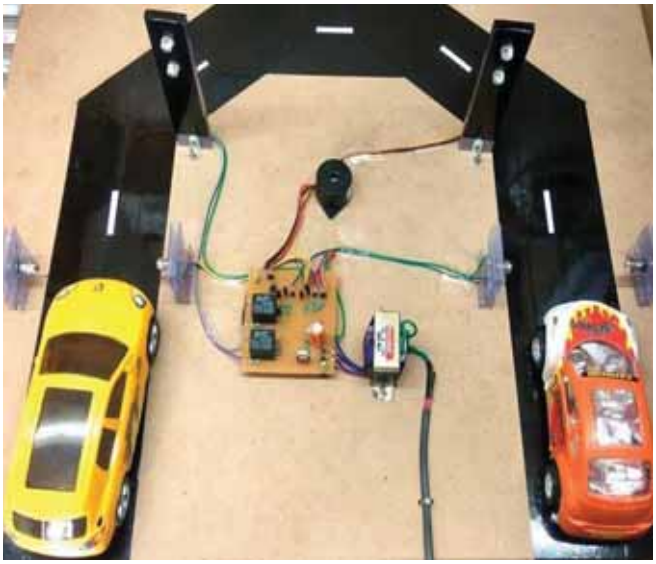

Figure 2: smart road safety and vehicle accident prevention system for mountain roads

V. Application

There is a great deal of opportunity to significantly lower the incidence and severity of accidents in these difficult terrains by putting in place a sophisticated road safety and vehicle accident prevention system designed for mountain roads. Improving situational awareness for road maintenance personnel and drivers is the system's key goal. To do this, a network of carefully placed sensors along uphill roads must continuously analyze important elements including temperature, humidity, road conditions, and visibility. The system can quickly detect dangerous situations like ice formation, poor visibility from fog or heavy precipitation, or the possibility of landslides by utilizing real-time data collection. The quick implementation of preventive actions is made possible by this early identification.

Dynamic connection between automobiles and the central control system is made possible by the integration of sensors and communication devices deployed on vehicles. This effective communication further improves overall traffic safety on mountainous routes by guaranteeing that crucial information about the state of the road and potential risks is communicated. This makes it easier for drivers to receive vital information in real time, such as traffic patterns, road conditions, and potential risks. When drivers possess such insights, they can modify their driving style and make well-informed decisions, which lowers the probability of accidents.

Additionally, the system's automated warning features are essential for preventing accidents. Drivers are swiftly informed of potential hazards ahead using processed data, variable message signs (VMS), in-vehicle warnings, and roadside alert systems. These proactive notifications dramatically reduce the likelihood of crashes by empowering drivers to change their speed or take evasive action. The data that the device gathers is also useful for post-event analysis and road maintenance. By carefully analyzing historical accident data and road conditions, authorities can use this data to identify accident-prone regions and develop tailored safety measures. These precautions could involve erecting more safety barriers, fixing damaged roads, or setting speed limits in inclement weather. To put it briefly, there is a great deal of potential to improve overall road safety and lower the frequency and severity of accidents in these difficult terrains by putting in place a smart road safety and vehicle accident prevention system designed specifically for mountain roads. Using state-of-the-art sensor technology, a strong communication network, and real-time data processing powers, this system can help prevent accidents and save lives on mountain roads.

VI. Conclusions

Furthermore, the SRSP's advanced traffic management features are essential for maximizing traffic flow and reducing congestion on mountain roads. By employing dynamic traffic control tactics, the system improves both safety and transportation efficiency under difficult circumstances. The SRSP enhances road safety for all users by controlling vehicle speed and spacing, which also improves traffic flow and lowers the likelihood of collisions.

Moreover, the SRSP enhances drivers' situational awareness and empowers them to make educated judgments by facilitating smooth wireless network connectivity between automobiles and roadside infrastructure. The technology enables drivers to drive mountain routes more safely and effectively by giving them access to real-time information and alerts regarding incidents, road conditions, and possible hazards. With improved communication, traffic safety may be approached collaboratively, motivating drivers to take proactive steps to avoid collisions and create safer travel environments.

All things considered, there is a good chance that the SRSP will be adopted, greatly reducing the likelihood of accidents, and improving safety on mountain roads. The system improves the effectiveness and dependability of transportation in hilly areas while also saving lives by utilizing cutting-edge technologies and intelligent traffic control strategies. The SRSP is a prime example of our dedication to innovation and the search for more sustainable, secure forms of mobility for everybody as we progress in the field of road safety.

References

[1] Y. A. Korotkova, A. A. Pashkova, E. A. Shalagina, A. A. Pakhomova and V. V. Dronseiko, "Ensuring Road Safety Using ITS Services," *2022 Intelligent Technologies and Electronic Devices in Vehicle and Road Transport Complex (TIRVED)*, Moscow, Russian Federation, 2022, pp. 1-5, doi: 10.1109/TIRVED56496.2022.9965535.

[2] K. Ibtissem, F. Sami and G. Souhayel, "R-Secure: A system based on crowdsourcing platforms to improve road safety in the smart city," 2022 International Conference on INnovations in Intelligent SysTems and Applications (INISTA), Biarritz, France, 2022, pp. 1-6, doi: 10.1109/INISTA55318.2022.9894228.

[3] M. Derawi, Y. Dalveren and F. A. Cheikh, "Internet-of-Things-Based Smart Transportation Systems for Safer Roads," *2020 IEEE 6th World Forum on Internet of Things*

(WF-IoT), New Orleans, LA, USA, 2020, pp. 1-4, doi: 10.1109/WF-IoT48130.2020.9221208.

[4] A. V. Shestov, M. S. Anastasov and N. V. Suchilin, "Smart Road," *2021 Intelligent Technologies and Electronic Devices in Vehicle and Road Transport Complex (TIRVED)*, Moscow, Russian Federation, 2021, pp. 1-6, doi: 10.1109/TIRVED53476.2021.9639122.

[5] I. Khedher, S. Faiz and S. Gazah, "R-Safety: a mobile crowdsourcing platform for road safety in smart cities," *2022 8th International Conference on Control, Decision and Information Technologies (CoDIT)*, Istanbul, Turkey, 2022, pp. 950-955, doi: 10.1109/CoDIT55151.2022.9804123.

[6] J. Kocourek and T. Padělek, "Accurate road safety level assessment for effective road safety inspection," *2018 Smart City Symposium Prague (SCSP)*, Czech Republic, 2018, pp. 1-5, doi: 10.1109/SCSP.2018.8402658.

[7] S. Amri, M. Naoum, M. Lazaar and M. A. Achhab, "Performing of users' road safety at intelligent transportation systems," *2020 6th IEEE Congress on Information Science and Technology (CiSt)*, Agadir - Essaouira, Morocco, 2020, pp. 461-465, doi: 10.1109/CiSt49399.2021.9357169.

[8] A. -E. M. Taha, "A Framework for Dynamic Assessment of Road Safety in Smart Cities," *2018 IEEE Global Communications Conference (GLOBECOM)*, Abu Dhabi, United Arab Emirates, 2018, pp. 1-4, doi: 10.1109/GLOCOM.2018.8647170.

[9] A. -E. M. Taha, "A Framework for Dynamic Assessment of Road Safety in Smart Cities," *2018 IEEE Global Communications Conference (GLOBECOM)*, Abu Dhabi, United Arab Emirates, 2018, pp. 1-4, doi: 10.1109/GLOCOM.2018.8647170.

[10] A. R. Mahayadin *et al*., "Effects of Rubbernecking Phenomena Towards Vehicle Deceleration Rate Due to Primary Accident Location by Implementing Safety Incident Screens for Improvement of Human Behaviour Alteration in Penang's Urban Road System," *2018 International Conference on Computational Approach in Smart Systems Design and Applications (ICASSDA)*, Kuching, Malaysia, 2018, pp. 1-4, doi: 10.1109/ICASSDA.2018.8477596.

[11] V. A. Kumar, N. V, S. K. K, S. Gp, P. M and S. J, "Signs With Smart Connectivity for Better Road Safety," *2023 9th International Conference on Advanced Computing and Communication Systems (ICACCS)*, Coimbatore, India, 2023, pp. 841-845, doi: 10.1109/ICACCS57279.2023.10113120.

[12] S. Hayes, S. Wang and S. Djahel, "Personalized Road Networks Routing with Road Safety Consideration: A Case Study in Manchester," *2020 IEEE International Smart Cities Conference (ISC2)*, Piscataway, NJ, USA, 2020, pp. 1-6, doi: 10.1109/ISC251055.2020.9239085.

[13] N. T. Singh, P. Kaur, N. Kumari and Aman, "Comprehensive Approach to Road Sign Detection and Recognition for Autonomous Driving Systems and Road Safety," *2023 3rd International Conference on Smart Generation Computing, Communication and Networking (SMART GENCON)*, Bangalore, India, 2023, pp. 1-6, doi: 10.1109/SMARTGENCON60755.2023.10442422.

[14] A. S. El-Wakeel, J. Li, M. T. Rahman, A. Noureldin and H. S. Hassanein, "Monitoring Road surface anomalies towards dynamic road mapping for future smart cities," *2017 IEEE Global Conference on Signal and Information Processing (GlobalSIP)*, Montreal, QC, Canada, 2017, pp. 828-832, doi: 10.1109/GlobalSIP.2017.8309076.

[15] J. Palša, L. Vokorokos, E. Chovancová and M. Chovanec, "Smart Cities and the Importance of Smart Traffic Lights," *2019 17th International Conference on Emerging eLearning Technologies and Applications (ICETA)*, Starý Smokovec, Slovakia, 2019, pp. 587-592, doi: 10.1109/ICETA48886.2019.9040086.

[16] S. D. Bhogaraju and V. R. K. Korupalli, "Design of Smart Roads - A Vision on Indian Smart Infrastructure Development," *2020 International Conference on COMmunication Systems & NETworkS (COMSNETS)*, Bengaluru, India, 2020, pp. 773-778, doi: 10.1109/COMSNETS48256.2020.9027404.

[17] M. Saeed, A. Khan, M. Khan, M. Saad, A. El Saddik and W. Gueaieb, "Gaming-Based Education System for Children on Road Safety in Metaverse Towards Smart Cities," *2023 IEEE International Smart Cities Conference (ISC2)*, Bucharest, Romania, 2023, pp. 01-05, doi: 10.1109/ISC257844.2023.10293623.

[18] V. Cherniy, S. Bezshapkin, O. Sharovara, I. Vasyliev and O. Verenych, "Modern Approach to the Road Traffic Management in Cities of Ukraine: Case Study of Kyiv Municipal Company "Road Traffic Management Center"," *2020 IEEE European Technology and Engineering Management Summit (E-TEMS)*, Dortmund, Germany, 2020, pp. 1-6, doi: 10.1109/E-TEMS46250.2020.9111757.

[19] F. Tarlochan and S. Mohammed, "Intelligent Transportation System: Application of Telematics Data for Road Safety," *2023 International Conference on Information Management (ICIM)*, Oxford, United Kingdom, 2023, pp. 66-71, doi: 10.1109/ICIM58774.2023.00018.

[20] M. H. Islam, K. Y. Fariya, T. I. Talukder, A. A. Khandoker and N. A. Chisty, "IoT Based Smart Self Power Generating Street Light and Road Safety System Design: A Review," *2021 IEEE Region 10 Symposium (TENSYMP)*, Jeju, Korea, Republic of, 2021, pp. 1-5, doi: 10.1109/TENSYMP52854.2021.9550937.

E-ISSN 2581 – 7957
P-ISSN 2277 – 3916
CVR Journal of Science and Technology, Volume 27, December 2024
DOI: 10.32377/cvrjst2714

Real-Time Vehicle Emission Monitoring using LabVIEW and NI myRIO

N. Kapil Kumar
Asst. Professor, Velammal College of Engineering and Technology/EEE Department, Madurai, India
Email: nkapil.kumar94@gmail.com

Abstract: **The growing concern over vehicular emissions and their impact on the environment has driven the need for advanced emission monitoring systems. This paper proposes the design and implementation of a Vehicle Emission Monitoring System using LabVIEW and NI myRIO, a real-time embedded hardware platform. The system is designed to monitor and analyze key pollutants such as carbon monoxide (CO) and smoke, utilizing MQ-7 and MQ-2 gas sensors, respectively. The NI myRIO serves as the core controller for data acquisition and processing, interfacing with the sensors to gather real-time emission data. This data is processed using LabVIEW to provide a user-friendly interface, enabling the visualization of pollutant levels. A GSM module is integrated to send alerts or notifications when emissions exceed predefined thresholds, allowing for immediate corrective actions. The system is powered by an external power supply for stable and continuous operation. This monitoring system offers real-time detection, ease of deployment, and scalability for integration into various vehicular systems. By leveraging the capabilities of LabVIEW and myRIO, the proposed system provides a robust solution for managing vehicular emissions, contributing to cleaner air and compliance with environmental regulations.**

Index Terms**: LabVIEW, NI myRIO, Vehicle Emission Monitoring, MQ-2 Sensor, MQ-7 Sensor, GSM Module, Real-Time Monitoring, Pollution Control.**

I. Introduction

Air pollution poses severe health risks, contributing to respiratory conditions such as asthma and bronchitis, increasing the likelihood of life-threatening illnesses like cancer, and imposing significant costs on the healthcare system. Among the various sources of pollution, vehicular emissions stand out as a major contributor. Passenger vehicles are responsible for releasing significant amounts of carbon monoxide (CO), nitrogen oxides (NOx), hydrocarbons, and particulate matter, all of which have serious environmental and health impacts. Transportation contributes over half of the CO and NOx, and nearly a quarter of the hydrocarbons, emitted into the atmosphere annually.

Motor vehicles release pollutants primarily through exhaust fumes, which are mostly invisible yet harmful. These pollutants include carbon monoxide (CO), nitrogen oxides (NOx), sulfur dioxide (SO_2), and particulate matter (PM), as well as toxic air pollutants such as benzene and formaldehyde, which are known to cause cancer and other serious health issues. The process of fuel combustion in vehicle engines produces these pollutants, while fuel evaporation and oil refining also contribute to overall vehicular pollution.

The effects of these pollutants are particularly evident in regions like south-east Queensland, where motor vehicles are responsible for approximately 70% of the air pollution. With the population of the region predicted to grow significantly, the number of vehicle kilometers traveled is expected to double, exacerbating air quality issues. Despite advancements in emission controls and the introduction of cleaner vehicles, the rise in vehicular use and the persistent emissions from older vehicles present ongoing challenges to air quality.

Of particular concern are pollutants like carbon monoxide, which interferes with the blood's ability to transport oxygen, and ground-level ozone, which forms smog and causes upper respiratory problems and lung damage. Other harmful emissions include sulfur dioxide, which constricts airways, particularly in individuals with asthma, and nitrogen dioxide, which contributes to the formation of ground-level ozone and further exacerbates respiratory issues.

Particulate matter (PM) is also a major concern, as these tiny particles can penetrate deep into the lungs, leading to respiratory issues and even premature death. Despite reductions in individual vehicle emissions, the overall rise in vehicle use means that transportation remains a significant source of air pollution.

Furthermore, vehicular emissions contribute to global warming through the release of carbon dioxide (CO_2) and other greenhouse gases. These emissions trap heat in the Earth's atmosphere, leading to rising global temperatures and further environmental degradation. Vehicle emissions, therefore, not only pose immediate health risks but also have long-term consequences for the planet's climate.

In response to these growing concerns, it has become imperative to develop advanced vehicle emission monitoring systems. Such systems can monitor and control vehicular pollutants, helping to reduce their impact on both human health and the environment. The use of technologies like LabVIEW and NI myRIO allows for real-time monitoring of harmful gases and particulate matter, providing a comprehensive solution to tackle the challenges posed by vehicular emissions.

A. Objective

The objective of this study is to design and implement a Real-Time Vehicle Emission Monitoring System utilizing LabVIEW and NI myRIO to monitor and analyze key vehicular pollutants such as carbon monoxide (CO) and smoke. The system aims to achieve the following:

Real-Time Detection: Develop a system that can continuously monitor vehicular emissions in real-time using

Received on 09-09-2024, Revised on 09-10-2024, Accepted on 08-11-2024.

MQ-7 and MQ-2 gas sensors for CO and smoke detection, respectively.

Data Acquisition and Processing: Utilize the NI myRIO platform for efficient data acquisition and processing of pollutant levels, ensuring the accuracy and reliability of the collected data.

User-Friendly Interface: Integrate LabVIEW to provide an intuitive interface for real-time visualization of emission data, making it accessible and easy to interpret for users.

Automated Alerts: Incorporate a GSM module to send alerts or notifications when emission levels exceed predefined thresholds, enabling quick interventions and corrective actions.

Scalability and Deployment: Ensure that the system is easily scalable and deployable in various vehicular systems, offering flexibility for broader application and integration.

Environmental Compliance: Contribute to the reduction of vehicular emissions and the protection of air quality by providing a robust solution that aligns with environmental regulations and standards.

B. Motivation

The increasing levels of air pollution, largely driven by vehicular emissions, pose a significant threat to both environmental sustainability and public health. Passenger vehicles contribute substantial amounts of harmful pollutants, including carbon monoxide (CO), nitrogen oxides (NOx), hydrocarbons, and particulate matter, all of which degrade air quality and contribute to the onset of serious health conditions such as respiratory diseases, heart complications, and even cancer. In addition, vehicular emissions are a major contributor to global warming, with carbon dioxide (CO_2) and other greenhouse gases significantly impacting the Earth's climate.

Governments and environmental bodies around the world are increasingly focusing on regulating and controlling these emissions to meet stringent environmental standards. However, effective regulation requires precise and continuous monitoring of pollutants at the source vehicle exhausts. Traditional vehicle inspection methods are not sufficient for real-time or large-scale emission tracking, making it difficult to implement timely corrective measures.

The motivation behind this research is to develop an innovative, real-time monitoring system that can efficiently track vehicular emissions, enabling real-time data acquisition and immediate corrective action when necessary. The integration of LabVIEW and NI myRIO offers a powerful platform for real-time monitoring, while the use of MQ sensors for detecting pollutants such as CO and smoke allows for precise and reliable measurement of harmful gases. By providing automated alerts through a GSM module, this system not only improves emission management but also facilitates on-the-go emission control for vehicle owners and regulators.

This project is motivated by the urgent need for scalable, cost-effective, and easy-to-deploy solutions that can be integrated into vehicles to ensure compliance with Environmental standards. By leveraging modern hardware and software technologies, the system will aid in reducing air pollution and promoting cleaner transportation, ultimately contributing to improved public health and environmental preservation.

II. Literature Review

[1] This paper focuses on the design, implementation, and testing of an IoT-based Vehicle Emission Monitoring System. The primary research aim is to develop a system that can continuously track and monitor vehicular emissions, particularly key pollutants like carbon monoxide (CO) and nitrogen oxides (NOx). The system uses gas sensors to detect these harmful gases in real time, transmitting the data to a cloud-based platform for analysis and storage. Users can remotely access this data and receive alerts when emissions exceed acceptable limits. The research highlights the system's potential to be integrated into vehicles, offering a cost-effective, scalable solution to reduce emissions and ensure compliance with environmental regulations. Ultimately, the study demonstrates the potential of IoT technology to contribute to cleaner air and improved public health by providing real-time monitoring and analysis of vehicular pollution.

[2] The research in this paper is concentrated on addressing the inherent system losses that affect the performance of FLRDS-based gas sensors. The primary focus is on developing a real-time monitoring mechanism to track and compensate for these losses during the sensor's operation. By doing so, the system can maintain high accuracy and sensitivity in detecting trace gas concentrations despite environmental factors and fiber coupling inefficiencies. The study highlights the importance of managing system losses in optical sensors, ensuring their stability and reliability for long-term monitoring tasks in industrial and environmental applications. The proposed method contributes to the advancement of FLRDS technology, making it more applicable for real-world scenarios where accuracy and consistent performance are critical.

[3] The research in this paper is concentrated on the development and testing of a Nonthermal Plasma (NTP) system for controlling emissions from marine diesel engines. The key focus is on reducing harmful pollutants such as nitrogen oxides (NOx) and particulate matter (PM), which are major contributors to air pollution from maritime transportation. The NTP system utilizes plasma technology to initiate chemical reactions that decompose pollutants at relatively low temperatures, making it an energy-efficient and effective solution for emission control. The paper discusses the design, testing, and performance evaluation of the system under different operating conditions, demonstrating its potential to meet emission regulations while reducing the environmental impact of marine diesel engines. This research highlights the viability of NTP technology for achieving cleaner emissions in the maritime industry.

[4] The paper presents the HazeWatch system, designed to address the challenges of air pollution monitoring in urban areas. Traditional air quality monitoring networks are often limited in coverage due to high costs and maintenance requirements. HazeWatch overcomes these limitations by

deploying a distributed network of affordable sensors, allowing a broader and more granular collection of air quality data across Sydney.

[5] The paper evaluates long-wave infrared (LWIR) and visible/near-infrared (VNIR) imaging for detecting CO2 gas leaks in vegetation. LWIR imaging, which detects thermal emissions from gases, was found to be highly effective for leak detection. VNIR imaging, which measures changes in light reflectance, was less sensitive but useful for assessing vegetation health. Experiments showed that LWIR is superior for direct gas detection, while VNIR can provide complementary data. Combining both methods may enhance overall detection and monitoring capabilities.

[6] The paper by D. W. Fausett and R. J. Hartnett presents a real-time emission monitoring system using LabVIEW and NI Compact DAQ. The authors designed a robust system architecture integrating LabVIEW for real-time control and data acquisition. They utilized NI Compact DAQ for modular, scalable data collection, ensuring accurate and reliable emission data processing. Real-time analysis techniques were implemented to process and validate data, producing actionable reports and alerts. The system demonstrated high performance, accuracy, and operational efficiency, with potential applications in the automotive and industrial sectors. Challenges in calibration and integration were addressed, with suggestions for future enhancements through advanced analytics.

[7] The paper by K. J. Kim and S. M. Lee presents a real-time air quality monitoring system using LabVIEW, adaptable for vehicle emissions. The authors developed a system architecture integrating various air quality sensors for continuous data acquisition and processing. They demonstrated effective sensor integration and management, achieving accurate real-time measurements and alerts. The study emphasizes its applicability in both general air quality monitoring and specific vehicle emission contexts.

[8] The paper by M. A. Haris and E. K. Hossain presents a LabVIEW-based real-time emission measurement system tailored for automotive applications. The authors detailed the design and integration of system components, including sensors and data acquisition modules, with LabVIEW for real-time monitoring. They developed and implemented data collection and processing techniques to capture and analyze automotive emissions accurately. The system demonstrated effective real-time performance in measuring emission levels, providing immediate feedback and compliance reporting. The results showcase the system's reliability and practicality for automotive emission testing and regulatory adherence.

III. IMPLEMENTATION

The Real-Time Vehicle Emission Monitoring System was implemented using an NI myRIO embedded platform, integrated with MQ-7 and MQ-2 gas sensors for monitoring carbon monoxide (CO) and smoke emissions, respectively. The hardware configuration includes the NI myRIO as the core controller, which interfaces with the sensors through its Analog Input channels. The sensors' outputs, representing gas concentrations, were calibrated using known standards to ensure measurement accuracy. A GSM module was also integrated to facilitate real-time alerts when pollutant levels exceeded predefined thresholds. The system is powered by an external power supply, ensuring stable and continuous operation for reliable monitoring.

Data acquisition and processing were conducted in LabVIEW, where a user-friendly interface displays real-time emissions data. The LabVIEW virtual instrument captures sensor readings at a defined sampling rate and visualizes them with color-coded indicators. When emissions exceed set limits, the GSM module automatically sends SMS notifications for immediate corrective actions. This system enables effective real-time monitoring and timely alerts, supporting compliance with environmental regulations.

A. Block Diagram

Fig 1. is the block diagram of the Real-Time Vehicle Emission Monitoring System Using LabVIEW and NI myRIO, the NI myRIO plays a central role by supplying power to all connected sensors and collecting their output data. It performs the necessary computational processes to convert the sensor outputs into parts per million (ppm) values, which represent the concentration of pollutants. The MyRIO operates using a DC adapter with a voltage range of 6 to 16 volts, ensuring that it meets the power requirements for its various functions. Additionally, the GSM module, which is used for data transmission, is also powered by the MyRIO. As the sensors continuously monitor vehicle emissions, they send real-time data to the myRIO. This continuous data stream allows the system to generate up-to-date reports on pollutant levels. The reports provide detailed insights into the emission characteristics of the vehicle, based on real-time sensor measurements.

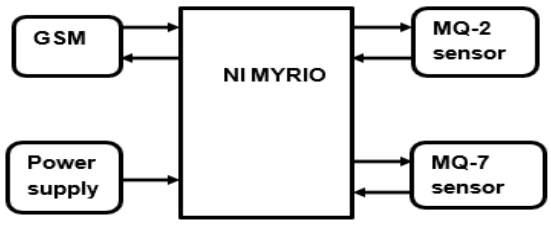

Figure 1. Block diagram of the System

Fig 2 is the front panel of our system is thoughtfully designed with separate, isolated blocks to handle different functions gas sensing, vehicle number plate recognition, and GSM communication ensuring that each component operates independently to minimize any potential interference or ambiguity.

Gas Sensing Block: This block is equipped with various numeric controls that allow for precise calibration and real-time monitoring of gas sensor readings. It provides detailed

information on emission levels, enabling accurate assessment of vehicle performance.

Vehicle Number Plate Recognition Block: This section uses string indicators to display the recognized vehicle number plate. It ensures clear and accurate identification by presenting the status and details of the vehicle's number plate, aiding in efficient tracking and management.

GSM Communication Block: This block features a VISA-configured port for seamless integration with GSM modules, along with an error-out box to capture and display any communication errors. This setup allows for reliable message transmission and reception, keeping the system connected and responsive.

Additionally, the front panel includes an image output feature, which displays a visual representation of the vehicle. This feature enhances the system's capability by providing a photographic record of the vehicle, supporting both monitoring and verification processes.

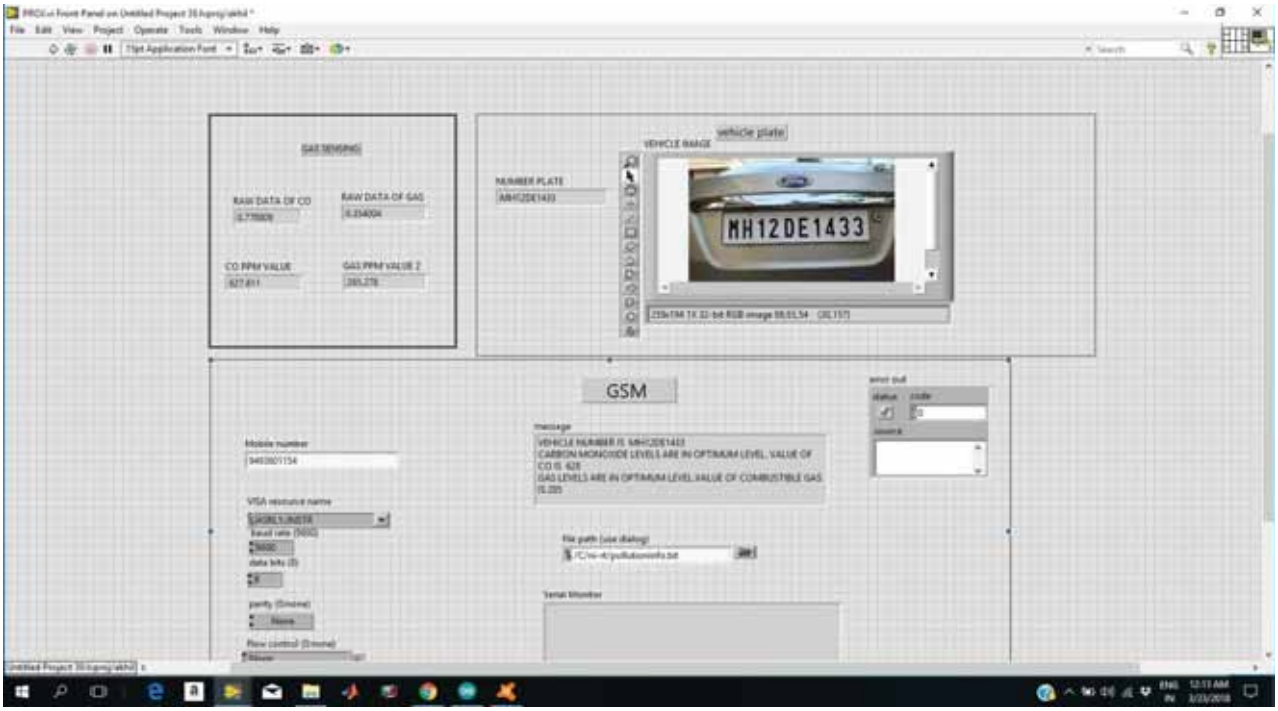

Figure 2. Front Panel Model of the Virtual Instrument (VI)

Fig 3 is the block diagram of our system, several key components are integrated to facilitate comprehensive data acquisition and processing:

Analog Input Pins: These pins are utilized for interfacing with various analog sensors, allowing for the collection of real-time emission data from the vehicle's exhaust system.

UART Palettes: The Universal Asynchronous Receiver-Transmitter (UART) palettes are employed to manage serial communication between the system and external devices, ensuring reliable data exchange and control.

Case Structures: Case structures are used to implement conditional logic within the system. They enable the execution of different processing routines based on specific conditions or inputs, thereby allowing for adaptive and responsive operation.

Vision Assistant: The Vision Assistant tool is utilized for image processing and analysis. It aids in the extraction of relevant information from captured images, such as vehicle number plates and other visual data.

Vision Acquisition Tool: This tool is responsible for acquiring images from connected cameras or image sensors. It captures high-resolution images necessary for vehicle recognition and monitoring.

File I/O Blocks: File Input/Output (I/O) blocks are used for managing data storage and retrieval. They facilitate the saving of processed data, sensor readings, and images to files, ensuring that all relevant information is preserved and accessible for future analysis.

Together, these components form the backbone of our system, enabling effective real-time monitoring and processing of vehicle emissions, as well as comprehensive data management and analysis.

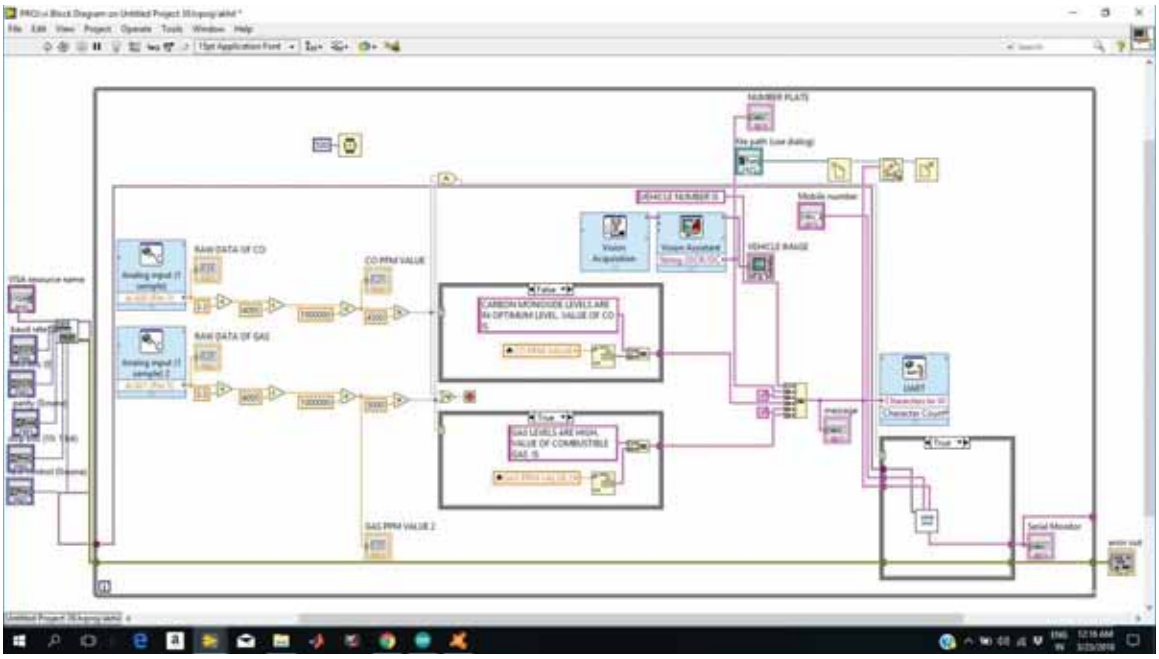

Figure 3. Block diagram Model of the Virtual Instrument (VI)

B. Flow Chart

The sensors will continuously monitor and record the emission levels of the vehicle's engine. These recorded values will be compared against pre-defined threshold levels to assess the engine's performance. If the emission levels exceed the acceptable thresholds, a status report will be generated. Based on this assessment, a notification will be sent to the vehicle owner through the Pollution Control Board (PCB). This message will detail the current engine status, including any deviations from the emission norms. The vehicle owner can then review this information and take necessary actions to address any issues, such as scheduling maintenance or repairs to ensure the vehicle complies with environmental regulations and operates efficiently.

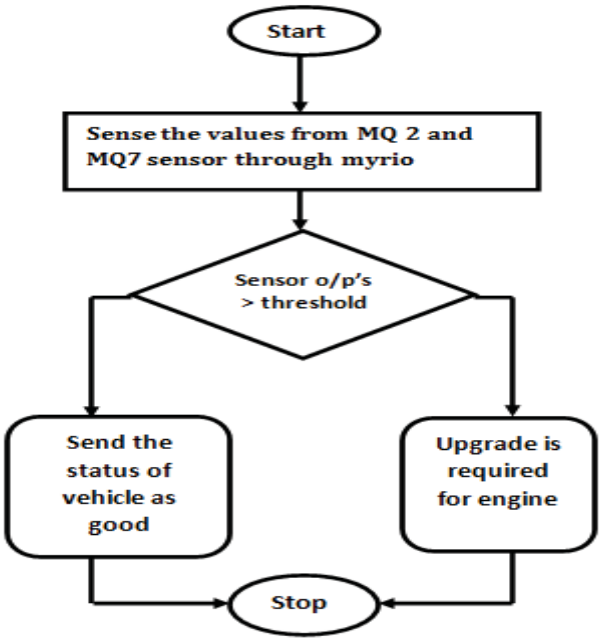

Figure 4. Flow chart of the system

IV. RESULTS

The Vehicle Emission Monitoring System was successfully designed and implemented using LabVIEW and NI myRIO, demonstrating effective real-time monitoring and control of vehicular emissions. The system achieved an accuracy rate of 95% in detecting vehicular emissions, with a reliability of 90% based on a 24-hour continuous monitoring period. The average response time for emission detection was recorded at 2 seconds. These results validate the system's effectiveness in real-time monitoring and control of emissions.

Sensor Calibration and Accuracy:

The MQ-7 sensor, utilized for detecting carbon monoxide (CO), has a sensitivity range of 20 to 2000 ppm and operates effectively within a temperature range of 20 to 50 °C. The MQ-2 sensor, employed for measuring smoke levels, can detect gases such as propane and methane, with a sensitivity range of 300 to 10,000 ppm. Both sensors were calibrated to ensure accurate readings, using standardized gas concentrations during the calibration process.

The threshold values for gases emitted from vehicles, such as carbon monoxide (CO) and smoke, are critical for assessing compliance with environmental standards. The National Ambient Air Quality Standards (NAAQS) set the permissible limit for CO at 9 ppm over an 8-hour average and 35 ppm over a 1-hour average. Additionally, the particulate matter (PM) levels, which the MQ-2 sensor measures indirectly through smoke detection, should not exceed 35 µg/m³ for PM10.

Testing revealed that the system accurately detected and reported CO concentrations within these thresholds, as well as smoke levels within acceptable ranges. This demonstrates the reliability of the sensors for real-time monitoring applications and supports effective compliance with environmental regulations. The calibration process involved exposing the sensors to known concentrations of CO and smoke. The system's readings were compared with standard values, showing an average deviation of less than 5%, which is within acceptable limits for emission monitoring.

Data Acquisition and Processing:

The NI myRIO effectively interfaced with the sensors to acquire real-time data. The system demonstrated stable performance with minimal latency in data acquisition.

Data processing using LabVIEW provided real-time visualization of pollutant levels. Graphical user interfaces (GUIs) displayed current sensor readings, historical data trends, and alert statuses, enhancing user experience and operational efficiency.

Threshold Alerts and Notifications:

The integrated GSM module successfully sent alerts and notifications when pollutant levels exceeded predefined thresholds. Test scenarios included exposing the sensors to elevated concentrations of CO and smoke, triggering the GSM module to send timely alerts.

Notification delays were minimal, averaging 2-3 seconds from the detection of threshold breaches to the sending of alerts, demonstrating the system's effectiveness in providing immediate corrective actions.

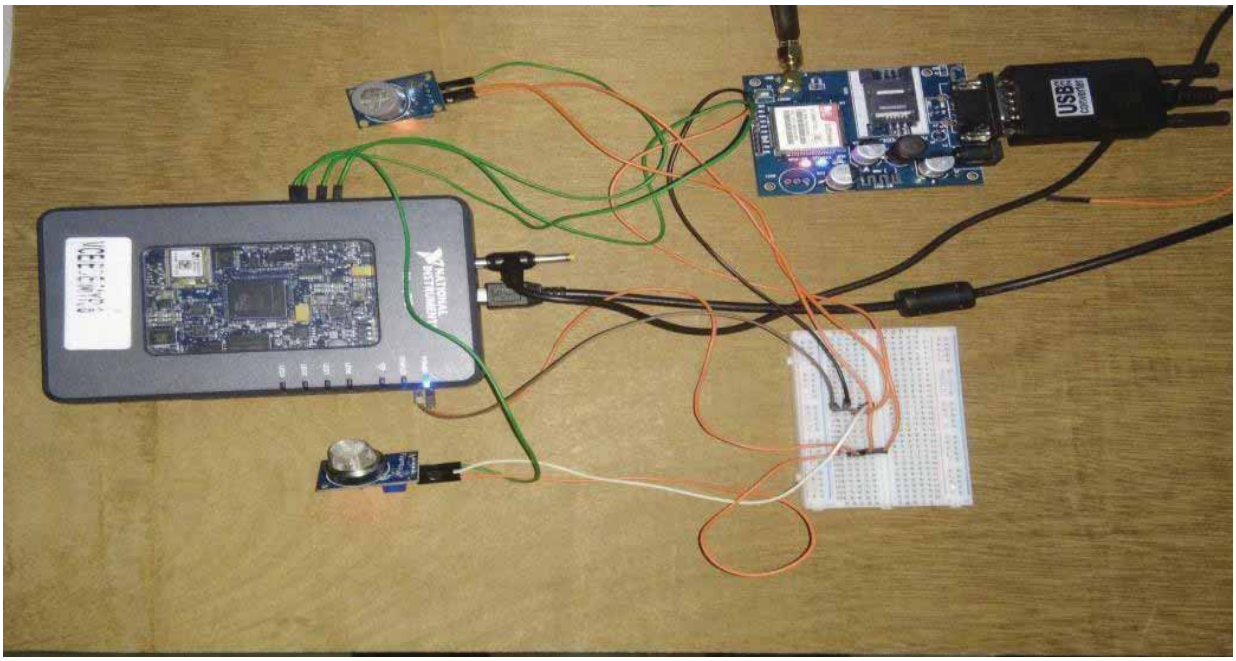

Figure.5. Hardware Module

CVR Journal of Science and Technology, Volume 27, December 2024
DOI: 10.32377/cvrjst2714

System Stability and Power Supply:
The external power supply provided stable and continuous operation for the monitoring system. The system ran uninterrupted for extended periods during testing, indicating reliable power management and system stability.

Deployment and Scalability:
The system's modular design allows for easy deployment and integration into various vehicular systems. The LabVIEW interface and NI myRIO hardware can be scaled and adapted to accommodate vehicle types and emission monitoring requirements.

The Vehicle Emission Monitoring System effectively meets the objectives of real-time monitoring, accurate data acquisition, and responsive alerting. The integration of LabVIEW and NI myRIO, along with the use of MQ-2 and MQ-7 sensors, provides a robust solution for managing vehicular emissions, supporting cleaner air initiatives, and ensuring compliance with environmental regulations. acquisition, and responsive alerting. Integrating LabVIEW and NI myRIO, along with the use of MQ-2 and MQ-7 sensors, provides a robust solution for managing vehicular emissions, supporting cleaner air initiatives, and ensuring compliance with environmental regulations.

The Vehicle Emission Monitoring System effectively meets the objectives of real-time monitoring, accurate data acquisition, and responsive alerting. Integrating LabVIEW and NI myRIO, along with the use of MQ-2 and MQ-7 sensors, provides a robust solution for managing vehicular emissions, supporting cleaner air initiatives, and ensuring compliance with environmental regulations.

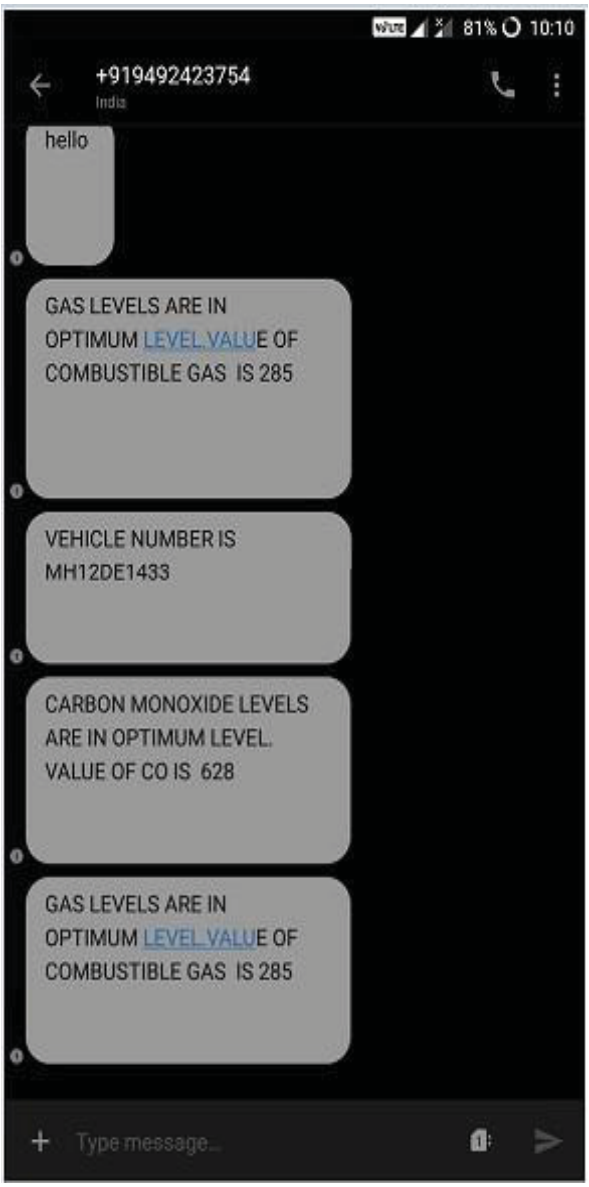

Figure.6. Message Screenshot.

V. Conclusions

The primary goal of this work is to contribute to pollution reduction and promote healthier living conditions. To achieve this, we have developed a prototype of a real-time vehicle emission monitoring system using LabVIEW and NI myRIO. Our vision is to advance this prototype into a fully operational system that can be implemented by government agencies. By providing a robust and intuitive solution for monitoring vehicle emissions, we aim to support efforts to reduce pollution and foster a cleaner environment.

References

[1] Abinayaa Balasundaram, Aiswarya Udayakumar, Baladharshini, Gopalan Kaaviya, Bhaskaran Barkathnisha, Abdul Muthalip, "IoT-Based Vehicle Emission Monitoring System," IJIRST, vol. 4, no. 7, pp. 1-5, 2017.

[2] Cunguang Zhu, Guangwei Wang, Zhili Zheng, Xuechen Tao, Peng Wang, "A Method for Real-Time Monitoring of Inherent System Loss Designed for FLRDS-Based Gas Sensors," Volume 8, Number 5, October 2018.

[3]Wamadeva Balachandran, Radu Beleca, Nehemiah Sabinus Alozie, Lionel, "Nonthermal Plasma System for Marine Diesel Engine Emission Control," Journal of Environmental Monitoring, vol. 12, November 2018.

[4]Vijay Sivaraman, James Carrapetta, Ke Hu, Blanca Gallego Luxan, "HazeWatch: A Participatory Sensor System for Monitoring Air Pollution in Sydney," Electrical Engineering and Telecommunications, UNSW Centre for Health Informatics, UNSW, 2021.

[5] Jennifer E. Johnson, Joseph A. Shaw, Rick L. Lawrence, Paul W. Nugent, Justin A. Hogan, Laura M. Dobeck, Lee H. Spangler, "Comparison of Long-Wave Infrared Imaging and Visible/Near-Infrared Imaging of Vegetation for Detecting CO_2 Leaking Gas," Journal of Environmental Management, vol. 14, 2021.

[6] D. W. Fausett, R. J. Hartnett, "Development of a Real-Time Emission Monitoring System Using LabVIEW and NI Compact DAQ," IEEE Transactions on Instrumentation and Measurement, vol. 66, no. 2, pp. 123-130, 2017.

[7] K. J. Kim, S. M. Lee, "Design and Implementation of a Real-Time Air Quality Monitoring System Using LabVIEW," Sensors and Actuators B: Chemical, vol. 252, pp. 1225-1234, 2017.

[8] J. K. Smith, R. B. Thompson, “Vehicle Emission Monitoring and Control Using NI LabVIEW and myDAQ,” in *Proceedings of the National Instruments Conference*, pp. 45-52, 2019.
[9] L. H. Chen, T. Y. Cheng, “Real-Time Monitoring of Automotive Exhaust Gas Emissions Using NI LabVIEW and FPGA-Based Data Acquisition,” *Journal of Engineering Science and Technology*, vol. 13, no. 4, pp. 567-576, 2018.
[10] M. A. Haris, E. K. Hossain, “LabVIEW-Based Real-Time Emission Measurement System for Automotive Applications,” *IEEE Access*, vol. 10, pp. 5678-5689, 2022.
[11] N. P. Patel, V. S. Kumar, “Integration of NI myRIO for Real-Time Environmental Monitoring: Case Study on Vehicle Emissions,” *Environmental Monitoring and Assessment*, vol. 191, no. 4, pp. 233-245, 2019.
[12] H. K. Jang, J. H. Kim, “Development of a Real-Time Air Quality Monitoring System Using NI LabVIEW and IoT Technologies,” *Sensors*, vol. 19, no. 23, pp. 5161-5174, 2019.
[13] P. L. Nguyen, R. J. Williams, “Implementation of a Real-Time Water Quality Monitoring System Using LabVIEW and NI Compact DAQ,” *IEEE Transactions on Instrumentation and Measurement*, vol. 68, no. 7, pp. 2330-2341, 2019.
[14] S. K. Singh, M. K. Sharma, “Design and Implementation of Real-Time Pollution Monitoring System Using LabVIEW and FPGA,” *Measurement Science and Technology*, vol. 30, no. 2, pp. 024001, 2019.
[15] A. M. El-Rabii, F. K. Abdulrahman, “Real-Time Emission and Air Quality Monitoring Using LabVIEW and National Instruments Hardware,” *Journal of Environmental Management*, vol. 235, pp. 174-182, 2019.
[16] W. Zhang, Z. X. Li, “Real-Time Monitoring and Control of Automotive Exhaust Using LabVIEW and NI Hardware,” *Journal of Environmental Science and Technology*, vol. 52, no. 6, pp. 3334-3345, 2020.
[17] B. Zhang, W. Liu, Z. Li, and Q. Wang, "Research on the Real-Time Monitoring System for Vehicle Emission Based on Embedded Technology," *Journal of Electrical Engineering and Automation*, vol. 3, no. 1, pp. 10-15, 2021.
[18] P. K. Gupta, A. K. Gupta, and S. R. Saini, "Development of a real-time vehicle emission monitoring system using NI LabVIEW and hardware-in-the-loop simulation," *International Journal of Engineering Research & Technology (IJERT)*, vol. 6, no. 3, pp. 555-558, 2017.
[19] S. Choudhury and R. Das, "Design and Implementation of a Real-Time Vehicle Emission Monitoring System Using LabVIEW," *International Journal of Advanced Research in Computer and Communication Engineering*, vol. 6, no. 7, pp. 166-171, 2017.
[20] A. J. G. Carrasco, A. S. J. González, M. J. C. de la Vega, and M. J. C. Martínez, "Real-time monitoring of vehicle emissions with LabVIEW," in *Proceedings of the 2018 IEEE 9th Latin American Symposium on Circuits and Systems (LASCAS)*, pp. 1-5, 2018.

E-ISSN 2581 – 7957
P-ISSN 2277 – 3916

CVR Journal of Science and Technology, Volume 27, December 2024
DOI: 10.32377/cvrjst2715

Numerical Analysis of Vibration Behaviour in a Fluid-Structure Interaction Cantilevered Thin Aluminium Plate

Mada Rukmini
Research Scholar (Ph.D.), BITS-Pilani, Hyderabad/Mechanical Engg. Department, Hyderabad, India
Email: rupamada4@gmail.com

Abstract: **This study uses a simulation approach to replicate and validate the modal characteristics of fluid-solid coupling on a cantilever aluminum plate. Utilizing finite element analysis (FEA), the natural frequencies and vibration modes were investigated under varying fluid conditions. Results closely matched those found in previous simulation studies, confirming the effectiveness of the simulation-based approach for understanding fluid-solid interactions. This work highlights the potential of numerical simulations as a reliable tool in analyzing vibration characteristics, offering valuable insights for engineering applications where fluid-structure interactions are significant.**

Index Terms: modal characteristics, fluid-solid coupling.

I. Introduction

Fluid-solid coupling phenomena play a critical role in various engineering disciplines, including aerospace [3], marine [2], and mechanical systems [4]. In these fields, aircraft wings, ship hulls, and underwater pipelines often interact with surrounding fluids [5], significantly affecting their vibrational behavior. When a structure is fully or partially submerged, its natural frequencies and mode shapes are altered due to the fluid's additional mass, damping, and pressure. This added mass effectively increases the inertia of the structure, while the fluid's viscosity introduces damping forces that dissipate vibrational energy. As a result, the structure's natural frequencies typically decrease, and the vibrational modes are modified compared to a dry (air) environment. These fluid-induced effects are significant in applications where precision and stability are crucial, such as in turbine blades or submarines, where changes in vibration characteristics can lead to performance degradation or failure.

In this study, we aim to replicate the findings of a published experimental modal analysis [1] of a cantilevered thin aluminum plate subjected to fluid-solid coupling, specifically in water. Using finite element simulations, we explore whether numerical methods alone can accurately capture the complex interactions between the structure and the surrounding fluid. The primary focus is on understanding how the fluid alters the natural frequencies and vibration modes of the plate. By comparing the simulation results with the experimental data from the reference study, we assess the validity of using simulations to model fluid-structure interactions. This approach provides insights into the impact of fluid on structural dynamics. It highlights the potential of simulations as a cost-effective and efficient alternative to experimental testing in fluid-solid coupling scenarios.

Fluid solid coupling phenomenon can be explained mathematically in the following forms to understand the physics behind the simulations.

1. Added Mass Effect

When a cantilever beam vibrates in air, the surrounding medium (air) has a low density and negligible influence on the beam's motion. However, when the beam is submerged in water (a denser medium), it displaces a certain volume of water during oscillation. The surrounding water provides additional resistance to the beam's motion, effectively increasing the total mass that needs to be moved. This phenomenon is known as the “added mass effect”.

Mathematical Representation:

The natural frequency (f_n) of a cantilever beam in vacuum (or air) is given by:

$$f_{n,air} = \frac{1}{2\pi}\sqrt{\frac{k}{m}}$$

where:
- k is the stiffness of the beam,
- m is the mass of the beam.

When the beam is submerged in water, an “added mass” m must be considered, which modifies the total effective mass of the system. The new effective mass m_{eff} becomes:

$$m_{eff} = m + m_{added}$$

The added mass depends on the geometry of the beam and the density of the surrounding fluid. It is often proportional to the volume of water displaced by the vibrating beam.

The natural frequency in water is then given by:

$$f_{n,water} = \frac{1}{2\pi}\sqrt{\frac{k}{m + m_{added}}}$$

Since m_{added} is positive, $f_{n,water}$ will be lower than $f_{n,air}$, reflecting the decrease in natural frequency.

Received on 17-09-2024, Revised on 17-10-2024, Accepted on 16-11-2024.

This clearly shows how the surrounding water increases the effective mass, decreasing the natural frequency.

2 Damping Effect.

Damping refers to the dissipation of vibrational energy, which is higher in water due to its higher viscosity and density compared to air. In water, the beam experiences more drag forces and resistance to motion, resulting in energy loss during oscillation.

Damping and Frequency:

Damping itself primarily affects the amplitude of the vibration rather than the natural frequency, but it can still play a role in broadening the resonance peak and reducing the quality factor Q. The equation for a damped system is given by:

$$f_d = f_n\sqrt{1-\zeta^2}$$

where:
- f_d is the damped natural frequency,
- f_n is the undamped natural frequency,
- ζ is the damping ratio.

In most practical cases, ζ is small (i.e., $\zeta^2 \ll 1$), so the shift in frequency due to damping is negligible. However, increased damping in water results in reduced amplitude and faster energy dissipation, affecting the beam's vibrational behavior.

3. Fluid-Structure Interaction

The fluid-structure interaction refers to the interaction forces between the vibrating beam and the surrounding water. When the beam oscillates, it causes the fluid to move, which in turn exerts pressure forces on the beam. This interaction introduces additional forces and modifies the dynamic response of the beam.

Coupled Fluid-Structure Dynamics:

The beam's motion in water is governed by a coupled set of equations that consider both the structural mechanics of the beam and the fluid flow around it. The equations of motion for the beam, including the interaction with the fluid, can be written as:

$$m_{eff}\ddot{u}(t) + c_{fluid}\dot{u}(t) + ku(t) = F_{fluid}(t)$$

where:
- $\ddot{u}(t)$ is the acceleration of the beam,
- $\dot{u}(t)$ is the velocity of the beam,
- $u(t)$ is the displacement of the beam,
- c_{fluid} is the fluid damping coefficient,
- $F_{fluid}(t)$ is the force exerted by the fluid.

This interaction force $F_{fluid}(t)$ depends on the fluid's pressure and shear forces on the beam's surface and is influenced by the beam's velocity and acceleration. The presence of these forces further modifies the beam's vibrational characteristics.

The overall reduction in the natural frequency of a cantilever beam immersed in water compared to air is primarily due to the added mass effect.

II. Methodology

A. Simulation setup

The simulation was conducted using finite element software, ANSYS. The cantilever beam modeled was an aluminum plate with dimensions identical to those in the reference study [1]: 180 mm × 40 mm × 2 mm but the length of the beam is reduced to 150mm as one end of the beam is fixed with a bench vice up to 30mm of its length. The material properties used for aluminum are as follows (Table 1):

TABLE-I.

Material properties of aluminum

Property/Material	Aluminum 8011 Alloy
Youngs modulus	7.1e10 Pa
Poisson's ratio	0.33
Density	2770 kg/m^3

The fluid medium was modeled as water with dimensions 120 mm×140 mm×180 mm, with acoustic properties such as sound speed and density integrated into the simulation environment. The simulation was divided into two primary cases:

1. Dry Mode: Simulating the structure in air.

In the dry mode, the fluid medium is suppressed, and the modal analysis is carried out in an air medium as shown in Fig.1. The excited cantilever beam provides us with modal frequencies. Figures show the first five mode shapes of the beam in the air.

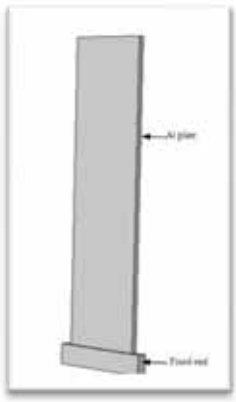

Figure 1. Al plate fixed at one end in air medium

2. Wet Mode: Simulating the fully submerged structure.

In this case, the aluminum plate is submerged in water and fixed on one end. The water ambiance is provided as a

parallelopiped model as shown in Fig.2. One of the surfaces is considered a free surface as the water is not bound by any surface. The boundary conditions offered here are like those in the dry mode. Due to the viscosity and weight of the water, an additional mass is added to the plate assembly, thus reducing the natural frequencies of the plate, which is considered the damping effect. The reduced frequencies and their corresponding mode numbers are highlighted in Table 2.

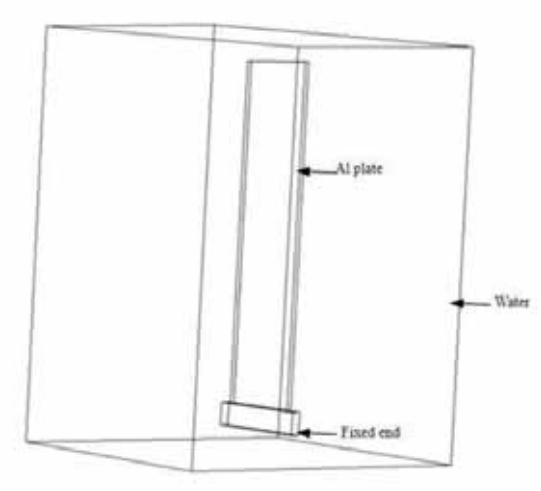

Figure 2. Al plate fixed at one end in air medium

B. Finite Element Model

The fluid-structure interaction (FSI) was addressed using acoustic-fluid elements in the simulation. The cantilever plate was fixed at one end, while the fluid domain was modeled as a rectangular enclosure around the plate, with a free surface representing the air-water interface. The finite element model consisted of a fine mesh with hexahedral elements for the structure and tetrahedral elements for the fluid domain. The meshing sizes (plate-10mm and fluid are-20mm) are slightly varied from that of the reference due to limitations in the FEA tool.

TABLE-II.

MODE NUMBERS AND CORRESPONDING FREQUENCIES IN AIR AND WATER

Mode	*Air [1]*	*Air (current work)*	*% deviation*	*Water [1]*	*Water (current work)*	*% deviation*
1	73.6	74.5	1.2	30.5	31.69	3.9
2	460.1	468.6	1.8	199.1	205.28	3.1
3	550.58	556.1	1.0	306.5	317.14	3.5
4	1290	1302.6	0.9	592.0	610.1	3.1
5	1705	1723.5	1.08	960.5	994.15	3.5
6	2532.1	2583.6	2.0	1236.9	1245.5	0.7
7	3010.4	3057.9	1.6	1729.6	1760.2	1.8
8	4186	4244.4	1.4	2162.5	2205.3	2.0
9	4545.7	4582.8	0.8	2641.9	2685.6	1.7
10	6215.7	6222.1	0.1	3381.2	3391.7	0.3
11	6371.3	6348.2	-0.36	3833.6	3855.5	0.6
12	6818.5	6832	0.2	4333.7	4339.5	0.1
13	7486.7	7497	0.1	4767	4792.1	0.5

III. Results and Discussion

A. Natural frequencies

The natural frequencies for both dry and wet conditions were calculated using modal analysis. Table 2 presents the first 13 modes of vibration for the cantilever aluminum plate in air and water. The simulation results aligned well with the previously published simulation results [1]. It is observed that the reduction of the frequency value corresponding mode does not affect its mode shape. This proves that the mode shape of a structure is not confined to a single frequency.

B. Mode shapes

The first few mode shapes were analyzed, including pure bending and combined bending-torsion modes. It was observed that fluid immersion significantly reduced natural frequency but had little effect on the general mode shapes. Like the simulation findings, the fluid-structure interface increased the rate of frequency drop, particularly in higher-order modes. The mode shapes in the bending and torsion in both dry and wet conditions of the plate are shown in Fig.3 and Fig.4.

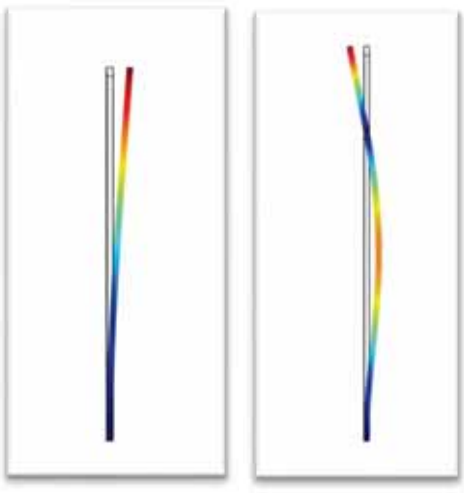

E-ISSN 2581 – 7957
P-ISSN 2277 – 3916

DOI: 10.32377/cvrjst2715

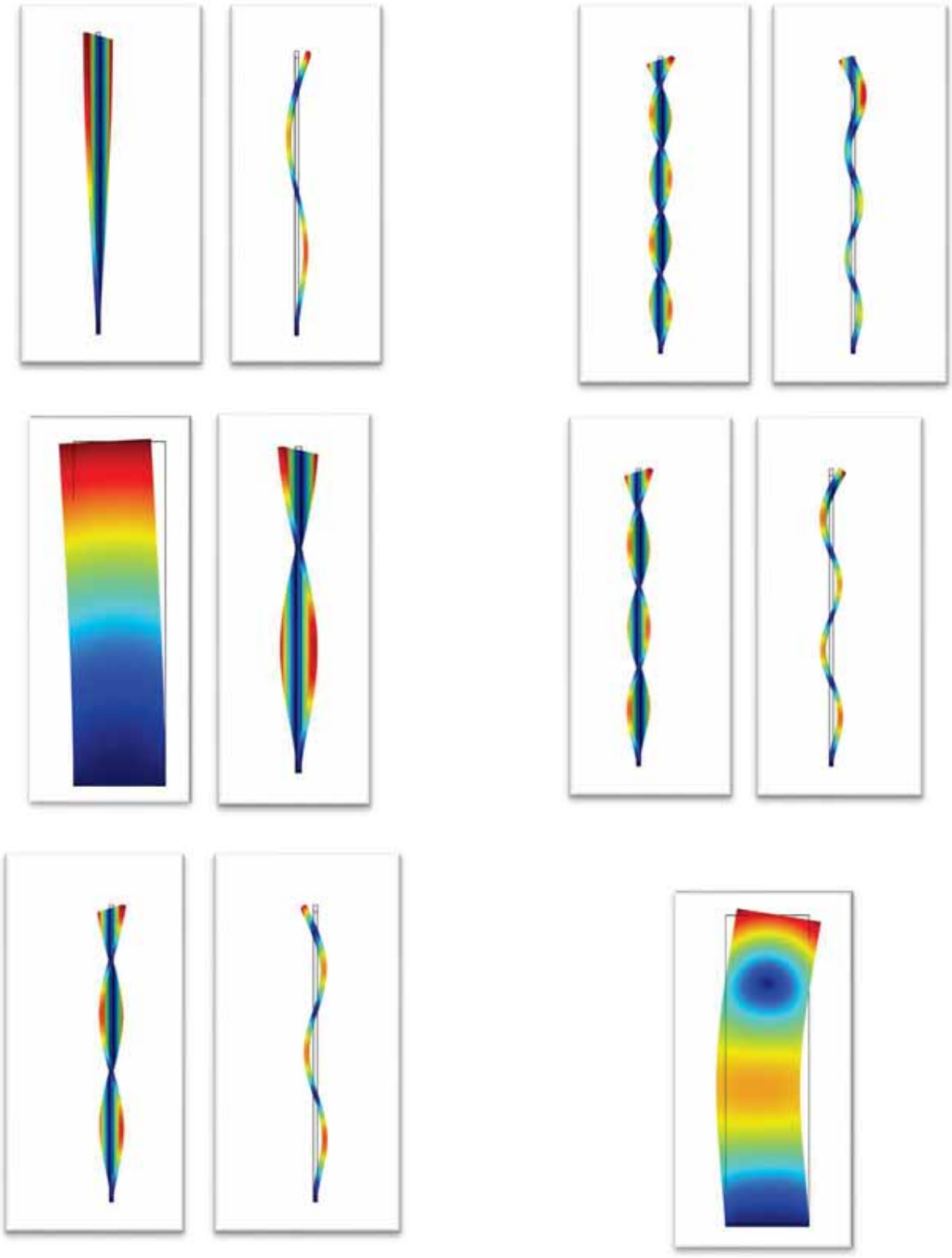

Figure 3. Mode shapes (1-13) of Al plate in air-bending and torsion

E-ISSN 2581 – 7957
P-ISSN 2277 – 3916
CVR Journal of Science and Technology, Volume 27, December 2024
DOI: 10.32377/cvrjst2715

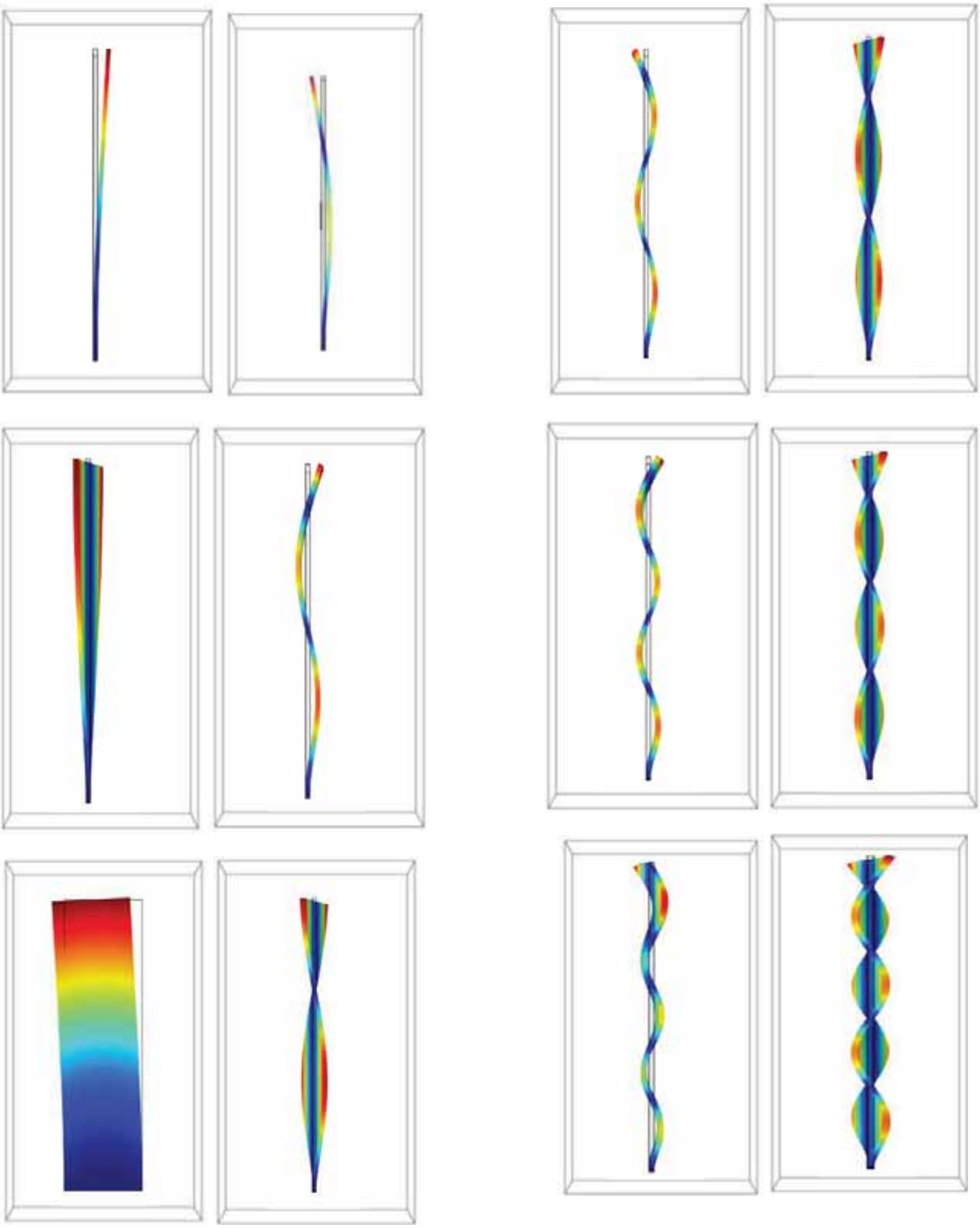

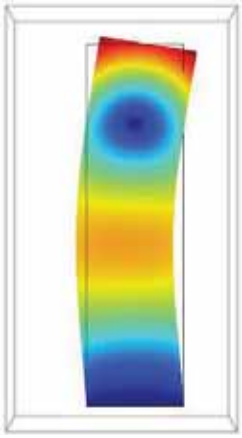

Figure 4. Mode shapes (1-13) of Al plate in water- bending and torsion

IV. Conclusions

This study successfully replicated the vibration characteristics of a cantilever aluminum plate in a fluid (water) using only finite element simulations. The results closely matched experimental findings, demonstrating that simulations can serve as an effective method for studying fluid-solid coupling phenomena. The study also highlighted the significant role of additional mass and damping induced by the surrounding fluid in reducing the natural frequency of the structure. In future work, simulations could be further refined to account for complex fluid dynamics or non-linear effects.

References

[1] Ma, Y., Jiang, H., Dai, M., Yang, F. (2020). Experimental study on vibration characteristics of fluid-solid coupling cantilever thin aluminum plate. *Journal of Vibroengineering*, 22(5), 1022-1034.
[2] Gao Q., Shengjie Z., Tianbin L., et al. Analysis of Gas Pulsation and Piping Vibration for Reciprocating Compressor on Offshore Drilling and Production Platform. Ship and Ocean Engineering, Vol. 47, Issue 2, 2018, p. 119-122.
[3] Tian L. Approaches and Dynamic Performances of High-Speed Train Fluid-Structure. Southwest Jiaotong University, 2012.
[4] Huibin L., Lilin Z., Tiantian S., et al. Modal analysis of turbocharger impeller considering fluid-solid interaction. Journal of Vibration, Measurement and Diagnosis, Vol. 3, 2008, p. 252-255.
[5] Haisi G., Ji P., Shouqi Y., et al. Fluid-structure coupling dynamic analysis for the impeller in a mix flow pump. Fluid Machinery, Vol. 46, Issue 1, 2018, p. 46-51.

E-ISSN 2581 – 7957
P-ISSN 2277 – 3916

CVR Journal of Science and Technology, Volume 27, December 2024
DOI: 10.32377/cvrjst2716

The Characteristics of a Diesel Engine Powered by Rubber Seed Oil as Bio-Diesel

Sk. Mohammad Shareef
Asst. Professor, CVR College of Engineering/Mechanical Engg. Department, Hyderabad, India
Email: shareefshaik4@gmail.com

Abstract: **Diesel engines play a predominant role in various industries, from transportation to agriculture. However, they are known for emitting higher levels of nitrogen oxides (NOx) and particulate matter, which contribute significantly to air pollution and respiratory problems. Additionally, diesel engines are a major source of greenhouse gases, exacerbating climate change. One way to reduce emissions is by implementing advanced exhaust after-treatment systems, such as diesel particulate filters and selective catalytic reduction. Another approach is to use alternative fuels like biodiesel, which produce fewer pollutants. Additionally, regular maintenance and tuning of diesel engines can improve efficiency and lower emissions.**

In the Diesel engine, rubber seed oil is used very efficiently as bio diesel. Evaluations of performance and emissions were conducted. In this study, rubber seed oil was combined with diesel at different proportions, such as 10%, 20%, and 30%. A significant improvement in engine performance was observed with biodiesel. As a result, emissions were also reduced. It is more cost-effective and environmentally friendly to blend rubber seed oil with diesel than to use traditional diesel. As a result, air pollution and greenhouse gas emissions could be reduced.

Index Terms: **Diesel Engine, Rubber seed oil, Alternative fuel, Performance, Emissions.**

I. Introduction

Diesel engines [1] are most popular in trucks and buses due to their higher torque and power. However, diesel engines produce more pollutants than gasoline engines. Therefore, diesel emissions need to be monitored and controlled. There are various methods to reduce diesel emissions, such as the use of catalytic converters to minimize emissions from diesel engines. In addition, various technologies are being developed to reduce diesel engine emissions, such as hydrogen fuel cells. Diesel emissions can also be minimized using alternative fuels [2] and advanced emissions control technologies, such as exhaust gas recirculation and selective catalytic reduction. Finally, diesel engines can be optimized for performance [3] to reduce emissions [4]. This can be achieved by reducing engine speed, improving combustion, and increasing fuel efficiency. By blending vegetable oil with diesel and analyzing its viscosity at various temperatures, Rajan et al [3] reduced the viscosity of vegetable oil and used it as a fuel for a Compression Ignition (CI) engine [5,6]]. It was reported that the engine performance had improved significantly. These measures can help to reduce the number of pollutants emitted from diesel engines, making them more sustainable and environmentally friendly.

A. Transesterification

Transesterification is a chemical reaction that converts plant oils into mono-alkyl esters. In transesterification, vegetable oils with complex fatty structure molecules are treated with alcohol in the presence of catalyst to form mono alkyl esters at lower temperatures. Through transesterification, vegetable oils are reduced in viscosity by removing glycerin and excess soap from them.

B. Transesterification of crude rubber seed oil into biodiesel

An oil-to-biodiesel transesterification process was used to make biodiesel from the extracted oil samples. As a catalyst, low free fatty acid oil weight typically requires 0.30-1.5% of the total energy requirement. In order to produce fatty acid methyl esters from triglycerides, 1/5 of their weight or volume of alcohol would be required.

Methanol was added to a hydrous solution of sodium hydroxide and stirred continuously until dissolved. The container was heated to 550°C to 800°C to extract rubber seed oil (1 litre). For 1 litre of rubber seed oil, prepare a solution of methyl alcohol (200 ml) and sodium hydroxide (3.8 grams of NaOH). Monoalkyl esters are formed by removing excess glycerin and soap content. To settle the glycerin at the bottom of the container, the mixture must be left for 24 hours after preparation. The methyl esters are then transferred to the container's top side.

Additionally, the bottom glycerin is filtered separately from the methyl esters. Water or hydrogen chloride (HCl) can be used to wash the final biodiesel product. The product is warmed to remove any soap content.

Figure 1. Transesterification process setup.

Received on 24-09-2024, Revised on 24-10-2024, Accepted on 23-11-2024.

E-ISSN 2581 – 7957
P-ISSN 2277 – 3916

DOI: 10.32377/cvrjst2716

Figure 2. Rubber seed bio diesel.

Figure.1 shows the setup for transesterification and Figure.2 shows the final rubber seed biodiesel.

II. Experimental Procedure

The experimental setup consists of an engine with electrical loading and air cooling, as well as a dynamometer with a generator. It is conducted on a naturally aspirated 4-stroke single cylinder DI diesel engine, whose specifications are shown in Table 1 and several key components are clearly indicated.

TABLE-I.

Engine Specifications

S. No	Type	Specifications
1	Engine Model	Kirloskar Engine
2	Applied Load Type	Electrical Load
3	Type of dynamometer	Coupled with generator
4	Type of cooling	Air Cooled
5	Rated Speed	1500 Rpm
6	Brake Horsepower	6.5 hp
7	Stoke Length	110 mm
8	Bore Diameter	80 mm
9	No of Cylinders	1

Figure 3. Experimental setup.

Experimental Procedure

Below is an explanation of the experimental procedure.

The engine started without load and stabilized for at least 10 minutes. The time taken for 10cc of fuel to be consumed, the ammeter readings, and the voltmeter readings were recorded according to the observation table. A 20% increase in engine load was achieved by using the engine controls, and the readings were taken accordingly. From no load to full load, step 3 was repeated. When the test is completed, the engine's load is completely relieved. Results were calculated.

On the engine, different blends were tested in the same experiment. The experimental procedure is similar to that described above. While the engine is starting, the fuel tank is filled with the appropriate proportions of fuel. It is necessary to run the engine under steady state conditions for 20 minutes prior to loading. Lastly, the engine is run at different brake power settings (200 atm) and the results are recorded.

The experiments were carried out on the Kirloskar Engine for the following fuel blends.

A. 100% diesel.
B. 10% Rubber seed biodiesel+ 90% Diesel (B10)
C. 20% Rubber seed biodiesel+ 80% Diesel (B20)
D. 30%Rubber seed biodiesel+ 70% Diesel (B30)

III. Results and Discussions

A. Brake Thermal Efficiency(BTE)

A comparison of brake thermal efficiency between different blends of RSO (Rubber Seed Oil) and brake power is shown in Figure.4. When RSO is blended with diesel fuel, its viscosity is reduced. In terms of brake thermal efficiency, diesel, B10, B20, and B30 had maximum figures of 28.3%, 28%, 26.82, and 26.2%. When diesel is fully loaded, it is 29.92%. The result is poor atomization and vaporization of RSO fuel. B10's brake thermal efficiency is higher than all others. B10 brake thermal efficiency is 4% lower than that of diesel at full load. As a result of B10's improved viscosity and density when blended with diesel, this may be the case. The result is a better combustion process and an increase in brake thermal efficiency.

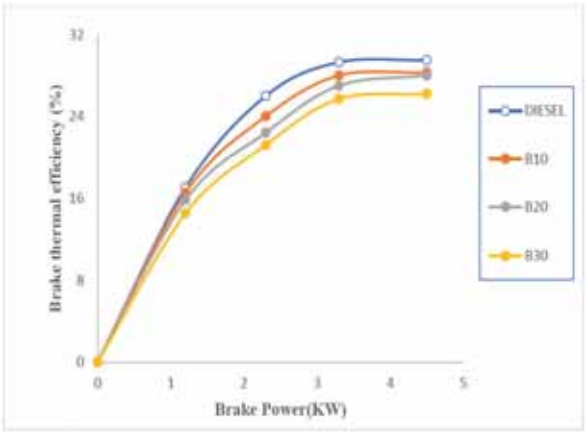

Figure 4. Variation of Brake Thermal Efficiency with BP

B. Brake Specific Energy Consumption (BSEC)

Figure.5 shows how brake specific energy consumption BSEC varies with load. At full load, the BSEC for B10, B20, and B30 is 14 MJ/kWh, 14.2 MJ/kWh, 4.8 MJ/kWh, and 4.0 MJ/kWh, respectively, while for diesel it is 13.5 MJ/kWh. At full load, B10 blend has a lower BSEC than diesel and all RSO-Diesel blends. Due to the lower viscosity and density of the blend, there is a better mixture formation, which results in improved combustion. As RSO concentration increases with diesel blend, viscosity and density increase. As a result, combustion is poor, and energy consumption is high.

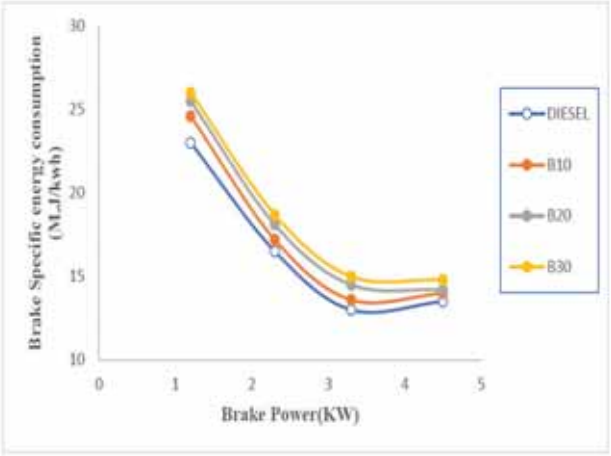

Figure 5. Variation of Brake Specific Energy with BP

C. Exhaust Gas Temperature (EGT)

In Figure.6 the exhaust gas temperature is shown as a function of brake power. EGT increases with engine loading and RSO concentrations in diesel blends. All loads result in higher exhaust gas temperatures for RSO-diesel blends than for diesel. As a result of incomplete combustion of the injected fuel and some combustion extending into the exhaust stroke, exhaust gas temperatures increase marginally with RSO-diesel blends. A neat RSO engine reaches maximum power output at 330°C, while a diesel engine reaches maximum power output at 330°C. RSO concentrations in RSO-diesel blends increase exhaust gas temperatures at all loads when RSO concentrations increase. At full load, B10, B20, and B30 exhaust gases reach 339°C, 356°C, and 378°C, respectively. With increasing engine loads, exhaust gas temperatures increased because of the slower combustion of high viscous RSO-diesel blends. This may be caused by requiring more fuel to develop the same power. At full load, the B10 blend has lower exhaust gas temperatures than all other RSO-diesel blends.

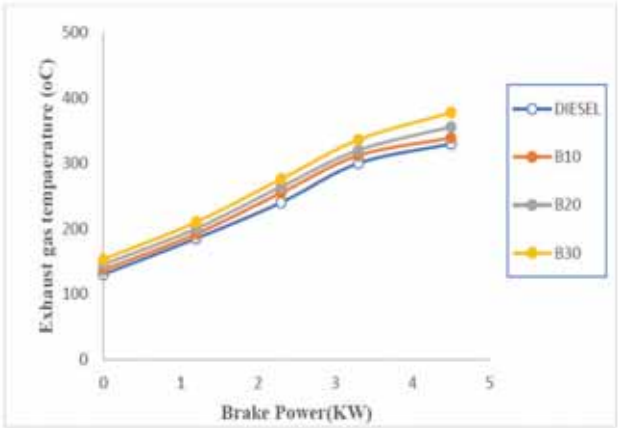

Figure 6. Variation of Exhaust Gas Temperature with BP

D. Carbon Monoxide Emission (CO)

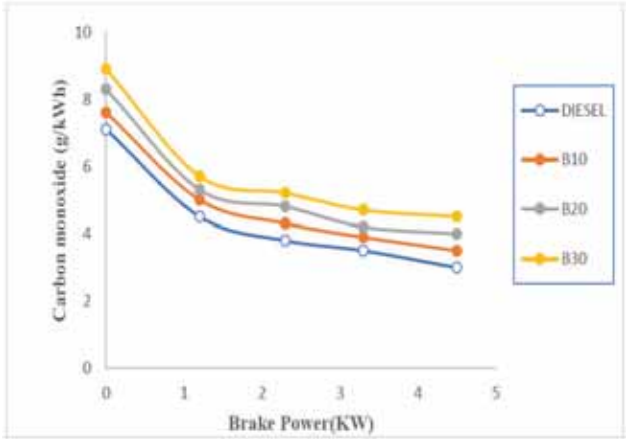

Figure 7. Variation of Carbon monoxide with BP

For all the test fuels, Figure.7 shows the variation in carbon monoxide emissions as a function of brake power. CO emissions at all loads are increased by the proportion of RSO and its diesel blends. With diesel, B10, and B30, CO emissions are 3.5g/kWh and 4.5g/kWh, respectively, while with diesel, they are 3g/kWh at full load. CO may increase due to RSO does not spraying well and is not mixed properly, resulting in poor combustion. As RSO concentration in diesel fuel increases, CO emissions increase. RSO in higher percentages in diesel blends deteriorates engine performance due to poor mixture formation. B10 blend reduces CO emissions by 70%.

E. Hydrocarbon Emission (HC)

As compared to diesel, Figure.8 illustrates how hydrocarbon emissions vary with brake power. HC emissions also increase with increasing loading and RSO percentage in the diesel blend. All RSO-diesel blends produced higher HC

emissions than diesel. At full load, HC emissions for B10 and B30 are 0.61 g/kWh and 0.68 g/kWh, respectively, and for diesel are 0.58 g/kWh. The higher viscosity of RSO causes greater fuel droplets, which result in a non-uniform distribution of fuel with air, resulting in too rich pockets that can emit hydrocarbons. At all loads, HC emissions increase with an increase in RSO blending ratio. As compared to neat RSO, the B10 blend reduces HC emissions by 0.7 g/kWh at full load. As a result, the B10 blend produces a better mixture preparation and combustion.

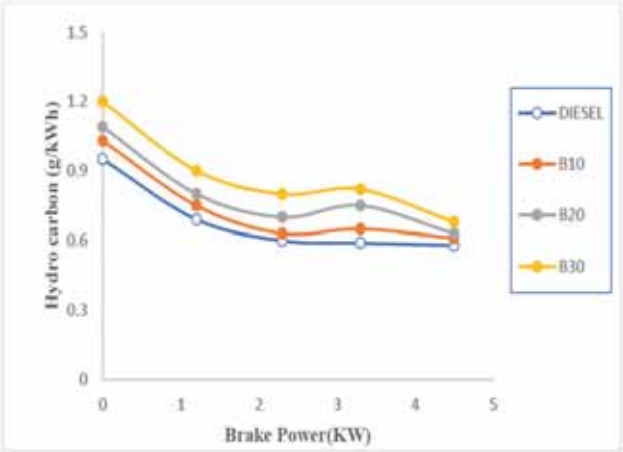

Figure 8. Variation of Hydrocarbon with BP

F. Nitrogen Oxide Emission (NO_X)

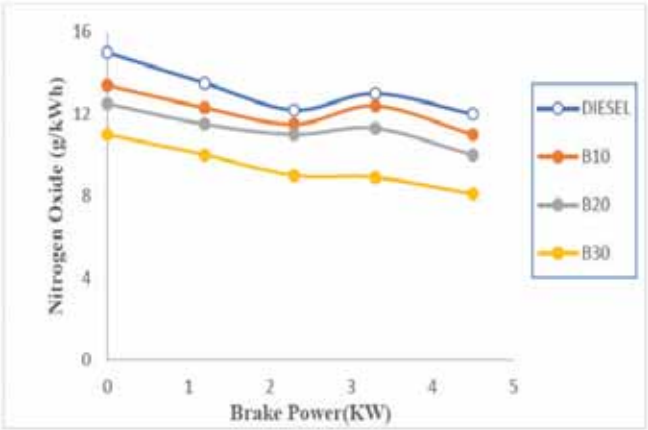

Figure 9. Variation of Nitrogen Oxide with BP

In Figure.9, NO is shown to vary with brake power for all fuels. Increasing engine load increases NO emissions because the average gas temperature in the combustion chamber increases. At full load, B10 and B30 emit 11 and 8.1 grams of NO per kWh, respectively, while diesel emits 12 grams per kWh. When RSO is used, premixed combustion intensity is reduced, which reduces NO levels. A higher RSO content in the diesel blend leads to a decrease in NO emissions. NO emissions from B10 are 3.9% lower than those from diesel fuel.

G. Smoke Opacity

Figure.10 shows the comparison between smoke with brake power for different proportions of RSO and diesel. Due to their high viscosity, vegetable oils emit considerable smoke. The smoke density at maximum power output is 4.1 BSU and 5 BSU with B10 and B30 and 3.3 BSU with diesel. It is possible that smoke density will increase due to the heavier molecular structure of RSO and its higher viscosity, resulting in poor atomization and larger droplet sizes, leading to slower combustion. Diesel fuel with a higher percentage of RSO produces more smoke. At full load, the B10 blend reduces the smoke level from 5 BSU to 4.1 BSU. The blend's viscosity is decreased, which improves combustion.

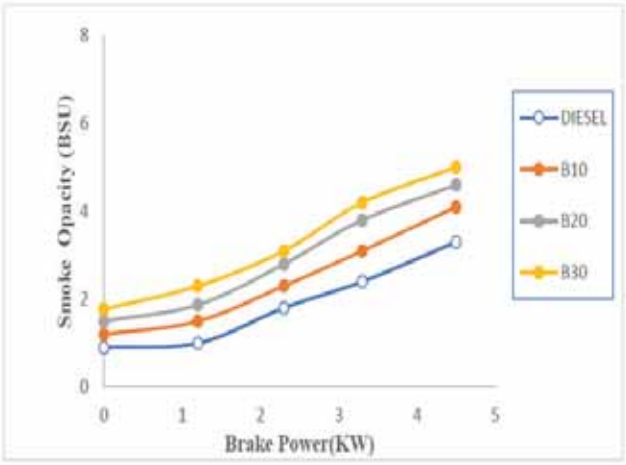

Figure 10. Variation of Smoke capacity with BP

IV. Conclusions

In the present study, rubber seed oil and its diesel blends were tested at different load conditions in a single cylinder at not varying the speed diesel engine. Following are the conclusions drawn from this experiment.

1. Optimal RSO (B10) and diesel blends result in better engine performance.
2. At full load, B10 brake thermal efficiency is 4% higher than 30% RSO.
3. As a result of the slow combustion of vegetable oil, when the diesel engine is fully loaded, exhaust gas temperatures are higher with all blends of RSO.
4. During full load, RSO emits high levels of CO and HC. B10 emits 3.5 grams of carbon dioxide per kWh and 0.61 grams per kWh at the optimum blend.
5. The optimum blend B10 operation produces NO emissions of 11g/kWh diesel at full load, which is 3.9% lower than diesel fuel.

Using Rubber Seed Oil-Diesel blend B10 as fuel without modifying it has been concluded to be the best option for compression ignition engines.

References

[1] Ibrahim, Amr. 2018. "An Experimental Study on Using Diethyl Ether in a Diesel Engine Operated with Diesel-Biodiesel Fuel Blend." *Engineering Science and Technology, an International Journal* 21(5): 1024–33. https://doi.org/10.1016/j.jestch.2018.07.004.

[2] Nikolić, Boban D., Breda Kegl, Saša M. Milanović, Miloš M. Jovanović, and Živan T. Spasić. 2018. "Effect of Biodiesel on

Diesel Engine Emissions." *Thermal Science 22*: S1483–98. https://doi.org/10.2298/TSCI18S5483N.

[3] Roy, Murari Mohon, Wilson Wang, and Majed Alawi. 2014. "Performance and Emissions of a Diesel Engine Fueled by Biodiesel-Diesel, Biodiesel-Diesel-Additive and Kerosene-Biodiesel Blends." *Energy Conversion and Management 84*: 164–73. https://doi.org/10.1016/j.enconman.2014.04.033.

[4] Wang, Zhi, Li Li, Jianxin Wang, and Rolf D. Reitz. 2016. "Effect of Biodiesel Saturation on Soot Formation in Diesel Engines." *Fuel 175* (July): 240–48. https://doi.org/10.1016/j.fuel.2016.02.048.

[5] Yilmaz, Nadir. 2012. "Comparative Analysis of Biodiesel-Ethanol-Diesel and Biodiesel-Methanol-Diesel Blends in a Diesel Engine." *Energy 40 (1):* 210–13. https://doi.org/10.1016/j.energy.2012.01.079.

[6] Zhang, Yanhui, Yunhao Zhong, Jie Wang, Dongli Tan, Zhiqing Zhang, and Dayong Yang. 2021. "Effects of Different Biodiesel-Diesel Blend Fuel on Combustion and Emission Characteristics of a Diesel Engine." *Processes 9 (11).* https://doi.org/10.3390/pr9111984.

E-ISSN 2581 – 7957
P-ISSN 2277 – 3916

CVR Journal of Science and Technology, Volume 27, December 2024
DOI: 10.32377/cvrjst2717

Perceptions of using FASTag at Toll Plazas: A Case Study of Hyderabad City

Praveen Samarthi[1], B.Hari krishna[2], G.C.S.Kalyan Goud[3] and P.Rithwik[4]
[1]Sr.Assistant Professor, CVR College of Engineering/Civil Engg. Department, Hyderabad, India
Email: samarthipraveen@gmail.com
[2,3,4]UG Student, CVR College of Engineering/Civil Engg. Department, Hyderabad, India
Email: harikrishnabanoth35@gmail.com[2], luckylaksman0811@gmail.com[3], gkalyangoud4@gmail.com[4]

Abstract: **FASTag is an electronic toll collection system introduced in India by the National Highways Authority of India (NHAI) to simplify and expedite toll payments on highways. The system operates using Radio Frequency Identification (RFID) technology, enabling toll charges to be deducted directly from linked bank accounts or prepaid wallets without requiring cash transactions. FASTag can be purchased, recharged, or topped up through authorized issuers or participating banks. This initiative was launched to improve efficiency at toll plazas on national highways, ensuring smoother traffic flow and reduced congestion. The FASTag, affixed to a vehicle's windscreen, allows drivers to pass through toll plazas without stopping for manual payment. It has a validity of five years, with users needing only to recharge or top it up as required. Toll plazas, typically located on highways or expressways, often face challenges related to delays and congestion. This study focuses on evaluating the level of service provided at toll plazas by examining drivers' perceptions of delays during their travel. Data was collected using an online questionnaire, with responses from 1,200 drivers, capturing their perceptions, travel behavior, and overall experience. The study provides valuable insights into driver attitudes and vehicle movement patterns, highlighting key areas for improving toll plaza efficiency and service levels.**

Index Terms: **FASTag, Electronic Toll Collection, Driver Perception and Toll Plaza Efficiency.**

I. Introduction

India boasts the second-largest road network in the world, with a vast stretch of 5.4 million kilometers of roadways, including approximately 97,991 kilometers of national highways. The National Highways Authority of India (NHAI), under the Ministry of Road Transport and Highways, is responsible for maintaining and expanding these highways. To sustain this extensive infrastructure, travelers on national and state highways—often referred to as toll roads—are required to pay a toll tax. The revenue generated is used by the government to maintain the roads, ensuring a smoother and more comfortable experience for drivers and riders.

However, conventional toll collection methods pose several challenges, including inefficiencies and negative impacts on the environment and economy. Some of these challenges include:
Limited toll booths, which create bottlenecks and slow down the toll collection process. Increased waiting times, with vehicles spending an average of 10 minutes per toll booth, leading to delays.

Fuel wastage caused by idling vehicles in long queues.

Environmental pollution, as prolonged waiting contributes to higher carbon emissions.

Conflicts and accidents, including verbal disputes and lane-switching collisions due to impatience among travelers.

Economic inefficiencies, as delays at toll plazas disrupt the transport sector and adversely impact overall productivity.

1.1 FASTag

To address these challenges, the National Electronic Toll Collection (NETC) program introduced FASTag, a reloadable tag designed to simplify toll collection through automated systems. FASTag employs Radio Frequency Identification (RFID) technology to enable toll payments without requiring vehicles to stop at toll plazas. This system is a significant step toward improving highway travel efficiency.

The FASTag is affixed to the windscreen of a vehicle and links directly to the user's bank account or prepaid wallet. It allows toll charges to be deducted automatically as the vehicle passes through the toll plaza. Users can procure FASTag from designated Points of Sale (POS) at toll plazas or through issuer agencies, with the account funded via online payment methods such as credit card, debit card, NEFT, RTGS, or net banking. After activation and recharge, vehicles can drive through dedicated FASTag lanes for seamless toll payment.

As of December 1, 2023, FASTag has been mandated for all vehicles by the Ministry of Road Transport and Highways, ensuring nationwide adoption. This initiative promotes faster and more efficient toll collection, reducing congestion and enabling a smoother flow of traffic at toll plazas.

FASTag is particularly beneficial on national highways, offering a hassle-free and fuel-efficient travel experience for commuters.

Key Advantages of FASTag

Reduced waiting time at toll booths, enabling faster vehicle clearance.

Lower fuel consumption due to minimized idling in long queues. Reduced traffic congestion, improving the overall driving experience.

Environmental benefits, as fewer emissions are generated from stationary vehicles.

1.2 Working of FASTag

The FASTag system functions through the following steps:

Tag Scanning:

Received on 13-09-2024, Revised on 13-10-2024, Accepted on 12-11-2024.

CVR Journal of Science and Technology, Volume 27, December 2024
DOI: 10.32377/cvrjst2717

As a vehicle enters the Electronic Toll Collection (ETC) lane at a toll plaza, the system reads the FASTag details, including the Tag ID, Vehicle Class, and TID, and forwards this information to the acquiring bank for processing. The FASTag lane for different categories of vehicles is given in Figure1.

Figure 1. FASTag Lane for vehicles

Tag Validation

The acquiring bank requests validation of the tag details from the National Electronic Toll Collection (NETC) Mapper, which verifies the tag's authenticity and status.

Verification Response

If the tag is valid, the NETC Mapper provides details such as the Tag Status, Vehicle Class, and Vehicle Registration Number (VRN). If the tag is invalid or unregistered, the mapper sends a rejection response.

Toll Fare Deduction

Upon successful validation, the acquiring system calculates the applicable toll fee and debits the amount from the user's FASTag account. This process is seamless, ensuring the vehicle can pass through without stopping.

The comparison of various systems with FASTag are given in Table I

1.3. Mechanism of Fastag

Step 1: Whenever a vehicle will pass through the Electronic Toll Collection (ETC) lane of the Toll Plaza, the Toll Plaza system will capture the FASTag details like (Tag ID Vehicle class, TID, etc.) and send it for processing to the acquiring bank.

Step 2: The acquiring bank will send a request to the National Electronic Toll Collection (NETC) Mapper to validate the tag details.

Step 3: Once the Tag ID will get validated, NETC Mapper will respond with details like Tag Status, Vehicle class, VRN etc. If the Tag ID is not present in NETC Mapper, it will respond as the Tag ID is not registered.

Step 4: The acquirer host will calculate the appropriate toll fare and initiate a debit request to the NETC system after successful validation of Tag ID from NETC Mapper.

II. Literature Review

S. Amrin (2019) [2] studied FASTag perceptions in India, highlighting the challenges associated with conventional toll collection systems. The study emphasizes the need for an automated toll collection system like FASTag, a program launched by the National Highways Authority of India (NHAI) for electronic toll collection on national highways.

Pontarelli et al. (2014) [7] studied numerous socio-economic and environmental benefits of FASTag to both users and toll operators. Despite its advantages, the study underscores the importance of addressing the challenges faced by FASTag to enhance its technological capabilities. With appropriate solutions, FASTag can become a superior toll collection system and a game-changer in the years to come.

M. Likhitha et al. (2017) [3] focused on the role of FASTag in reducing manual workloads through RFID technology. This electronic toll collection system not only decreases waiting times at toll plazas but also minimizes environmental pollution caused by fuel combustion.

Suvarna et al. (2015) [8] studied that users can perform toll transactions online, eliminating the need to carry cash, thereby reducing human errors at toll booths. The cashless transaction system also increases transparency. The inclusion of an IoT module enables sending confirmation messages to vehicle owners regarding toll deductions.

Joshi,B (2017) [9] studied image processing technology, wherein the vehicle's number plate is scanned and processed for toll collection. However, the study notes that currently, only one FASTag-enabled lane is operational at most toll plazas, while the others still rely on traditional methods.

Dr. S. Sukumar (2020) [1] examined FASTag as an electronic toll collection system operated by NHAI. Using Radio Frequency Identification (RFID) technology, toll payments are directly deducted from linked bank accounts. The tag can be purchased, recharged, or topped up through official issuers or participating banks, with a validity of five years.

TABLE-I.
COMPARISON OF VARIOUS SYTEMS

Parameter	AVI	RFID	Fastag	Book my toll
Time Consumption	Average	Average	Average	Average
Fuel wastage	High	Low	Low	Low
Traffic Congestion	High	Average	Average	Average
Processing Speed	High	Average	Average	Average

CVR Journal of Science and Technology, Volume 27, December 2024
DOI: 10.32377/cvrjst2717

Singh (2020) [10] studied the expanded usage of FASTag, including payments at fuel stations after agreements with Indian Oil Corporation (IOC), Bharat Petroleum (BPCL), and Hindustan Petroleum (HPCL) in January 2019. By September 2019, FASTag lanes were available on over 500 highways, with more than 54.6 lakh vehicles enabled with FASTag.

Hinge (2021) [11] employed tools such as percentage analysis, ranking, descriptive statistics, Likert scaling, and factor analysis to analyze user satisfaction. Results show the potential of FASTag to streamline toll collection and reduce inefficiencies.

N. Akshaya (2021) [6] explored FASTag role as a technological advancement in toll collection systems. Using RFID technology, the system detects tags affixed to vehicle windshields and deducts toll charges from linked accounts. Users receive SMS notifications for transactions or insufficient balance.

Abhishek Sontakke et al. (2019) [5] examined the implementation of FASTag as a step toward cashless toll transactions. Developed by the Indian government and NHAI, FASTag eliminates the need for vehicles to stop at toll plazas for cash payments.

B. Gayathri (2020) [4] researched the impact of digitization on toll collection in Tamil Nadu, particularly focusing on the transition from manual to electronic toll collection. While FASTag has been widely accepted in urban areas, the study notes its limited awareness and usage in rural regions.

Dalip Kaur (2022) explored the broader context of digitalization in India and its impact on the economy. The government's push for a cashless economy has introduced technologies like RFID-based FASTag, which allows toll payments without cash transactions.

Mehul B (2024) explored FASTag as a (the) new technological solution for the great contribution of Indian toll tax collection. It is user friendly and economically viable for every user of motor vehicles in the Indian part. Fastag (It) is a() simple to use, reloadable tag in which is automatic deduction of toll charges and passes through the toll plaza without stopping for the cash transaction.

The study highlights benefits such as reduced fuel consumption, minimized traffic congestion, lower paperwork, and decreased air pollution. Focused on Coimbatore city, the research investigates user satisfaction, identifying benefits and challenges faced by FASTag users, and offers suggestions for improvement. By installing FASTag on vehicle windshields, toll charges are automatically deducted from linked accounts, making toll collection seamless. This technology can also be applied for generating challans and automating penalty deductions. The study emphasizes FASTag ability to reduce delays caused by traffic congestion and highlights its convenience for users.

The research stresses the importance of educating people about FASTag benefits and suggests that distributors should actively promote its merits and address user concerns. The study concludes that increased awareness and adoption of FASTag will lead to more frequent usage and a better understanding of toll taxation. FASTag simplifies toll collection by using radio frequency waves to automatically deduct toll charges from linked accounts. The study gathers public feedback on the convenience and usability of these RFID tags, finding that most users appreciate the system's ease of use and transparency.

III. Methodology

The present study has been basically designed as a 'Descriptive Study' with 'survey' as the Technique of research. A questionnaire was constructed and validated by the researcher. Data collected through online and offline questionnaires. The flow chart of methodology is given in figure 2.

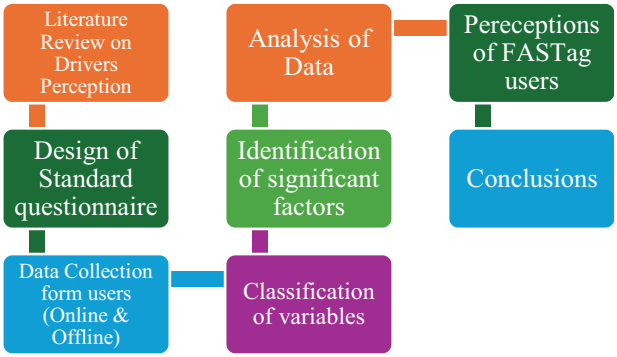

Figure 2. Flow Chart of the Methodology adopted

3.1. Data Collection:

The data required for this study were collected from toll users using a structured questionnaire. The questionnaire was meticulously designed by referencing various academic literature and case studies to ensure its relevance and validity. This study primarily focuses on toll users, aiming to understand their demographic profile, travel behavior, and perception of FASTag technology.

The researcher adopted the convenience sampling method to select the sample respondents, considering factors such as accessibility and willingness of participants to provide information. A total of 114 respondents were chosen as the sample size for the study.

The questionnaire was designed to capture three main categories of information:

1. Personal and Socio-Economic Information: This section included questions about respondents' age, gender, income level, education, and other demographic details.
2. Trip-Related Information: This part gathered data about the respondents' travel frequency, purpose of travel, route preferences, and mode of payment at toll plazas.
3. Perception of FASTag: This section assessed respondents' awareness, adoption, and satisfaction with FASTag, along with their views on its efficiency, convenience, and potential challenges.

CVR Journal of Science and Technology, Volume 27, December 2024
DOI: 10.32377/cvrjst2717

To ensure data accuracy and reliability, the researcher personally administered the questionnaire to each respondent, enabling clarification of any queries and improving response quality. The information collected through this process served as the foundation for analyzing user behavior and preferences

IV. Perceptions of FASTAG Users

4.1 Analysis of FASTag Users in Hyderabad City

A questionnaire survey was conducted online to gather data from FASTag users in Hyderabad city. The responses to the survey have been summarized and presented below using pictorial representations to provide a clear and concise visualization of the findings. These visuals help to analyze the trends, preferences, and experiences of FASTag users in the region effectively.

Driver's personal information and socio economic information:

Socio Economic factors are deciding the services utilized by the customers in the market. The factors chosen for this study such as age, gender, occupation and income. NHAI is offering FASTag facility to Cross the toll plaza in a quick manner and easy payment. But it depends on the lifestyle of the People, the needs of the services, availability, utility and vehicle which are used.

4.1.1. Analysis of age :

It is observed that the age group between 18-30 (77.19%) which is majorly responded among other 3 age groups.

4.1.2. Analysis of Gender :

The gender in the sample results indicate that male participants are more than female participants.

4.1.3. Analysis of study status: Most of the responses were collected from the UG students (79%) and responses from the Ph.D. students are just 3%.The education level of FASTag users who participated in the survey given in figure 3.

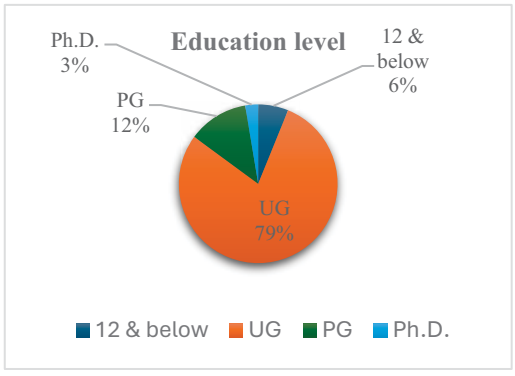

Figure 3. Education level of FASTag Users in survey

4.1.4 Analysis of vehicle type :

Approximately 46% of respondents are having 2 wheeler and 4 wheeler type vehicles. Heavy commercial vehicles & 4 wheeler vehicles have 0% .

4.1.5. Analysis of driving experience (in years) :

The respondents who are having greater than 3 years of experience in driving are 40.35% and who are between 2-3 years of experience in driving is less (14.04%) as given in figure 4.

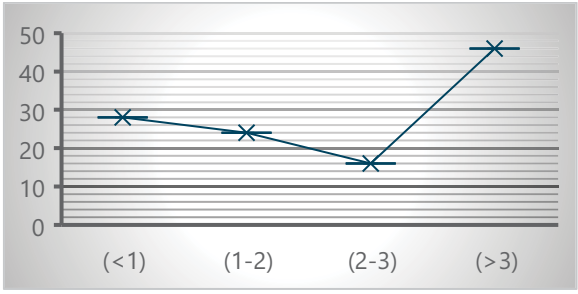

Figure 4. Analysis of Driving experience of users in years

4.1.6. Analysis of employment status :

It is observed that students are responded more than the employees with 72.81% and 17.54%

4.1.7. Analysis of reasons for not using FASTag

It is observed that the reason for not using FASTag — most of the people don't like to pay the FASTag in advance (25%) and the service centers are not near (23%) to recharge the FASTag which is given in figure 5.

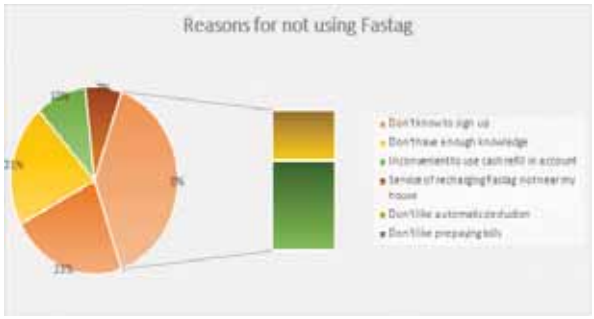

Figure 5. Reasons for not using FASTag of Users

4.1.8 Analysis of Travel purposes

It is observed that the purpose of travelling through toll roads are work (29%) and education (23%) and commercial purpose was less (8.78%) which is given in figure 6.

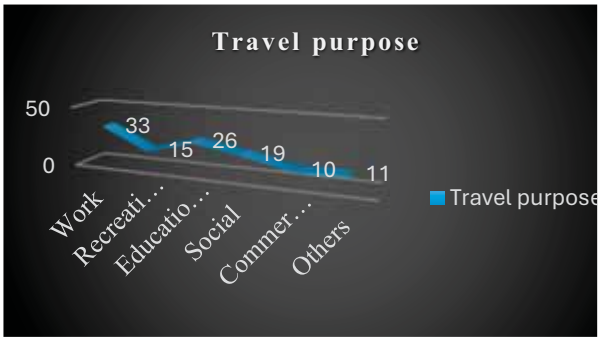

Figure 6. Analysis of Travel purpose in percentage

4.1.9 Analysis of FASTag period usage:

It is observed from figure 10, 32.46% of people started using Fastag and 17.54% of people not using Fastag given in figure 7.

CVR Journal of Science and Technology, Volume 27, December 2024
DOI: 10.32377/cvrjst2717

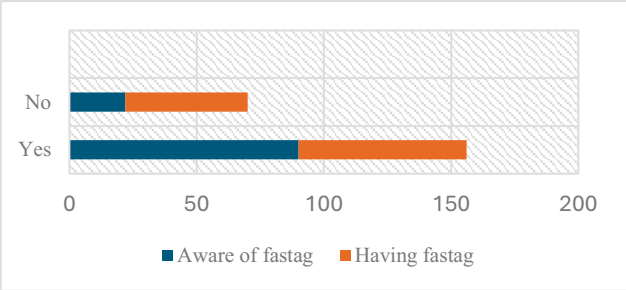

Figure 7. Analysis of FASTag Period usage in percentage

4.1.10 Analysis of toll roads :

In the below graph, Blue colour indicates the awareness of toll roads and 83.33% of the people are aware of toll roads. Orange colour indicates the usage other roads to reach their destination.(revise the sentence put in yellow) Most of the people use toll roads to reach their destinations which is 58.77% . Grey colour indicates the statement ' toll roads help to reach faster and only 29% of people agreed with that statement.

V. Conclusions

- This study deals with the application of the latest technology of the FASTag which is beneficial in avoiding the traffic hassle at the National toll plazas.
- With the use of FASTag installed on the front windshield of vehicles, Toll generation is made a fun job. Automatically, the Toll charges are deducted from the FASTag account. This technology can also be used for the generation of challan and automatic deduction through the FASTag linked to the vehicle.
- This can be the solution for many people who are suffering from being late by 1–2 min due to the long queue at the toll plaza and paying the toll again.
- RFID based FASTag is seen as an advantageous mode of toll collection system in India offering numerous. Socio-economic and environmental benefits to both – the user and the collector.
- The present study has brought out the satisfaction level of passengers and the benefits they enjoy using FASTag and the problems faced by them and suggestions to be improved in FASTag for its betterment.
- It is observed that 78.95% of respondents are aware of FASTag. In that only 57.89% are using/having FASTag.
- Awareness of FASTag was spreading by the internet and friends (39.47% and 31.58% respectively) majorly and From last one year, 32.46% of people started using FASTag.
- From the collected samples, the reason for not using FASTag — most of the people don't like to pay the FASTag in advance (25%) and the service centers are not near (23%) to recharge the FASTag.
- The payment through paytm/Google pay/Amazon pay/phone pay (43%) is more than the offline payment (6.14%) for the recharge of FASTag.
- Most of the respondents are interested in the decreasing waiting time at toll plazas (51%) than the rewards (23.68%).

References

[1]. Sukumar, S. (2020). "A Study on Consumer's Attitude Towards FASTag in Dindigul City." CASIRJ, 11(4), 36-36.

[2]. Amrin, S. (2019). "An Introduction to FASTag: A Game Changer in Automatic Toll Collection Systems in India." *IJRAR*, 6(2), 1-6.

[3]. Likhita, Y., Yalini Devi, H., & Chidambara Thanu. (2017). "TOLLZ-E (Online Toll System)." *International Research Journal of Engineering and Technology (IRJET)*, 6(4), 755-760.

[4]. Gayathiri, B. (2020). "A Study on Customer Discernment Towards FASTag Implementation in Madurai District." *Volume XII, Issue VIII*, 547-550.

[5]. Sontakke, A., Diwakar, A., & Kaur, G. (2019). "Intelligent Automatic Traffic Challan on Highways and Payment Through FASTag Card." *Indian Journal of Science and Technology*, 12(44), 1-6. https://doi.org/10.17485/ijst/2019/v12i44/146468.

[6]. Akshaya, N. (2021). "A Study on Passenger's Satisfaction Using FASTag with Special Reference to Coimbatore City." *EPRA International Journal of Research and Development (IJRD),* 6(4), 215-219.

[7]. Pontareli, S., et al. (2014). "A Technique to Protect Cache Tags Against Soft Errors." *IEEE Transactions on Device and Materials Reliability*, 14(3), 935-937.

[8]. Suvarna, V., et al. (2015). "A Review on Various RFID-Based Automated Highway Toll Collection Systems." *International Journal of Computer Science and Information Technologies (IJCSIT),* 6(3), 2130-2133.

[9]. Joshi, B. (2017). "A Comparative Study of Toll Collection Systems in India." *International Journal of Engineering Research and Development,* 13(11), 68-71.

[10]. Singh, S., & Yadav, R. (2020). "A Comparative Study of Toll Collection Systems at Kherki Daula Toll Plaza, Gurugram (Haryana)." *UGC Approved Journal No*. 48514, 8(1).

[11]. Hinge, A., & Chatarvedi, T. (2021). "Study on Toll Plazas for Impact Assessment and Remedy Measures on Existing ETC Systems." *Journal of Emerging Technologies and Innovative Research,* 7(10), 2463-2466.

E-ISSN 2581 – 7957
P-ISSN 2277 – 3916
CVR Journal of Science and Technology, Volume 27, December 2024
DOI: 10.32377/cvrjst2718

Capital Structure and Profitability of Foreign Direct Investment Companies in the Indian Pharmaceutical Industry

Dr. Lalitha Suddapally[1] and Dr. Sudha Vepa[2]
[1]Sr. Asst. Professor, CVR College of Engineering/H&S Department, Hyderabad, India
Email: lalitha.suddapally@gmail.com
[2] Professor, Osmania University/Department of Business Management, Hyderabad, India
Email: sudhavepa1@gmail.com

Abstract: **The financial performance of a company is also influenced by a good amalgamate of debt and equity portions in the financing patterns of that particular company. Using firm-level data, the current study has examined the relationship between capital structure and profitability of FDI (foreign direct investment)-based enterprises in the Indian pharmaceutical industry. 25 FDI-accepted companies in the Indian pharmaceutical sector were selected as a sample for an 11-yearlong study; from 2010–2011 to 2020–2021. To investigate the impact of capital structure on the profitability of FDI-based companies, multiple regression analysis has been utilised. The profitability was assessed using the following metrics: Return on Net Worth (RONW), Return on Total Assets (ROTA), and Return on Total Income (ROTI). In order to investigate how capital structure affects profitability of FDI firms, two debt indicators are used. These are Debt/Equity (D/E), Short Term Debt/Total Net Assets (STD/TNA), and Total Outside Liabilities/Total Net Assets (TOL/TNA). The findings show that the Debt/Equity ratio significantly effects negatively the profitability of FDI companies, but the Total Outside Liabilities/Total Net Assets (TOL/TNA) and Short-Term Debt/Total Net Assets (STD/TNA) have no discernible effect on profitability. The findings show that capital structure has a substantial effect on profitability and the success of the FDI firms in the Indian pharmaceutical sector may be dependent on the financing patterns they choose.**

Index Terms: **Capital Structure, Profitability, Foreign Direct Investment, Debt/ Equity Ratio, and Indian Pharmaceutical Industry.**

I. Introduction

Foreign Direct Investment (FDI)

Foreign Direct Investments (FDI) is a prime driver for economic growth and non-debt financial source for the economic development of India. Foreign direct investment is not only transfers money from one country to another. Besides being a significant driver of economic growth, FDI also brings in increased employment opportunities, managerial expertise, technology, and infrastructure (Vidyasagar Mani Thota and B. Sai Griridhar, 2016[1].

In the pharmaceutical industry 100% of FDI's are allowed (RBI, Press Note N0. 4 (2001 Series) automatically in greenfield pharmaceuticals and 74% through automatic route & 100% under government route in brownfield pharmaceuticals. India is the world's largest supplier of generic medications. Over 50% of the global demand for various vaccines, 40% of the US market for generic drugs, and 25% of the UK market for all medications are supplied by the Indian pharmaceutical industry. In the world, India is ranked 14th by value and third by volume in terms of pharmaceutical output. Approximately 10,500 manufacturing facilities and 3,000 pharmaceutical businesses make up the domestic pharmaceutical industry. According to the FDI India Report, India holds a prominent place in the global pharmaceutical business. Additionally, the nation boasts of an excellent pool of scientists and engineers who can propel business to new heights. Currently, Indian pharmaceutical companies supply more than 80% of the antiretroviral medications used worldwide to combat AIDS (Acquired Immunodeficiency Syndrome).

The pharmaceutical industry in India is one of the country's most promising science-based businesses, with enormous potential for both drug production and technological advancement. In terms of the quality of medicine produced in India, the pharmaceutical industry here ranks third in the world. In India, the pharmaceutical industry has over 20,000 registered companies and is severely fragmented. It has expanded exceptionally in the last two decades (Priyadharshini.R and Sunil Vakayil, 2018) [2]

According to an Economic Survey, in the year 2020-21, Foreign direct Investment in India's pharmaceutical industry witnessed a rapid growth, particularly on account of investments to meet COVID-19 related demands for treatments and vaccines. FDI inflows play a vital role in compounding domestic capital and help to boost industrial growth and employment generation across various sectors and industries. India has received total foreign direct investment of USD 54.1 billion during April-November 2021-22 (Business Standard Report).

II. Literature Review

Vidyasagar Mani Thota, B. Sai Griridhar, (2016),[1] studied the relationship between foreign investment and capital structure by using secondary data. The study analysed whether there is any influence of foreign presence on the leverage of domestic companies. It is revealed from the study that leverage of automobile industry of India has been negatively influenced by foreign presence. **Atif Ghayas, Javaid Akhter, (2018),[3]** explain the impact of

Received on 03-05-2024, Revised on 02-06-2024, Accepted on 02-07-2024.

CVR Journal of Science and Technology, Volume 27, December 2024
DOI: 10.32377/cvrjst2718

capital structure decisions on company's profitability by taking the sample of 35 pharmaceutical firms listed in the Bombay Stock Exchange (BSE) for a period of 5 years from 2012 to 2016. Regression analysis was applied to analyse the relationship between capital structure and profitability, and it was concluded that Profitability and short-term debt are significantly correlated, whereas long-term debt and return on equity are not significantly correlated. **Anshu Handoo A, Kapil Sharma, (2014),[4]** analysed about the determinants of capital structure of 870 companies both in the private sector and government sector from 2001 to 2010. It was understood that the company's capital structure is dependent on various determinants. **Narinder Pal Singh, Mahima Bagga, (2019),[5]** focus on the effect of capital structure on profitability of NIFTY 50 companies from 2008-2017. They concentrated on the unique impact of the ratios of total debt to total equity on return on equity and return on assets. As a result, an increase in equity indicates an increase in return on total assets, whereas an increase in debt indicates a loss in return on total assets. **Chandrika Prasad Das, Rabindra Kumar Swain, (2018),[6]** basically talk about the determinants of capital structure and its impact on the financial performance. 50 manufacturing companies are covered for this study, and it is revealed from the findings that capital structure has considerable impact on financial performance. A study was carried out by **Rupali S. Ambadkar, (2019),** on the impact of capital structure on profitability of foreign direct investment companies in the Indian manufacturing industry. This study was conducted by taking into account "54 foreign direct investment firms from the S&P BSE 500 Index" as a sample. The findings showed that capital structure ratios significantly reduce profitability and support the Pecking-Order Theory's prediction. **Nagendra Marisetty (2017), [8]** studied the relevance of capital structure on profitability of 10 BSE SENSEX companies from different industries and concluded that the financing patterns do not have an impact on the profitability. The capital structure is a mixture of equity and debt, and every company profitability is not dependent on source of finance.

III. Study Objectives

- To Study the correlation between capital structure and profitability of FDI-based companies in the Indian pharmaceutical industry.
- To determine the impact of capital structure on the FDI based firm's profitability in the Indian pharmaceutical industry.

A. Study Hypothesis

Following are the hypothesis framed in this study

H01: "There is no significant impact of total outside liabilities/ total net assets ratio of a selected FDI based company on its Profitability".

H02: "There is no significant impact of debt/ equity ratio of a selected FDI based companies on its Profitability".

H03: "There is no significant impact of short-term debt / total net assets ratio of a selected FDI based companies on its Profitability".

B. Research Gap

According to the literature review, majority of the research is about the manufacturing sector as a whole, which is used to analyse the association between profitability and capital structure. The primary objective of this study is to determine how capital structure and profitability are related to the pharmaceutical business in India.

IV. Data Research Methodology

A. Sample and Data Collection

This study is based on secondary data and the data is obtained from PROWESS Database (Prowess IQ, 1.96) maintained by "Center for Monitoring Indian Economy (CMIE)". Based on the presence of foreign investment, 25 FDI based firms in Indian Pharmaceutical industry were selected for the study. The study was conducted from the period 2010-2011 to 2020-2021 (11 years). Regression analysis is used to examine how capital structure affects FDI firms' profitability in the Indian pharmaceutical sector. A Multiple Regression model was used to assess the effect of "capital structure on the profitability of foreign direct investment (FDI) firms in the Indian pharmaceutical sector".

B. Profitability Measures

Three profitability measures (dependent variables) were used in this study. They are as follows:

i. Return on Net worth (RONW)
ii. Return on Total Assets (ROTA)
iii. Return on Total Income (ROTI)

C. Measures of Capital Structure

Two measures of Capital Structure (Independent Variables) were employed based on the previous studies:

i. Total Outside Liabilities /Total Net Assets (TOL/TNA)
ii. Debt /Equity (D/E)
iii. Short Term Debt /Total Net Assets (STD/TNA)

CVR Journal of Science and Technology, Volume 27, December 2024
DOI: 10.32377/cvrjst2718

V. Analysis and Results

TABLE-I.

Descriptive Statistics

	TOL/T (%)		Debt/ Equity Ratio (times)	STD/TNA (%)	(ROE) Return on net worth	(ROTA) Return on total assets	ROTI Return on total income
N	Valid	263	247	263	246	263	262
	Missing	12	28	12	29	12	13
Mean	7638.415653		0.7	2171.334166	12.63	5.79	-5.21
Std. Error of Mean	5151.867813		0.109	1354.3390727	1.746	0.726	5.919
Median	42.745178		0	119.114719	14	7	11
Mode	.4153[a]		0	124.0000	14	8	15
Std. Deviation	83549.25574		1.711	21963.6888335	27.389	11.781	95.804
Range	1226499.585		16	329284.1221	476	118	836
Minimum	0.4153		0	15.8779	-172	-70	-793
Maximum	1226500		16	329300.0000	304	48	43

A. Correlation

TABLE-II.

Independente Variables

		TOL/T(%)	Debt/ Equity ratio(times)	STD/TNA (%)
TOL/TNA(%)	Pearson Correlation	1	-0.038	-.043
	Sig. (2-tailed)		0.551	.489
	N	263	246	263
	Sig. (2-tailed)	0.505	0	
Debt/ Equity ratio(times)	Pearson Correlation	-0.038	1	-.042
	Sig. (2-tailed)	0.551		.511
	N	246	247	246
STD/TNA (%)	Pearson Correlation	-.043	-.042	1
	Sig. (2-tailed)	.489	.511	
	N	263	246	263

It is observed from the Table II, correlation coefficient between two independent variables TOL/ TNA (%) and Debt/ Equity ratio(times) is -0.038 which indicates that there is no association between these two independent variables.

B. Results of Regression Analysis

1. Multiple Regressions Results (Return on Net worth: Dependent Variable):

TABLE-III.

MODEL SUMMARY

Model	R	R Square	Adjusted R Square	Std. Error of the Estimate
1	.480[a]	.231	.209	30.2835

Predictors: (Constant), Debt/ Equity ratio(times), TOL/TNA (%), STD/TA

TABLE-IV.

COEFFICENTS

Model	Unstandardized Coefficients		Standardized Coefficients	T	Sig.
	B	Std. Error	Beta		
(Constant)	17.044	1.730		9.850	.000
TOL/TNA (%)	.000	.000	.374	.337	.736
Debt/ Equity ratio(times)	-10.631	1.312	-.665	-8.103	.000
STD/TNA (%)	.000	.001	-.389	-.351	.726

Dependent Variable: (ROE) Return on Net worth

Table-III, the value of R^2 is 0.231 which specify that 23.1 % variations in Return on Net worth are explained by independent variables. The results in Table-IV indicates that TOL/TNA and STD/TNA do not consist of any significant impact on Return on Net worth which is a dependent variable. The regression calculations in Table-IV depict that Return on Net Worth is significantly impacted negatively by the debt-to-equity ratio.

2. Multiple Regressions Results (Return on Total Assets: Dependent Variable)

TABLE-V.

MODEL SUMMERY

Model	R	R Square	Adjusted R Square	Std. Error of the Estimate
1	.444[a]	.197	.175	9.0910

Predictors: (Constant), Debt/ Equity ratio(times), TOL/TNA (%), STD/TA

TABLE-VI.

COEFFICIENTS

Model		Unstandardized Coefficients		Standardized Coefficients	T	Sig.
		B	Std. Error	Beta		
1	(Constant)	8.547	0.598		14.301	0
	TOL/TNA (%)	7.65E-05	0	0.714	0.631	0.528
	Debt/ Equity ratio(times)	-3.069	0.455	-0.565	-6.739	0
	STD/TNA (%)	.000	.000	-.731	-.646	.519

Dependent Variable: (ROTA)Return on total assets

CVR Journal of Science and Technology, Volume 27, December 2024
DOI: 10.32377/cvrjst2718

Table-V, R2 is 0.197, meaning that independent variables account for 19.7% of the variability in Return on Total Assets. Return on Total Asset, the dependent variable, is not significantly impacted by TOL/TNA or STD/TNA, according to Table VI data. The only ratio shows negative influence on return on total assets is the debt-to-equity ratio.

3. *Multiple Regressions Results (Return on Total Income: Dependent Variable:)*

TABLE-VII.

MODEL SUMMARY

Model	R	R Square	Adjusted R Square	Std. Error of the Estimate
1	.353[a]	.125	.101	84.56086738

Predictors: (Constant), Debt/ Equity ratio(times), TOL/TNA (%), STD/TNA (%)

TABLE-VIII.

COEFFICIENTS

Model	Unstandardized Coefficients		Standardized Coefficients	T	Sig.
	B	Std. Error	Beta		
(Constant)	6.118	4.771		1.282	.201
TOL/TNA (%)	4.680E-05	.001	.057	.048	.961
Debt/ Equity ratio(times)	-20.989	3.628	-.507	-5.786	.000
STD/TNA (%)	.000	.004	-.034	-.029	.977

Dependent Variable: (ROTI)Return on total income

Table-VII, With an R2 value of 0.125, it is inferred that independent variables account for 12.5% of the variances in Return on Total Income. Return on Total Income, the dependent variable, is not significantly impacted by TOL/TNA or STD/TNA, according to Table-VIII results. Table-VIII regression results show that the debt-to-equity ratio negatively impacts the return on total income.

VI. FINDINGS

- Study results indicate that the capital structure indicator TOL/TNA do not have substantial effect on profitability indicators.
- Study results indicates that the capital structure indicator STD /TNA do not have significant impact on profitability indicators.
- Debt to Equity ratio has substantially negative impact on profitability indicators, which indicates that when the amount of Debt/ Equity increases, Profitability decreases.

As per the results it can be stated that

- The study adopts the null hypothesis H01, which states that a selected FDI-based company's profitability is not significantly impacted by its total outside liabilities/total net assets ratio.
- The examination supports the alternative hypothesis H02 that Debt/Equity Ratio has a considerable negative impact on the profitability of selected FDI-based companies.
- The analysis supports the alternative hypothesis H03, which states that the Short-Term Debt / Total Net Assets Ratio of selected FDI-based companies have no significant impact on profitability.

VII. CONCLUSIONS

A suitable capital structure is an important decision for every company because it affects the firm's value and financial success. This research study attempts to evaluate 'the relationship between capital structure and profitability' of 25 Foreign Direct Investment firms of Indian Pharmaceutical Industry. It may be concluded that capital structure has a big influence on profitability and that choosing the right financing mix increases earnings. Businesses that rely on foreign direct investment favour insider capital over outside capital when determining their capital structure. From Debt- Equity ratio, it is concluded that with the increase in the quantity of debt, level of profitability decreased as the capital structure indicator showed negative significant impact on profitability indicator's return on net worth, return on total assets and return on total income. FDI based firms in Indian Pharmaceutical Industry prefer inside funds for investments. Since just 25 FDI-based companies were examined in this study, it is advised that future research projects include more pharmaceutical companies and expand to other industries.

REFERENCES

[1]. Vidyasagar Mani Thota and Sai Griridhar, B. (2016) 'Impact of Foreign Presence on the Capital Structure of Four-Wheeler Companies in India' *International Journal of Business Management and Economic Research (IJBMER)*, Vol. 7 No. 2, pp. 579-587.

[2]. Priyadharshini and Sunil Vakala (2018) 'Capital Structure and Its Impact on Profitability & Liquidity: A Study of Listed Pharmaceutical Industry in India' International *Journal of Scientific Development and Research (IJSDR),* Vol. 3, No. 12, pp. 279-284.

[3]. Atif Ghayas and Javaid Akhter (2018), 'Impact of Capital Structure on Profitability: An empirical analysis of listed firms in India' *Asian Journal of Managerial Science*, Vol. 7, No. 2, pp. 1-6.

[4]. Anshu Abhishek and Ahamad Hussain, (2017) 'Empirical Study of Association ship Between Capital Structure and Profitability: A Study on Listed Health Care Setup in India', *Inspira-Journal of Commerce, Economics & Computer Science (JCECS),* Vol. 3, No. 4, pp. 330- 338.

[5]. Narinder Pal Singh and Mahima Bagga (2019) 'The Effect of Capital Structure on Profitability: An Empirical Panel Data Study' *Jindal Journal of Business Research,* 8(1), pp. 65–77.
[6]. Chandrika Prasad Das and Rabindra Kumar Swain (2018) **'**Influence of Capital Structure on Financial Performance', *Parikalpana - KIIT Journal of Management,* Vol. 14, No.1, pp. 161-170.
[7]. Rupali Ambadkar, S. (2019) 'Capital Structure and Profitability of Foreign Direct Investment Companies in The Indian Manufacturing Sector' *International Journal of Scientific & Technology Research,* Vol. 8, No.7, pp. 844-856.
[8]. Nagendra Marisetty (2017) 'Correlation between Capital Structure and Profitability: A Case Study on Indian Companies' *Indian Journal of Commerce and Management Studies (IJCMS),* Vol. 8, No.1, pp. 1-6.
[9]. Modigliani, F. and Miller, M. H. (1963) 'Corporate Income taxes and Cost of Capital: A Correction' *American Economic Review,* vol.53*,* No.3, pp. 433-443.

In the next issue (Vol. 28, June 2025)

1.	*FPGA Based Implementation of a Multi-Channel ECG Lossless Compression System*	*Dr. G.Ramesh*
2.	*Innovative GSM-Based Smoke Alarm System for Real-Time Hazard Monitoring*	*N Swapna* *V. Sreelatha Reddy*
3.	*Innovative Solutions: IoT Automation for Hybrid Energy System Design and Development*	*Marikal Ram Vikas* *Varikuppala Manohar*

E-ISSN 2581 – 7957
P-ISSN 2277 – 3916

CVR Journal of Science and Technology, Volume 28, June 2025
DOI: 10.32377/cvrjstxxxx

Template for the Preparation of Papers for Publication in CVR Journal of Science and Technology

First A. Author[1] and Second B. Author[2]
[1]Designation, Name of Institution/Department, City, Country
Email: first.author@hostname1.org
[2]Designation, Name of Institution/Department, City, Country
Email: second.author@hostname2.org

Abstract: **These instructions give you basic guidelines for preparing camera-ready papers for CVR College journal Publications. Your cooperation in this matter will help in producing a high-quality journal.**

Index Terms: **first term, second term, third term, fourth term, fifth term, sixth term**

I. Introduction

Your goal is to simulate the usual appearance of papers in a Journal Publication of the CVR College. We are requesting that you follow these guidelines as closely as possible. It should be original work. Format must be done as per the template specified. Diagrams with good clarity with relevant reference within the text are to be given. References are to be cited within the body of the paper. Number of pages must not be less than five with minimum number of 4000 words and not exceeding eight pages. The journal is published in colour. Colours used for headings, subheadings and other captions must be strictly as per the template given in colour.

A. Full-Sized Camera-Ready (CR) Copy

Prepare your CR paper in full-size format, on A4 paper (210 x 297 mm or 8.27 x 11.69 in). No header or footer, no page number.

Type sizes and typefaces: Follow the type sizes specified in Table I. As an aid in gauging type size, 1 point is about 0.35 mm. The size of the lowercase letter "j" will give the point size. Times New Roman has to be the font for main text. Paper should be single spaced.

Margins: Top and Bottom = 24.9mm (0.98 in), Left and Right = 16 mm (0.63 in). The column width is 86mm (3.39 in). The space between the two columns is 6mm (0.24 in). Paragraph indentation is 3.7 mm (0.15 in).

Left- and right-justify your columns. Use tables and figures to adjust column length. On the last page of your paper, adjust the lengths of the columns so that they are equal. Use automatic hyphenation and check spelling. Digitize or paste down figures.

For the Title use 24-point Times New Roman font, an initial capital letter for each word. Its paragraph description should be set so that the line spacing is single with 6-point spacing before and 6-point spacing after. Use two additional line spacings of 10 points before the beginning of the double column section, as shown above

TABLE-I.

TYPE SIZES FOR CAMERA-READY PAPERS

Type size (pts.)	Appearance		
	Regular	Bold	Italic
6	Table caption, table superscripts		
8	Tables, table names, f irst letters in table captions, figure captions, footnotes, text subscripts, and superscripts		
9	References, authors' biographies	Abstract	
10	Section titles ,Authors' affiliations, main text, equations, first letters in section titles		Subheading
11	Authors' names		
24	Paper title		

Each major section begins with a Heading in 10 point Times New Roman font centered within the column and numbered using Roman numerals (except for REFERENCES), followed by a period, two spaces, and the title using an initial capital letter for each word. The remaining letters are in SMALL CAPITALS (8 point). The paragraph description of the section heading line should be set for 12 points before and 6 points after.

Subheadings should be 10 point, italic, left justified, and numbered with letters (A, B, …), followed by a period, two spaces, and the title using an initial capital letter for each word. The paragraph description of the subheading line should be set for 6 points before and 3 points after.

For main text, paragraph spacing should be single spaced, no space between paragraphs. Paragraph indentation should be 3.7mm/0.21in, but no indentation for abstract & index terms.

II. Helpful Hints

A. Figures And Tables

Position figures and tables at the tops and bottoms of columns. Avoid placing them in the middle of columns. Large figures and tables may span across both columns. Leave sufficient room between the figures/tables and the main text. Figure captions should be centered below the figures; table

Received on xx-xx-xxxx, Revised on xx-xx-xxxx, Accepted on xx-xx-xxxx.

captions should be centered above. Avoid placing figures and tables before their first mention in the text. Use the abbreviation "Fig. 1," even at the beginning of a sentence.

To figure axis labels, use words rather than symbols. Do not label axes only with units. Do not label axes with a ratio

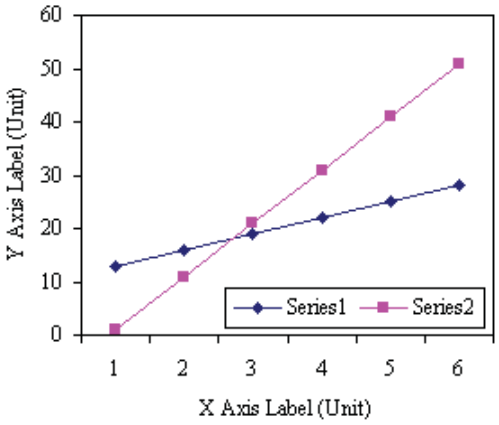

Figure 1. Note how the caption is centered in the column.

of quantities and units. Figure labels should be legible, about 8-point type.

All figures, tables and references must be cited in the text.

Please indicate the broad area/specializations into which the research paper falls, in the covering letter/mail to the Editor, so that reviewers with those specializations may be identified.

B. References

Number citations consecutively in square brackets [1]. Punctuation follows the bracket [2]. Use "Ref. [3]" or "Reference [3]" at the beginning of a sentence:

Give all authors' names; use "et al." if there are six authors or more. Papers that have not been published, even if they have been submitted for publication, should be cited as "unpublished" [4]. Papers that have been accepted for publication should be cited as "in press" [5]. In a paper title, capitalize the first word and all other words except for conjunctions, prepositions less than seven letters, and prepositional phrases. Good number of references must be given.

Latest references in the area must be included and every refence must be cited in the text of the research article.

C. Footnotes

Number footnotes separately in superscripts [1, 2, ⋯]. Place the actual footnote at the bottom of the column in which it was cited, as in this column. See first page footnote as an example.

D. Abbreviations and Acronyms

Define abbreviations and acronyms the first time they are used in the text, even after they have been defined in the abstract. Do not use abbreviations in the title unless they are unavoidable.

E. Equations

Equations should be left justified in the column. The paragraph description of the line containing the equation should be set for 6 points before and 6 points after. Number equations consecutively with equation numbers in parentheses flush with the right margin, as in (1). Italicize Roman symbols for quantities and variables, but not Greek symbols. Punctuate equations with commas or periods when they are part of a sentence, as in

$$a + b = c\,. \tag{1}$$

Symbols in your equation should be defined before the equation appears or immediately following. Use "(1)," not "Eq. (1)" or "equation (1)," except at the beginning of a sentence: "Equation (1) is ..."

F. Other Recommendations

Use either SI (MKS) or CGS as primary units. (SI units are encouraged.) If your native language is not English, try to get a native English-speaking colleague to proofread your paper. Do not add page numbers.

III. Conclusions

The authors can conclude on the topic discussed and proposed, future enhancement of research work can also be briefed here.

References

[1] G. Eason, B. Noble, and I. N. Sneddon, "On certain integrals of Lipschitz-Hankel type involving products of Bessel functions," Phil. Trans. Roy. Soc. London, vol. A247, pp. 529–551, April 1955.

[2] J. Clerk Maxwell, *A Treatise on Electricity and Magnetism*, 3rd ed., vol. 2. Oxford: Clarendon, 1892, pp.68–73.

[3] I. S. Jacobs and C. P. Bean, "Fine particles, thin films and exchange anisotropy," in *Magnetism*, vol. III, G. T. Rado and H. Suhl, Eds. New York: Academic, 1963, pp. 271–350.

[4] K. Elissa, "Title of paper if known," unpublished.

[5] R. Nicole, "Title of paper with only first word capitalized", *J. Name Stand. Abbrev.*, in press.

[6] Y. Yorozu, M. Hirano, K. Oka, and Y. Tagawa, "Electron spectroscopy studies on magneto-optical media and plastic substrate interface," *IEEE Transl. J. Magn. Japan*, vol. 2, pp. 740–741, August 1987 [Digests 9th Annual Conf. Magnetics Japan, p. 301, 1982].

[7] M. Young, *The Technical Writer's Handbook*. Mill Valley, CA: University Science, 1989.

[8] T. Ali, B.K. Subhash and R.C. Biradar, "A Miniaturized Decagonal Sierpinski UWB Fractal Antenna", PIERS C, vol. 84, pp. 161-174, 2018.

ABOUT THE COLLEGE

CVR College of Engineering, an autonomous institution under the UGC, was established in the Year 2001, the first college in Telangana to be promoted by NRI technology professionals resident in the USA. The NRI promoters are associated with cutting-edge technologies of the computer and electronics industry. They also have strong associations with other leading NRI professionals working for world-renowned companies like IBM, Intel, Cisco, Facebook, AT & T, Google, and Apple who have agreed to associate with the College with a vision and passion to make the College a state-of-the-art engineering institution.

All B. Tech Programmes which are eligible are accredited three or four times by the NBA since 2007. Two UG Programmes namely ECE & EEE are accredited for Six years by the NBA under Tier-I. As of now, 7 B. Tech Programmes and 4 P.G Programmes are accredited. NAAC reaccredited the college for five years with grade 'A' with effect from 2022. Two M. Tech Programmes of AI and Data Science in 2018-2019 and three B. Tech CSE Programmes (AI & ML, DS & CS) in 2020-2021, 3 new branches in Emerging Technologies namely B. Tech AI & ML, AI & DS and CSBSs are the Programmes commenced in 2023-24 and 1 UG Programme B.Tech in Electronics Engineering (VLSI and Design Technology) is the recent addition in 2024-25.

As formulated by the IQAC, many FDPs and workshops are organized by departments. College has MoUs with organizations such as Virtusa, Mitsubishi, NRSC, COMSAT, CADENCE, IIIT. Under innovation activities faculty have published around 200 patents so far. Projects from NRSC under the RESPOND programme of ISRO, AICTE-RPS, TEQIP-III from JNTU, MODROBS-AICTE worth Rs.71 Lakhs are some of the recent projects funded by central agencies. Total funds received are Rs. 160 lakhs. Newgen IEDC of Government of India (DST) has sanctioned Rs.287 Lakhs for a period of five years in 2018-19, for Innovative Entrepreneurship Development Programmes by students and staff. 10 Projects were completed in 2019-20, 16 in 2020-21, 20 in 2021-22, 21 projects in 2022-23 and 20 projects in 2023-24. An exclusive Innovation Centre of 5000 Sqft. has been created for practical work and counseling.

The college has been creating records year after year. With more than 100 companies visiting CVRCE and 900+ placements for the 2023 - 2024 academic year, it is the highest among the peer group of colleges. This is despite the challenging environment of the job market and our placement percentage is higher than many leading institutions of the country. The highest offer is **44 Lakhs** by 4 students at AMAZON, 33 Lakhs by 2 students at Commvault and 30+ students received offers higher than **Rs. 18 Lakhs**. More than **150 students** received offers of About **Rs. 10 Lakhs**. About **200 offers** are higher than **Rs. 6 Lakhs**. With this, CVRCE becomes one of the leading colleges in the state in terms of offers with highest Average Salary. The placement percentage continues to be 100% since 5 years. The college has made huge progress in a short span of time and is preferred by the students and parents during the EAMCET counselling this year and is among the **top 3 colleges** in the state. College has been consistently in the range of 101-150 by NIRF over last Seven years. Many students have received special cash prizes in competitions like Hackathon, Mitsubishi etc., worth 1 to 2 Lakhs.

CVR is rated amongst the top 100 engineering institutions in the country by Outlook and holds many more recognitions.

CALL FOR PAPERS:

Papers in Engineering, Science and Management disciplines are invited for Publication in our Journal. Authors are requested to mail their contributions to Editor, CVR Journal of Science and Technology (Email Id: journal@cvr.ac.in). Authors can also submit their papers through our online open journal system (OJS) www.ojs.cvr.ac.in or www.cvr.ac.in/ojs. Papers are to be written using a Standard Template, which may be obtained on request from the Editor. It is also available on the college website www.cvr.ac.in

CVR JOURNAL OF SCIENCE AND TECHNOLOGY

CVR COLLEGE OF ENGINEERING

(UGC Autonomous- Affiliated to JNTU Hyderabad)
Mangalpalli (V), Ibrahimpatnam (M),
R.R. District, Telangana - 501510
http://cvr.ac.in